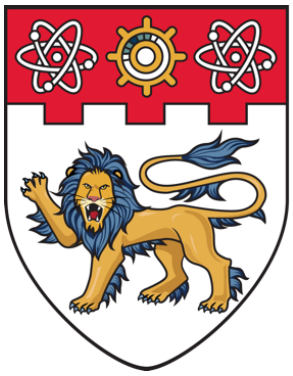

NANYANG TECHNOLOGICAL UNIVERSITY
SINGAPORE

# SYNTHESIS OF FUNCTIONAL POLYMERS: SELF-CATALYSED SYNTHESIS OF FUNCTIONAL POLYMERS AND NANO-CAPSULES AND SYNTHESIS OF DEGRADABLE POLYMERS USING CYCLIC KETENE HEMIACETAL ESTER MONOMERS

**OH XIN YI**

**SCHOOL OF PHYSICAL AND MATHEMATICAL SCIENCES**

**2022**

# SYNTHESIS OF FUNCTIONAL POLYMERS: SELF-CATALYSED SYNTHESIS OF FUNCTIONAL POLYMERS AND NANO-CAPSULES AND SYNTHESIS OF DEGRADABLE POLYMERS USING CYCLIC KETENE HEMIACETAL ESTER MONOMERS

**OH XIN YI**

SCHOOL OF PHYSICAL AND MATHEMATICAL SCIENCES

A thesis submitted to the Nanyang Technological University in partial fulfilment of the requirement for the degree of Doctor of Philosophy

**2022**

# Statement of Originality

I hereby certify that the work embodied in this thesis is the result of original research done by me except where otherwise stated in this thesis. The thesis work has not been submitted for a degree or professional qualification to any other university or institution. I declare that this thesis is written by myself and is free of plagiarism and of sufficient grammatical clarity to be examined. I confirm that the investigations were conducted in accord with the ethics policies and integrity standards of Nanyang Technological University and that the research data are presented honestly and without prejudice.



5th January 2022
. . . . . .
Date

. . . . . .
[Oh Xin Yi]

# Supervisor Declaration Statement

I have reviewed the content and presentation style of this thesis and declare it of sufficient grammatical clarity to be examined. To the best of my knowledge, the thesis is free of plagiarism and the research and writing are those of the candidate's except as acknowledged in the Author Attribution Statement. I confirm that the investigations were conducted in accord with the ethics policies and integrity standards of Nanyang Technological University and that the research data are presented honestly and without prejudice.

5 Jan 2022

.....
Date

.....
[Atsushi GOTO]

# Authorship Attribution Statement

This thesis contains material from [2] paper(s) published in the following peer-reviewed journal(s) in which I am listed as a co-first author with equal contribution for Chapter 2 and first author for Chapter 3.

Chapter 2 is published as Wang, C.–G.; Oh, X. Y.; Xu, L.; Goto, A. Self-Catalyzed Living Radical Polymerization Using Quaternary–Ammonium–Iodide–Containing Monomers. *Macromolecules* **2019**, *52*, 2712−2718.

The contributions of the co-authors are:

- Prof. A. Goto presented the initial project.
- I conducted all the experiments and analysis for the synthesis of monomers, homopolymerizations and random copolymerizations of these monomers used in this chapter at the Division of Chemistry and Biological Chemistry, School of Physical and Mathematical Sciences, Singapore.
- Prof. A. Goto and Dr. C.–G. Wang guided on the explanation of the experimental data.
- Dr. C.–G. Wang performed the experiments for the block copolymerizations and a surface-initiated polymerization. These results were not included in this chapter.
- Dr. C.–G. Wang and I prepared the draft of the manuscript. Prof. A. Goto edited and finalized the manuscript. Prof. A. Goto, Dr. C.–G. Wang, Dr. X. Liu, and I proofread the accepted manuscript.

Chapter 4 is published as Oh, X. Y.; Ge, Y.; Goto, A. Synthesis of Degradable and Chemically Recyclable Polymers Using 4,4-Disubstituted Five-Membered Cyclic Ketene Hemiacetal Ester (CKHE) Monomers. *Chem. Sci.* **2021**, *12*, 13546–13556.

The contributions of the co-authors are:

- Prof. A. Goto presented the initial project.
- I conducted all the experiments and analysis at the Division of Chemistry and Biological Chemistry, School of Physical and Mathematical Sciences, Singapore.

- Prof. A. Goto and Dr. Y. Ge guided on the explanation of the experimental data.
- I prepared the draft of the manuscript. Prof. A. Goto edited and finalized the manuscript. Prof. A. Goto and I proofread the accepted manuscript.

5th January 2022

. . . . . .

Date

. . . . . .

[Oh Xin Yi]

# Abstract

Sustainability in chemistry has raised significant interest since 1980s. The objective of this doctoral thesis is to prepare sustainable functional polymers.

In chapter 1, the general concept of radical polymerization was described. Also, several controlled radical polymerization (CRP) systems were discussed, including their principles and mechanisms. The concept of self-catalysis, polymerization-induced self-assembly (PISA), and degradable vinyl polymers were explained. The motivations and aims of each chapter were discussed.

In chapter 2, self-catalyzed CRP using reversible complexation mediated polymerization (RCMP) was reported. Quaternary ammonium iodide (QAI)-containing monomers were synthesized and used in RCMP as a monomer and as well as a catalyst. The polymerization was performed without the addition of an extra catalyst. QAI-containing monomers were copolymerized with functional methacrylates and acrylates.

In chapter 3, synthesis of nano-capsule was reported using self-catalyzed CRP and the nano-capsule was used as a heterogeneous RCMP catalyst. The nano-capsule was prepared using self-catalyzed polymerization-induced self-assembly (PISA). This vesicular nano-capsule possessing QAI functionality worked as a heterogeneous catalyst for the polymerization of several monomers. Also, good recyclability of this heterogeneous catalyst was demonstrated with ten cycles of methyl methacrylate (MMA) polymerization. The nano-capsule was further used as a nano-reactor to synthesize poly(methyl methacrylate) (PMMA) inside the cavity.

In chapter 4, synthesis of degradable and chemically recyclable polymers was reported. 4,4-disubstituted five-membered cyclic ketene hemiacetal ester (CKHE) (i.e., 4,4-dimethyl-2-methylene-1,3-dioxolan-5-one (DMDL) and 5-methyl-2-methylene-5-phenyl-1,3-dioxolan-4-one (PhDL)) monomers were synthesized and used for conventional radical polymerization.

CKHE monomers were copolymerized with various co-monomers. Poly(4,4-dimethyl-2-methylene-1,3-dioxolan-5-one) (PDMDL) was degraded in hydroxide- and amine-assisted conditions. Degradations of hydrophilic and hydrophobic random copolymers of PDMDL were also studied. Chemical recycling was demonstrated with the recovery of DMDL monomer precursor from PDMDL degradation.

In chapter 5, CRP of CKHE monomers (i.e., DMDL) was studied using reversible addition-fragmentation chain transfer (RAFT) polymerization and RCMP. Low-dispersity homopolymers, random copolymers, and a block copolymer of DMDL were prepared. A random copolymer of DMDL (i.e., PDMA-*r*-PDMDL, where PDMA is poly(*N*,*N*-dimethylacrylamide)) was degraded in a hydroxide-assisted condition.

In this thesis, synthesis of functional polymers was demonstrated and their contribution to sustainability was presented. In Chapter 2 and 3, we used the catalytic monomers to catalyze polymerizations without additional catalyst. In Chapter 3, we prepared a heterogeneous catalyst with the catalytic monomer for recycle use in polymerizations. In Chapter 4 and 5, we synthesized degradable polymers and recovered the degradation product for monomer synthesis.

# Acknowledgements

I would like to express my warmest gratitude to my supervisor, Prof. Goto. The completion of my Ph.D.'s journey would be impossible without his guidance and support. His expertise and encouragement constantly guided me through this tough journey. I am extremely grateful to him and it is a great honor to learn from Prof. Goto.

I would also like to convey my gratefulness to my current TAC members, Prof. Zhao Yanli and Prof. Shingo Ito, and also Prof. Naohiko Yoshikai (ex-TAC member) for their valuable comments and pointers. Also, I am thankful to the assistance provided by technical staff to support me when using analytical instruments.

I would like to thank my fellow lab mates (present and past) for their continued help. I want to thank Dr. Sarkar Jit, Dr. Ge Yicen, and Dr. Wang Chen–Gang for their valuable suggestions to my projects. And I would also like to thank Dr. Zheng Jie, Chew Ye Qiu, Yong (Seankongsuk Pattarakiat), and Chen Jiahua for their encouragement during my tough times in this journey.

Lastly, I am very glad to have my family's unconditional support especially to my parents who have always got my back.

# Table of Contents

**List of Abbreviations**

| | |
|---|---|
| AIBN | 2,2’-azobis(2-methylpropionitrile) |
| AN | Acrylonitrile |
| ATRP | Atom transfer radical polymerization |
| BA | Butyl acrylate |
| BNI | Tetrabutylammonium iodide |
| BzMA | Benzyl methacrylate |
| BMA | Butyl methacrylate |
| CP-I | 2-Iodo-2-methylpropionitrile |
| CRP | Controlled radical polymerization |
| CTA | Chain transfer agent |
| CKAs | Cyclic ketene acetals |
| CDPA | 4-Cyano-4[[(dodecylthio)carbonothioyl]thio]pentanoic acid |
| CMPC | 2-Cyanopropan-2-yl *N*-methyl-*N*-(pyridin-4-yl)carbamodithioate |
| CKHE | 4,4-Disubstituted five-membered cyclic ketene hemiacetal ester |
| CMs | Catalytic monomers |
| $C_6$MAI | [2-(Methacryloyloxy)ethyl]dimethylhexylammonium iodide |
| *Đ* | Polymer dispersity |
| DSC | Differential scanning calorimetry |
| DMAEMA | 2,2-(Dimethylamino)ethyl methacrylat |
| DMAEA | 2,2-(Dimethylamino)ethyl acrylate |
| DMDL | 4,4-Dimethyl-2-methylene-1,3-dioxolan-5-one |
| DMA | *N*,*N*-dimethylacrylamide |
| EC | Ethylene carbonate |

| | |
|---|---|
| EHMA | 2-Ethylhexyl methacrylate |
| ECP | Ethyl 2-[(ethoxycarbonothioyl)thio]propionate |
| GPC | Gel permeation chromatography |
| GMA | Glycidyl methacrylate |
| HIBA | 2-Hydroxyisbutyric acid |
| $k_{add}$ | Addition rate constant |
| $k_{fr}$ | Fragmentation rate constant |
| $k_p$ | Propagation rate constant |
| $k_a$ | Activation rate constant |
| $k_{da}$ | Deactivation rate constant |
| LMA | Lauryl methacrylate |
| LAMs | “Less activated” monomers |
| LRP | Living radical polymerization |
| MAMs | “More activated” monomers |
| MMA | Methyl methacrylate |
| MEA | 2-Methoxyethyl acrylate |
| MEMA | 2-Methoxyethyl methacrylate |
| MBDO | 2-Methylene-4*H*-benzo[d][1,3]dioxin-4-one |
| $M_n$ | Number-average molecular weight |
| $M_w$ | Weight-average molecular weight |
| NMP | Nitroxide mediated radical polymerization |
| NMR | Nuclear magnetic resonance |
| NVP | *N*-vinylpyrrolidone |
| PhDL | 5-Methyl-2-methylene-5-phenyl-1,3-dioxolan-4-one |
| PDMDL | Poly(4,4-dimethyl-2-methylene-1,3-dioxolan-5-one) |

| | |
|---|---|
| PISA | Polymerization-induced self-assembly |
| PAN | Poly(acrylonitrile) |
| PDMA | Poly(*N*,*N*-dimethylacrylamide) |
| PBA | Poly(butyl acrylate) |
| PEGMA | Poly(ethylene glycol) methyl ether methacrylate |
| PMEA | Poly(2-methoxyethyl acrylate) |
| PMMA | Poly(methyl methacrylate) |
| PPEGMA | Poly(poly(ethylene glycol) methyl ether methacrylate) |
| PSt | Poly(styrene) |
| QAI | Quaternary ammonium iodide |
| RAFT | Reversible addition-fragmentation chain transfer polymerization |
| RCMP | Reversible complexation mediated polymerization |
| RDRP | Reversible-deactivation radical polymerization |
| ROP | Ring-opening polymerization |
| rROP | Radical ring-opening polymerization |
| St | Styrene |
| TGA | Thermogravimetric analysis |
| TEM | Transmission electron microscope |
| TEA | Triethylamine |
| TBPB | *t*-Butyl peroxybenzoate |
| V65 | 2,2'-Azobis(2,4-dimethylvaleronitrile) |
| VAc | Vinyl acetate |

## Chapter 1. Introduction

### 1.1. Conventional Radical Polymerization

Synthetic polymers are widely used in our daily lives. Global plastics production increased from 15 million metric tons in 1964 then to 311 million in 2014, increasing twentyfold in just 50 years.[1] In recent years, production has reached close to 400 million tons. And this number will increase further over years.

Radical polymerization is one of the most widely used methods to produce synthetic polymers in industry. It is advantageous over other methods because it is tolerant to water and other small quantity of impurities, liable to a wide range of monomers, and suitable for large scale production. All these factors make radical polymerization economically attractive to industry.[2]

In conventional radical polymerization, peroxide or azo compounds are used as radical initiators, for example. They decompose either by light or heat, producing free radicals by the cleavage of labile bonds (initiation in Scheme 1.1a). The generated active radical propagates with monomer, and the polymer chain grows (propagation in Scheme 1.1a). The propagating radical can be added by multiple monomers, generating another propagating polymer radicals. Alternatively, two propagating polymer radicals can undergo termination via recombination or disproportionation, generating a dead chain that is unable to propagate further (termination in Scheme 1.1c). This irreversible termination occurs randomly among the propagating radicals, resulting in broad molecular weight distributions and uncontrolled molecular weights. The dispersity ($Đ = M_w/M_n$) is 1 when all polymers have the same chain length and is generally larger than 1.5 when polymers are prepared by conventional radical polymerization, where $M_w$ and $M_n$ are weight-average of molecular weight and number-average molecular weight, respectively.

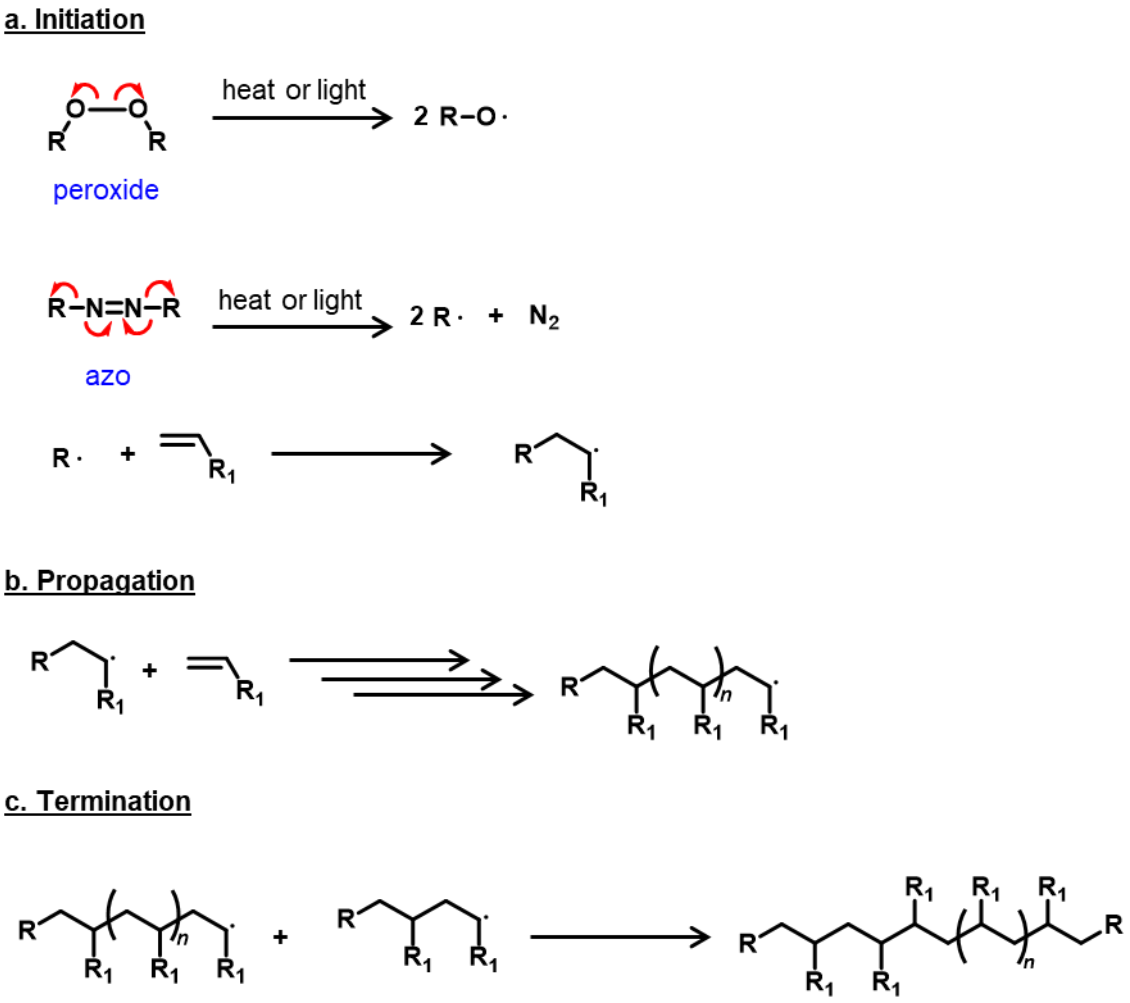


**Scheme 1.1.** Elementary reactions in conventional radical polymerization.

## 1.2. Controlled Radical Polymerization (CRP)

To address the problems (i.e., broad molecular weight distributions and uncontrolled molecular weights) of conventional radical polymerization, Szwarc et al. introduced anionic "living polymerization" in 1956 which did not include a termination step, therefore enabling the polymer chains to continue to grow when more monomers were added.[3] In radical polymerization, this kind of "living polymerization" is termed as controlled radical polymerization (CRP). It is also named as reversible-deactivation radical polymerization (RDRP) (Scheme 1.2). RDRP is based on the reversibly activation of a dormant polymer species (Polymer–X), generating a propagating polymer radical (Polymer•) which undergoes

addition of monomers. X is a capping agent. Polymer• is subsequently capped by X, undergoing deactivation and regenerating Polymer–X. Upon frequent activation-deactivation cycles, each polymer chain has a nearly identical opportunity to propagate, thereby achieving low dispersities ($Đ$ < 1.5) with controlled molecular weights.

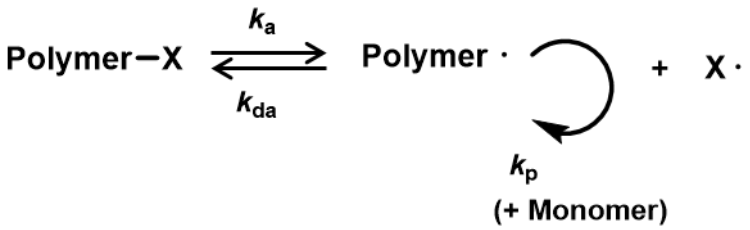


**Scheme 1.2.** Reversible activation in LRP/CRP/RDRP.

Based on the concept of reversibly generating Polymer• from Polymer–X, atom transfer radical polymerization (ATRP), nitroxide-mediated radical polymerization (NMP), reversible addition-fragmentation chain transfer (RAFT) polymerization, and reversible complexation mediated polymerization (RCMP) were developed, for example. These methods utilize different capping agents (X).

In 1995, Matyjaszewski et al. [4] and Sawamoto et al.[5] independently developed ATRP. ATRP uses a halogen (Cl, Br or I) as an X and a transition metal complex ($LM_t^n$ where $M_t$ is transition metal and L is the ligand) as a catalyst. The catalyst abstracts the halogen (X) from Polymer-X via a redox process and reversibly generates Polymer• and an oxidized metal complex ($LM_t^{n+1}X$) (Scheme 1.3). The transition metals used in ATRP include copper (Cu) (most frequently used), iron (Fe), nickel (Ni), and ruthenium (Ru). Different ligands such as nitrogen species (pyridine or aliphatic amine) are chosen to control the polymerization rate and the dispersity for different monomers, solvents, and temperatures.

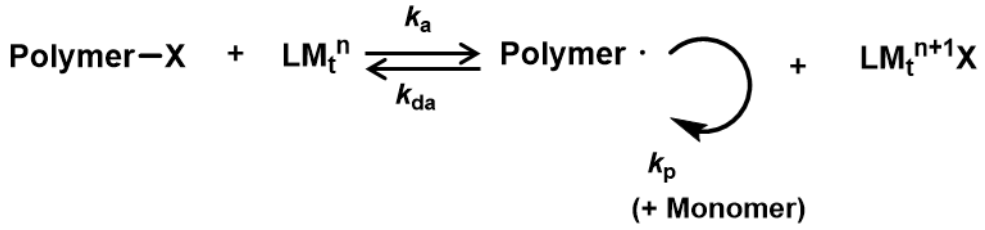


**Scheme 1.3.** Reversible activation and deactivation in ATRP.

NMP was first introduced by Solomon et al. in 1984 at CSIRO, generating oligomers.[6] Georges et al. subsequently achieved the synthesis of low-dispersity polymers.[7] Alkoxyamines (Polymer–X) are used in NMP to reversibly generate Polymer$^{\bullet}$ and a nitroxide radical (X$^{\bullet}$) (Scheme 1.4). Nitroxides are persistent radicals. In NMP, Polymer–X (X = $ONR_1R_2$) decomposes under heat to generate Polymer$^{\bullet}$ and X$^{\bullet}$ (Scheme 1.4).

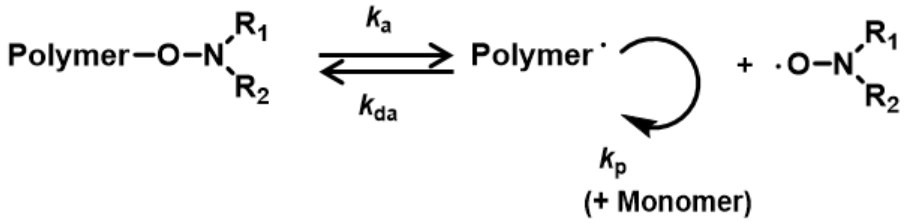


**Scheme 1.4.** Reversible activation in NMP.

Other than ATRP and NMP, RAFT polymerization and RCMP are also useful to synthesize low-dispersity polymers. They are used in the present thesis (chapters 2, 3, and 5) and are explained more in the following sub-sections (chapters 1.3 and 1.4).

### 1.3. Reversible Addition-Fragmentation Chain Transfer (RAFT) Polymerization

RAFT polymerization was first reported in 1998 by the CSIRO group.[8] RAFT is a degenerative chain transfer of Polymer$^{\bullet}$ ($P_m^{\bullet}$) to thiocarbonylthio compounds (S=C(Z)S–$P_n$). $P_m^{\bullet}$ undergoes addition to S=C(Z)S–$P_n$, generating an intermediate radical ($P_n$–SC$^{\bullet}$(Z)S–$P_m$). The intermediate radical undergoes fragmentation into S=C(Z)S–$P_m$ and $P_n^{\bullet}$ (Scheme 1.5).

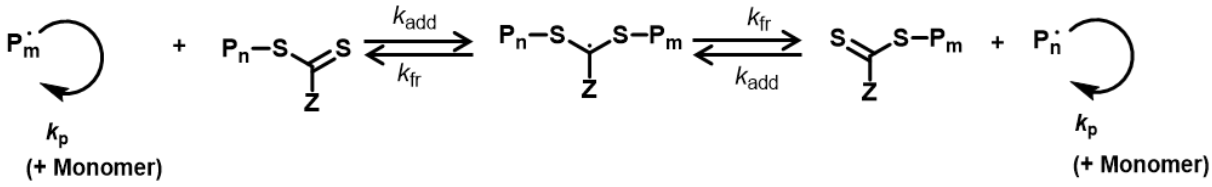


**Scheme 1.5.** RAFT polymerization mechanism.

A RAFT agent, also termed as a chain transfer agent (CTA) (S=C(Z)SR), contains a leaving alkyl group (R group) and a stabilizing group (Z group). Examples of RAFT agents are dithioesters (Z = alkyl), trithiocarbonates (Z = *S*-alkyl), xanthates (Z = *O*-alkyl), and dithiocarbamate (Z = *N*-alkyl) (Figure 1.1). To ensure a frequent chain transfer, the C=S bond of the CTA must be sufficiently reactive for the addition of the propagating radical. Different Z groups are used to control the stability of the intermediate radical generated in the RAFT process. The addition rate constant ($k_{add}$) increases with an increase in the stability of the intermediate radical by the Z group, resulting in a more frequent chain transfer. The $k_{add}$ values increase in the order of Z = *N*-alkyl < *O*-alkyl < *S*-alkyl < alkyl.

Vinyl monomers can be categorized into "more activated" monomers (MAMs) and "less activated" monomers (LAMs) based on the stability of generated propagating radical. MAMs refer to monomers containing a polymerizable vinyl group conjugating to substituents such as a phenyl (e.g., styrene), a carbonyl group (e.g., methacrylates), or a nitrile (e.g., acrylonitrile) with their generated propagating radicals stabilized. LAMs usually do not carry such substituents that help to stabilize the propagating radicals.

In general, dithioesters and trithiocarbonates are used to control polymerization of MAMs while xanthates are used for polymerization of LAMs. The selection of RAFT agents is important for monomers with different reactivities, i.e., MAMs and LAMs. Dithioesters and trithiocarbonates have higher $k_{add}$ values and are generally efficient CTAs for MAMs such as styrene and methacrylates. In contrast, for LAMs, the propagating radicals are less stable. Therefore, the equilibrium shifts to the intermediate radical and results in accumulation of the

intermediate radical (Scheme 1.5). Hence, terminations between an intermediate radical and a propagating radical and between intermediate radicals can be significant, generating dead polymer chains and resulting in a retardation in the polymerization rate. Thus, CTAs with higher fragmentation rate constants ($k_{fr}$) values such as xanthates and dithiocarbamates are used for LAMs because their intermediate radicals are less stable.


**Figure 1.1.** Examples of RAFT agents (CTAs).

### 1.4. Reversible Complexation Mediated Polymerization (RCMP)

In 2007, Goto et al.[9] developed RCMP, which is an organocatalyzed CRP. This organocatalyzed CRP system uses alkyl iodides as initiators (X = iodide) and organic compounds such as amines (triethylamine and tributylamine) and an iodide anion ($I^-$) as catalysts. $I^-$ is used in a form of tetrabutylammonium iodide ($Bu_4N^+I^-$), for example. $Bu_4N^+I^-$ is a quaternary ammonium iodide (QAI). The catalyst ($I^-$) coordinates the iodide of Polymer-I through a halogen bonding, forming a complex (Polymer–I···catalyst) that can reversibly generate Polymer• (Scheme 1.6).

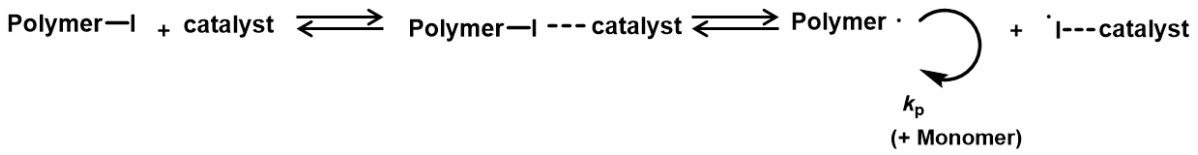


**Scheme 1.6.** Reversible activation in RCMP.

Initially, amines were used as catalysts in RCMP. Amines were suitable for methacrylates and styrene while not suitable for acrylates and acrylonitrile.[10] This is because

the amines were not strong enough to abstract the iodide from polyacrylate- and polyacrylonitrile-based Polymer–I. Later, ionic catalysts were used as more reactive catalysts and were effective to control the polymerization of methacrylates, styrene, acrylates, and acrylonitrile due to their ability to form stronger halogen bonding with Polymer-I, thus effectively generate Polymer•.[11–14] In RCMP, besides heating, photoirradiation can be used to control the polymerization with the use of amines[15] or organic photocatalysts[16]. Also, RCMP is applied in the polymerization of several monomers in polar solvents, i.e., water or ethanol.[14,17]

At the polymer chain-end (Polymer–I), the weak carbon-iodine bond is utilized in RCMP to generate Polymer•. Furthermore, the weak-iodine bond is exploited for chain-end transformation, converting Polymer–I to chain-end functionalized polymers.[18,19] RCMP is advantageous in which no metals or odorous compounds are used. Polymers obtained with the organic catalysts can be used in biomedical applications due to no toxicity imposed.

### 1.5. Self-catalysis

Self-catalysis is a process in which a reactant or product works as a catalyst and catalyzes the reaction without the need of an extra catalyst. This technique offers a major advantage in which no additional catalyst is needed, therefore simplifying the purification and reducing the waste generation.

Endo et al. reported the synthesis of random copolymers containing spiroorthoester and benzyl sulfonium salt moieties and later the polymers were cured without the need of an extra catalyst.[20] A self-catalysis was reported for ring-opening polymerization (ROP) with phthaloylchitosan (PHCS). PHCS contains phthalimido compound (working as a catalyst) and polymers of PHCS were grafted to a polycaprolactone without an additional catalyst.[21] Wang et al. prepared a diol with a catalytic property that catalyzes a polycondensation of the diol and

an isocyanate to form a polyurethane without the addition of an extra catalyst.[22] In the field of CRP, self-photocatalytic initiators (not catalytic "monomers") were successfully used for methacrylate and styrene copolymerizations using RAFT polymerizations.[23,24]

### 1.6. Polymerization-Induced Self-Assembly (PISA)

Nano-objects including spheres, rods and vesicles have been prepared by self-assemblies of block copolymers in solution (Figure 1.2). They can be prepared via a post polymerization process in which a block copolymer solution is prepared in a good solvent and then a selective poor solvent is added dropwise into the solution in a highly diluted condition. The selective poor solvent leads to the insolubility of the block copolymer and triggers it to self-assemble into various nano-objects. This process needs to be conducted in a very diluted condition (i.e., 1–3 wt% polymer in the solvent) (i.e., at a low solid content) which requires a large amount of solvent and is therefore unfavorable for commercial applications.[25]

Polymerization-induced self-assembly (PISA) is a process that drives a block copolymer to self-assemble during polymerization.[26] It is an efficient method to overcome the limitation (the low solid content) of the post-polymerization method. In the first step of PISA, a soluble first polymer block is prepared in a good solvent. Then, the soluble (solvophilic) first polymer block is chain-extended to form an insoluble (solvophobic) second segment in a selected good solvent for the first block. As the chain-extension proceeds, the growing second block becomes insoluble, forming spheres first. Continuation of the second block polymerization drives the reorganization of the block copolymers to form other morphologies such as rods and vesicles.

PISA is advantageous as it can be performed at relatively high solid contents (up to 50/50 (w/w %) polymer/solvent ratio).[27,28] Also, PISA usually enables high monomer conversions to be achieved within short reaction times compared to conventional solution

polymerization.[29,30] In addition, different morphologies can be prepared via PISA by just adjusting the molecular weights of the two block segments.

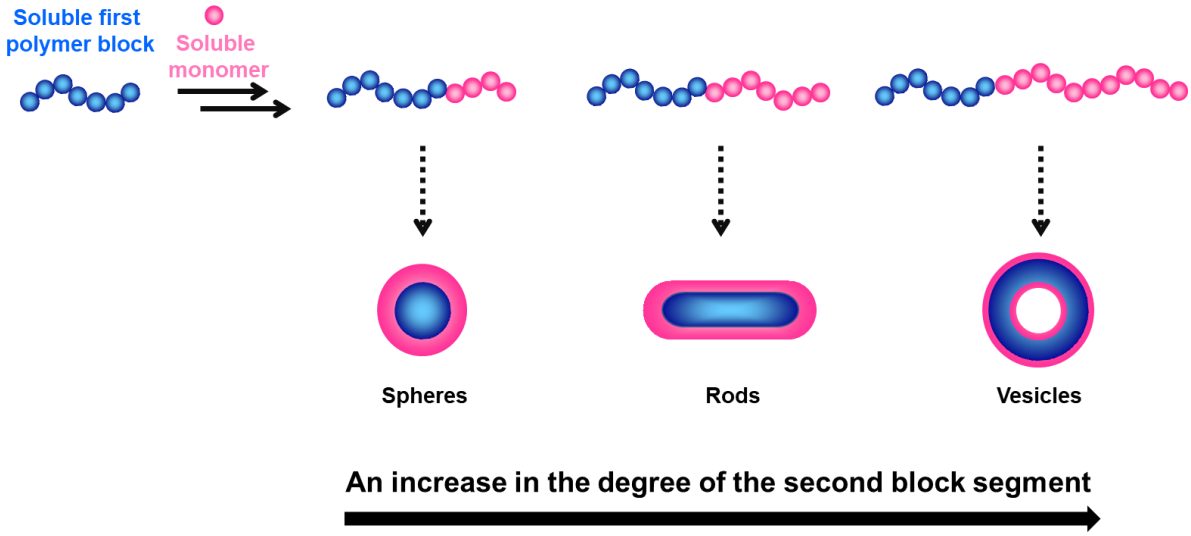


**Figure 1.2.** Nano-objects generated by polymerization-induced self-assembly (PISA).

### 1.7. Degradable Vinyl Polymers

Vinyl polymers are a group of polymers that are obtained from vinyl monomers ($CH_2$=CHR). The polymer backbones consist of –$CH_2$CHR– repeating units. The backbone carbon-carbon bonds are strong and resist to degradation. Thus, the polymers are durable from hydrolysis and enzymatic degradation in natural environments. The good durability is beneficial for pro-longed use of the polymer in outdoor environments but is disadvantageous with respect to possible plastic pollution in the environment upon improper treatment after use. In addition, degradability is desired in biomedical applications such as drug delivery and tissue engineering.

One approach to introduce degradability to polymers is to insert labile units within the polymer backbone. The degradation can lead to a reduced molecular weight of polymer by half, partially or to a monomer unit size.

The introduction of a labile unit in the polymer backbone was realized using difunctional initiators containing a cleavable bond. Employing difunctional initiators in CRP systems such as ATRP[31] and RAFT[32] polymerization, diblock polymers with a cleavable junction in the center were prepared (Figure 1.3). This method was also used for synthesizing degradable complex architectures, i.e., multiple arms star polymers,[33] which was utilized in drug delivery applications. Random copolymers synthesized using difunctional initiator can be degraded. However, there is only one degradable linkage (from the difunctional initiator) per polymer chain. Upon degradation, the single polymer chain degrades into two shorter polymer chains which may still be too high in molecular weight for desired applications. Synthesis of degradable random copolymers with multiple degradable sites in the polymer backbones is not attainable using this method.

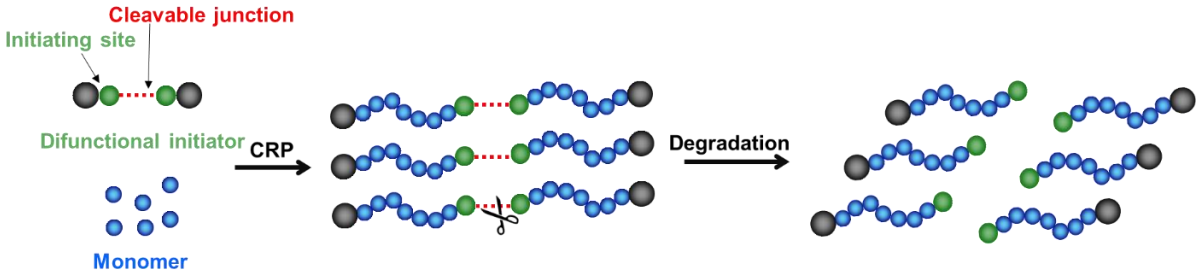


**Figure 1.3.** Degradable polymers synthesized with difunctional initiator.

Another way to prepare degradable polymer was to utilize a click reaction. For instance, a RAFT agent with $\alpha,\omega$-dialkyne functionality was used to yield a polymer with dialkyne ends. The obtained polymer was subsequently reacted with an $\alpha,\omega$-diazide peptide containing degradable linkages via copper-catalysed azide–alkyne Huisgen cycloaddition (CuAAC) (Figure 1.4).[32]

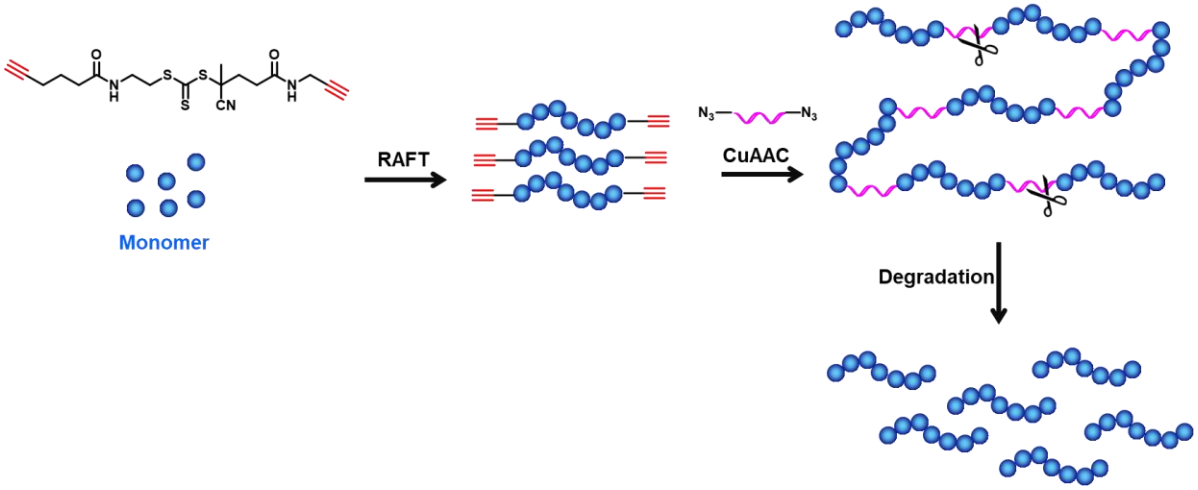


**Figure 1.4.** Degradable polymers synthesized via click reaction.

In recent years, radical ring-opening polymerization (rROP) of cyclic monomers[34-36] has attracted numerous research interest to incorporate degradable linkages into the polymer backbone. Among several classes of cyclic monomers, cyclic ketene acetals (CKAs) are the most studied monomers, as first reported by Bailey and co-workers in the early 80s.[37,38] CKAs are copolymerized with other vinyl monomers to confer degradability in the polymers upon the random insertion of ester groups (Figure 1.5). Although the homopolymerization of CKAs is challenging but it can copolymerize with various functional vinyl monomers via conventional radical polymerization and CRP techniques. Also, different structures of CKAs such as 5-membered and 7-membered rings species are explored with different ring opening abilities.

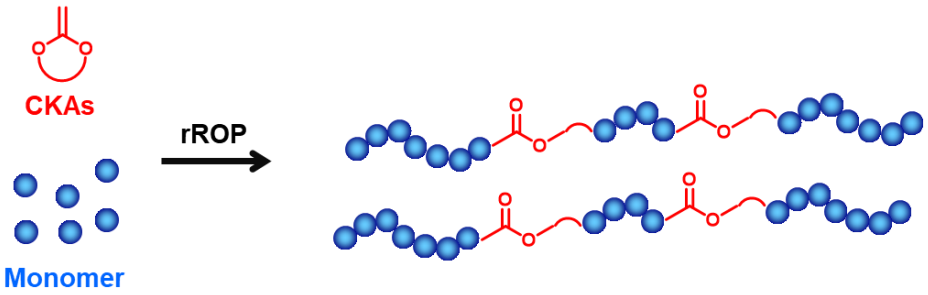


**Figure 1.5.** Degradable polymers prepared by cyclic ketene acetals (CKAs).

## 1.8. Thesis Objectives

Sustainable chemistry aims to improve the efficiency of natural resources being used to satisfy human needs with more environmentally benign design.[39] CRP techniques need catalysts (i.e., transition metal complex for ATRP, CTAs for RAFT polymerization, and iodide anion for RCMP). After polymerization, a purification step is needed to remove the catalyst. In addition, the catalysts are used for one-time (i.e., unable to recover after use). Polymers are widely used in numerous applications. Without proper treatment after use (i.e., recycling), the polymers accumulate in the environment and causes environmental issue.

In this doctoral thesis, the primary motivation was to design a sustainable polymerization process or functional polymers contributing to the sustainability. The present work aimed to conduct RCMP in a more sustainable way (i.e., without the need of an extra catalyst or a reusable catalyst) and prepare degradable vinyl polymers with chemical recyclability.

This thesis includes self-catalyzed RCMP (chapter 2), synthesis of a functional nano-capsule (chapter 3) and synthesis of functional polymers with degradability and chemical recyclability (chapters 4 and 5). In Chapter 2 and 3, we used the catalytic monomers to catalyze polymerizations without additional catalyst. In Chapter 3, we prepared a heterogeneous catalyst with the catalytic monomer for recycle use in polymerizations. In Chapter 4 and 5, we synthesized degradable polymers and recovered the degradation product for monomer synthesis.

Outcomes of chapters 2 and 3 contribute to the sustainability in which fewer chemical wastes are generated (i.e., easy purification after polymerization and reusable catalyst). Also, the degradable vinyl polymers reported in chapters 4 and 5, devoting to the sustainability with their chemical recycling abilities.

### 1.9. Aim in Chapter 2

In RCMP, catalysts are added to control the polymerization and need to be removed after the polymerization. The removal process (i.e., purification) generates chemical waste. In this chapter, a monomer with catalytic property was designed to catalyze RCMP without the need for an additional catalyst.

As mentioned, QAI is an RCMP catalyst to activate Polymer–I to reversibly generate Polymer$^{\bullet}$ (Scheme 1.6). Chapter 2 describes the use of QAI-containing vinyl monomer for synthesizing QAI-containing polymers (Figure 1.6). The polymerization is a self-catalyzed RCMP without the addition of an extra catalyst. Because of the QAI functionality, QAI-containing monomer serves as a monomer and an RCMP catalyst. No additional catalyst is required to proceed the polymerization. Purification (i.e., removal of catalyst) is simple without the presence of additional catalyst. Less chemical waste (i.e., solvent for purification) is generated for the whole polymerization process. Thus, this work contributes to the sustainability with less generation of chemical waste.

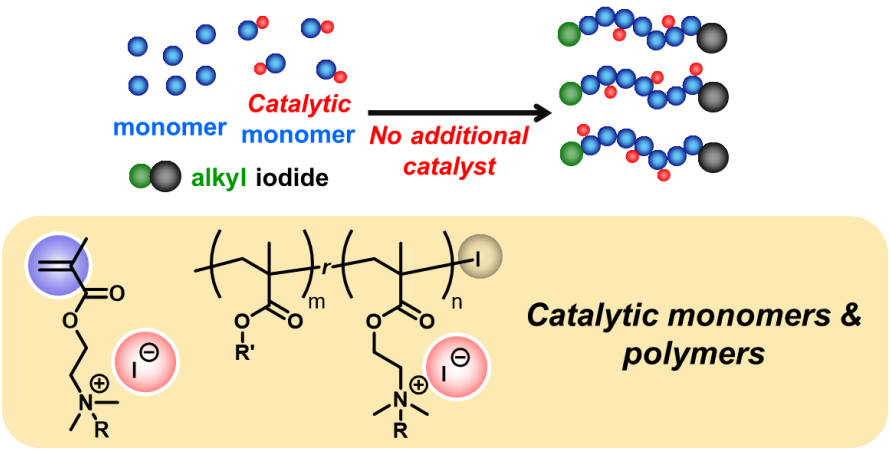


**Figure 1.6.** RCMP of QAI-containing CMs.

## 1.10. Aim in Chapter 3

Chapter 3 described an application of the self-catalyzed RCMP (developed in chapter 2) for the synthesis of a nano-capsule (vesicle). The nano-capsule was further utilized as a unique nano-reactor. A solvophilic first block was synthesized using QAI-containing monomer (i.e., also worked as a catalyst) without an extra catalyst to obtain a QAI-containing polymer block. Then, this block was chain-extended to form a solvophobic second segment which self-assembled into a nano-capsule in situ via self-catalyzed PISA (i.e., without additional catalyst). The obtained nano-capsule bears QAI functionalities (i.e., catalyst for RCMP) on both outer and inner surfaces of the shell (Figure 1.7). Thus, the nano-capsule was further used as a heterogeneous catalyst of RCMP of methyl methacrylate (MMA). The nano-capsule catalyzed the RCMP of MMA on both outer surface and inner core. Outer surface QAI catalyzed the RCMP of MMA, generating PMMA outside the nano-capsule. When some stirring time had been allowed before polymerization, small molecules (i.e., MMA monomer and alkyl iodide initiator) diffused into the inner core. The RCMP of MMA was catalyzed by inner surface QAI and poly(methyl methacrylate) (PMMA) was generated in the inner core. Thus, PMMA was generated on both the inside and outside of the nano-capsule. This QAI-containing nano-capsule worked as a heterogeneous RCMP catalyst which was recycled and reused for MMA polymerization up to ten cycles using the outer surface QAI. It is also amenable to other vinyl monomers (i.e., functional methacrylates, styrene, and acrylonitrile). This nano-capsule serves as dual catalysts for RCMP with QAI groups on both outer and inner surfaces of the nano-capsule. The inner core of the nano-capsule works as a nano-reactor enabling micro-phase separation polymerization (i.e., polymerization inside the nano-capsule).

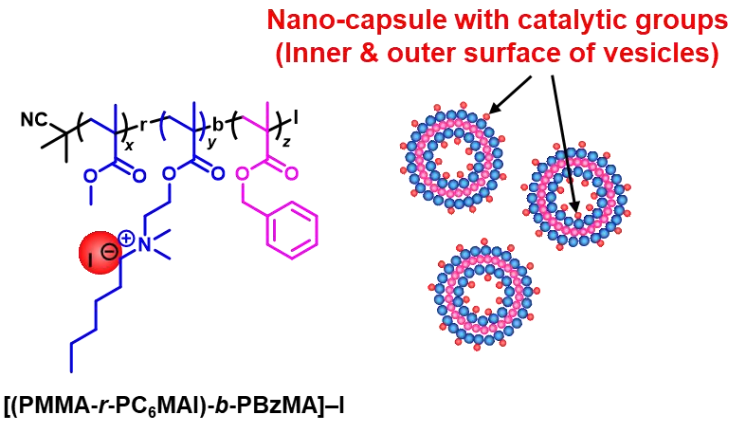


**Figure 1.7.** Nano-capsule with catalytic sites on both outer surface and inner core.

### 1.11. Aim in Chapter 4

Vinyl polymers that are non-degradable cause pollution in the environment if they are not treated properly after use. In addition, polymer degradability is important for applications such as controlled drug delivery and tissue engineering scaffold. In chapter 4, novel degradable and chemically recyclable polymers were developed. 4,4-disubstituted five-membered cyclic ketene hemiacetal ester (CKHE) monomers were used as novel monomers. CKHE monomers were homopolymerized and copolymerized with several vinyl co-monomers via conventional radical polymerization. In the random copolymerizations, a kinetic study was conducted to determine the monomer reactivity ratios. The obtained CKHE homopolymer and random copolymers are degradable upon base treatment. CKHE homopolymer was degraded to a precursor (i.e., 2-hydroxyisbutyric acid (HIBA)) of the monomer and recycled to synthesize the monomer. Chemical recycling is a process that polymers degrade into their raw materials which can be further utilized. The CKHE homopolymer is degradable and chemically recyclable which may contribute to the circular materials economy.

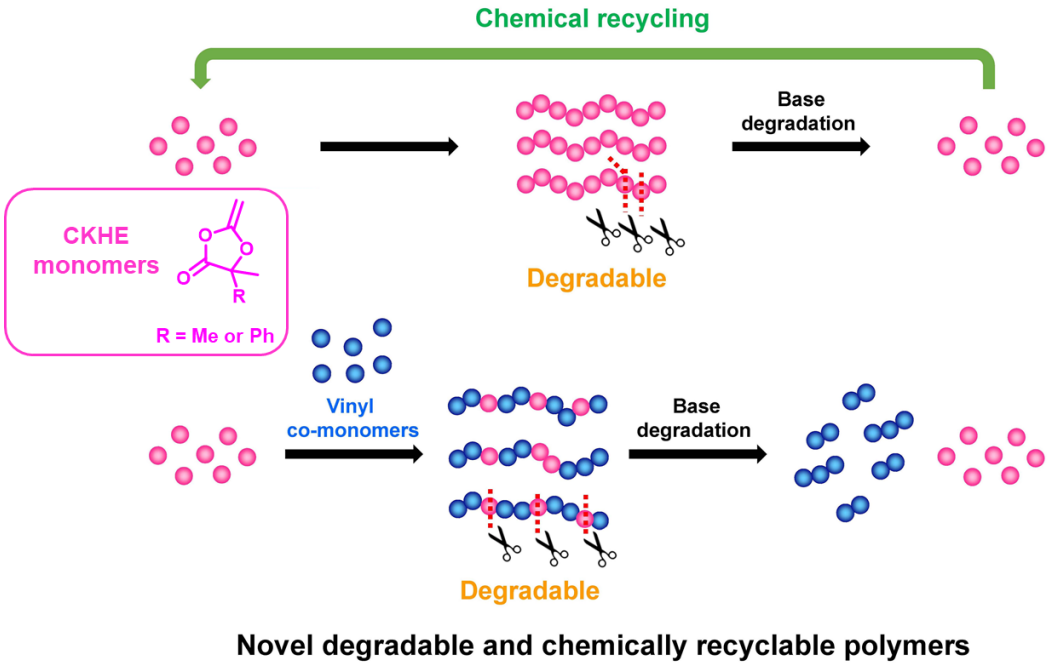


**Figure 1.8.** Synthesis and degradation of CKHE polymers.

## 1.12. Aim in Chapter 5

In chapter 5, CRP was used to synthesize low-dispersity CKHE containing polymers (while conventional radical polymerization was used in chapter 4). A CKHE monomer was polymerized via CRP, i.e., RAFT polymerization and RCMP, yielding low-dispersity homo-polymers and random (gradient) copolymers. A block copolymer was synthesized using RAFT polymerization. Upon degradation, gradient copolymers generate mostly short oligomers while block copolymers generate small molecules (from degradable segment) and polymer chains (from non-degradable segment). Both gradient and block copolymers are useful in biomedical applications.

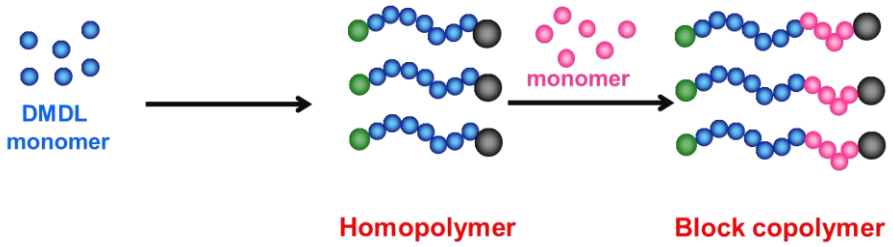


**Figure 1.9.** CRP of DMDL homo- and block copolymers.

## References


1. The future of plastics: a new global treaty? https://www.c2es.org/2021/08/the-future-of-plastics-a-new-global-treaty/ (accessed 30 Dec 21).
2. Grishin, D. F.; Grishin, I.D. *Russ. J. Appl. Chem.* **2011**, *84*, 2021-2028.
3. Szwarc, M. *Nature* **1956,** *178*, 1168-1169.
4. Kato, M.; Kamigaito, M.; Sawamoto, M.; Higashimura, T. *Macromolecules* **1995,** *28*, 1721-1723.
5. Wang, J.-S.; Matyjaszewski, K. *J. Am. Chem. Soc.* **1995,** *117*, 5614-5615.
6. Solomon, D. H.; Rizzardo, E.; Cacioli, P. U. S. Patent 4, 581, 429, 1986.
7. Georges, M. K.; Veregin, R. P. N.; Kazmaier, P. M.; Hamer, G. K. *Macromolecules*, **1993**, *26*, 2987-2988.
8. Chiefari, J.; Chong, Y. K.; Ercole, F.; Krstina, J.; Jeffery, J.; Le, T. P. T.; Mayadunne, R. T. A.; Meijs, G. F.; Moad, C. L.; Moad, G.; Rizzardo, E.; Thang, S. H. *Macromolecules* **1998,** *31*, 5559-5562.
9. Goto, A.; Zushi, H.; Hirai, N.; Wakada, T.; Tsujii, Y.; Fukuda, T. *J. Am. Chem. Soc.* **2007,** *129*, 13347-13354.
10. Goto, A.; Suzuki, T.; Ohfuji, H.; Tanishima, M.; Fukuda, T.; Tsujii, Y.; Kaji, H. *Macromolecules* **2011,** *44*, 8709-8715.
11. Goto, A.; Ohtsuki, A.; Ohfuji, H.; Tanishima, M.; Kaji, H. *J. Am. Chem. Soc.* **2013,** *135*, 11131-11139.
12. Xu, H.; Wang, C.-G.; Lu, Y.; Goto, A. *Macromolecules* **2019,** *52*, 2156-2163.
13. Wang, C.-G.; Goto, A. *J. Am. Chem. Soc.* **2017,** *139*, 10551-10560.
14. Wang, C.-G.; Hanindita, F.; Goto, A. *ACS Macro Lett.* **2018,** *7*, 263-268.
15. Ohtsuki, A.; Goto, A.; Kaji, H. *Macromolecules* **2013,** *46*, 96-102.
16. Ohtsuki, A.; Lei, L.; Tanishima, M.; Goto, A.; Kaji, H. *J. Am. Chem. Soc.* **2015,** *137*, 5610-5617.
17. Sarkar, J.; Xiao, L.; Goto, A. *Macromolecules* **2016,** *49*, 5033-5042.
18. Chen, C.; Wang, C.-G.; Xiao, L.; Goto, A. *Chem. Commun.* **2018,** *54*, 13738-13741.
19. Chen, C.; Xiao, L.; Goto, A. *Macromolecules* **2016,** *49*, 9425-9440.
20. Kume, M.; Hirano, A.; Ochiai, B.; Endo, T. *J. Polym. Sci. A Polym. Chem.* **2006**, *44*, 3666-3673.
21. Liu, L.; Chen, L.; Fang, Y. *Macromol. Rapid Commun.* **2006**, *27*, 1988-1994.
22. Liu, Z.; Wu, B.; Jiang Y.; Lei, J.; Zhou, C.; Zhang, J.; Wang, J. *Polymer* **2018**, *143*, 129-136.
23. Xu, J.; Shanmugam, S.; Boyer, C. *ACS Macro Lett.* **2015**, *4*, 926-932.
24. Zeng, G.; Liu, M.; Jiang, R.; Huang, Q.; Huang, L.; Wan, Q.; Dai, Y.; Wen, Y.; Zhang, X.; Wei, Y. *Mater. Sci. Eng.* **2018**, *83*, 154-159.
25. Blanazs, A.; Madsen, J.; Battaglia, G.; Ryan, A. J.; Armes, S. P. *J. Am. Chem. Soc.* **2011**, *133*, 16581-16587.
26. Warren, N. J.; Armes, S. P. *J. Am. Chem. Soc.* **2014**, *136*, 10174– 10185.
27. Cunningham, V. J.; Alswieleh, A. M.; Thompson, K. L.; Williams, M.; Leggett, G. J.; Armes, S. P.; Musa, O. M. *Macromolecules* **2014**, *47*, 5613– 5623.
28. Derry, M. J.; Fielding, L. A.; Armes, S. P. *Polym. Chem.* **2015**, *6*, 3054– 3062.

29. Blanazs, A.; Madsen, J.; Battaglia, G.; Ryan, A. J.; Armes, S. P. *J. Am. Chem. Soc.* **2011**, *133*, 16581– 16587.
30. Chaduc, I.; Girod, M.; Antoine, R.; Charleux, B.; D'Agosto, F.; Lansalot, M. *Macromolecules* **2012**, *45*, 5881– 5893.
31. Rikkou-Kalourkoti, M.; Loizou, E.; Porcar, L.; Matyjaszewskic, K.; Patrickios, C. S. *Polym. Chem.* **2012**, *3*, 105-116.
32. Luo, K.; Yang, J.; Kopečková, P.; Kopeček, J. *Macromolecules* **2011**, *44*, 2481-2488.
33. Wiltshire, J. T.; Qiao, G. G. *Macromolecules* **2006**, *39*, 9018-9027.
34. Tardy, A.; Nicolas, J.; Gigmes, D.; Lefay, C.; Guillaneuf, Y. *Chem. Rev.* **2017**, *117*, 1319-1406.
35. Pesenti, T.; Nicolas, J. *ACS Macro Lett.* **2020**, *9*, 1812-1835.
36. Mothe, S. R.; Tan, J. S. J.; Chennamaneni, L. R.; Aidil, F.; Su, Y.; Kang, H. C.; Lim, F. C. H.; Thoniyot, P. *J Polym Sci.* **2020**, *58*, 1728-1738.
37. Bailey, W.J.; Ni, Z.; Wu, S.R. *J. Polym. Sci., Part A: Polym. Chem.* **1982**, *20*, 3021-3030.
38. Bailey, W.J.; Ni, Z.; Wu, S.R. *Macromolecules* **1982**, *15*, 711-714.
39. Sustainable Chemistry. https://www.oecd.org/chemicalsafety/risk-management/sustainablechemistry.htm (accessed on 2 Jan 2022).

## Chapter 2. Self-catalyzed Living Radical Polymerization Using Quaternary-Ammonium-Iodide-Containing Monomers


### Abstract

Self-catalyzed living radical polymerization using quaternary ammonium iodide (QAI)-containing monomers is reported. The monomer contains a polymerizable methacrylate or acrylate moiety and QAI as a catalytic moiety at the side chain. Several (functional) methacrylates and acrylates were successfully copolymerized with QAI-containing monomers without additional catalysts, generating QAI-containing copolymers. This technique is attractive for its wide range of amenable monomers and metal-free nature. The obtained QAI-containing polymers may find biomedical and antibacterial applications.

## 2.1 Introduction

Self-catalysis is a unique process in which a reactant carries a reacting group and also a catalytic group to trigger a reaction.[1–4] The reactant is self-catalyzed to convert to the product without need for additional catalysts. Self-catalysis offers simple purification processes (no need for the catalyst removal), which is advantageous in practical applications.

Living radical polymerization (LRP), also known as reversible-deactivation radical polymerization, is widely used for synthesizing well-defined polymers with controlled molecular weights and narrow molecular weight distributions.[5–8] Our research group has developed an organocatalyzed LRP using an alkyl iodide (R−I) as an initiator (Scheme 2.1).[9–15] The catalysts include an iodide anion ($I^-$),[11–13] and $I^-$ is used in the form of quaternary ammonium iodide (QAI) such as tetrabutylammonium iodide ($Bu_4N^+I^-$). Mechanistically, the polymer−iodide dormant species (polymer−I) coordinates the catalyst (I−) via halogen bonding to form a complex (polymer−I···catalyst). The complex reversibly generates a propagating radical (Polymer•). We termed this polymerization reversible complexation mediated polymerization (RCMP).[10,11] The use of nonspecial capping agents and nonmetal catalysts are attractive features of RCMP.

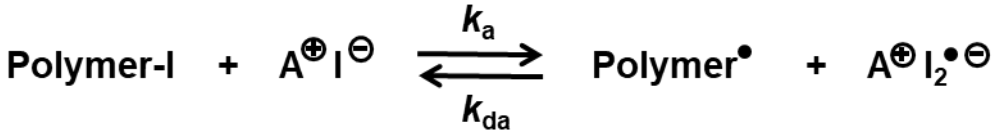


**Scheme 2.1.** Reversible activation in RCMP.

In material chemistry, polymers possessing quaternary ammonium halides such as QAI at the side chains are widely used for functional materials due to their hydrophilic, antifouling, and antibacterial properties.[16–19] Their structures such as block, comb-shaped, and brush have successfully been controlled via LRP.[20–25] In many cases, polymers containing tertiary amino

groups are first prepared by LRP and the subsequent quaternization using alkyl halides generates polymers with quaternary ammonium halides.[20,21] Despite the successful synthesis, the removal of metallic catalysts or odorous capping agents and the time-consuming postquaternization may pose possible issues in further applications.

In this chapter, self-catalyzed RCMP using QAI-containing monomers (Figure 2.1) was reported. The monomer contains a polymerizable methacrylate or acrylate moiety and also QAI as a catalytic moiety, offering self-catalyzed RCMP. The monomer is termed as catalytic monomer (CM) in this chapter. The QAI-containing monomers contain the catalytic QAI group that works as a catalyst in RCMP. The iodide of the QAI group coordinates the polymer-iodide dormant via halogen bonding, the polymer iodide bond is weakened, forming active polymer radical and iodine-catalyst complex. Therefore, the QAI-containing monomers control the polymerization and thus improving the dispersity of the polymers. The self-catalyzed RCMP directly yields QAI-containing polymers without postquaternization. The QAI-containing polymers also helps to control polymerization. Self-catalysis was used in other polymerizations (ring-opening polymerizations) and polymer degradation.[26–28] In the field of LRP, self-photocatalytic initiators (not catalytic "monomers") were successfully used.[29,30] In the present work, we report the first use of CMs for self-catalyzed LRP.

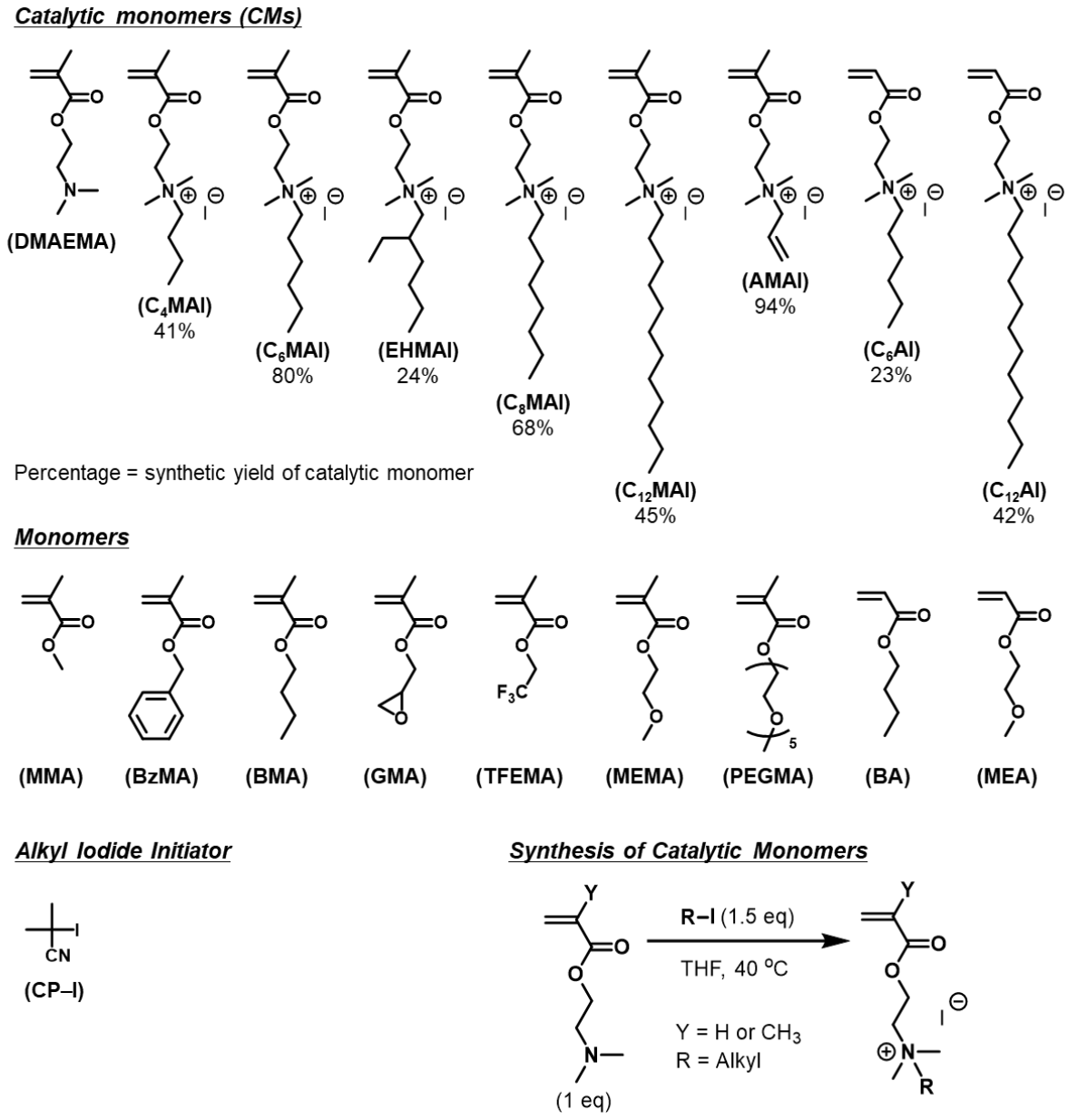


**Figure 2.1.** Structures of catalytic monomers (CMs), monomers, and alkyl iodide used in this work and the synthesis of catalytic monomers.

## 2.2 Results and Discussion

### Synthesis of Catalytic Monomers (CMs) Containing Quaternary Ammonium Iodide (QAI).

The QAI-containing catalytic monomers (Figure 2.1) were synthesized via the Menshutkin reaction in high yields (up to 94%) in a simple manner. 2,2-(Dimethylamino)ethyl methacrylate (DMAEMA) (1 equiv.) or 2,2-(dimethylamino)ethyl acrylate (DMAEA) (1 equiv.) was reacted with an alkyl iodide (1.5 equiv.) in tetrahydrofuran (THF) at 40 °C for 24 h to generate the corresponding CM. Several CMs with different alkyl chains (Figure 2.1) were synthesized for tuning the solubility of CMs in monomers and solvents. The structures and abbreviations of the studied CMs are given in Figure 2.1. A 90 g scale synthesis of $C_6$MAI (Figure 2.1) was achieved using DMAEMA and hexyl iodide ($C_6H_{13}$−I), for example (Figure 2.4). The purification was simple; namely, the solid $C_6$MAI was rinsed with cold THF, giving an 80% yield after purification in the mentioned 90 g synthesis. The use of 1.1 equiv. of hexyl iodide gave a lower yield (57%) than that of 1.5 equiv. (yield = 80%). The scalable synthesis and facile purification are beneficial for practical use.

### Self-Catalyzed RCMP of Methyl Methacrylate (MMA) and $C_6$MAI.

We carried out self-catalyzed RCMP using methyl methacrylate (MMA) as a main monomer and $C_6$MAI as a comonomer with different ratios of $[MMA]_0/[C_6MAI]_0$ ranging from 99/1 to 75/25 (Table 2.1, entries 1−4). We heated a mixture of the two monomers (100 equiv. in total) and a 2-iodo-2-methylpropionitrile (CP−I (Figure 2.1)) initiator (1 equiv.) at 70 °C. The QAI moiety of $C_6$MAI plays a catalytic role to generate propagating radicals from CP−I and polymer−I. Ethylene carbonate (EC) was used as a solvent to dissolve $C_6$MAI for the high $C_6$MAI-content systems ($[MMA]_0/[C_6MAI]_0$ = 90/10 and 75/25).

**Table 2.1.** Self-catalyzed RCMP of methacrylates and acrylates with catalytic monomers.

| Entry | M[a] | CM[b] | Solvent[c] | $[M]_0/[CM]_0/[CP-I]_0$ | $T$ (°C) | $t$ (h) | Conv (M/CM, %)[d] | $M_n$[e] ($M_{n,theo}$[f]) | $Đ$[e] |
|---|---|---|---|---|---|---|---|---|---|
| 1 | MMA | $C_6$MAI | none | 7920/80/80 | 70 | 12 | 62/59 | 7800 (6400) | 1.28 |
| 2 | MMA | $C_6$MAI | none | 7800/200/80 | 70 | 8 | 72/76 | 11000 (7300) | 1.29 |
| 3 | MMA | $C_6$MAI | EC | 7200/800/80 | 70 | 4 | 69/68 | 8800 (8700) | 1.34 |
| 4 | MMA | $C_6$MAI | EC | 6000/2000/80 | 70 | 3 | 66/89 | 8700 (7500) | 1.24 |
| 5 | none | $C_6$MAI | EC | 0/8000/80 | 80 | 8 | −/73 | NA[g] (27000) | NA[g] |
| 6 | MMA | DMAEMA | none | 7200/800/80 | 70 | 12 | 64/59 | 6700 (6700) | 1.46 |
| 7 | MMA | $C_4$MAI | EC | 7200/800/80 | 70 | 8 | 61/95 | 5500 (8700) | 1.26 |
| 8 | MMA | $C_8$MAI | EC | 7200/800/80 | 70 | 8 | 60/93 | 8300 (9700) | 1.25 |
| 9 | MMA | EHMAI | EC | 7200/800/80 | 70 | 7 | 81/81 | 8000 (11000) | 1.28 |
| 10 | MMA | $C_{12}$MAI | EC | 7200/800/80 | 70 | 6 | 70/66 | 6300 (11000) | 1.33 |
| 11 | MMA | AMAI | EC | 7200/800/80 | 70 | 8 | 37/37 | 5300 (4500) | 1.19 |
| 12 | BMA | $C_6$MAI | EC | 7200/800/80 | 70 | 10 | 51/55 | 8000 (8600) | 1.39 |
| 13 | GMA | $C_6$MAI | EC | 7200/800/80 | 70 | 4 | 82/55 | 16000 (13000) | 1.35 |
| 14 | BzMA | $C_6$MAI | EC | 7200/800/80 | 70 | 8 | 70/69 | 18000 (14000) | 1.37 |
| 15 | MEMA | $C_6$MAI | none | 7200/800/80 | 70 | 7 | 52/57 | 6500 (7900) | 1.32 |
| 16 | PEGMA | $C_6$MAI | none | 7200/800/80[h] | 60 | 10 | 56/98 | 9900 (10000) | 1.40 |
| 17 | DMAEMA | $C_6$MAI | none | 7200/800/80[i] | 50 | 3 | 93/94 | 12000 (16000) | 1.39 |
| 18 | BA | $C_{12}$AI | none | 7200/800/80[j] | 110 | 48 | 40/60 | 8300 (7400) | 1.17 |
| 19 | MEA | $C_6$AI | none | 7200/800/80 | 110 | 24 | 66/72 | 8100 (10000) | 1.18 |
| 20[k] | MMA | $C_6$MAI | EC | 7200/800/8 | 60 | 8 | 19/15 | 20000 (25000) | 1.27 |

[a]Main monomer. [b]Catalytic monomer. The structures and abbreviations are given in Figure 2.1 [c] EC means dilution with 25wt% ethylene carbonate (EC). [d]$^1$H NMR calculated monomer conversion. [e]PMMA-calibrated THF-GPC values for entries 1−3, 7−15, 18, and 19. PMMA-calibrated DMF-GPC values for entries 4, 6, 16, 17, and 20. [f]Theoretical $M_n$ calculated with $[M]_0$, $[CM]_0$, $[CP-I]_0$, and monomer conversion. [g]The polymer tended to be adsorbed on columns in THF and DMF eluents and was not able to analyze with GPC. [h]Addition of V65 (160 mM). [i]Addition of V65 (40 mM). [j]Addition of $I_2$ (5 mM).

Figure 2.2a shows the time evolution of the conversions of MMA (squares) and $C_6$MAI (triangles) for $[MMA]_0/[C_6MAI]_0$ = 90/10 (Table 2.1, entry 3). The rate of the monomer consumption was very similar for MMA (monomer 1) and $C_6$MAI (monomer 2), meaning that the reactivity ratios ($r_1$ and $r_2$) are nearly 1. The nearly unity reactivity ratios are reasonable because both monomers are methacrylates (the same type of monomer). The polymerization was relatively fast; the total monomer conversion reached 69% for 4 h. The number-average molecular weight ($M_n$) well matched with the theoretical value, and the dispersity ($Đ = M_w/M_n$) was low (1.17−1.34) from an early stage of polymerization (Figure 2.2b), where $M_w$ is the weight-average molecular weight. This result shows a good catalytic activity of $C_6$MAI.

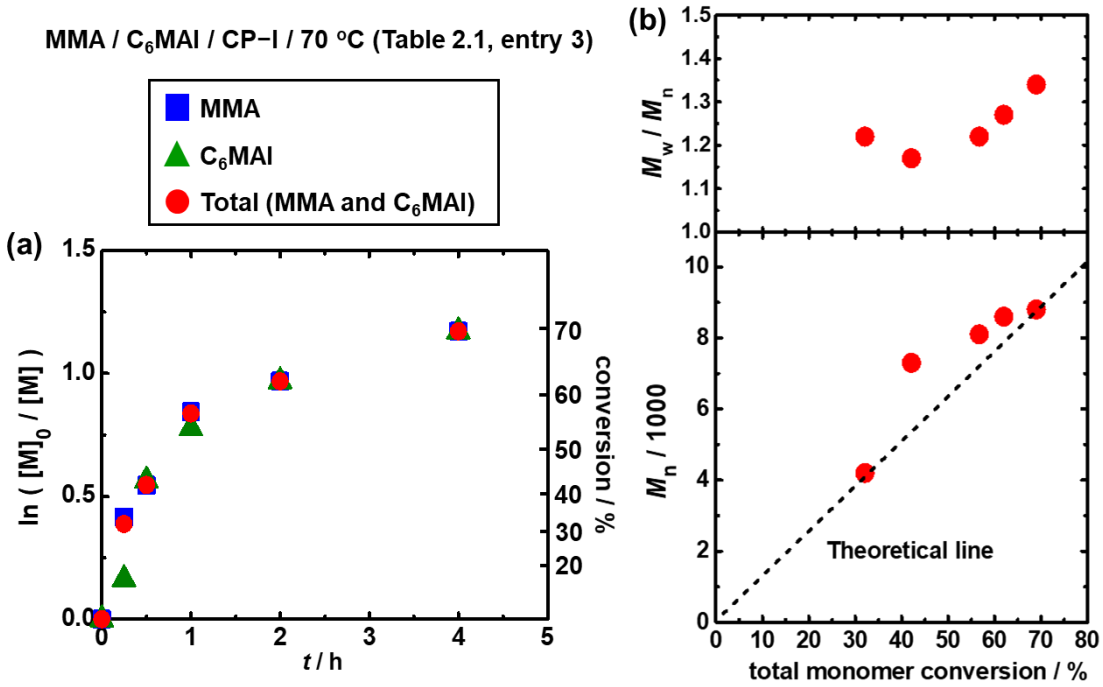


**Figure 2.2.** Plots of (a) $\ln([M]_0/[M])$ *vs.* $t$ and (b) $M_n$ and $M_w/M_n$ *vs.* conversion for the MMA/CP−I/$C_6$MAI system (70 °C): $[MMA]_0$ = 7200 mM; $[CP-I]_0$ = 80 mM; $[C_6MAI]_0$ = 800 mM. The $M_n$ and $M_w/M_n$ values are obtained by PMMA-calibrated GPC. The symbols are indicated in the Figure.

Figure 2.3 shows the $^1$H NMR spectrum of the random copolymer (PMMA-*r*-P$C_6$MAI) obtained at 4 h ($M_n$ = 8800 and $Đ$ = 1.34) after purification. The methyl (*d* in Figure 2.3) and methylene (*c* and *e*) protons of the quaternary amino group in the $C_6$MAI unit clearly appeared at 3.53 ppm (*d*), 3.73 ppm (*e*), and 4.15 ppm (*c*), showing the existence of $C_6$MAI moieties in the copolymer. From the peak areas of the methyl proton (*a*) in the MMA unit and the ethylene proton (*c*) in the $C_6$MAI unit, the polymer composition (MMA/$C_6$MAI) was calculated to be 92/8, which matched the feed monomer composition (90/10) and the nearly unity reactivity ratio. This result means that the fraction of $C_6$MAI in the copolymer can be manipulated in a predictable manner by simply tuning the feed MMA/$C_6$MAI monomer ratio. Thus, the self-catalyzed RCMP using a QAI-containing monomer offers a facile access for preparing well-defined QAI-containing polymers.

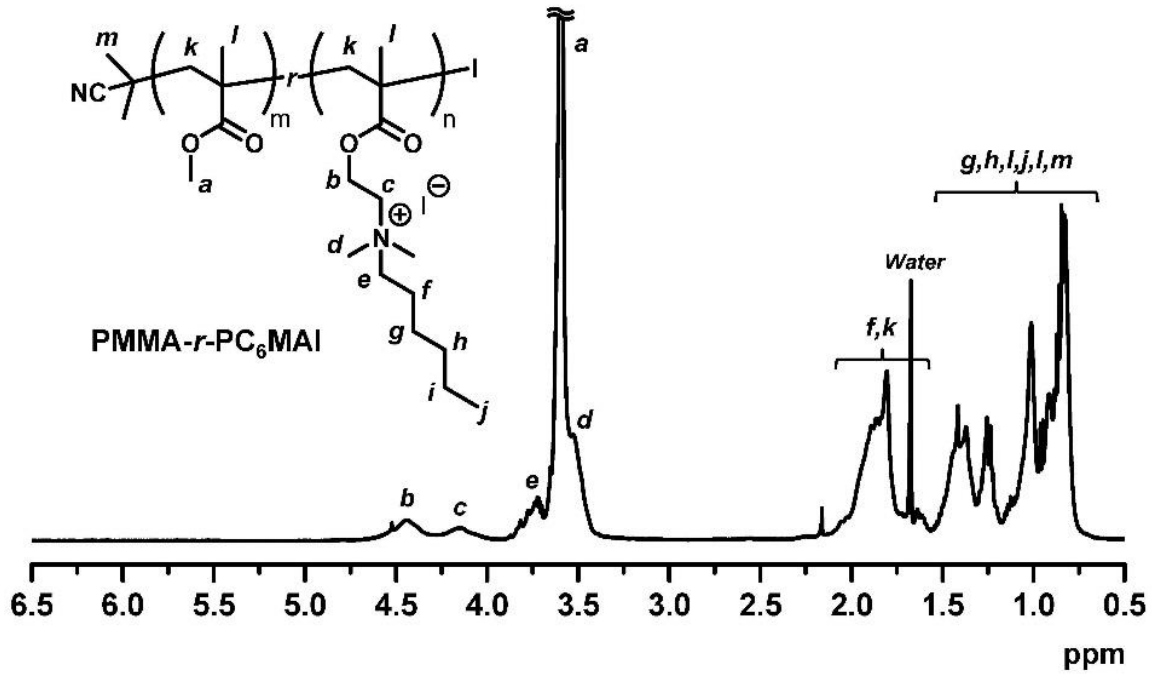


**Figure 2.3.** $^1$H NMR spectrum of PMMA-*r*-P$C_6$MAI (Table 2.1, entry 3) after purification (400 MHz, 298 K, $CDCl_3$).

With an increase in the $C_6$MAI fraction (ranging the $[MMA]_0/[C_6MAI]_0$ ratio from 99/1 to 75/25) (Table 2.1, entries 1−4), the polymerization rate reasonably increased because of the higher catalyst ($C_6$MAI) concentration. The total monomer conversion reached 72% for a short time of 3 h for $[MMA]_0/C_6MAI]_0$ = 75/25 (Table 2.1, entry 4). The homopolymerization of $C_6$MAI was also performed at 80 °C for 8 h to give $PC_6$MAI with 73% monomer conversion (Table 2.1, entry 5 and Figure 2.29). We increased the temperature from 70 ℃ to 80 ℃ to fully dissolve $C_6$MAI monomer. However, the obtained polymer was not able to analyze with gel permeation chromatography (GPC) because the polymer tended to be adsorbed on the GPC columns. Nonquaternized DMAEMA (Figure 2.1) with a tertiary amine also served as a CM to copolymerize with MMA (Table 2.1, entry 6). Tertiary amines are known to work as moderately efficient RCMP catalysts.[10] However, compared with QAI-containing $C_6$MAI (Table 2.1, entry 3), DMAEMA provided a 3 times slower polymerization (64% total monomer conversion for 12 h) and a higher $Đ$ value (1.46) because of the lower catalytic activity.

**Polymerization of MMA and Other CMs.**

Besides $C_6$MAI, CMs possessing different alkyl chains (Figure 2.1), i.e., butyl ($C_4$MAI), 2-ethylhexyl (EHMAI), octyl ($C_8$MAI), dodecyl ($C_{12}$MAI), and allyl (AMAI) chains, were effective for the MMA polymerizations (Table 2.1, entries 7−11), yielding low-dispersity polymers ($Đ$ = approximately 1.3). The use of AMAI successfully provided functional allyl groups in the copolymer chain (Table 2.1, entry 11 and Figure 2.30). The suppression of chain transfer to ally group is due to the steric hindrance of neighboring vinyl group and quaternary ammonium alkyl iodide group. We also observed that the length of alkyl chains largely affected the hydrophobicity of QAI-containing polymers. Whereas PMMA-*r*-$PC_6$MAI ($M_n$ = 8800 and $Đ$ = 1.34, Table 2.1, entry 3) (5.0 wt %) was dissolved in an acetone/water (40/60) mixture, PMMA-*r*-$PC_{12}$MAI with a longer alkyl chain ($M_n$ = 6300 and $Đ$ = 1.33, Table 2.1, entry 10)

(5.0 wt %) was precipitated even in a more acetone-containing mixture (acetone/water = 46/54). This observation demonstrates that the hydrophobicity of QAI-containing polymers is tunable through the side chains in CMs. The facile synthesis and functionalization of CMs are highly beneficial for practical use and design of functional polymers.

**Polymerization of Functional Methacrylates and Acrylates.**

QAI-containing monomers were compatible with various functional methacrylates and acrylates (Figure 2.1). The polymerization results of butyl methacrylate (BMA), glycidyl methacrylate (GMA), benzyl methacrylate (BzMA), 2-methoxyethyl methacrylate (MEMA), poly(ethylene glycol) methyl ether methacrylate (PEGMA), and 2-(dimethylamino)-ethyl methacrylate (DMAEMA) with $C_6$MAI are summarized in Table 2.1 (entries 12−17). QAI-containing copolymers with low-dispersity ($Đ \leqslant 1.40$) were successfully synthesized. The relatively slow polymerization of BMA could be attributed to the low solubility of $C_6$MAI in the highly hydrophobic BMA (Table 2.1, entry 12). Whereas 70 °C was used for hydrophobic monomers (Table 2.1, entries 1−4 and 6−15), a milder temperature (50−60 °C) was used for hydrophilic PEGMA and DMAEMA monomers to suppress a side reaction (elimination of HI from the polymer chain end to generate a dead polymer, which is enhanced in polar media) (Table 2.1, entries 16 and 17). In the two systems, an azo initiator (2,2′-azobis(2,4-dimethyl-valeronitrile) (V65)) was added to increase the polymerization rate. Azo initiators are often used to decrease the deactivator concentration and hence increase the polymerization rate in RCMP and other LRP systems.[31]

Table 2.1 (entries 18 and 19) shows the polymerizations of acrylates. Two QAI-containing acrylates, i.e., $C_{12}$AI and $C_6$AI (Figure 2.1), were used to polymerize butyl acrylate (BA) and 2-methoxyethyl acrylate (MEA) (Figure 2.1), respectively, yielding low-dispersity polymers ($Đ$ = 1.17−1.18). ($C_{12}$AI exhibited a good solubility in the hydrophobic BA.) RCMP

of acrylates requires highly active catalysts because of the stronger secondary alkyl C−I bond in an acrylate polymer than the tertiary alkyl C−I bond in a methacrylate polymer. The successful polymerizations of the acrylates demonstrate the high catalytic activities of the QAI-containing monomers.

Quaternary ammonium halide-containing polymers are of great interest in antibacterial applications. The introduction of QAI in the biocompatible polymers, i.e., MEMA, PEGMA, and MEA polymers, can significantly increase their antibacterial properties.[32,33] The self-catalyzed RCMP is a metal-free, odor free, and straightforward synthetic route for QAI-containing copolymers with quantitative quaternization. The technique does not require postquaternization or time-consuming removal of unreacted quaternizing agents from the polymers.

## 2.3 Conclusions

Self-catalyzed RCMP using QAI-containing CMs was developed. QAI-containing CMs are easy to synthesize, which is attractive for large-scale use. The amenable monomers encompassed MMA, BA, and several functional methacrylates and acrylates. The system does not require additional catalysts and generates QAI-containing polymers without postquaternization. The high versatility in amenable monomers and CMs and the metal-free nature are beneficial aspects, and the obtained polymers may find biomedical and antibacterial applications.

## 2.4 Experimental Section

### Materials.

Methyl methacrylate (MMA) (>99.8%, Tokyo Chemical Industry (TCI)), 2-(dimethylamino)ethyl methacrylate (DMAEMA) (≥98.5%, TCI), 2-(dimethylamino)ethyl acrylate (DMAEA) (≥98%, TCI), 2-methoxyethyl methacrylate (MEMA) (≥98%, TCI), poly(ethylene glycol) methyl ether methacrylate (PEGMA) (average molecular weight = 300) (98%, Sigma-Aldrich, USA), butyl acrylate (BA) (>99%, TCI), 2-methoxyethyl acrylate (MEA) (>98%, TCI), benzyl methacrylate (BzMA) (>98%, TCI), and 2,2,2-trifluoroethyl methacrylate (TFEMA) (99%, Sigma-Aldrich) were purified through an alumina column. 2-Iodo-2-methylpropionitrile (CP−I) (>95%, TCI), 1-iodobutane (99%, Sigma-Aldrich), 1-iodohexane (≥98%, Sigma-Aldrich), 1-iodooctane (98%, Sigma-Aldrich), 1-iododododecane (98%, Sigma-Aldrich), 2-ethylhexyl iodide (97%, Sigma-Aldrich), allyl iodide (98%, Sigma-Aldrich), 2,2'-azobis(2,4-dimethylvaleronitrile) (V65) (95%, Wako Pure Chemical, Japan), ethylene carbonate (EC, >99%, TCI), diethylene glycol dimethyl ether (diglyme, >99%, TCI), isopropyl alcohol (>99.5%, TCI), ammonia solution (28% in water, TCI), acetone (≥99.5%, Fisher Scientific, USA), chloroform (>99.2%, VWR Chemicals, USA), ethanol (≥99.5%, absolute, Fisher Scientific), tetrahydrofuran (THF) (>99.5%, Kanto Chemical, Japan), *N*,*N*-dimethylformamide (DMF) (>99.5%, Kanto), diethyl ether (ACS reagent grade, VWR International), and hexane (>99%, International Scientific, Singapore) were used as received.

### Measurements.

The THF-GPC analysis was performed on a Shimadzu i-Series Plus liquid chromatograph LC-2030c Plus (Kyoto, Japan) equipped with two Shodex KF-804L mixed gel columns (300 × 8.0 mm; bead size = 7 $\mu$m; pore size = 20–200 Å). The DMF-GPC analysis

was performed on a Shodex GPC-101 liquid chromatograph (Tokyo, Japan) equipped with two Shodex KF-804L mixed gel columns. The flow rate was 0.7 mL/min (THF) and 0.8 mL/min (DMF). The DMF eluent included LiBr (10 mM). The sample detection was conducted using a refractive index detector (RID-20A) for THF-GPC and a Shodex differential refractometer RI-101 for DMF-GPC. The column system was calibrated with standard poly(methyl methacrylate)s (PMMAs) for both THF-GPC and DMF-GPC systems.

The NMR spectra were recorded on Bruker (Germany) AV500 spectrometer (500 MHz), BBFO400 spectrometer (400 MHz), or AV 300 (300 MHz) at ambient temperature. $CDCl_3$ and acetone-$d_6$ (Cambridge Isotope Laboratories, USA) were used as the solvents for the NMR analysis, and the chemical shift was calibrated using residual undeuterated solvents or tetramethylsilane (TMS) as the internal standard. The monomer conversion and the monomer composition in the obtained polymer were determined with $^1$H NMR. The mass spectra were obtained with a Q-Tof Premier (Waters, USA) high-resolution liquid chromatography mass spectrometer (HRLC-MS). The IR spectra were recorded on a Bruker ALPHA FTIR spectrometer with KBr (spectroscopic grade, Sigma-Aldrich, USA) as a matrix.

**General Procedure for the Synthesis of Quaternary Ammonium Iodide (QAI)-Containing Monomer.**

In a typical run, a mixture of DMAEMA (50.0 g, 0.32 mol) and hexyl iodide (100 g, 0.47 mol) in THF (300 mL) was heated at 40 °C with magnetic stirring under argon atmosphere to avoid moisture. After 24 h, the reaction solution was cooled in an ice bath. The generated precipitate was filtered and washed with cold THF. The solid was collected and dried in vacuum to give **$C_6$MAI** (93.3 g, 0.26 mol) in an 80% yield as a white solid. Other QAI-containing monomers were also synthesized similarly. For **EHMAI,** the reaction solution was

evaporated to produce insoluble solid. The solid was washed with diethyl ether for several times to remove unreacted starting materials, yielding **EHMAI** as a light orange solid. For **AMAI**, a mixture of DMAEMA (5.0 g, 32 mmol) and allyl iodide (8.01 g, 48 mol) in THF (20 mL) was heat at 40 °C with magnetic stirring under argon atmosphere for 12 h, yielding **AMAI** as a red solid. For synthesizing **$C_6$AI** and **$C_{12}$AI**, DMAEA was used instead of DMAEMA.

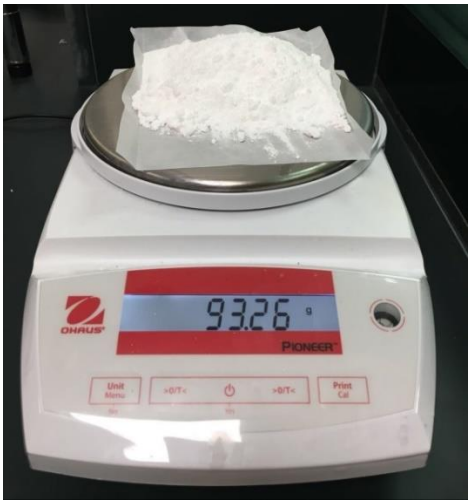


**Figure 2.4.** Image of 90-gram synthesis of $C_6$MAI.

**$C_4$MAI**: Yield: 41%. $^1$H NMR (400 MHz, 298 K, $CDCl_3$) $\delta$ 6.15 (s, 1H, –C=C$\underline{H}_2$), 5.67 (s, 1H, –C=C$\underline{H}_2$), 4.66 (m, 2H, –COC$\underline{H}_2$CH$_2$–), 4.13 (m, 2H, –COCH$_2$C$\underline{H}_2$–), 3.68 (t, $J$ = 8.0 Hz, 2H, –N$^+$C$\underline{H}_2$–), 3.49 (s, 6H, – N$^+$(C$\underline{H}_3$)$_2$), 1.95 (s, 3H, CH$_2$=CC$\underline{H}_3$), 1.78 (quintet, $J$ = 8.0 Hz, 2H, –N$^+$CH$_2$C$\underline{H}_2$–), 1.43 (*sextet*, $J$ = 4.0 Hz, 2H, –N$^+$(CH$_2$)$_2$C$\underline{H}_2$–), 1.00 (t, $J$ = 4 Hz, 3H, –C$\underline{H}_3$) ppm; $^{13}$C NMR (100 MHz, 298 K, $CDCl_3$) $\delta$ 166.3, 135.1, 127.5, 65.6, 62.6, 58.2, 52.2, 24.8, 19.5, 18.3, 13.7 ppm. IR (KBr) $\upsilon$ 1719 (C=O), 1636 (C=C), 1168 (C–O) cm$^{-1}$. HRLC-MS (*m/z*): calcd for $C_{12}H_{24}NO_2^+$ [M–I$^-$]$^+$, 214.1807; found, 214.1807.

**$C_6$MAI**: $^1$H NMR (400 MHz, 298 K, $CDCl_3$) $\delta$ 6.13 (s, 1H, –C=C$\underline{H_2}$), 5.65 (s, 1H, –C=C$\underline{H_2}$), 4.64 (m, 2H, –COC$\underline{H_2}$CH$_2$–), 4.12 (m, 2H, –COCH$_2$C$\underline{H_2}$–), 3.64 (t, $J$ = 6.92 Hz, –N$^+$C$\underline{H_2}$–), 3.47 (s, 6H, – N$^+$(C$\underline{H_3}$)$_2$), 1.92 (s, 3H, CH$_2$=CC$\underline{H_3}$), 1.76 (quintet, $J$ = 6.92 Hz, 2H, –N$^+$CH$_2$C$\underline{H_2}$–), 1.31 (m, 6H, –N$^+$CH$_2$CH$_2$(C$\underline{H_2}$)$_3$–), 0.85 (t, $J$ = 6.92 Hz, –C$\underline{H_3}$) ppm; $^{13}$C NMR (100 MHz, 298 K, $CDCl_3$) $\delta$ 166.3, 135.1, 127.5, 65.8, 62.6, 58.1, 52.2, 31.2, 25.8, 22.9, 22.4, 18.3, 13.9 ppm. IR (KBr) $\upsilon$ 1729 (C=O), 1637 (C=C), 1167 (C–O) cm$^{-1}$. HRLC-MS (*m/z*): calcd for $C_{14}H_{28}NO_2^+$ [M–I$^-$]$^+$, 242.2122; found, 242.2120.

**EHMAI**: Yield: 24%. $^1$H NMR (300 MHz, 298 K, $CDCl_3$) $\delta$ 6.18 (s, 1H, –C=C$\underline{H_2}$), 5.69 (s, 1H, –C=C$\underline{H_2}$), 4.69 (m, 2H, –COC$\underline{H_2}$CH$_2$–), 4.24 (m, 2H, –COCH$_2$C$\underline{H_2}$–), 3.60 (m, 2H, –N$^+$C$\underline{H_2}$–), 3.47 (s, 6H, – N$^+$(C$\underline{H_3}$)$_2$), 1.96 (s, 3H, CH$_2$=CC$\underline{H_3}$), 1.88 (m, 1H, –N$^+$CH$_2$C$\underline{H}$–), 1.80-1.19 (m, 8H, –N$^+$CH$_2$CH(C$\underline{H_2}$)$_4$–), 0.95 (t, $J$ = 7.50 Hz, –C$\underline{H_3}$), 0.92 (t, $J$ = 6.00 Hz, –N$^+$CH$_2$CHC$\underline{H_3}$) ppm; $^{13}$C NMR (100 MHz, 298 K, $CDCl_3$) $\delta$ 166.3, 135.1, 127.7, 70.7, 63.8, 58.0, 51.8, 34.3, 32.9, 28.3, 26.2, 22.8, 18.3, 14.0, 10.5 ppm. IR (KBr) $\upsilon$ 1722 (C=O), 1640 (C=C), 1167 (C–O) cm$^{-1}$. HRLC-MS (*m/z*): calcd for $C_{16}H_{32}NO_2^+$ [M–I$^-$]$^+$, 270.2433; found, 270.2439.

**$C_8$MAI**: Yield: 68%. $^1$H NMR (400 MHz, 298 K, $CDCl_3$) $\delta$ 6.09 (s, 1H, –C=C$\underline{H_2}$), 5.61 (s, 1H, –C=C$\underline{H_2}$), 4.61 (m, 2H, –COC$\underline{H_2}$CH$_2$–), 4.07 (m, 2H, –COCH$_2$C$\underline{H_2}$–), 3.60 (t, $J$ = 8.40 Hz, –N$^+$C$\underline{H_2}$–), 3.43 (s, 6H, – N$^+$(C$\underline{H_3}$)$_2$), 1.96 (s, 3H, CH$_2$=CC$\underline{H_3}$), 1.71 (quintet, $J$ = 6.80 Hz, 2H, –N$^+$CH$_2$C$\underline{H_2}$–), 1.30-1.19 (m, 10H, –N$^+$CH$_2$CH$_2$(C$\underline{H_2}$)$_5$–), 0.80 (t, $J$ = 6.40 Hz, –C$\underline{H_3}$) ppm; $^{13}$C NMR (100 MHz, 298 K, $CDCl_3$) $\delta$ 166.3, 135.1, 127.5, 65.8, 62.6, 58.1, 52.2, 31.6, 29.1, 29.0, 26.1, 23.0, 22.5, 18.3, 14.0 ppm. IR (KBr) $\upsilon$ 1718 (C=O), 1633 (C=C), 1160 (C–O) cm$^{-1}$. HRLC-MS (*m/z*): calcd for $C_{16}H_{32}NO_2^+$ [M–I$^-$]$^+$, 270.2433; found, 270.2439.

**$C_{12}$MAI**: Yield: 45%. $^1$H NMR (400 MHz, 298 K, $CDCl_3$) $\delta$ 6.16 (s, 1H, –C=C$\underline{H_2}$), 5.68 (t, $J$ = 1.6 Hz, 1H, –C=C$\underline{H_2}$), 4.66 (m, 2H, –COC$\underline{H_2}$CH$_2$–), 4.14 (m, 2H, –COCH$_2$C$\underline{H_2}$–), 3.63 (t, $J$ = 8.8 Hz, 2H, –N$^+$C$\underline{H_2}$–), 3.50 (s, 6H, –N$^+$(C$\underline{H_3}$)$_2$), 1.95 (s, 3H, CH$_2$=CC$\underline{H_3}$), 1.77 (quintet, $J$ = 8.8 Hz, 2H, –N$^+$CH$_2$C$\underline{H_2}$–), 1.36 (s, 4H, –N$^+$(CH$_2$)$_2$(C$\underline{H_2}$)$_2$–), 1.25 (s, 14H, –N$^+$(CH$_2$)$_4$(C$\underline{H_2}$)$_7$–), 0.87 (t, $J$ = 6.4 Hz, 3H, –C$\underline{H_3}$) ppm; $^{13}$C NMR (100 MHz, 298 K, $CDCl_3$) $\delta$ 166.4, 135.1, 127.6, 65.9, 62.6, 58.2, 52.3, 31.9, 29.6, 29.6, 29.5, 29.5, 29.4, 29.3, 26.2, 23.1, 22.7, 18.4, 14.2 ppm. IR (KBr) $\upsilon$ 1722 (C=O), 1637 (C=C), 1167 (C–O) cm$^{-1}$. HRLC-MS (*m/z*): calcd for $C_{20}H_{40}NO_2^+$ [M–I$^-$]$^+$, 326.3059; found, 326.3060.

**AMAI**: Yield: 94%.$^1$H NMR (400 MHz, 298 K, $CDCl_3$) $\delta$ 6.19–6.09 (m, 1H, H$_2$C=C$\underline{H}$), 6.17 (s, 1H, $\underline{H_2}$C=C–CH$_3$), 5.97 (d, 1H, $\underline{H_2}$C=CH, $J$ = 8.4 Hz), 5.81 (d, 1H, $\underline{H_2}$C=CH, $J$ = 8.4 Hz), 5.69 (s, 1H, $\underline{H_2}$C=C–CH$_3$), 4.71 (br, 2H, –COC$\underline{H_2}$CH$_2$–), 4.50 (d, 1H, H$_2$C=C$\underline{H}$, $J$ = 3.6 Hz), 4.13 (m, 2H, –COCH$_2$C$\underline{H_2}$–), 3.47 (s, 6H, –N$^+$(C$\underline{H_3}$)$_2$), 1.96 (s, 3H, CH$_2$=CC$\underline{H_3}$) ppm; $^{13}$C NMR (100 MHz, 298 K, $CDCl_3$) $\delta$ 165.7, 134.5, 130.2, 127.0, 123.6, 66.8, 61.9, 57.6, 50.9, 17.8 ppm. IR (KBr) $\upsilon$ 1719 (C=O), 1636 (C=C), 1178 (C–O) cm$^{-1}$. HRLC-MS (*m/z*): calcd for $C_{11}H_{20}NO_2^+$ [M–I$^-$]$^+$, 198.1494; found, 198.1499.

**$C_6$AI**: Yield: 23%. $^1$H NMR (500 MHz, 298 K, $CDCl_3$) $\delta$ 6.48 (d, $J$ =, 8.6 Hz, 1H, –C=C$\underline{H_2}$), 6.12 (dd, $J$ = 8.6, 5.3 Hz, 1H, –C=C$\underline{H_2}$), 5.95 (d, $J$ = 8.6 Hz, 1H, –CH$_2$=C$\underline{H}$–), 4.67 (m, 2H, –COC$\underline{H_2}$CH$_2$–), 4.12 (m, 2H, –COCH$_2$C$\underline{H_2}$–), 3.63 (t, $J$ = 8.8 Hz, 2H, –N$^+$C$\underline{H_2}$–), 3.49 (s, 6H, –N$^+$(C$\underline{H_3}$)$_2$), 1.77 (m, 2H, –N$^+$CH$_2$C$\underline{H_2}$–), 1.33 (m, 6H, –N$^+$(CH$_2$)$_2$(C$\underline{H_2}$)$_3$–), 0.88 (t, $J$ = 6.8 Hz, 3H, –C$\underline{H_3}$) ppm; $^{13}$C NMR (100 MHz, 298 K, $CDCl_3$) $\delta$ 165.1, 133.1, 127.1, 65.9, 62.5, 58.0, 52.3, 31.2, 25.8, 22.9, 22.4, 13.9 ppm. IR (KBr) $\upsilon$ 1729 (C=O), 1637 (C=C), 1186 (C–O) cm$^{-1}$. HRLC-MS (*m/z*): calcd for $C_{13}H_{26}NO_2^+$ [M–I$^-$]$^+$, 228.1964; found, 228.1961.

**$C_{12}$AI**: Yield: 42%. $^1$H NMR (400 MHz, 298 K, $CDCl_3$) $\delta$ 6.42 (d, $J$ = 8.6 Hz, 1H, –C=C$\underline{H_2}$), 6.12 (dd, $J$ = 8.6, 5.3 Hz, 1H, –C=C$\underline{H_2}$), 5.95 (d, $J$ = 8.6 Hz, 1H, –$CH_2$=C$\underline{H}$–), 4.67 (s, 2H, –COC$\underline{H_2}CH_2$–), 4.12 (s, 2H, –$COCH_2C\underline{H_2}$–), 3.63 (t, $J$ = 8.6 Hz, 2H, –$N^+C\underline{H_2}$–), 3.49 (s, 6H, –$N^+(C\underline{H_3})_2$), 1.77 (m, 2H, –$N^+CH_2C\underline{H_2}$–), 1.35 (s, 4H, –$N^+(CH_2)_2(C\underline{H_2})_2$–), 1.24 (s, 14H, –$N^+(CH_2)_4(C\underline{H_2})_7$–), 0.86 (t, $J$ = 7.0 Hz, 3H, –C$\underline{H_3}$) ppm; $^{13}$C NMR (100 MHz, 298 K, $CDCl_3$) $\delta$ 165.0, 133.0, 127.0, 65.8, 62.4, 57.9, 52.3, 31.8, 29.5, 29.5, 29.4, 29.3, 29.2, 29.2, 26.1, 22.9, 22.6, 14.0 ppm. IR (KBr) $\upsilon$ 1729 (C=O), 1633 (C=C), 1185 (C–O) $cm^{-1}$. HRLC-MS (*m/z*): calcd for $C_{19}H_{38}NO_2^+$ $[M–I^–]^+$, 312.2903; found, 312.2901.

**General Procedure for Polymerization.**

In a typical run, a mixture of a (main) monomer (1.5 g), a catalytic monomer, CP−I (alkyl iodide initiator), and ethylene carbonate (solvent, 25wt%) was heated in a Schlenk flask at 50–110 °C under argon atmosphere with magnetic stirring. After a prescribed time *t*, an aliquot (0.1 mL) of the solution was taken out by a syringe, quenched to room temperature, and analyzed with GPC and $^1$H NMR. At the last date point of the reaction, the polymer solution was diluted with acetone, and the polymer was reprecipitated in a mixture of hexane/ethanol (7/3 (v/v)) twice for purification. The collected polymer was dried in vacuo.

**Spectral Data.**

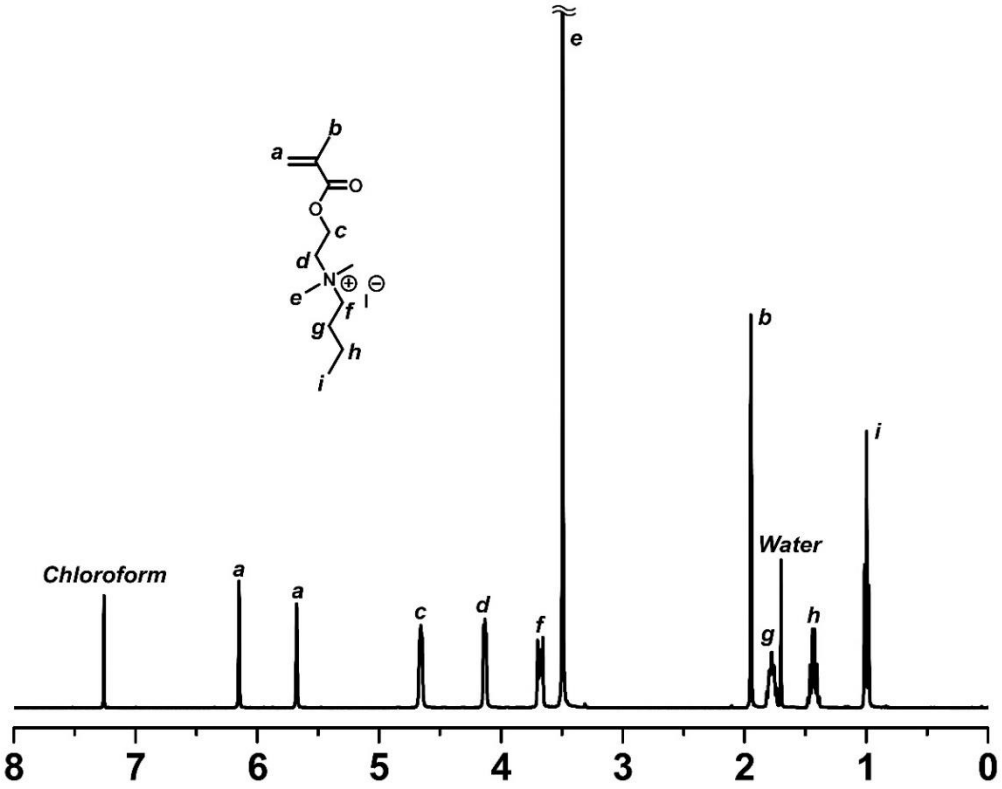


**Figure 2.5.** $^{1}H$ NMR spectrum of $C_4MAI$ (400 MHz, 298 K, $CDCl_3$).

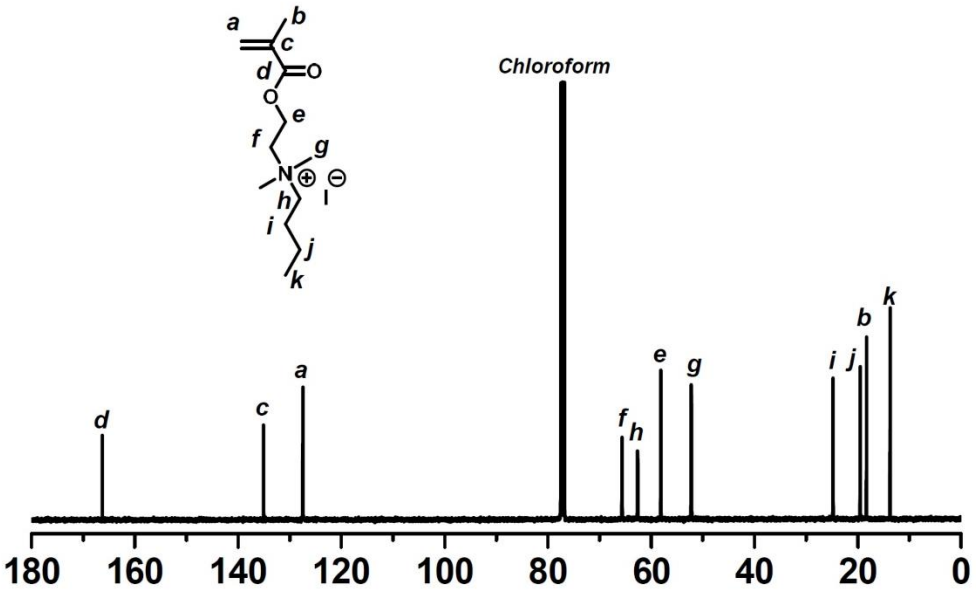


**Figure 2.6.** $^{13}C$ NMR spectrum of $C_4MAI$ (100 MHz, 298 K, $CDCl_3$).

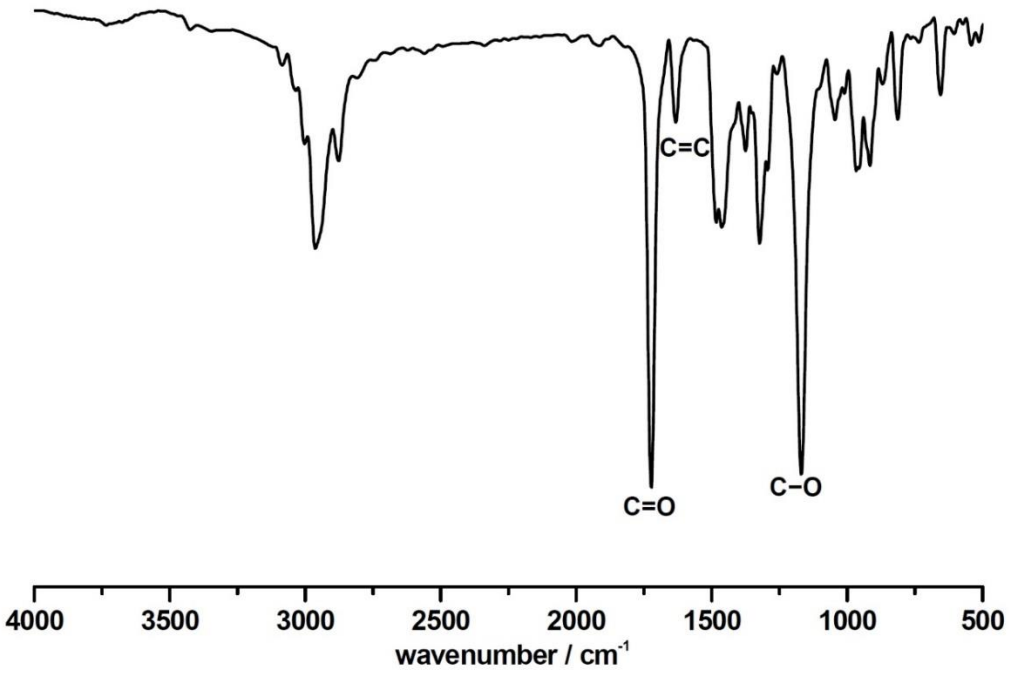


**Figure 2.7.** IR spectrum of $C_4$MAI (KBr).

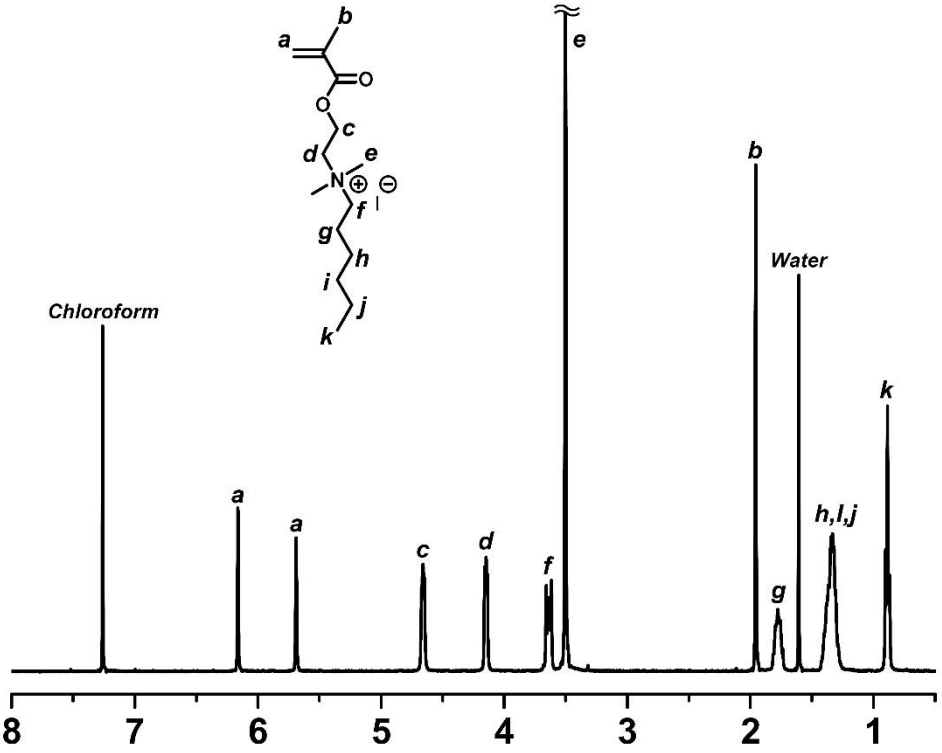


**Figure 2.8.** $^1$H NMR spectrum of $C_6$MAI (400 MHz, 298 K, $CDCl_3$).

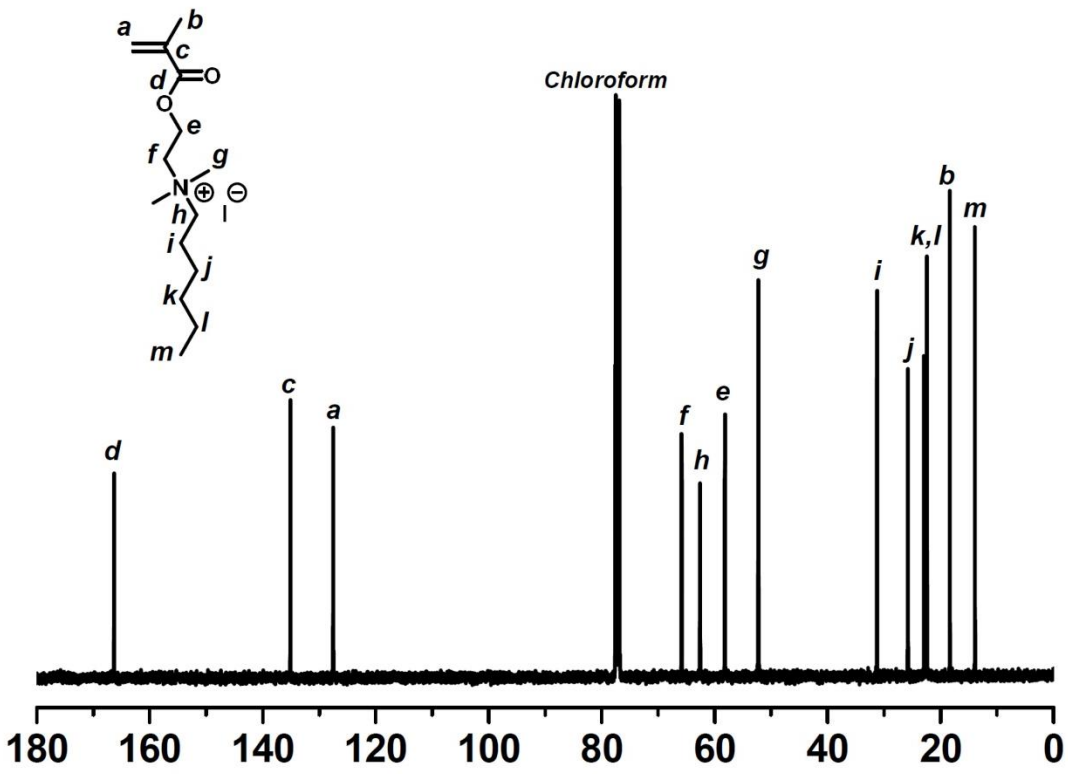


**Figure 2.9.** $^{13}C$ NMR spectrum of $C_6MAI$ (100 MHz, 298 K, $CDCl_3$).

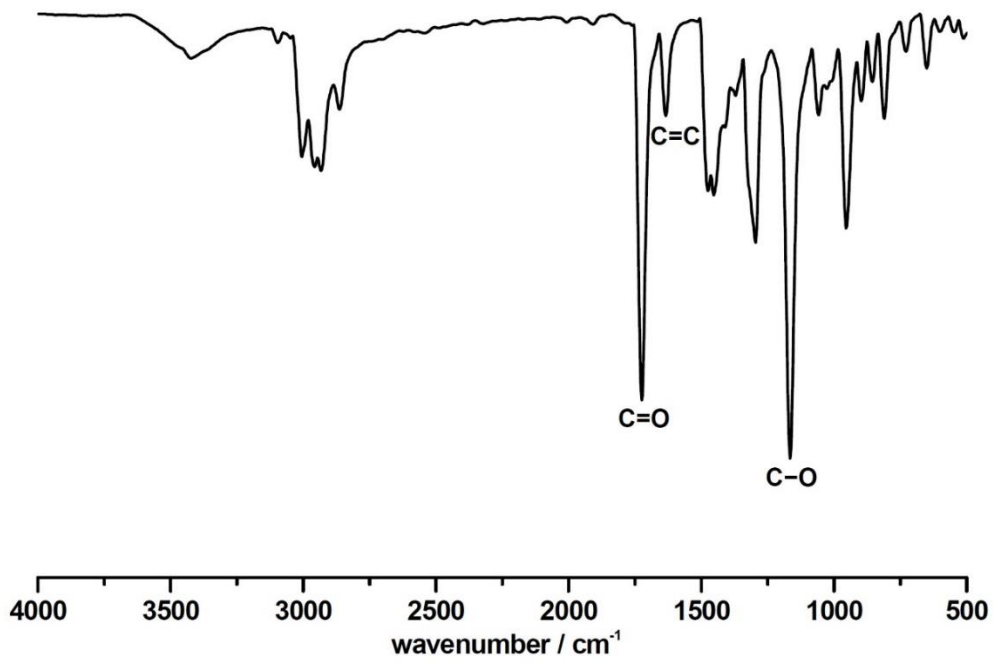


**Figure 2.10.** IR spectrum of $C_6MAI$ (KBr).

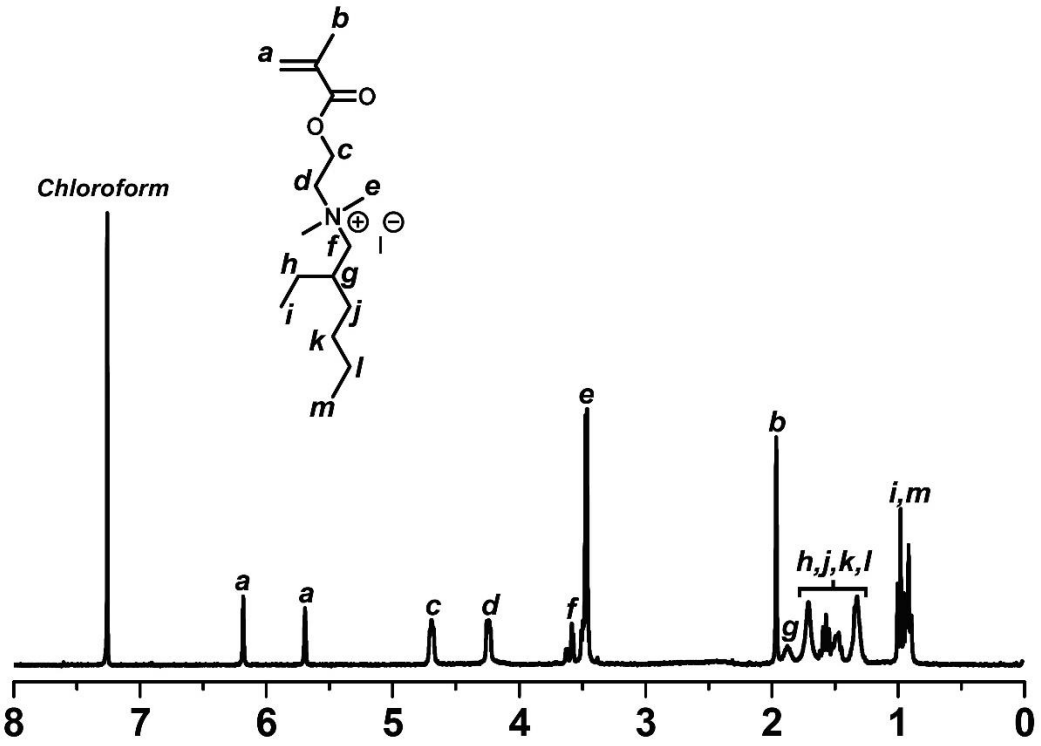


**Figure 2.11.** $^{1}H$ NMR spectrum of EHMAI (300 MHz, 298 K, $CDCl_3$).

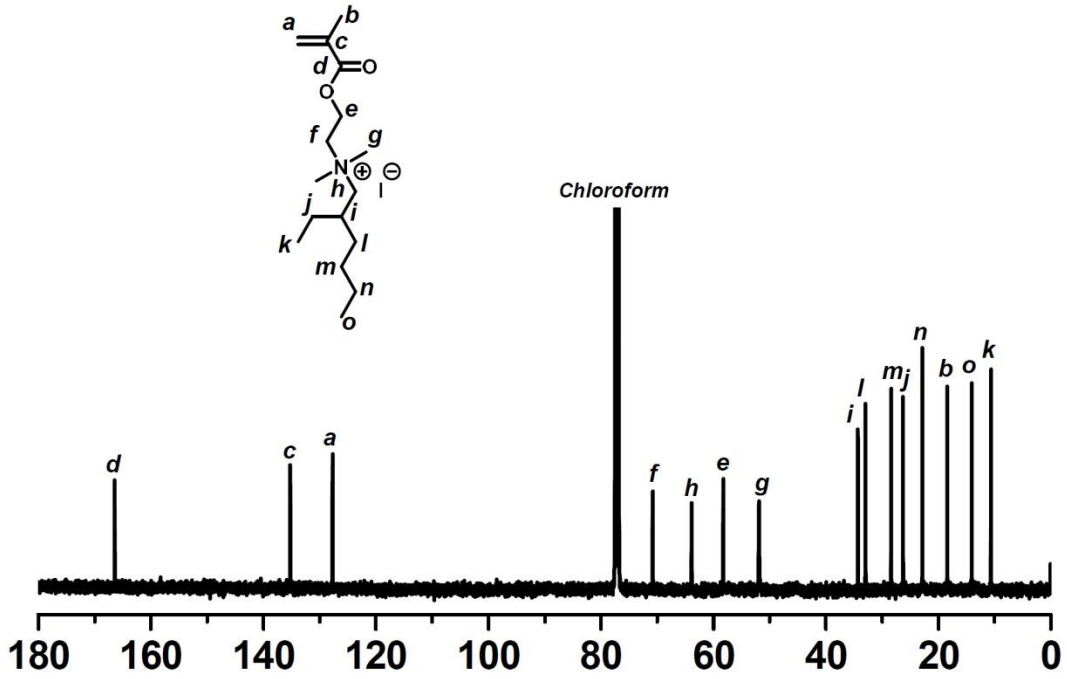


**Figure 2.12.** $^{13}C$ NMR spectrum of EHMAI (100 MHz, 298 K, $CDCl_3$).

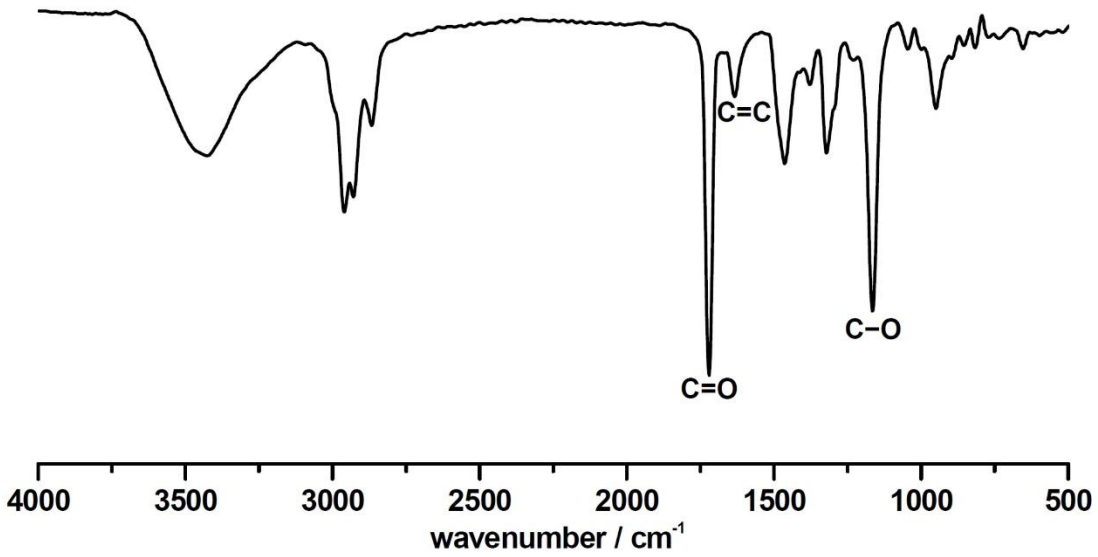


**Figure 2.13.** IR spectrum of EHMAI (KBr).

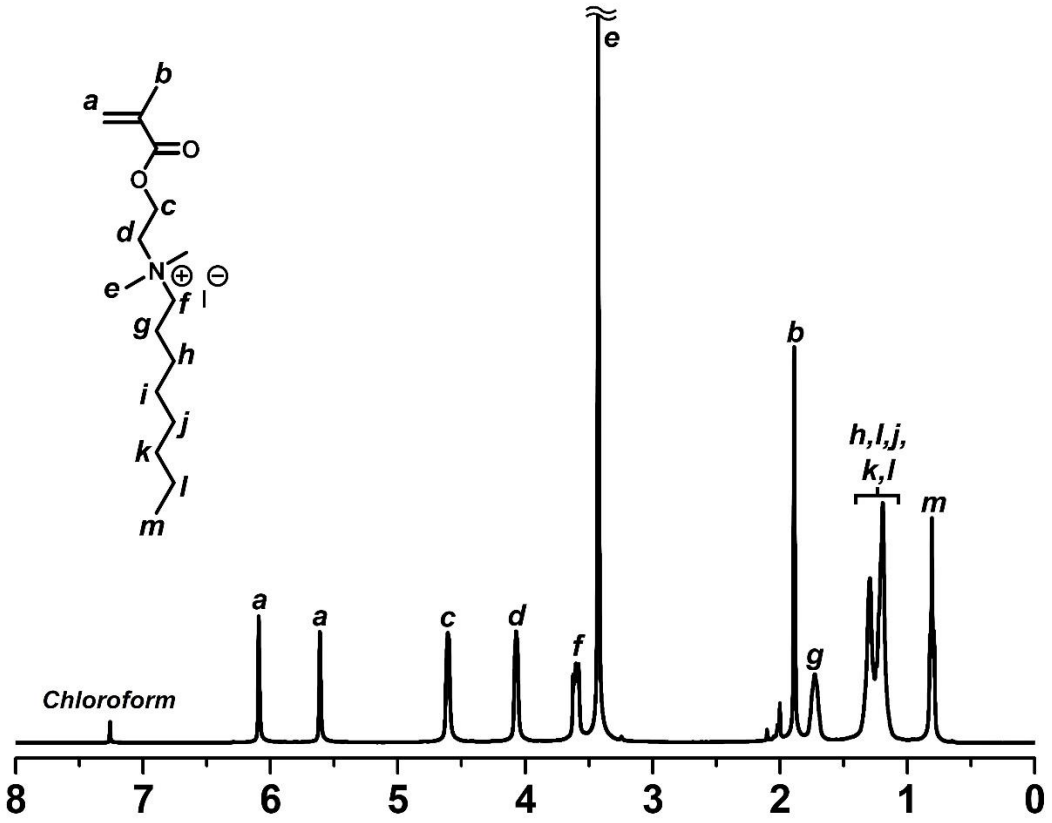


**Figure 2.14.** $^{1}H$ NMR spectrum of $C_8$MAI (400 MHz, 298 K, CDCl3).

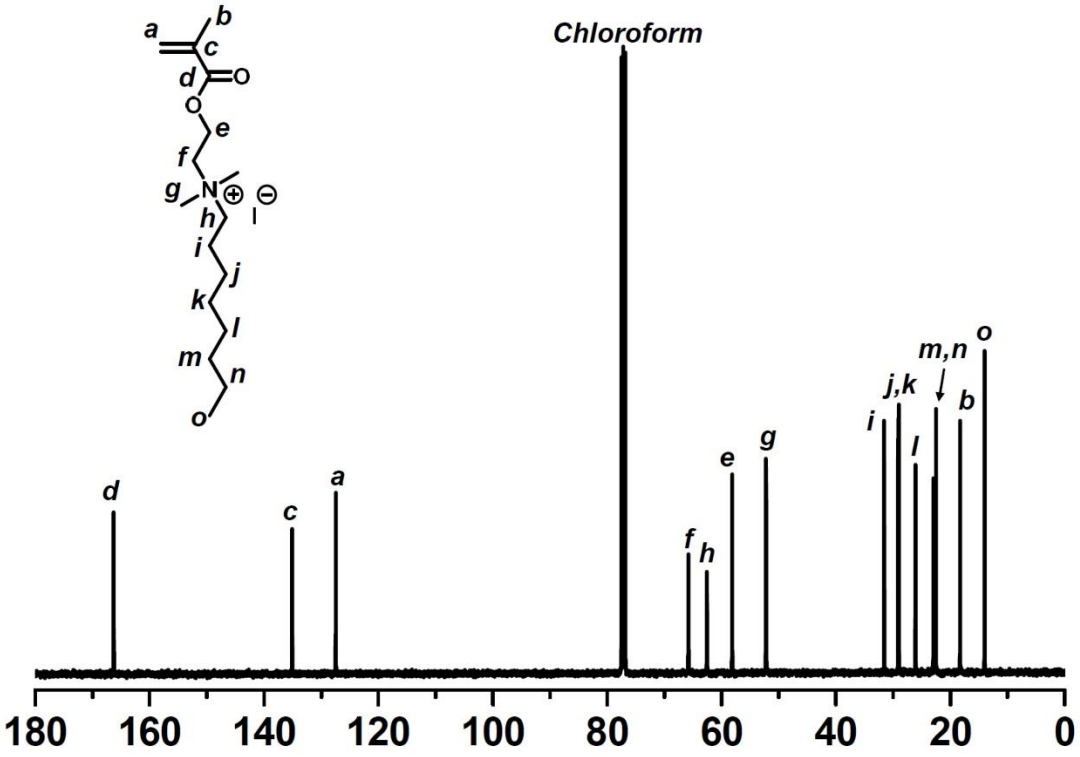


**Figure 2.15.** $^{13}C$ NMR spectrum of $C_8MAI$ (100 MHz, 298 K, $CDCl_3$).

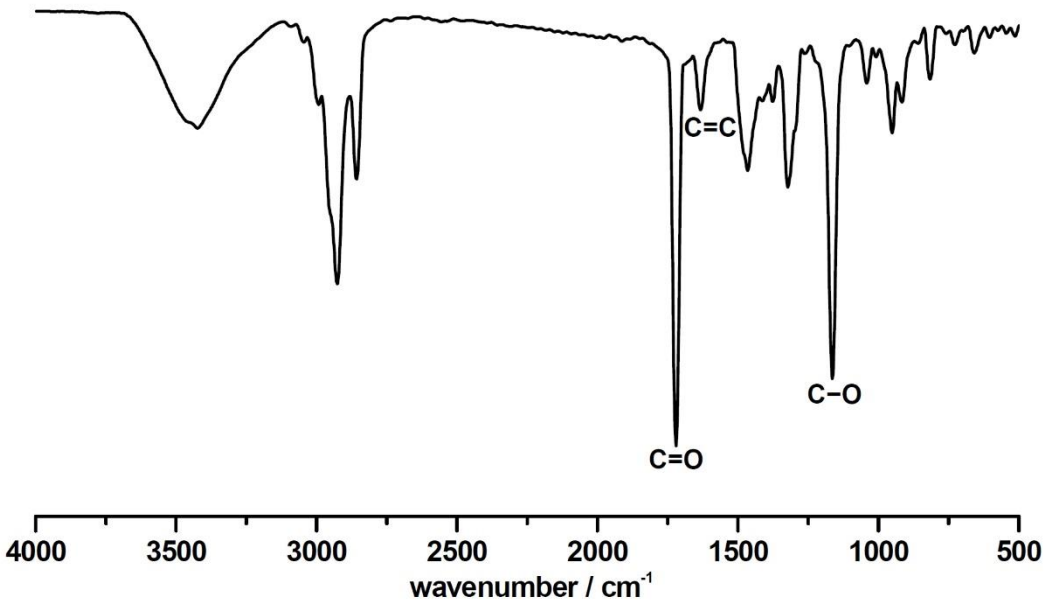


**Figure 2.16.** IR spectrum of $C_8MAI$ (KBr).

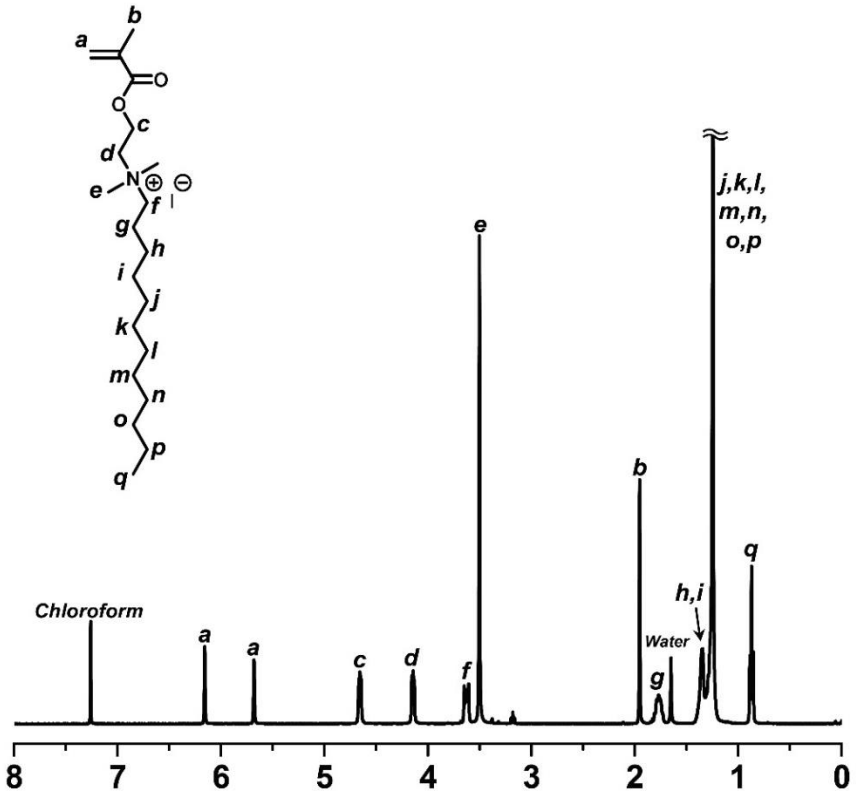


**Figure 2.17.** $^{1}H$ NMR spectrum of $C_{12}MAI$ (400 MHz, 298 K, CDCl3).

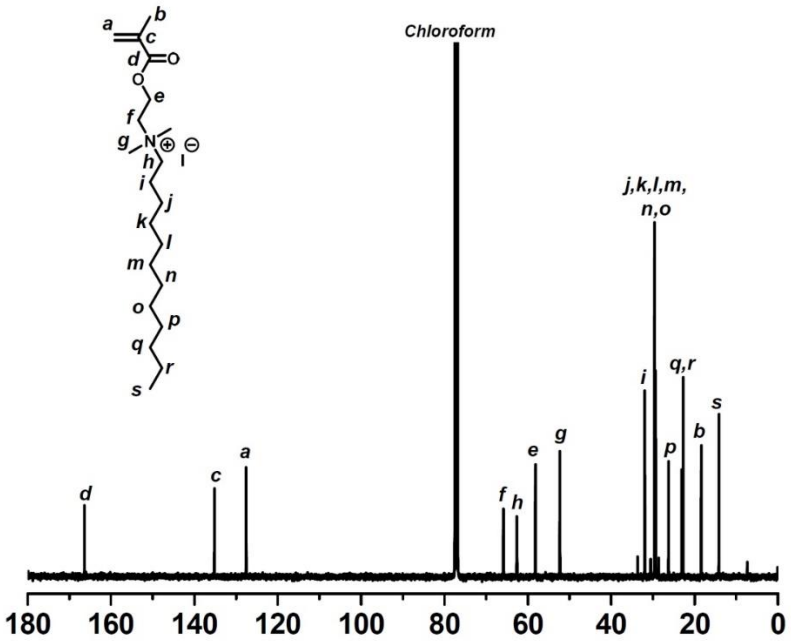


**Figure 2.18.** $^{13}C$ NMR spectrum of $C_{12}MAI$ (100 MHz, 298 K, $CDCl_3$).

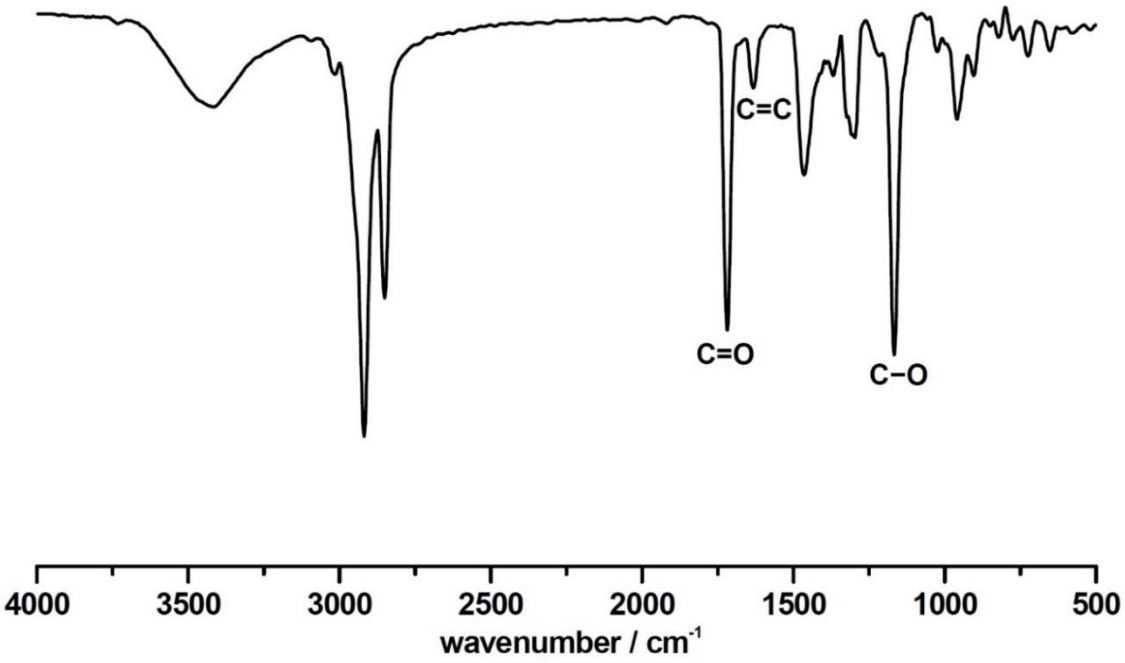


**Figure 2.19.** IR spectrum of $C_{12}$MAI (KBr).

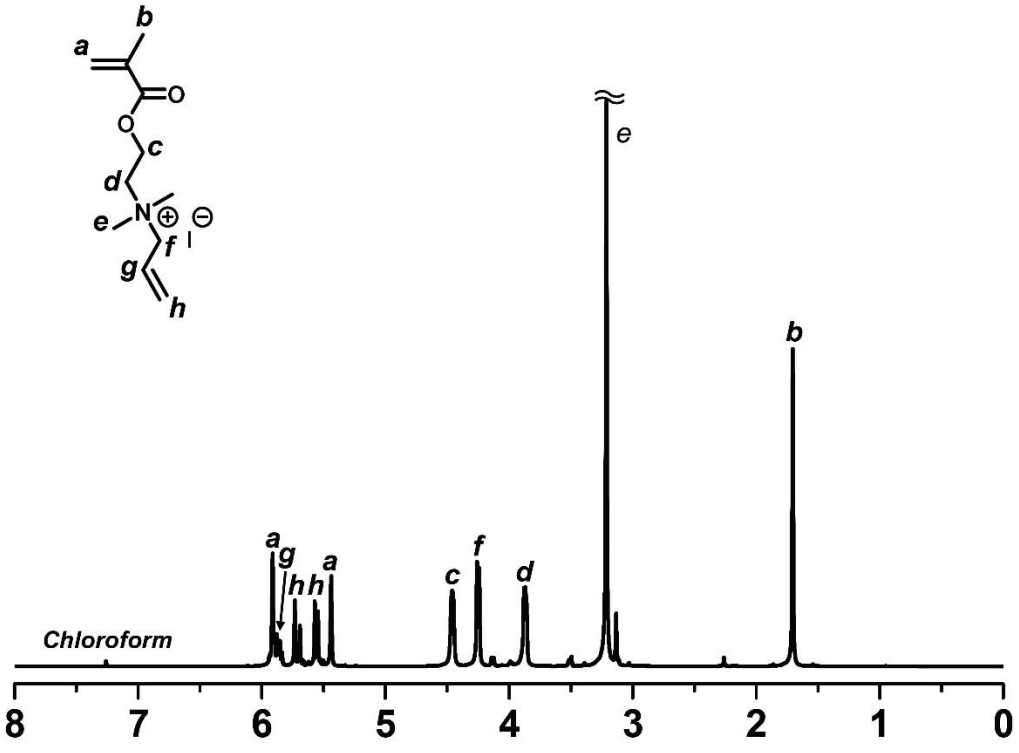


**Figure 2.20.** $^1$H NMR spectrum of AMAI (400 MHz, 298 K, $CDCl_3$).

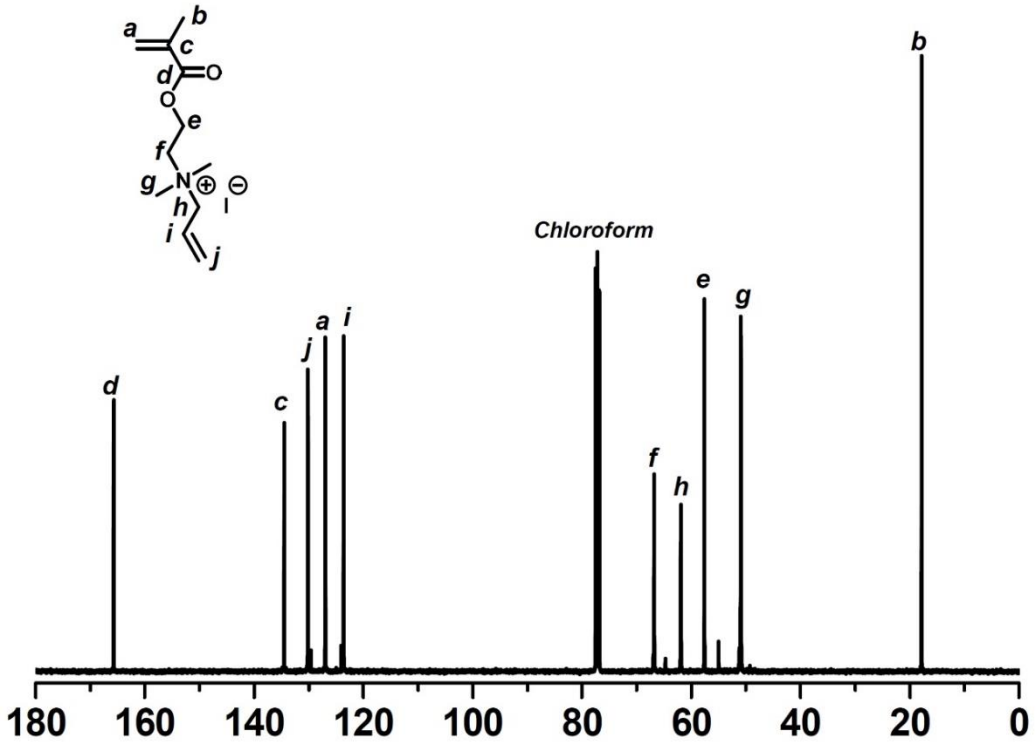


**Figure 2.21.** $^{13}C$ NMR spectrum of AMAI (100 MHz, 298 K, $CDCl_3$).

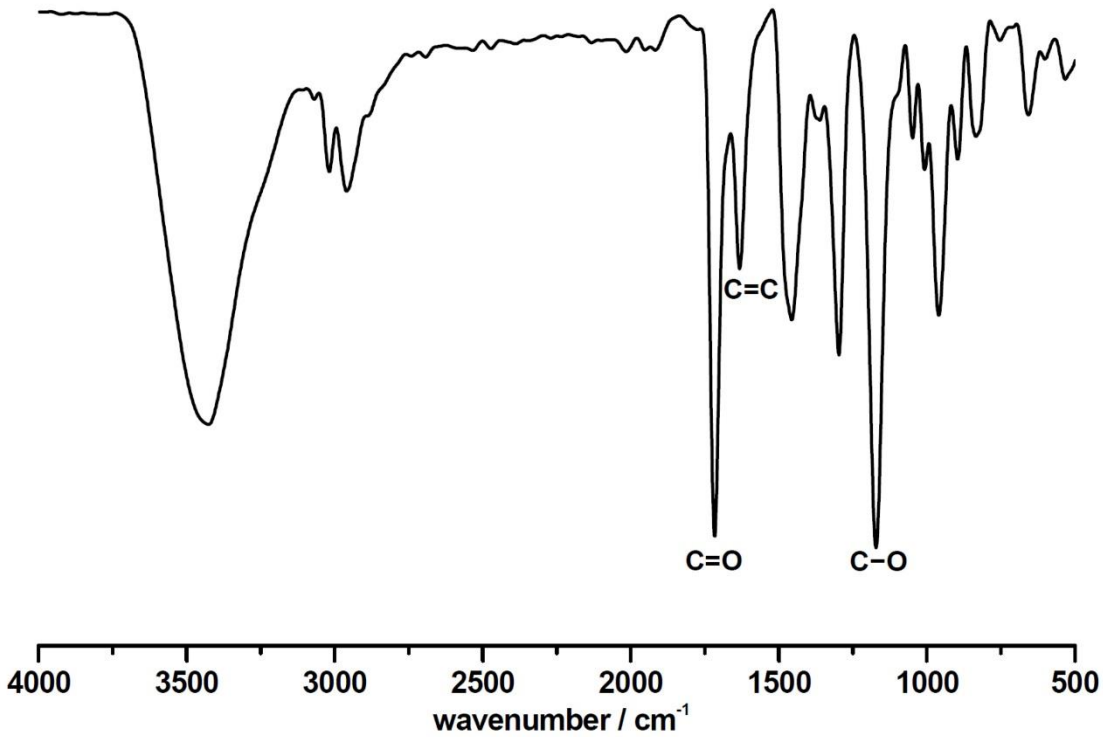


**Figure 2.22.** IR spectrum of AMAI (KBr).

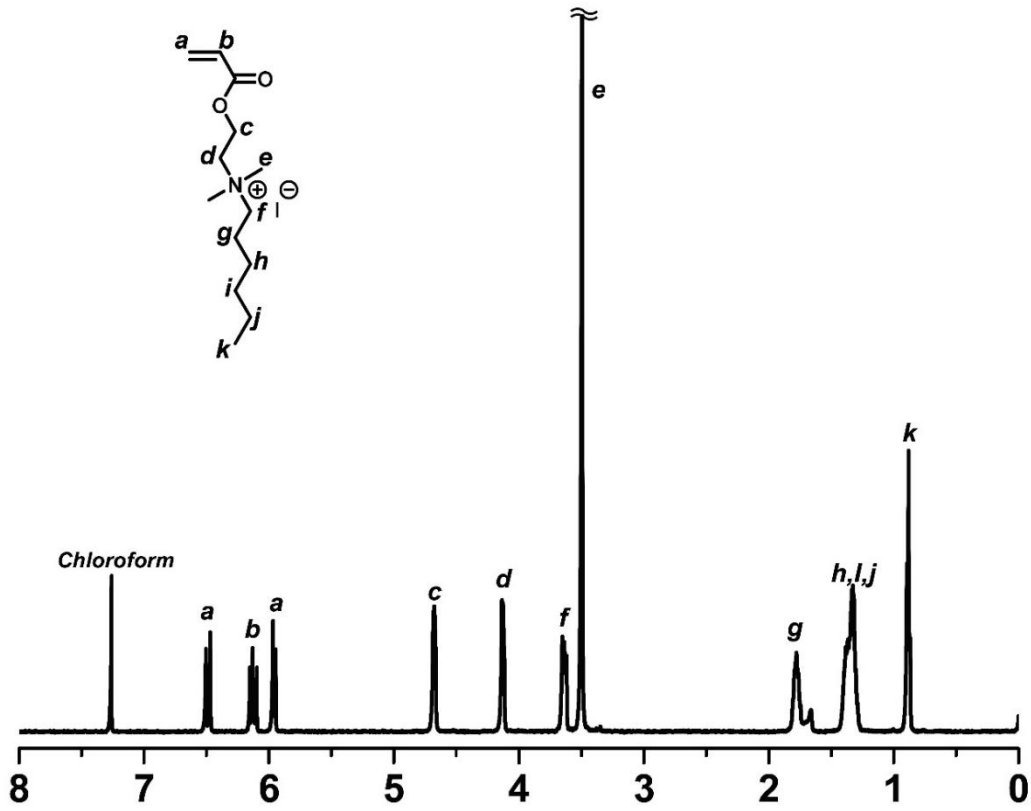


**Figure 2.23.** $^{1}$H NMR spectrum of $C_6AI$ (500 MHz, 298 K, $CDCl_3$).

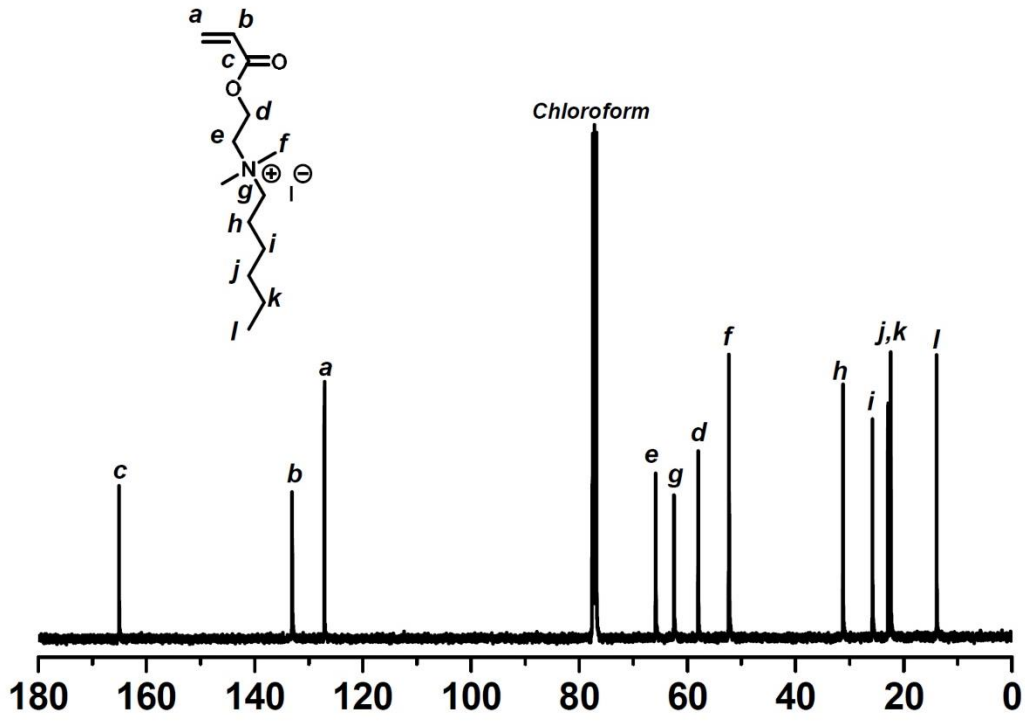


**Figure 2.24.** $^{13}$C NMR spectrum of $C_6AI$ (100 MHz, 298 K, $CDCl_3$).

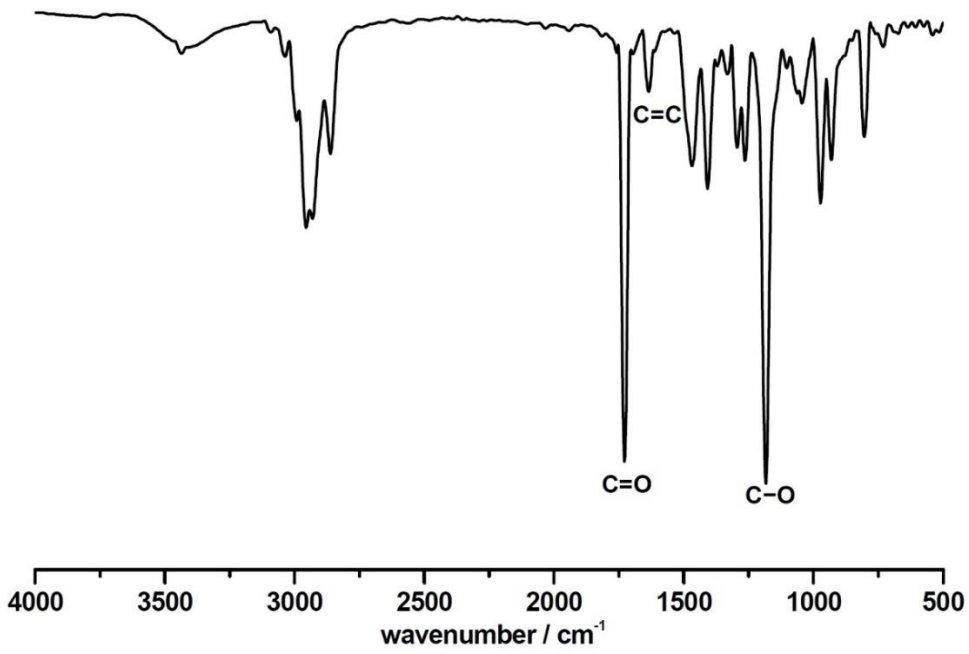


**Figure 2.25.** IR spectrum of $C_6$AI (KBr).

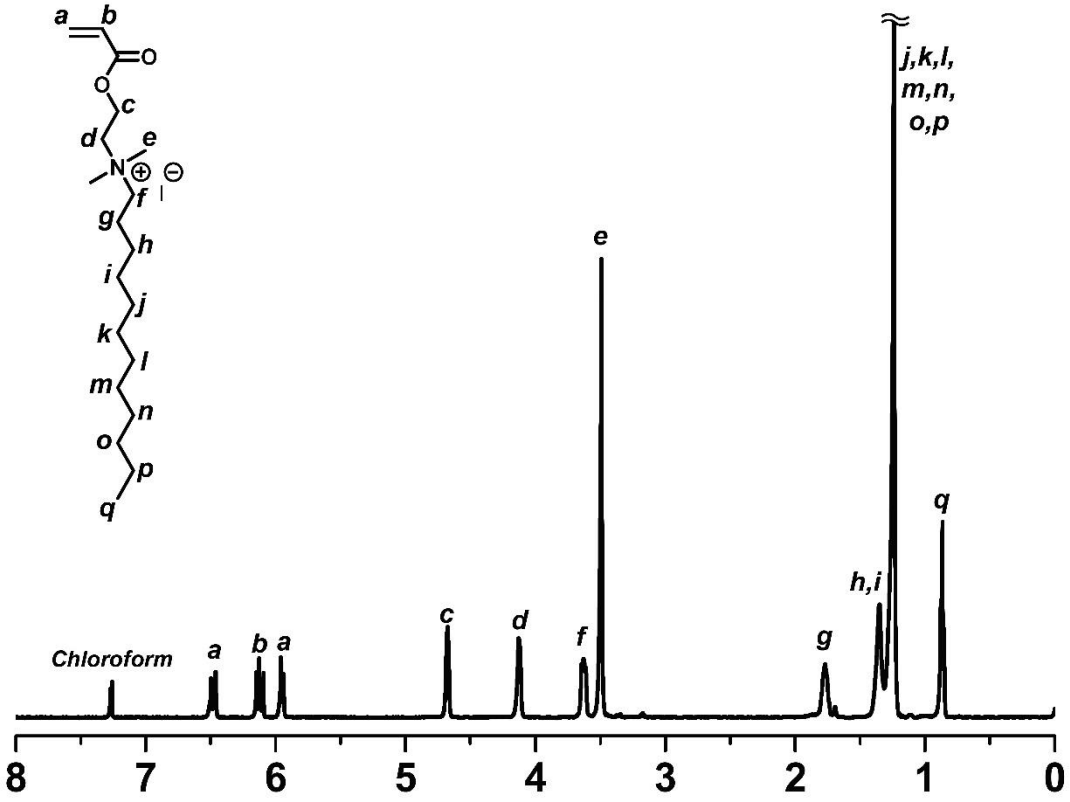


**Figure 2.26.** $^1$H NMR spectrum of $C_{12}$AI (500 MHz, 298 K, $CDCl_3$).

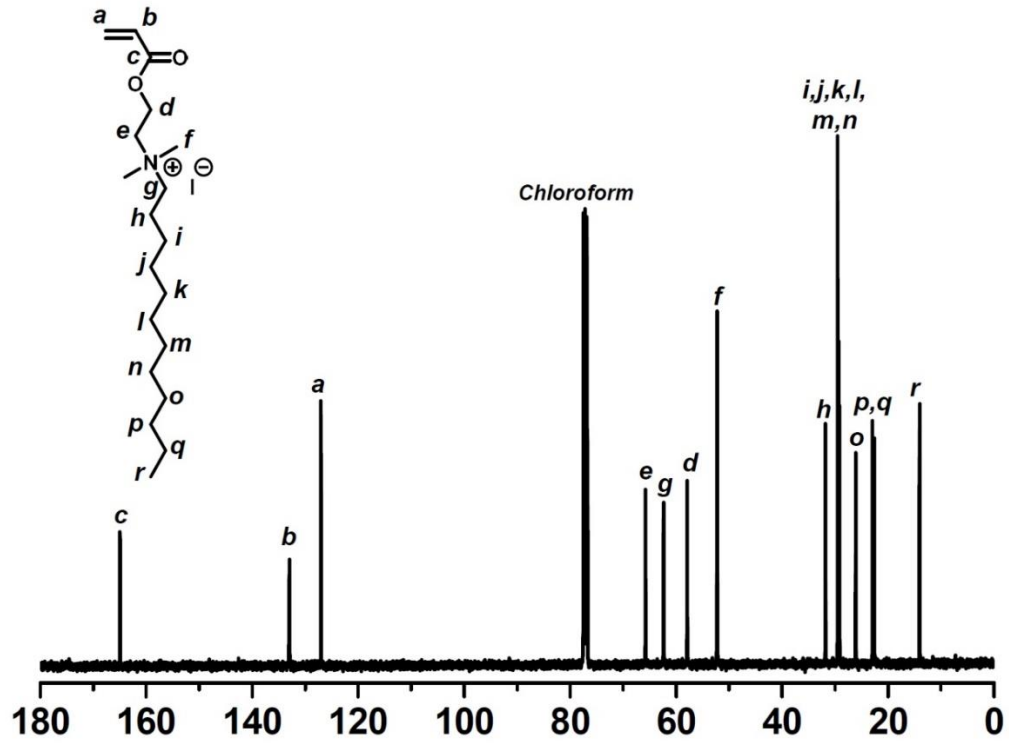


**Figure 2.27.** $^{13}C$ NMR spectrum of $C_{12}AI$ (100 MHz, 298 K, $CDCl_3$).

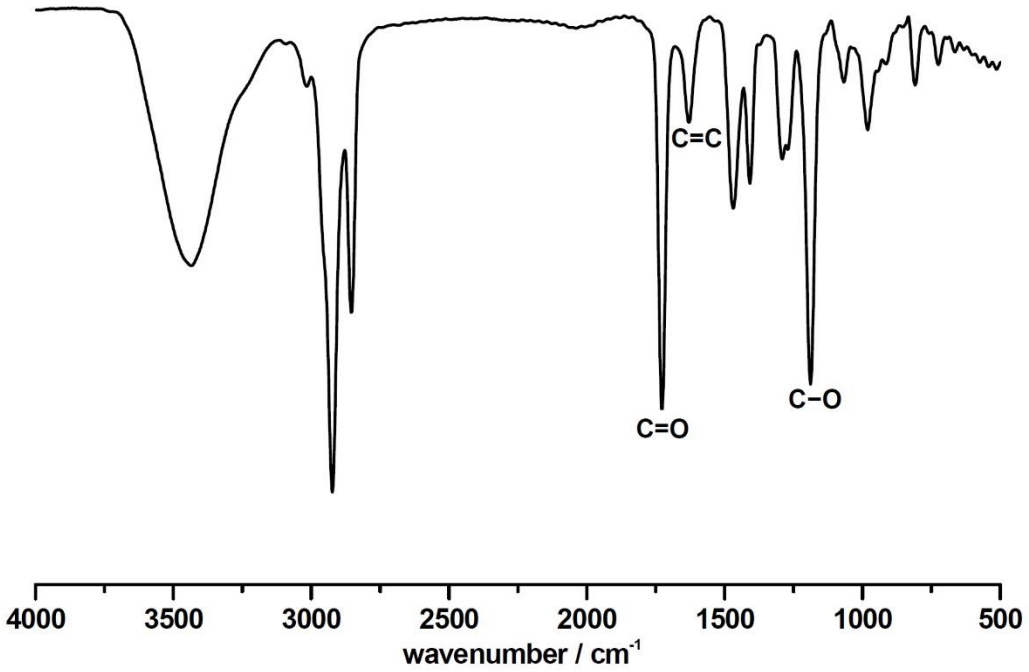


**Figure 2.28.** IR spectrum of $C_{12}AI$ (KBr).

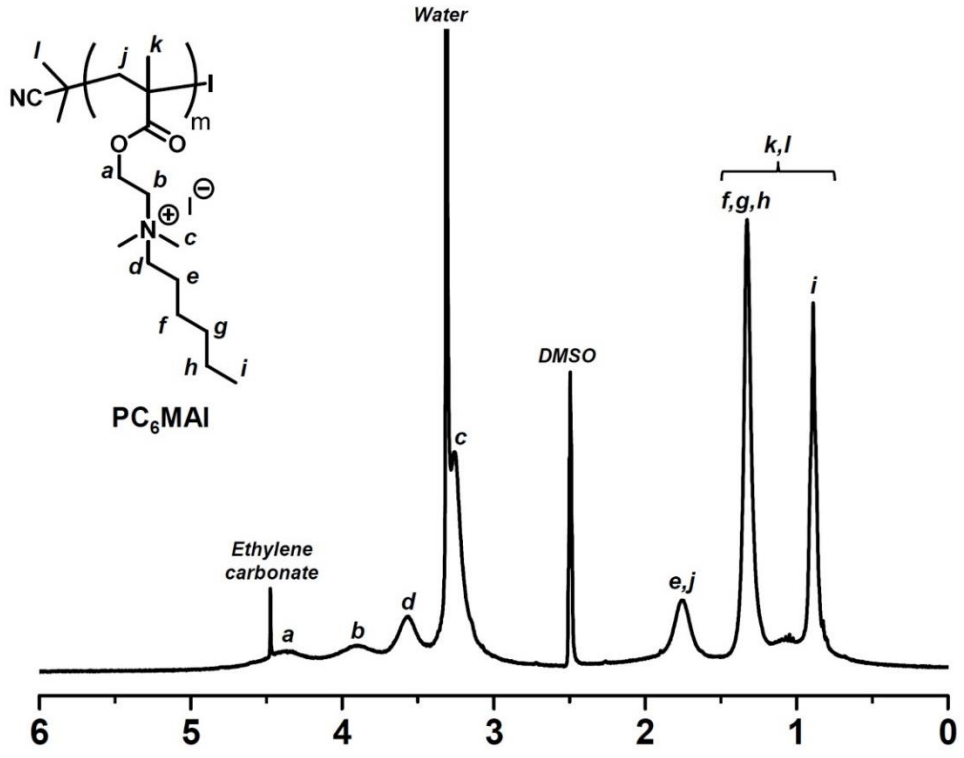


**Figure 2.29.** $^{1}$H NMR spectrum of $PC_6MAI$ (300 MHz, 298 K, DMSO).

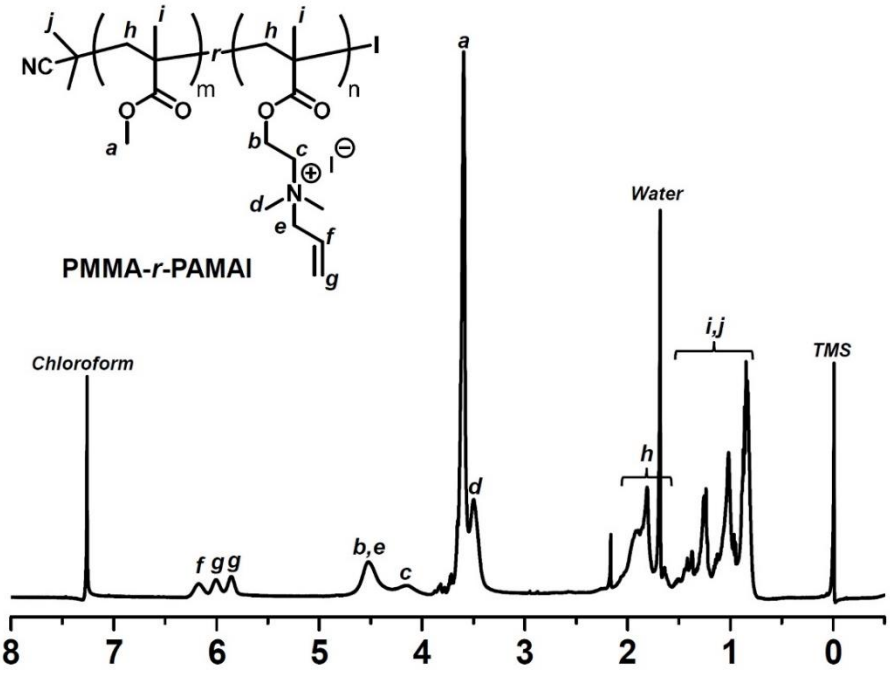


**Figure 2.30.** $^{1}$H NMR spectrum of PMMA-*r*-PAMAI (400 MHz, 298 K, $CDCl_3$).

## References


1. The description of self-catalysis here is different from autocatalysis. In autocatalysis, the reaction products serve as the catalysts to accelerate the reactions.
2. Krawczyk, H. *Synth. Commun.* **2000**, *30*, 657-664.
3. Bachmann, J.; Zierold, R.; Chong, Y. T.; Hauert, R.; Sturm, C.; Schmidt-Grund, R.; Rheinländer, B.; Grundmann, M.; Gösele, U.; Nielsch K. *Angew. Chem. Int. Ed.* **2008**, *47*, 6177-6179.
4. MacLeod, P. D.; Li, Z.; Li, C.-J. *Tetrahedron* **2010**, *66*, 1045-1050.
5. Matyjaszewski, K. *Adv. Mater.* **2018**, *30*, 1706441.
6. Keddie, D. J.; Moad, G.; Rizzardo, E.; Thang, S. H. *Macromolecules* **2012**, *45*, 5321-5342.
7. Matyjaszewski, K.; Tsarevsky, N. V. *J. Am. Chem. Soc.* **2014**, *136*, 6513-6533.
8. Nicolas, J.; Guillaneuf, Y.; Lefay, C.; Bertin, D.; Gigmes, D.; Charleux, B. *Prog. Polym. Sci.* **2013**, *38*, 63-235.
9. Goto, A.; Zushi, H.; Hirai, N.; Wakada, T.; Tsujii, Y.; Fukuda, T. *J. Am. Chem. Soc.* **2007**, *129*, 13347-13354.
10. Goto, A.; Suzuki, T.; Ohfuji, T.; Tanishima, M.; Fukuda, T.; Tsujii, Y.; Kaji, H. *Macromolecules* **2011**, *44*, 8709-8715.
11. Goto, A.; Ohtsuki, A.; Ohfuji, H.; Tanishima, M.; Kaji, H. *J. Am. Chem. Soc.* **2013**, *135*, 11131-11139.
12. Ohtsuki, A.; Lei, L.; Tanishima, M.; Goto, A.; Kaji, H. *J. Am. Chem. Soc.* **2015**, *137*, 5610-5617.
13. Wang, C.-G.; Goto, A. *J. Am. Chem. Soc.* **2017**, *139*, 10551-10560.
14. Wang, C.-G.; Hanindita, F.; Goto, A. *ACS Macro Lett.* **2018**, *7*, 263-268.
15. Wang, C.-G.; Chen, C.; Sakakibara, K.; Tsujii, Y.; Goto, A. *Angew. Chem. Int. Ed.* **2018**, *57*, 13504-13508.
16. Konai, M. M.; Bhattacharjee, B.; Ghosh S.; Haldar, J. *Biomacromolecules* **2018**, *19*, 1888-1917.
17. Jiao, Y.; Niu, L.; Ma, S.; Li, J.; Tay, F. R.; Chen, J. *Prog. Polym. Sci.* **2017**, *71*, 53-90.
18. Xue, Y.; Xiao, H.; Zhang, Y. *Int. J. Mol. Sci.* **2015**, *16*, 3626-3655.
19. Jaeger, W.; Bohrisch, J.; Laschewsky, A. *Prog. Polym. Sci.* **2010**, *35*, 511-577.
20. Lenoir, S.; Pagnoulle, C.; Detrembleur, C.; Galleni, M.; Jérôme, R. *J. Polym. Sci., Part A: Polym. Chem.* **2006**, *44*, 1214-1224.
21. Murata, H.; Koepsel, R. R.; Matyjaszewski, K.; Russell, A. J. *Biomaterials* **2007**, *28*, 4870-4879.
22. Li, Y.; Armes, S. P.; Jin, X.; Zhu, S. *Macromolecules* **2003**, *36*, 8268-8275.
23. Kobayashi, M.; Terada, M.; Terayama, Y.; Kikuchi, M.; Takahara, A. *Macromolecules* **2010**, *43*, 8409-8415.
24. Roy, D.; Knapp, J. S.; Guthrie, J. T.; Perrier, S. *Biomacromolecules* **2008**, *9*, 91-99.
25. Siegwart, D. J.; Oh, J. K.; Matyjaszewski, K. *Prog. Polym. Sci.* **2012**, *37*, 18-37.
26. Tagoshi, H.; Endo, T. *J. Appl. Polym. Sci.* **1991**, *43*, 1933-1939.
27. Truong, N. P.; Jia, Z.; Burges, M.; McMillan, N. A. J.; Monteiro, M. J. *Biomacromolecules* **2011**, *12*, 1876-1882.

28. Liu, L.; Chen, L.; Fang, Y. *Macromol. Rapid Commun.* **2006**, *27*, 1988-1994.
29. Xu, J.; Shanmugam, S.; Boyer, C. *ACS Macro Lett.* **2015**, *4*, 926-932.
30. Zeng, G.; Liu, M.; Jiang, R.; Huang, Q.; Huang, L.; Wan, Q.; Dai, Y.; Wen, Y.; Zhang, X.; Wei, Y. *Mater. Sci. Eng. C* **2018**, *83*, 154-159.
31. Goto, A.; Fukuda, T. *Prog. Polym. Sci.* **2004**, *29*, 329-385.
32. Sellenet, P. H.; Allison, B.; Applegate, B. M.; Youngblood, J. P. *Biomacromolecules* **2007**, *8*, 19−23.
33. Han, H.; Wu, J.; Avery, C. W.; Mizutani, M.; Jiang, X.; Kamigaito, M.; Chen, Z.; Xi, C.; Kuroda, K. *Langmuir* **2011**, *27*, 4010–4019.

# Chapter 3. Self-catalyzed Synthesis of Nano-capsule and Its Application to Heterogeneous RCMP Catalyst


## Abstract

A quaternary ammonium iodide (QAI)-containing macroinitiator was used in self-catalyzed polymerization-induced self-assembly (PISA), yielding a nano-capsule (vesicle) bearing QAI groups on both outer and inner surfaces of the nano-capsule. QAI is a catalyst for reversible complexation mediated polymerization (RCMP). Thus, the obtained nano-capsule was utilized as a heterogeneous catalyst in RCMPs of several monomers. A good recyclability of the catalytic nano-capsule was demonstrated in ten cycles. Polymers are generated not only outside the capsule (via QAI-catalysis on the outer surface) but also inside the capsule (cavity) (via QAI-catalysis on the inner surface), latter of which afforded a polymer-loaded nano-capsule. Thus, the nano-capsule served as a dual catalyst for yielding polymers outside and inside the capsule.

## 3.1. Introduction

Polymerization-induced self-assembly (PISA) is a technique to generate nano-assemblies such as micelles, worms, and vesicles in situ during the polymerization.[1–9] PISA can generate assemblies at high solid contents, which is an attractive feature. In PISA, a solvophilic macroinitiator is extended via polymerization to form an amphiphilic block copolymer. As the second block segment grows, the block copolymer becomes insoluble in the polymerization solvent, forming nano-assemblies during the polymerization. PISA utilizes living polymerizations such as living radical polymerizations (also termed reversible deactivation radical polymerizations) including reversible addition-fragmentation chain transfer (RAFT) polymerization[10–12], atom transfer radical polymerization (ATRP)[13–15], and nitroxide mediated polymerization (NMP)[16–17]. Our research group has conducted PISA using reversible complexation mediated polymerization (RCMP)[3–5].

RCMP[18-21] utilizes a polymer-iodide (polymer–I) as a dormant species and an iodide anion ($I^-$) as a catalyst. $I^-$is used in the form of a quaternary ammonium iodide (QAI) ($R_4N^+$ $I^-$), for example. The polymer–I dormant species coordinates the $I^-$ catalyst to form a halogen bonding complex (polymer–I···$I^-$). The complex subsequently reversibly generates a propagating radical (polymer$^\bullet$) (Scheme 3.1). An advantage of RCMP is use of no metals or odorous compounds.

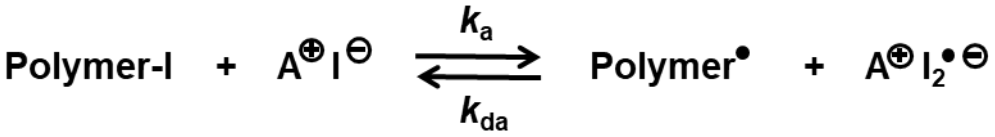


**Scheme 3.1.** Reversible activation in RCMP.

Our research group previously utilized QAI-containing monomers such as [2-(methacryloyloxy)ethyl]dimethylhexylammonium iodide ($C_6$MAI) (Scheme 3.2) and attained self-catalyzed RCMP of QAI-containing monomers.[22] The monomer contains a polymerizable methacrylate moiety and also a catalytic QAI moiety. Because the monomer contains the catalytic moiety, the polymerization (RCMP) proceeds without adding extra catalysts.

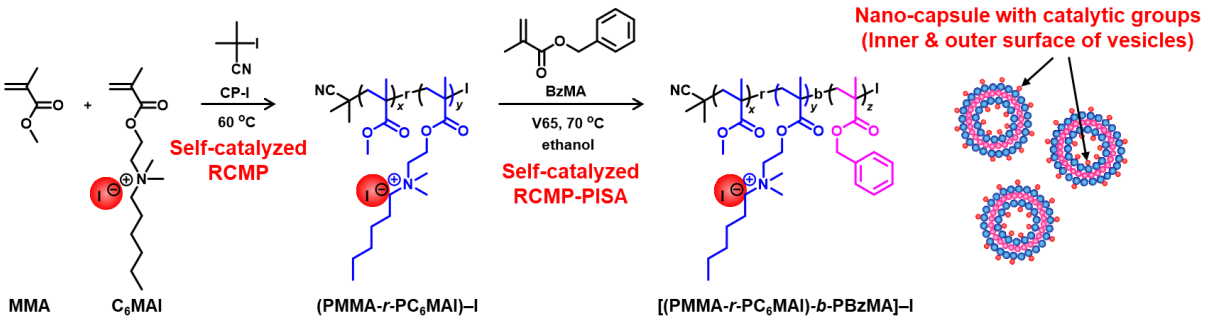


**Scheme 3.2.** Self-catalyzed synthesis of nano-capsules via RCMP-PISA.

Herein, we report a combination of self-catalyzed RCMP with PISA for synthesizing a nano-capsule (vesicle). As Scheme 3.2 shows, we prepared a QAI-containing macroinitiator via self-catalyzed RCMP and subsequently used the macroinitiator to conduct self-catalyzed RCMP-PISA for synthesizing a nano-capsule. The macroinitiator served as an initiator and a catalyst. This is the first self-catalyzed synthesis of a nano-assembly in the fields of living radical polymerization and PISA.

Importantly, the surface of the obtained nano-capsule bears QAI groups (Scheme 3.2). Hence, as an application, we further utilized the obtained nano-capsule as a supported (heterogeneous) catalyst for RCMP. Heterogeneous catalysts have been extensively studied for polymerizations since the development of Ziegler-Natta catalysts in 1970s for producing polyethylene and polypropylene.[23] An advantage of heterogeneous catalysts is recyclability of the catalysts, which is beneficial for sustainability. Heterogeneous catalysts have also

extensively been studied in ATRP[24–35] and RAFT polymerizations[36–38]. The present catalytic nano-capsule for RCMP is purely organic (with no inorganic support) and recyclable, which are attractive features. A marked unique feature of the present catalytic nano-capsule is that the nano-capsule bears QAI groups on both outer and inner surfaces of the nano-capsule (Scheme 3.2) and hence can serve as dual catalysts to conduct RCMP outside and inside the nano-capsule. Monomers can undergo polymerization outside the nano-capsule via the outer surface catalysts or diffuse into the inner core and undergo polymerization inside the nano-capsule (nano-reactor) via the inner surface catalysts. Such dual catalysts are novel in the field of living radical polymerization.

### 3.2. Results and Discussion

#### Synthesis of Macroinitiator ((PMMA-*r*-PC$_6$MAI)–I).

A mixture of methyl methacrylate (MMA) (19.3 equiv., main monomer), C$_6$MAI (1 equiv., co-monomer and catalyst), and 2-iodo-2-methylpropionitrile (CP–I, initiating dormant species) was heated at 60 ℃ for 1 h (Scheme 3.2 and Table 3.1). C$_6$MAI contains both methacrylate and QAI groups and acts as a monomer and a polymerization catalyst. Hence, the polymerization proceeded without an extra catalyst. We intentionally stopped the polymerization for a short period of time (1 h) and at low monomer conversions (30% for MMA and 41% for C$_6$MAI) in order to retain the chain-end iodide. The obtained polymer was purified by reprecipitation in a hexane/ethanol mixture (7/3 (v/v)). The number-average molecular weight ($M_n$) and dispersity ($Đ = M_w/M_n$) of the purified (PMMA-*r*-PC$_6$MAI)–iodide ((PMMA-*r*-PC$_6$MAI)–I) random copolymer were 1700 and 1.08, respectively, where $M_w$ is the weight-average molecular weight, PMMA is poly(methyl methacrylate), and PC$_6$MAI is poly([2-(methacryloyloxy)ethyl]dimethylhexylammonium iodide) (Table 3.1). These values are PMMA-calibrated gel permeation chromatography (GPC) values. Figure 3.1 shows the $^1$H

NMR spectrum of the purified PMMA-*r*-P$C_6$MAI. The methyl ($CH_3$) protons (*a*) of the MMA unit appeared at 3.56–3.88 ppm. For $C_6$MAI unit, the ethylene ($OCH_2$) protons (*b*) appeared at 4.31–4.74 ppm, the ethylene ($OCH_2\underline{CH_2}N^+$) protons (*c*) appeared at 3.91–4.31 ppm, the ethylene ($CH_2N^+$) protons (*d*) appeared at 3.69–3.91 ppm, the dimethyl protons ($(CH_3)_2N^+$) (*e*) appeared at 3.15–3.56 ppm, the ethylene ($N^+CH_2\underline{CH_2}CH_2$) protons (*f*) and the ethylene ($\underline{CH_2}CCH_3$) protons (*k*) appeared at 1.56–2.31 ppm, the ethylene ($N^+(CH_2)_2\underline{(CH_2)_3}$) protons (*g*, *h*, *i*) and the methyl ($N^+(CH_2)_2(CH_2)_3\underline{CH_3}$) protons (*j*) and the methyl ($CH_2C\underline{CH_3}$) protons (*l*) and the dimethyl ((CN)C($\underline{CH_3}$)$_2$) protons (*m*) appeared at 0.51–1.56 ppm. The molar ratio of the MMA units to the $C_6$MAI units is calculated according to [(integral for *a*, *e*, and *d*) – (integral for *b* and *c*)×(8H for *e* and *d*)/(4H for *b* and *c*)]/(3H for *a*) to (integral for *b* and *c*)/(4H for *b* and *c*). We calculated the molar compositions of the MMA and $C_6$MAI units to be 79% and 21%, respectively. The original amounts (19.3 equiv. and 1 equiv.) and conversions (30% and 41%) of MMA and $C_6$MAI suggest that the polymer compositions before the purification were 93% and 7% for MMA and $C_6$MAI, respectively. During the reprecipitation, MMA-rich polymers seemed to be removed more, which would result in the observed increase in the $C_6$MAI composition (21%) after the purification. Using these $M_n$ value (1700) and molar compositions (79% and 21% for the MMA and $C_6$MAI units, respectively), we estimate the degree of polymerization (DP) to be approximately 9 and 2 (8.6 and 2.3) for the MMA and $C_6$MAI units, respectively. Because the $M_n$ value is not an absolute value but a PMMA-calibrated GPC value, these DP values are viewed as rough estimate. We use these estimated DP values in the present paper. Thus, we obtained (P$MMA_9$-*r*-P$C_6MAI_2$)–I. In the present paper, the subscript in the polymer denotes a DP of each monomer.

**Table 3.1.** Synthesis of (PMMA-*r*-$PC_6MAI$)–I.

| $[MMA]_0/[C_6MAI]_0/[CP–I]_0$ (equiv.) | *T* (°C) | *t* (h) | Conv. (%)[a] (MMA/$C_6MAI$) | $M_n$[b] | *Đ*[b] | DP[c] (MMA/$C_6MAI$) |
|---|---|---|---|---|---|---|
| 19.3/1/1 | 60 | 1 | 30/41 | 1700 | 1.08 | 9/2 |

[a]Monomer conversions were determined with $^1$H NMR. [b]PMMA-calibrated GPC (THF eluent) values of the purified polymer. [c] The DP values of the MMA and $C_6MAI$ units were calculated from the $M_n$ value and the polymer compositions obtained from the $^1$H NMR spectrum of the purified polymer.

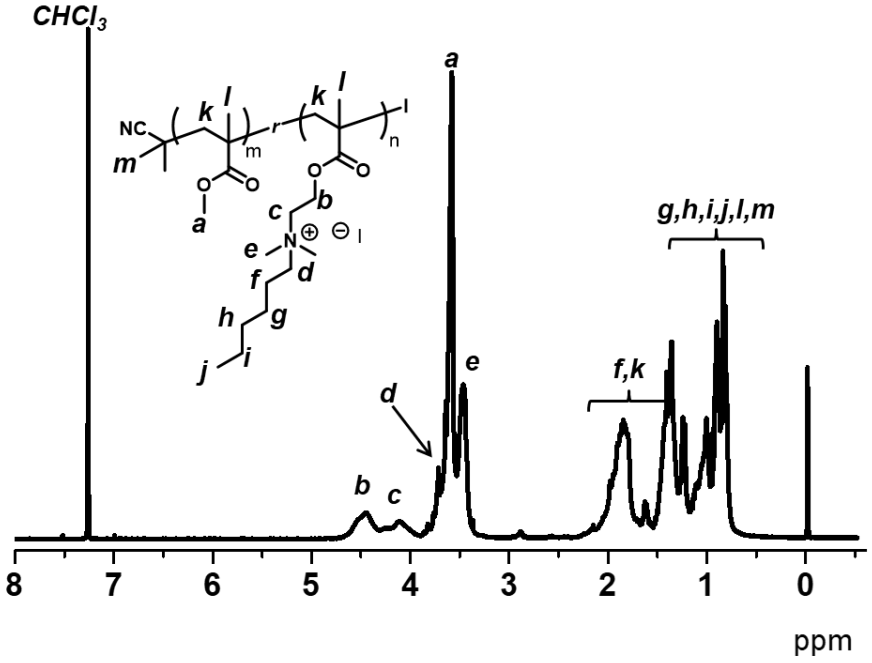


**Figure 3.1.** $^1$H NMR spectrum of PMMA-*r*-$PC_6MAI$ (Table 3.1) (400 MHz, 298 K, $CDCl_3$).

**Self-catalyzed PISA.**

Using the obtained ($PMMA_9$-*r*-$PC_6MAI_2$)–I as a macroinitiator, we carried out PISA. We heated a mixture of benzyl methacrylate (BzMA) (100 equiv., monomer), ($PMMA_9$-*r*-$PC_6MAI_2$)–I (1 equiv., macroinitiator), 2,2'-azobis(2,4-dimethylvaleronitrile) (V65) (0.5 equiv., azo initiator), and ethanol (70 wt% of the total mixture) at 70 °C (Scheme 3.2 and Table 3.2). The total fraction of the macroinitiator (2.7 wt%) and monomer (BzMA) (27.3 wt%) was 30 wt%, and hence the solid (polymer) content expected at a full (100%) monomer conversion was 30 wt%. V65 was added to increase the polymerization rate. Azo initiators are used to

decrease the deactivator concentration, hence, effectively increase the polymerization rate in RCMP[22] and other living radical polymerization systems[39].

The polymerization mixture turned cloudy at 1 h, suggesting the formation of a self-assembly as the PBzMA segment became long enough to be insoluble in ethanol (solvent), where PBzMA is poly(benzyl methacrylate). An aliquot of the polymerization mixture was taken out at 1, 1.25, 1.5, and 2 h and diluted with $CDCl_3$ for the NMR analysis (to determine the monomer conversion) or tetrahydrofuran (THF) for the GPC analysis. The monomer conversion reached 62 % for 2 h (Table 3.2 and Figure 3.2a). The GPC chromatogram at 2 h (Figure 3.2b) show that a large fraction of the macroinitiator chains smoothly extended to block copolymer chains, suggesting a high block efficiency. The $M_n$ value increased with an increase in the monomer (BzMA) conversion and the $Đ$ value was 1.19–1.38 during the polymerization (Table 3.2 and Figure 3.2c), suggesting that the $C_6$MAI units in the macroinitiator worked as effective catalysts in the polymerization.

**Table 3.2.** PISA of BzMA using ($PMMA_9$-*r*-$PC_6MAI_2$)–I and V65 (in 70% Ethanol) at 70 °C.

| $[BzMA]_0/[(PMMA_9$-*r*-$PC_6MAI_2)$–$I]_0/[V65]_0$ (equiv.)[a] | *t* (h) | Conv. (%)[b] | $M_n$[c] ($M_{n,theo}$[d]) | $Đ$[c] | Hydrodynamic size in DLS (*d*(DLS)) (nm)[e] | DLS size distribution index[f] |
|---|---|---|---|---|---|---|
| 100/1/0.5 | 1 | 33 | 6100 (7500) | 1.38 | - | - |
| | 1.25 | 40 | 7500 (8700) | 1.22 | - | - |
| | 1.5 | 52 | 8400 (11000) | 1.22 | - | - |
| | 2 | 62 | 12000 (13000) | 1.19 | 220 | 0.139 |

[a] Solvent was ethanol (70 wt%). [b]Monomer (BzMA) conversion determined with $^1$H NMR. [c]PMMA-calibrated GPC values (THF eluent). [d]Theoretical $M_n$ values calculated according to ($[BzMA]_0/[macroinitiator]_0$)×(monomer conversion) + (molecular weight of macroinitiator (1700)). [e]Intensity-average DLS peak-top value (in water/ethanol mixture (98.6/1.4 (v/v))). [f]The intensity-average size distribution index in DLS defined as [(standard deviation)/(peak-top value)]$^2$ (in water/ethanol mixture (98.6/1.4 (v/v))).

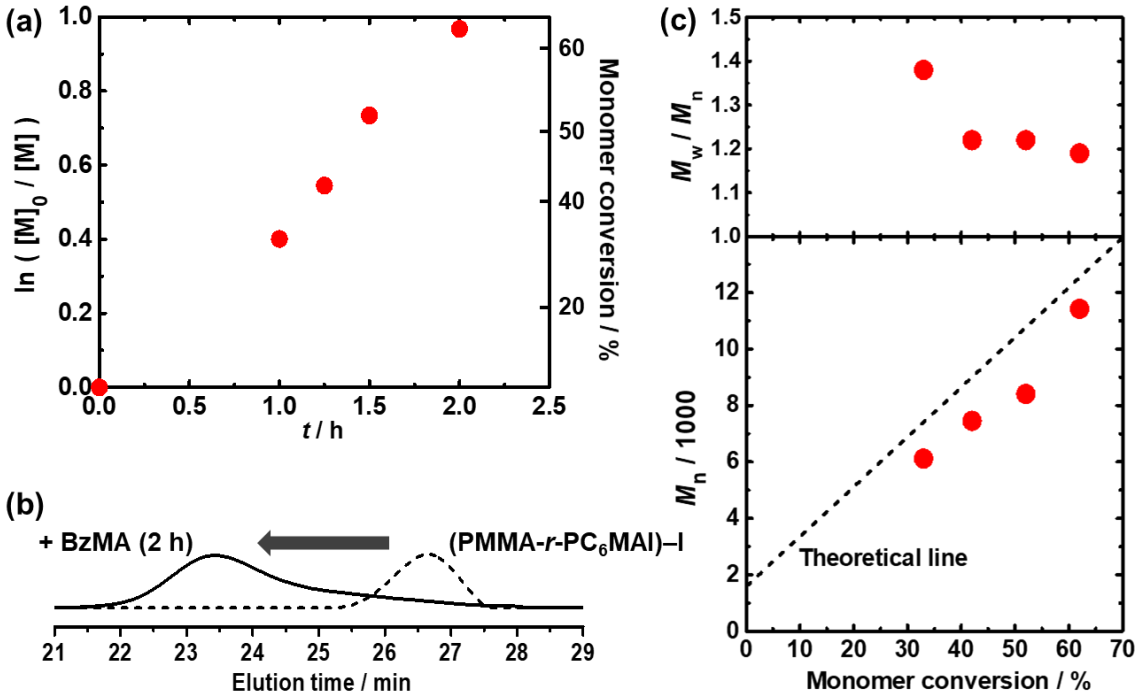


**Figure 3.2**. (a) Plot of ln([M]$_0$/[M]) *vs.* time (*t*), (b) GPC chromatograms at 0 and 2 h, and (c) plots of $M_n$ and $M_w/M_n$ *vs.* monomer conversion for the BzMA/(PMMA$_9$-*r*-PC$_6$MAI$_2$)–I/V65/ethanol system (70 °C): [BzMA]$_0$ = 8 M; [(PMMA$_9$-*r*-PC$_6$MAI$_2$)–I]$_0$ = 80 mM; [V65]$_0$ = 40 mM; ethanol = 70 wt% (Table 3.2).

At 2 h, the DP of PBzMA is estimated to be 62 from the original amount of BzMA (100 equiv. to the macroinitiator) and the conversion of BzMA (62%). We use this estimated DP value in the present paper and denote the block copolymer as (PMMA$_9$-*r*-PC$_6$MAI$_2$)-*b*-PBzMA$_{62}$. The self-assembly obtained at 2 h was studied using transmission electron microscopy (TEM) and dynamic light scattering (DLS) (Figure 3.3). For the TEM analysis, the polymerization mixture was diluted with ethanol (50 times), dropped on a TEM grid, and dried under vacuum condition. The TEM image (image A in Figure 3.3a, median size of the vesicles is 140 nm) suggests the generation of a vesicle. For the DLS analysis, the polymerization mixture was diluted with water (50 times). The DLS analysis (Figure 3.3 and Table 3.2) shows that the hydrodynamic size (intensity-average DLS peak top value) of the assembly was 220 nm (in a water/ethanol (98.6/1.4 (v/v)) mixture). The size (diameter = 220 nm) of the assembly was larger than the two-fold (ca. 37 nm) of the contour length (ca. 18 nm = 0.25 nm × 73 (= 9

+ 2 + 62) monomer units in total) of the block copolymer, suggesting that the generated assembly was not a micelle but a vesicle. (The size of the assembly shown in the TEM image is somewhat smaller than that determined using DLS, because the assembly was dry in the TEM analysis and swollen in the DLS analysis (in the solvent).) The solid content at 2 h was 19.6 wt% (2.7 wt% of the macroinitiator and 16.9 wt% of the PBzMA segment generated during the PISA). Thus, we successfully obtained a ($PMMA_9$-*r*-$PC_6MAI_2$)-*b*-$PBzMA_{62}$ nano-capsule with a relatively high solid content.

**Synthesis of Crosslinked Nano-capsules.**

In order to stabilize (fix) the nano-capsule structure, we co-used a crosslinkable divinyl monomer, i.e., ethylene glycol dimethacrylate (EGDMA), as well as BzMA in PISA. A small amount of EGDMA (6.25% molar fraction of EGDMA and 93.75% molar fraction of BzMA) was used to crosslink the polymer at a later stage of polymerization, i.e., after the assembly (nano-capsule) was formed.

**Table 3.3.** Synthesis of Crosslinked Nano-capsule at 70 °C.

| $[BzMA]_0/[EGDMA]_0/[(PMMA_9$-*r*-$PC_6MAI_2)$–$I]_0/[V65]_0$ (equiv.)[a] | *t* (h) | Hydrodynamic size in DLS (*d*(DLS)) (nm)[b] | DLS size distribution index[c] |
|---|---|---|---|
| 93.75/6.25/1/0.5 | 2 | 234 | 0.139 |

[a] Solvent was ethanol (70 wt%). [b]Intensity-average DLS peak-top value (in water/ethanol mixture (98.6/1.4 (v/v))). [c]The intensity-average size distribution index in DLS defined as [(standard deviation)/(peak-top value)]$^2$ (in water/ethanol mixture (98.6/1.4 (v/v))).

We carried out the same polymerization as above (Table 3.2) except co-using EGDMA (Table 3.3) for 2 h. Both BzMA and EGDMA are methacrylates. We assume that the two monomers have same reactivity and that the total monomer conversion was the same as that using BzMA only (62% (Table 3.2)). Thus, we denote the obtained polymer as ($PMMA_9$-*r*-$PC_6MAI_2$)-*b*-$(PBzMA$-*r*-$PEGDMA)_{62}$. As the TEM image (image B in Figure 3.3b, median

size of the vesicles is 310 nm) shows, a vesicle was generated. The DLS analysis (Figure 3.3b and Table 3.3) showed that the hydrodynamic size (DLS peak top) of the assembly in a water/ethanol (98.6/1.4 (v/v)) mixture was 234 nm, which is close to that (220 nm) of the non-crosslinked vesicle obtained using BzMA only (Figure 3.3a and Table 3.2).

We added THF to the non-crosslinked (Figure 3.3a) and crosslinked (Figure 3.3b) vesicles. The non-crosslinked vesicle decomposed to single polymer chains with a hydrodynamic size of 7 nm (in a THF/ethanol (98.6/1.4 (v/v)) mixture), because the PBzMA segment is soluble in THF. In contrast, the crosslinked vesicle was stable in THF (THF/ethanol (98.6/1.4 (v/v)) mixture) with a hydrodynamic size of 191 nm, which is close to that (234 nm) in water (water/ethanol (98.6/1.4 (v/v)) mixture). The TEM analysis confirmed that the assembly structure (vesicle structure) was unchanged in water (image B in Figure 3.3) and THF (image C in Figure 3.3, median size of the vesicles is 183 nm). Thus, we successfully obtained the crosslinked vesicle. We observed that the outline of the vesicle (shell layer) in image C is much obvious than that in image B. It could be due to the different contrast in TEM image B and C. Another possible reason might be due to the different drying speed of different solvents (ethanol for TEM image B and THF for TEM image C).

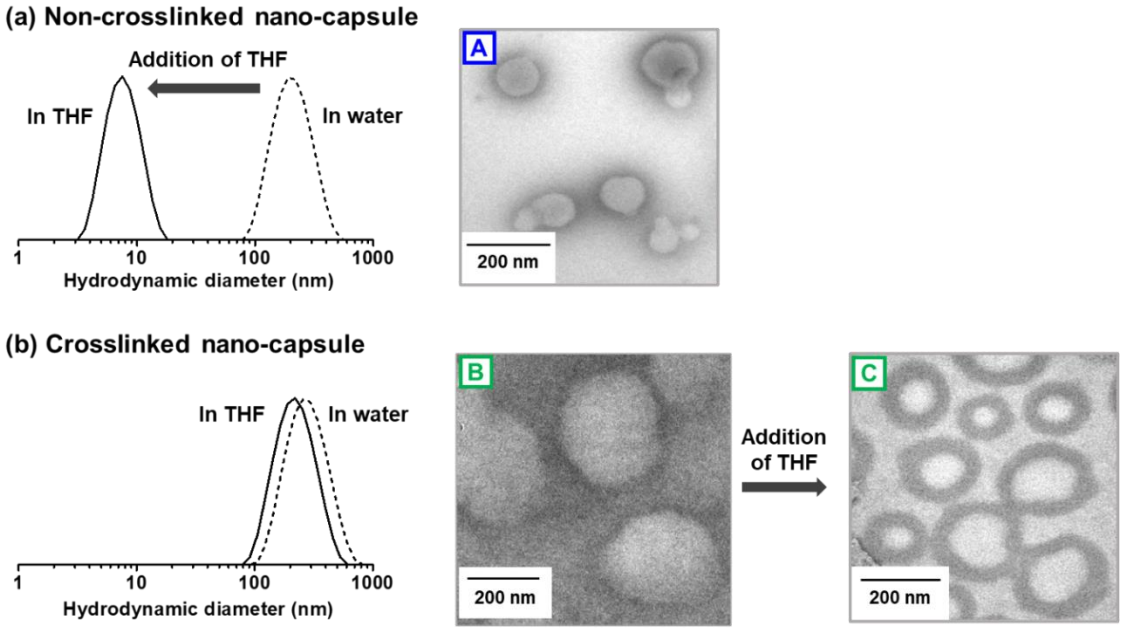


**Figure 3.3.** DLS curves in water (water/ethanol mixture (98.6/1.4 (v/v)) (dashed line) and in THF (THF/ethanol mixture (98.6/1.4 (v/v)) (solid line) for (a) $(PMMA_9$-*r*-$PC_6MAI_2)$-*b*-$PBzMA_{62}$ and (b) $(PMMA_9$-*r*-$PC_6MAI_2)$-*b*-$(PBzMA$-*r*-$PEGDMA)_{62}$ nano-capsules. TEM images for A = $(PMMA_9$-*r*-$PC_6MAI_2)$-*b*-$PBzMA_{62}$, B = $(PMMA_9$-*r*-$PC_6MAI_2)$-*b*-$(PBzMA$-*r*-$PEGDMA)_{62}$ in ethanol, and C = $(PMMA_9$-*r*-$PC_6MAI_2)$-*b*-$(PBzMA$-*r*-$PEGDMA)_{62}$ in THF.

**Polymerizations of MMA Using Catalytic Nano-capsule.**

The obtained crosslinked nano-capsule (Table 3.3) contains QAI ($C_6MAI$) units on both outer and inner surfaces of the nano-capsule (Scheme 3.2). The QAI unit can work as a RCMP catalyst, motivating us to use this crosslinked nano-capsule as a unique catalytic nano-capsule. We exploited the outer and inner QAI groups in a dual manner and conducted RCMP outside and inside the nano-capsule.

A mixture of MMA (52 wt% of total reaction mixture, 100 equiv., monomer), CP–I (1 equiv., initiator), and the crosslinked nano-capsule (13 wt% of total reaction mixture, 0.5 equiv. of the $C_6MAI$ unit, catalyst), and toluene (35 wt% of total reaction mixture, solvent) was heated at 70 °C (Table 3.4 (entry 1) and Figure 3.4 (circles)). The monomer (MMA) conversion reached 42% for 24 h. For 24 h, the polymer generated outside the nano-capsule had a $M_n$ value of 5100, which is close to the theoretical value (4400), and a $Đ$ value of 1.22. In order to further

decrease the *Đ* value, we added a small amount of $I_2$ (0.0125 equiv. to CP–I) (Table 3.4 (entry 2) and Figure 3.4 (squares)). The *Đ* value slightly decreased to 1.20 for 24 h (monomer conversion = 28% and $M_n$ = 3200). $I_2$ is a good deactivator of Polymer$^\bullet$ and its addition can ensure a sufficiently high deactivation rate.[22, 40]

While a low-dispersity polymer was successfully obtained, the polymerization was relatively slow (Table 3.4 (entry 2) and Figure 3.4 (squares)). To increase the polymerization rate, we added a small amount (0.25 equiv.) of an azo initiator, i.e., 2,2'-azobis(2-methylpropionitrile) (AIBN) (Table 3.4 (entry 3) and Figure 3.4 (triangles)). With the addition of AIBN, the polymerization rate increased by a factor of approximately 21 (Figure 3.4), even though the amount of the crosslinked nano-capsule was approximately halved (6 wt% for Table 3.4 (entry 3) *vs.* 13 wt% for Table 3.4 (entry 1)). The monomer (MMA) conversion reached 91% for 9 h, while keeping a small *Đ* value (1.23). These results (Table 3.4 and Figure 3.4) demonstrate that the crosslinked nano-capsule successfully worked as a heterogeneous catalyst in RCMP of MMA (outside the nano-capsule). (The RCMP inside the nano-capsule will be described below.) We supposed the PMMA was formed by dissolving in the solvent but not absorbing on the nano-capsule. The nano-capsule works as a catalyst to coordinate to the polymer-iodide, generating polymer radical chain which dissolve in the solvent.

**Table 3.4.** RCMPs of MMA using Catalytic Nano-capsule.

| Entry | $[MMA]_0/[CP–I]_0/[I_2]_0/[AIBN]_0$ (equiv.)[a] | Catalytic nano-capsule | $T$ (°C) | $t$ (h) | Conv. (%)[b] | $M_n$ ($M_{n,theo}$[c]) | $Đ$ |
|---|---|---|---|---|---|---|---|
| 1 | 100/1/0/0 | 13 wt% (0.5 equiv. $C_6$MAI unit) | 70 | 24 | 42 | 5100 (4200) | 1.22 |
| 2 | 100/1/0.0125/0 | 13 wt% (0.5 equiv. $C_6$MAI unit) | 70 | 24 | 28 | 3200 (2800) | 1.20 |
| 3 | 100/1/0.0125/0.25 | 6 wt% (0.2 equiv. $C_6$MAI unit) | 70 | 9 | 91 | 9800 (9100) | 1.23 |

[a]52 wt% MMA, 13 wt% catalytic nano-capsule, and 35 wt% solvent (toluene) for entries 1 and 2 and 56 wt% MMA, 6 wt% catalytic nano-capsule, and 38 wt% solvent (toluene) for entry 3. [b]Monomer conversions determined with $^1$H NMR. [c]Theoretical $M_n$ values calculated according to ($[MMA]_0/[CP–I]_0$)×(monomer conversion).

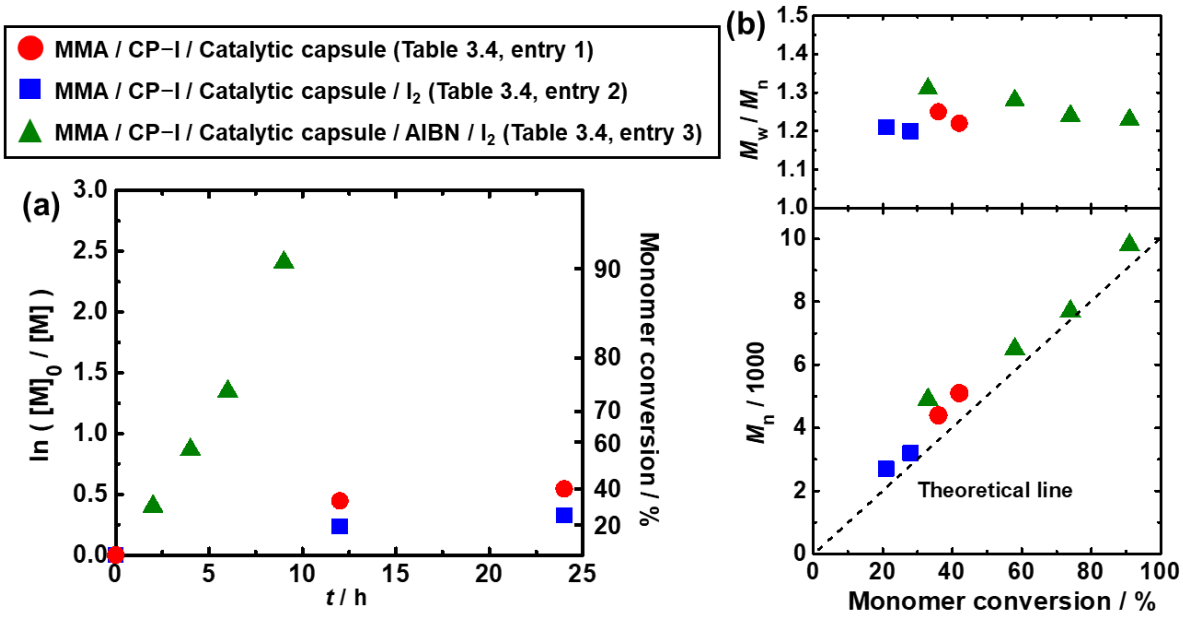


**Figure 3.4.** Plots of (a) $\ln([M]_0/[M])$ *vs.* time ($t$) and (b) $M_n$ and $M_w/M_n$ *vs.* monomer conversion for the MMA/CP−I/(catalytic capsule)/$I_2$/AIBN systems (70 °C). The reaction conditions are given in Table 4. The symbols are indicated in the figure.

**Polymerizations of Several Monomers Using Catalytic Nano-capsule.**

Besides MMA, we studied RCMPs of other functional methacrylates, i.e., BzMA and poly(ethylene glycol) methyl ether methacrylate (PEGMA) (molecular weight = 300), and other families of monomer, i.e., styrene (St) and acrylonitrile (AN) using the catalytic nano-

capsule (Table 5). Relatively low-dispersity polymers ($Đ$ = 1.34–1.48) were obtained with 75–89% monomer conversions for 1–8 h. The results suggest a wide monomer scope of the catalytic nano-capsule.

**Table 3.5.** RCMPs of BzMA, PEGMA, St, and AN using Catalytic Nano-capsule.

| Entry | Monomer | $[Monomer]_0$/ $[CP–I]_0$/ $[Azo\ initiator]_0$ (equiv.)[a,b] | Catalytic nano-capsule | $T$ (°C) | $t$ (h) | Conv. (%)[c] | $M_n$[d] ($M_{n,theo}$[e]) | $Đ$[d] |
|---|---|---|---|---|---|---|---|---|
| 1 | BzMA | 100/1/0.25 | 9 wt% (0.8 equiv.) | 70 | 2 | 89 | 14000 (16000) | 1.48 |
| 2 | PEGMA | 100/1/1 | 6 wt% (0.6 equiv.) | 60 | 2 | 89 | 23000 (27000) | 1.35 |
| 3 | St | 100/1/1 | 9 wt% (0.5 equiv.) | 80 | 8 | 75 | 5500 (7800) | 1.34 |
| 4 | AN | 100/1/0.125 | 6 wt% (0.1 equiv.) | 75 | 1 | 86 | 19000 (4600) | 1.48 |

[a]38 wt% monomer, 9 wt% catalytic nano-capsule, and 53 wt% solvent (toluene) for entries 1 and 3, 58 wt% monomer, 6 wt% catalytic nano-capsule, and 36 wt% solvent (toluene) for entry 2 and 4. [b]Azo intiator = AIBN for entries 1, 3, and 4 and V65 for entry 2. [c]Monomer conversions determined with $^1$H NMR. [d]PMMA-calibrated THF-GPC values for entries 1 and 3 and PMMA-calibrated DMF-GPC values for entries 2 and 4. [e]Theoretical $M_n$ values calculated according to ($[monomer]_0/[CP–I]_0$)×(monomer conversion).

**Recycling of Catalytic Nano-capsule.**

The catalytic nano-capsule was able to be recovered from the polymerization solution through precipitation (using toluene as a good solvent to dilute reaction mixture and collect the nano-capsule by subsequent centrifugation). To demonstrate the recyclability of the catalytic nano-capsule, we used the recovered catalytic nano-capsule in the polymerizations of MMA under the same condition (condition in Table 3.4 (entry 3)) in recycled manners. We added $I_2$ in each run, because $I_2$ was washed out from the nano-capsule in the recovery process. In ten polymerization cycles, similar monomer conversions (83–91%) and $M_n$ values (9200–9800) were consistently achieved for the 9 h polymerization (Figure 3.5 and Table 3.6). The $Đ$ value gradually increased from 1.23 (first cycle) to 1.39 (tenth cycle), suggesting a gradual loss of the catalytic activity. Nevertheless, the $Đ$ value was still relatively small (1.39) even in the tenth cycle. The results show the good recyclability of the catalytic nano-capsule. The size of

the catalytic nano-capsule might increase after first cycle due to the occupancy of polymer (PMMA) in the core and thus expanding the nano-capsule. But the increase in size should be minor since the vesicular structure was crosslinked (covalently stabilized).

**Table 3.6.** RCMPs of MMA using Recycled Catalytic Nano-capsule.

| Cycle[a] | $[MMA]_0/[CP–I]_0/[AIBN]_0/[I_2]$ (mM)[b] | Catalytic nano-capsule | $T$ (°C) | $t$ (h) | Conv. (%)[c] | $M_n$ ($M_{n,theo}$[d]) | $Đ$ |
|---|---|---|---|---|---|---|---|
| 1 | 8000/80/20/1 (100/1/0.25/0.0125) (equiv.) | 6 wt% (0.2 equiv. $C_6$MAI unit) | 70 | 9 | 91 | 9800 (9100) | 1.23 |
| 2 | 8000/80/20/1 (100/1/0.25/0.0125) (equiv.) | 6 wt% (0.2 equiv. $C_6$MAI unit) | 70 | 9 | 87 | 9200 (8700) | 1.22 |
| 3 | 8000/80/20/1 (100/1/0.25/0.0125) (equiv.) | 6 wt% (0.2 equiv. $C_6$MAI unit) | 70 | 9 | 84 | 9400 (8400) | 1.24 |
| 4 | 8000/80/20/1 (100/1/0.25/0.0125) (equiv.) | 6 wt% (0.2 equiv. $C_6$MAI unit) | 70 | 9 | 85 | 9500 (8500) | 1.31 |
| 5 | 8000/80/20/1 (100/1/0.25/0.0125) (equiv.) | 6 wt% (0.2 equiv. $C_6$MAI unit) | 70 | 9 | 90 | 9500 (9000) | 1.33 |
| 6 | 8000/80/20/1 (100/1/0.25/0.0125) (equiv.) | 6 wt% (0.2 equiv. $C_6$MAI unit) | 70 | 9 | 86 | 9800 (8600) | 1.33 |
| 7 | 8000/80/20/1 (100/1/0.25/0.0125) (equiv.) | 6 wt% (0.2 equiv. $C_6$MAI unit) | 70 | 9 | 85 | 9800 (8500) | 1.36 |
| 8 | 8000/80/20/1 (100/1/0.25/0.0125) (equiv.) | 6 wt% (0.2 equiv. $C_6$MAI unit) | 70 | 9 | 83 | 9600 (8300) | 1.32 |
| 9 | 8000/80/20/1 (100/1/0.25/0.0125) (equiv.) | 6 wt% (0.2 equiv. $C_6$MAI unit) | 70 | 9 | 86 | 10400 (8600) | 1.38 |
| 10 | 8000/80/20/1 (100/1/0.25/0.0125) (equiv.) | 6 wt% (0.2 equiv. $C_6$MAI unit) | 70 | 9 | 86 | 10400 (8600) | 1.39 |

[a]Polymerization cycle. [b]56 wt% MMA, 6 wt% catalytic nano-capsule, and 38 wt% solvent (toluene). [c]Monomer conversions determined from NMR. [d]Theoretical $M_n$ calculated according to $([MMA]_0/[CP–I]_0)\times$(monomer conversion).

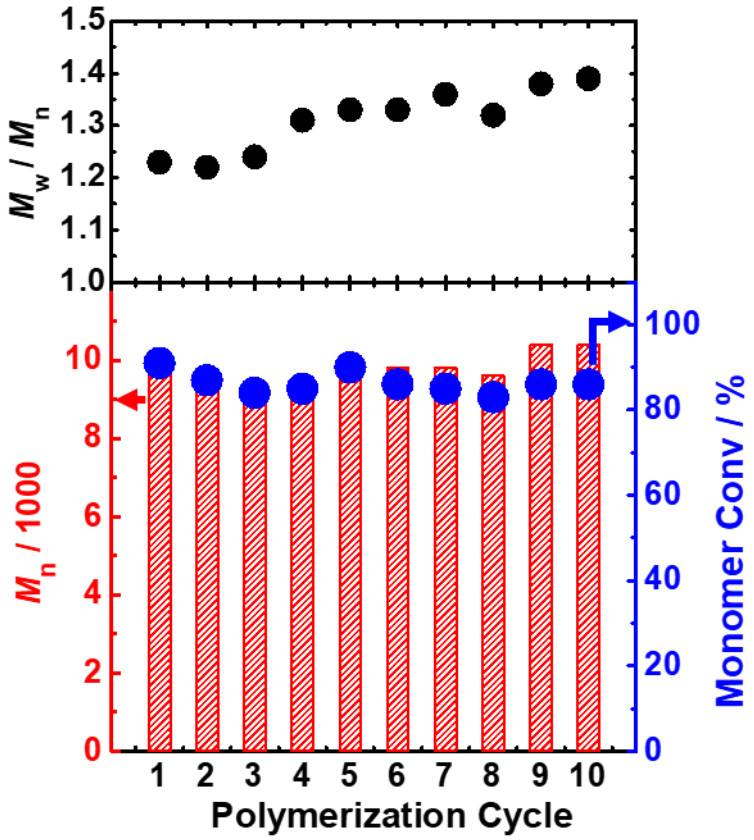


**Figure 3.5.** RCMPs of MMA using catalytic nano-capsule in a recycled manner. The reaction condition for each cycle was the same as Table 4 (entry 3): MMA/CP−I/(catalytic capsule)/$I_2$/AIBN system (70 °C) where $[MMA]_0$ = 8 M; $[CP\text{-}I]_0$ = 80 mM; $[AIBN]_0$ = 20 mM; $[I_2]_0$ = 1 mM.

**Use of Catalytic Nano-capsule as Nano-reactor.**

We also utilized the nano-capsule as a catalytic nano-reactor. The present nano-capsule bears QAI groups not only on the outer surface but also on the inner surface, and hence we conducted RCMP in the cavity of the nano-capsule. We first dispersed the catalytic nano-capsule (6 wt% of total reaction mixture) in toluene (38 wt% of total reaction mixture) at room temperature. After stirring for 2 h, we added a mixture of MMA (100 equiv.), CP–I (1 equiv.), AIBN (0.25 equiv.), and $I_2$ (0.025 equiv.) and stirred the whole mixture for another 2 h at room temperature to ensure that the monomer (MMA), initiating dormant species (CP–I), and other species diffuse into the cavity of the nano-capsule. (We did not conduct the pre-stirring (totally 4 h) in the above-mentioned study for polymers outside the nano-capsule. However, the

monomer, initiating dormant species, and other species should diffuse in the cavity and the polymerization should occur in the cavity in the above-mentioned study, too. Here, to study RCMP in the cavity in more detail, we conducted the pre-stirring to ensure their diffusion into the cavity.) We subsequently heated the mixture at 70 ℃ for 6 h. The polymerization took place in both inside and outside the nano-capsule. After the polymerization, we collected the catalytic nano-capsule by immersion in toluene to fully remove small molecules from the cavity. We suppose that the polymer formed outside the nano-capsule was rinsed out while the polymer formed inside the nano-capsule stayed in the cavity because large molecules (polymer chains) were not able to penetrate the nano-capsule shell.

The collected nano-capsule was analyzed with DLS and TEM. The DLS analysis showed that the hydrodynamic size (DLS peak top) increased from 191 nm (before the polymerization in the cavity) in THF (solvent) to 396 nm (after the polymerization in the cavity) in THF (solvent). The increase in the particle size suggests an increase in the osmotic pressure in the cavity and hence the presence of polymers in the cavity. The TEM image (Figure 3.6) shows that the cavity of the nano-capsule was loaded with the polymer (PMMA). The cavity was empty before the MMA polymerization (Figure 3.3c). After the MMA polymerization, the cavity was dark in color (Figure 3.6) which is different from Figure 3.3c. The results demonstrate that the polymerization occurred in the cavity and that the nano-capsule served as a catalytic nano-reactor for RCMP. Interestingly, in the present system, the hydrophobic (PMMA) nanoparticle was obtained in a stable manner in the hydrophobic (MMA and toluene) medium, unlike conventional emulsion and polymerizations utilizing hydrophilic media to generate hydrophobic particles. This aspect is a unique feature to use the nano-reactor. However, it is not possible to remove, isolate and characterize the PMMA synthesized within the cavity of the nano-capsule, because ester linkages present in EGDMA, PMMA, PBzMA,

and PMMA-*r*-$PC_6MAI$. With base degradation, it is not possible to selectively cleave the ester linkages in EGDMA from others.

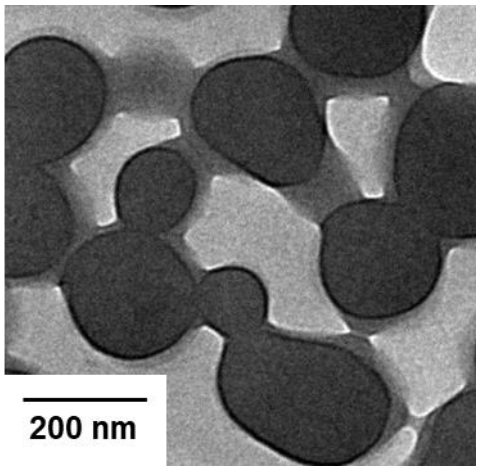


**Figure 3.6.** TEM image of PMMA-loaded catalytic nano-capsule.

### 3.3. Conclusions

QAI-containing nano-capsule was obtained via self-catalyzed RCMP-PISA at a relatively high (19.6 wt%) solid content. The obtained nano-capsule was successfully utilized as a heterogeneous catalyst in RCMPs of MMA, BzMA, PEGMA, St, and AN, yielding relatively low-dispersity ($Đ$ = 1.23–1.48) polymers at high monomer conversions (75–91%). A good recyclability of the catalytic nano-capsule was demonstrated in RCMPs of MMA in ten cycles. The nano-capsule bears QAI groups on the inner surface (as well as the outer surface) and hence worked as a catalytic nano-reactor, yielding a PMMA-loaded nano-capsule. In the future, the nano-reactor may be used for block copolymerizations to create functional micro-phase separation nanoparticles and selective polymerization for monomers with different property (i.e., hydrophilic and hydrophobic monomers) for example. The self-catalyzed synthesis of a nano-capsule at a relatively high solid content and a unique application of the obtained nano-capsule as a dual heterogeneous catalyst are attractive and interesting features of this study.

## 3.4 Experimental Section

### Materials.

Tetrahydrofuran (THF) (>99.5%, Kanto Chemical, Japan), 1-iodohexane (≥98%, Sigma-Aldrich), 2,2′-azobis(2-methylpropionitrile) (AIBN) (95%, Wako Pure Chemical, Japan), 2-(dimethylamino)ethyl methacrylate (DMAEMA) (≥98.5%, TCI), 2-iodo-2-methylpropionitrile (CP−I) (>95%, TCI), acetone (≥99.5%, Fisher Scientific, USA), benzyl methacrylate (BzMA) (>98%, TCI), chloroform (>99.2%, VWR Chemicals, USA), methyl methacrylate (MMA) (>99.8%, Tokyo Chemical Industry (TCI)), poly(ethylene glycol) methyl ether methacrylate (PEGMA) (average molecular weight = 300) (98%, Sigma-Aldrich, USA), acrylonitrile (AN) (>99%, TCI), 2,2'-azobis(2,4-dimethylvaleronitrile) (V65) (95%, Wako), styrene (St) (>99.8%, TCI), ethylene carbonate (EC, >99%, TCI), ethanol (≥99.5%, absolute, Fisher Scientific), toluene (ACS reagent grade, VWR International), hexane (>99%, International Scientific, Singapore) and *N*,*N*-dimethylformamide (DMF) (>99.5%, Kanto), were used as received.

### Measurement.

A Shimadzu i-Series Plus liquid chromatograph LC-2030c Plus (Kyoto, Japan) equipped with a Shodex (Japan) KF-804L mixed gel column (300 × 8.0 mm; bead size = 7 μm; pore size = 1500 Å) and a Shodex LF-804 mixed gel column (300 × 8.0 mm; bead size = 6 μm; pore size = 3000 Å) was used with THF eluent for the GPC analysis. The flow rate was 0.7 mL/min (40 $^{o}$C). A Shimadzu LC-2030c Plus equipped with two Shodex LF-804 mixed gel columns (300 × 8.0 mm; bead size = 6 μm; pore size = 3000 Å) and a Shodex KD-802 (300 × 8.0 mm; bead size = 6 μm; pore size = 150 Å) was used with DMF eluent for the GPC analysis. The flow rate was 0.34 mL/min (40 °C). The DMF eluent contained LiBr (10 mM). A refractive

index detector (RID-20A) was used for sample detection for THF-GPC and for DMF-GPC. For both THF-GPC and DMF-GPC systems, standard poly(methyl methacrylate)s (PMMAs) was used to calibrate the column system.

The NMR spectra were recorded on Bruker (Germany) BBFO400 spectrometer (400 MHz) at ambient temperature. $CDCl_3$ (Cambridge Isotope Laboratories, USA) were used as the solvents for the NMR analysis, and the chemical shift was calibrated using residual undeuterated solvents or tetramethylsilane (TMS) as the internal standard. The monomer conversions and the monomer compositions in the obtained polymers were determined with $^1H$ NMR.

A JEM-1400 transmission electron microscope (JEOL, Japan) operated at 100 kV was used to obtain transmission electron microscopy (TEM) images. The TEM grid was carbon-coated on 200 mesh (copper) (Ted Pella, USA).

A Malvern Zetasizer Nano ZSP (Worcestershire, UK) was used for the dynamic light scattering (DLS) measuremen. The test angle for the DLS analysis was 173° (backscattering detection). Ethanol, water or THF were used as the solvent.

**Synthesis of Macroinitiator (PMMA-*r*-PC$_6$MAI–I).**

A mixture of MMA (7.5 g, 75 mmol), $C_6$MAI (1.46 g, 3.95 mmol), and CP−I (0.77 g, 3.95 mmol) was heated in a 50 mL flask at 60 °C under argon atmosphere with magnetic stirring. After 1 h, the mixture was quenched to room temperature and diluted with acetone (10 mL). The solution was dropped into a mixture of hexane/ethanol (7/3 (v/v), 100 mL) for purification. The reprecipitation was repeated twice to complete remove the monomers. The polymer was collected and dried in vacuo to give PMMA-*r*-$PC_6$MAI as a yellow solid. Yield: 36% (3.54 g). $M_n$ = 1700 and $Đ$ = 1.08 after purification.

**Self-catalyzed PISA.**

In a typical run, a mixture of BzMA monomer (1 g), a macroinitiator (PMMA-*r*-$PC_6MAI$), and V65 was heated in a Schlenk flask at 70 °C under argon atmosphere with magnetic stirring. After a prescribed time *t*, an aliquot (0.1 mL) of the solution was taken out by a syringe, quenched to room temperature, and analyzed with GPC and $^1$H NMR. An aliquot (0.1 mL) was diluted with ethanol, water or THF for DLS and TEM.

**General Procedure for Polymerization.**

In a typical run, a mixture of a monomer (1 g), catalytic nano-capsules, CP−I (alkyl iodide initiator), and solvent was heated in a Schlenk flask at 60–80 °C under argon atmosphere with magnetic stirring. After a prescribed time *t*, an aliquot (0.1 mL) of the solution was taken out by a syringe, quenched to room temperature, and analyzed with GPC and $^1$H NMR.

**Recyclability Test (Recovery of Catalytic Nano-capsule).**

In a typical run, a mixture of an MMA (4.5 g, 56 wt% of total reaction mixture, 100 equiv.), catalytic nano-capsules (0.5 g, 6 wt% of total reaction mixture, 0.2 equiv.), CP−I (alkyl iodide initiator, 1 equiv.), $I_2$ (0.0125 equiv.), AIBN (0.25 equiv.), and toluene (38 wt%) of total reaction mixture was heated in a Schlenk flask at 70 °C under argon atmosphere with magnetic stirring. After 9 h, the reaction mixture was quenched to room temperature, and analyzed with GPC and $^1$H NMR. The reaction mixture was diluted with toluene and the catalytic nano-capsule was collected by centrifugation. The catalytic nano-capsule was dried in vacuum overnight then used for next MMA polymerization cycle.

**RCMP in the Cavity of Nano-capsule.**

In a typical run, a mixture of a catalytic nano-capsule (6 wt% of total reaction mixture) and toluene (38 wt% of total reaction mixture) was stirred at room temperature. After 2 h, a mixture of MMA (100 equiv., 56 wt% of total reaction mixture), CP–I (1 equiv.), AIBN (0.25 equiv.), and $I_2$ (0.025 equiv.) was added and stirred the whole mixture for another 2 h at room temperature. The whole mixture was then heated at 70 ℃ for 6 h. After 6 h, the mixture was quenched to room temperature, and stirred with excess toluene then centrifuged to collect the nano-capsule. The collected capsule was dried in vacuum overnight and analyzed by TEM.

## References


1. Shi, Q.; Chen, Y.; Yang, J.; J. Yang. *Chem. Commun.* **2021**, *57*, 11390-11393.
2. Hou, W.; Li, Z.; Xu, L.; Li, Y.; Shi, Y.; Chen, Y. *ACS Macro Lett.* **2021**, *10*, 1260-1265.
3. Sarkar, J.; Lim, Y.F.; Goto, A. *Macromol. Chem. Phys.* **2021**, *222*, 2100349.
4. Sarkar, J.; Jackson, A. W.; Herk, A. M. V.; Goto, A. *Polym. Chem.* **2020**, *11*, 3904-3912.
5. Sarkar, J.; Xiao, L.; Jackson, A. W.; Herk, A. M. V.; Goto, A. *Polym. Chem.* **2018**, *9*, 4900-4907.
6. Chen, C.; Wylie, R. A. L.; Klinger, D.; Connal, L. A. *Chem. Mater.* **2017**, *29*, 1918–1945.
7. Gaitzsch, J.; Huang, X.; Voit, B. *Chem. Rev.* **2016**, *116*, 1053–1093.
8. Cui, J.; Koeverden, M. P. V.; Müllner, M.; Kempe, K.; Caruso, F. *Adv. Colloid Interface Sci.* **2014**, *207*, 14–31.
9. Warren, N. J.; Armes, S. P. *J. Am. Chem. Soc.* **2014**, *136*, 10174– 10185.
10. Canning, S. L.; Smith, G. N.; Armes, S. P. *Macromolecules* **2016**, *49*, 1985-2001.
11. Zhang, Y.; Yu, L.; Dai, X.; Zhang, L.; Tan, J. *ACS Macro Lett.* **2019**, *8*, 1102-1109.
12. Haye, J. L. d. l.; Zhang, X.; Chaduc, I.; Brunel, F.; Lansalot, M.; D'Agosto, F. *Angew. Chem. Int. Ed.* **2016**, *55*, 3739.
13. Wang, G.; Schmitt, M.; Wang, Z.; Lee, B.; Pan, X.; Fu, L.; Yan, J.; Li, S.; Xie, G.; Bockstaller, M. R.; Matyjaszewski, K. *Macromolecules* **2016**, *49*, 8605-8615.
14. Alzahrani, A.; Zhou, D.; Kuchel, R. P.; Zetterlund, P. B.; Aldabbagh, F. *Polym. Chem.* **2019**, *10*, 2658-2665.
15. Shi, B.; Zhang, H.; Liu, Y.; Wang, J.; Zhou, P.; Cao, M.; Wang, G. *Macromol. Rapid Commun.* **2019**, *40*, 1900547.
16. Qiao, X. G.; Lansalot, M.; Bourgeat-Lami, E.; Charleux, B. *Macromolecules* **2013**, *46*, 4285-4295.
17. Yoshida, E. *Colloid Polym. Sci.* **2013**, *291*, 2733–2739.
18. Goto, A.; Zushi, H.; Hirai, N.; Wakada, T.; Tsujii Y.; Fukuda, T. *J. Am. Chem. Soc.* **2007**, *129*, 13347–13354.
19. Goto, A.; Suzuki, T.; Ohfuji, H.; Tanishima, M.; Fukuda, T.; Tsujii, Y.; Kaji, H. *Macromolecules* **2011**, *44*, 8709–8715.
20. Goto, A.; Ohtsuki, A.; Ohfuji, H.; Tanishima, M.; Kaji, H. *J. Am. Chem. Soc.* **2013**, *135*, 11131–11139.
21. Ohtsuki, A.; Lei, L.; Tanishima, M.; Goto, A.; Kaji, H. *J. Am. Chem. Soc.* **2015**, *137*, 5610–5617.
22. Wang, C-G; Chang, J. J.; Yong, E. J. F.; Niino, H.; Chatani, S.; Hsu, S. Y.; Goto, A. *Macromolecules* **2020**, *53*, 51-58.
23. Böhm, L. L. *Angew. Chem., Int. Ed.* **2003**, *42*, 5010−5030.
24. Kickelbick, G.; Paik, H.-j.; Matyjaszewski, K. *Macromolecules* **1999**, *32*, 2941−2947.
25. Haddleton, D. M.; Duncalf, D. J.; Kukulj, D.; Radigue, A. P. *Macromolecules* **1999**, *32*, 4769−4775.
26. Shen, Y.; Zhu, S.; Zeng, F.; Pelton, R. H. *Macromolecules* **2000**, *33*, 5427−5431.
27. Nguyen, J. V.; Jones, C. W. *Macromolecules* **2004**, *37*, 1190−1203.
28. Bernhardt, C.; Osman, C. B.; Charleux, B.; Stoffelbach, F. *Polymer* **2015**, *77*, 199−207.
29. Taskin, O. S.; Kiskan, B.; Yagci, Y. *Polym. Int.* **2018**, *67*, 55−60.

30. Munirasu, S.; Aggarwal, R.; Baskaran, D. *Chem. Commun.* **2009**, 4518−4520.
31. Barrientos-Ramírez, S.; Oca-Ramírez, G. M. d.; Ramos- Fernández, E. V.; Sepúlveda-Escribano, A.; Pastor-Blas, M. M.; González-Montiel, A. *Appl. Catal.* **2011**, *406*, 22−33.
32. Ding, S.; Xing, Y.; Radosz, M.; Shen, Y. *Macromolecules* **2006**, *39*, 6399−6405.
33. Kanazawa, A.; Satoh, K.; Kamigaito, M. *Macromolecules* **2011**, *44*, 1927−1933.
34. Lee, H.-C.; Antonietti, M.; Schmidt, B. V. K. J. *Polym. Chem.* **2016**, *7*, 7199−7203.
35. Lee, H.-C.; Fantin, M.; Antonietti, M.; Matyjaszewski, K.; Schmidt, B. V. K. J. *Chem. Mater.* **2017**, *29*, 9445−9455.
36. Shanmugam, S.; Xu, S.; Adnan, N. N. M.; Boyer, C. *Macromolecules* **2018**, *51*, 779−790.
37. Huang, Y.;Li, X.; Le Li, J.;Zhang,B.; Cai, T. *Macromolecules* **2018**, *51*, 7974− 7982.
38. Chu, Y.; Corrigan, N.; Wu, C.; Boyer, C.; Xu, J. *ACS Sustainable Chem. Eng.* **2018**, *6*, 15245− 15253.
39. Goto, A.; Fukuda, T. *Prog. Polym. Sci.* **2004**, *29*, 329−385.
40. Hong, S. C.; Matyjaszewski, K. *Macromolecules* **2002**, *35*, 7592−7605.

## Chapter 4. Synthesis of Degradable and Chemically Recyclable Polymers Using 4,4-Disubstituted Five-Membered Cyclic Ketene Hemiacetal Ester (CKHE) Monomers.


### Abstract

Novel degradable and chemically recyclable polymers were synthesized using five-membered cyclic ketene hemiacetal ester (CKHE) monomers. The studied monomers were 4,4-dimethyl-2-methylene-1,3-dioxolan-5-one (DMDL) and 5-methyl-2-methylene-5-phenyl-1,3-dioxolan-4-one (PhDL). The two monomers were synthesized in high yields (80–90%), which is an attractive feature. DMDL afforded its homopolymer with a relatively high molecular weight ($M_n$ >100 000, where $M_n$ is the number-average molecular weight). DMDL and PhDL were copolymerized with various families of vinyl monomers, i.e., methacrylates, acrylates, styrene, acrylonitrile, vinyl pyrrolidinone, and acrylamide, and various functional methacrylates and acrylate. Such a wide scope of the accessible polymers is highly useful for material design. The obtained homopolymers and random copolymers of DMDL degraded in basic conditions (in the presence of a hydroxide or an amine) at relatively mild temperatures (room temperature to 65 °C). The degradation of the DMDL homopolymer generated 2-hydroxyisobutyric acid (HIBA). The generated HIBA was recovered and used as an ingredient to re-synthesize DMDL monomer, and this monomer was further used to re-synthesize the DMDL polymer, demonstrating the chemical recycling of the DMDL polymer. Such degradability and chemical recyclability of the DMDL polymer may contribute to the circular materials economy.

## 4.1. Introduction

Degradable polymers find numerous applications in, e.g., drug delivery, packaging, and agriculture fields.[1–9] In the field of radical polymerization, degradable polymers are prepared via radical ring-opening polymerization of cyclic ketene acetals (CKAs),[10–14] for example, gaining significant attention. Examples of CKA are 2-methylene-1,3-dioxepane (MDO),[15–23] 5,6-benzo-2-methylene-1,3-dioxepane (BMDO),[24–26] and 2-methylene-4-phenyl-1,3-dioxolane (MPDL)[27–30] (Scheme 4.1). CKAs are homo-polymerized and co-polymerized with other vinyl monomers, affording degradable ester linkages in the polymer backbones. Mechanistically (Scheme 4.1), the radical addition to the carbon–carbon double bond of CKA generates a ring-retained radical. The subsequent intramolecular fragmentation (ring opening) generates a ring-opened radical and provides a degradable ester linkage in the backbone. MDO and BMDO are seven-membered ring, and the ring strain would promote the ring opening. BMDO and MPDL produce benzylic ring-opened radicals, and the stabilization of the radical by the phenyl group would promote the ring opening. The obtained homopolymers and copolymers have been exploited for applications in, e.g., packaging, agrochemical, personal care, and biomedical applications.[10–13]

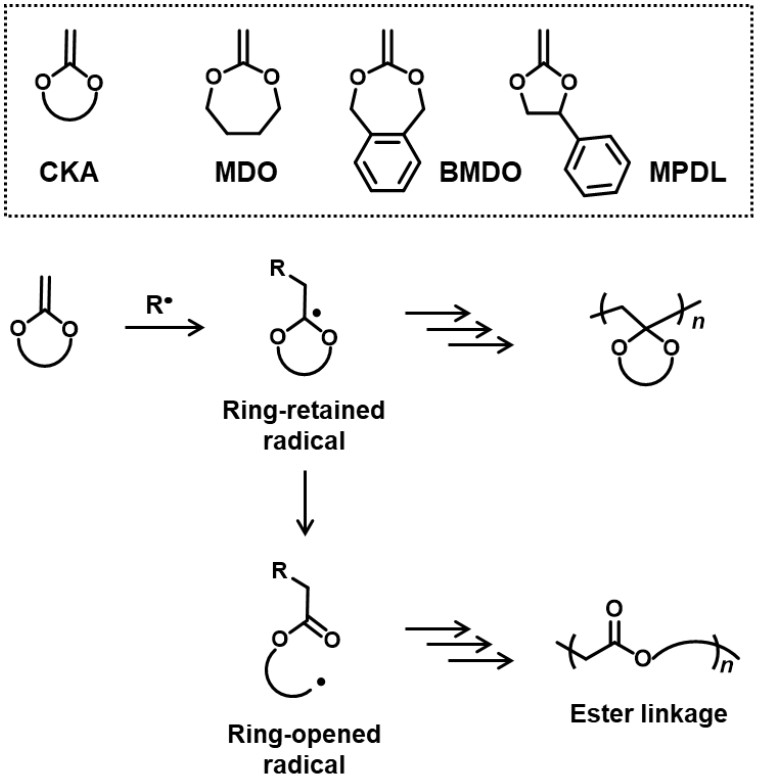


**Scheme 4.1.** CKA monomers and their possible polymerization mechanisms.

In the present work, we are motivated to use cyclic ketene hemiacetal esters (CKHEs) (Scheme 4.2) as alternatives to CKAs. A CKHE bears a carbonyl group, while a CKA does not. We choose 4,4-disubstituted five-membered CKHEs, i.e., 4,4-dimethyl-2-methylene-1,3-dioxolan-5-one (DMDL) and 5-methyl-2-methylene-5-phenyl-1,3-dioxolan-4-one (PhDL) (Scheme 4.2). If their ring opening occurs (Scheme 4.2), a relatively stable polymethacrylate-like radical (a tertiary radical with an ester group and two alkyl groups) is generated. Hence, we hypothesize that the polymerizations of these monomers would prefer ring opening and provide polymers with anhydride degradable linkages in the backbone, which is our initial motivation, although this hypothesis is found to be incorrect as described below.

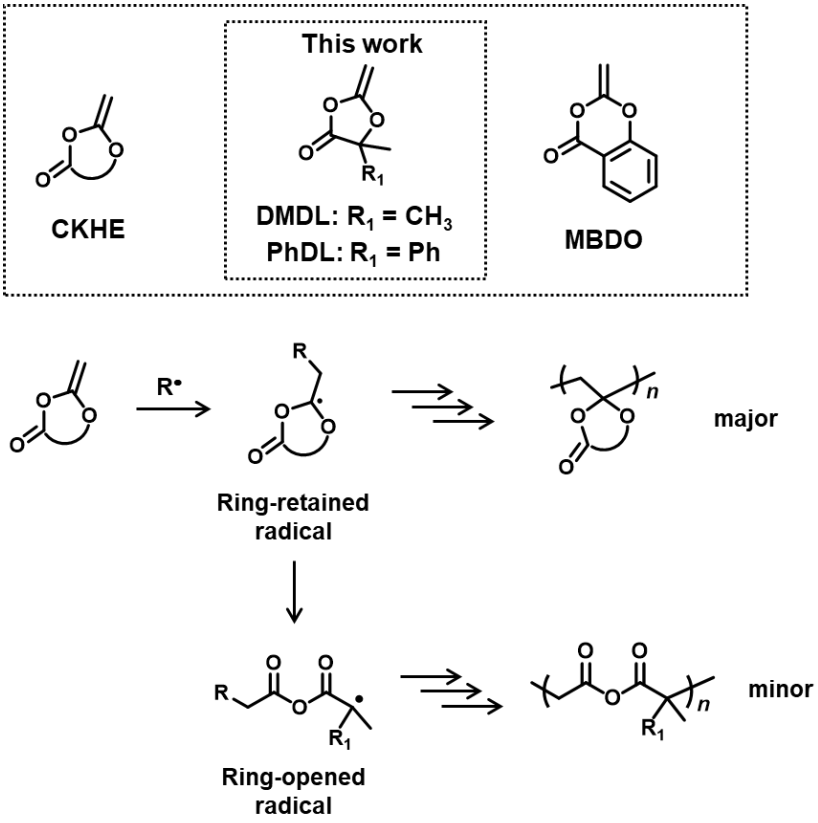


**Scheme 4.2.** CKHE monomers and their possible polymerization mechanisms.

To the best of our knowledge, there is one report of radical polymerization of a CKHE. The studied CKHE was a six-membered CKHE, i.e., 2-methylene-4*H*-benzo[d][1,3]dioxin-4-one (MBDO (Scheme 4.2)).[31] MBDO yielded polymers with ring-retained structures, possibly because its ring-opened radical is a phenyl radical, which is unlikely to generate. The homopolymer of MBDO was insoluble in most of common organic solvents. MBDO was copolymerized with vinyl acetate (VAc), yielding soluble random copolymers. Interestingly, the obtained polymers degraded via acid-assisted hydrolysis. After 5 days of the hydrolysis, only small molecules were detected. The authors suggested the backbone (main chain) scission of the polymers. The nuclear magnetic resonance (NMR) analysis showed that the polymers degraded to acetic acid and salicylic acid, which are raw ingredients of MBDO. Therefore, the authors suggested that the polymers are potentially recyclable, although the recycling was not demonstrated experimentally. These results are interesting findings.

In the present paper, we report the use of DMDL and PhDL as CKHEs to synthesize their homopolymers and random copolymers with several co-monomers. DMDL and PhDL are 4,4-disubstituted five-membered CKHEs bearing two methyl groups (DMDL) or a phenyl group and a methyl group (PhDL) at the 4-position. Unlike the previously reported MBDO, DMDL was able to generate homopolymers soluble in common organic solvents. DMDL and PhDL were also able to be copolymerized with a range of co-monomers. Mechanistically, contrary to our initial hypothesis, DMDL and PhDL generated polymers with ring-retained structures (Scheme 4.2) like MBDO, meaning that the activation energy for generating the ring-opened radical is still high for DMDL and PhDL. Nevertheless, despite the ring-retained structure, the PDMDL homopolymers and copolymers degraded via the backbone scission in basic conditions, where PDMDL is poly(4,4-dimethyl-2-methylene-1,3-dioxolan-5-one). Importantly, NaOH-assisted degradation of PDMDL homopolymers generated 2-hydroxyisobutyric acid (HIBA), which is a raw ingredient of DMDL (Scheme 4.3). We recovered HIBA to synthesize the DMDL monomer and PDMDL, demonstrating the recycling of PDMDL (Scheme 4.3). In this recycling, four of the six carbons of DMDL are recycled via HIBA (four carbons). Thus, the polymers serve as (partly) recyclable polymers. Markedly, the degradation of our polymers does not generate mere $CO_2$ but generates their raw ingredient. This type of polymers is classified to chemically recyclable polymers that can degrade into their raw ingredients or useful oligomers to build other new polymeric materials.[2] Chemically recyclable polymers are attractive in sustainability and may provide more economic values compared with polymers that can degrade into mere $CO_2$.

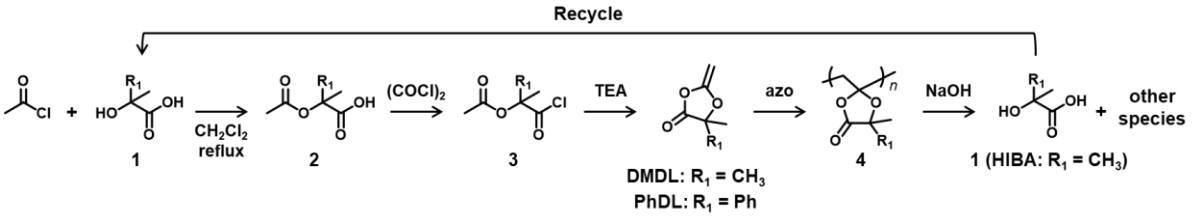


**Scheme 4.3.** Synthesis of monomer, polymerization, hydroxide-assisted degradation of polymer, and recycle of HIBA.

## 4.2. Results and Discussion

### Synthesis of DMDL and PhDL.

DMDL was previously synthesized in the field of synthetic organic chemistry[32] but has not been utilized in polymerization. According to the literature,[32] we synthesized DMDL via an intramolecular cyclization of commercially available compound **3** ($R_1$ = $CH_3$ in Scheme 4.3) (1 equiv.) using triethylamine (TEA) (1.2 equiv.) in dichloromethane under reflux for 5 h. The conversion determined with $^1$H NMR was nearly 100%. There was no report for the synthesis of PhDL. We synthesized PhDL from commercially available compound **1** ($R_1$ = Ph in Scheme 4.3) by referring to the synthesis of a similar compound.[33,34] The compound **1** (1 equiv.) was reacted with acetyl chloride (2.8 equiv.) in dichloromethane under reflux for 2 h, giving compound **2** ($R_1$ = Ph in Scheme 4.3) in a 96% yield after purification (recrystallization). The purified compound **2** (1 equiv.) was subsequently reacted with oxalyl chloride (1.1 equiv.) in a mixture of dichloromethane (99%) and dimethyl formamide (1%) at room temperature overnight, giving compound **3** ($R_1$ = Ph in Scheme 4.3) in a 99% conversion (as determined with $^1$H NMR). The crude compound **3** (1 equiv.) was used for its intramolecular cyclization in the presence of TEA (4.7 equiv.) in dichloromethane under reflux for 2 h, yielding PhDL (Figures 4.7 and 4.8 in Experimental Section). Both DMDL and PhDL were purified by distillation, and we obtained pure DMDL and PhDL in 80% and 90% yields (based on the amount of compound **3**), respectively. The high yields of these two monomers are attractive features in practical use.

In a synthetic point of view, the 4-position of compound **3** must be di-substituted. If the 4-position is not di-substituted (but mono-substituted or non-substituted), the compound **3** is unstable, spontaneously generating an undesired compound (a ketene).[35] This requirement is also another reason why we studied 4,4-disubstituted DMDL and PhDL. The stability of the DMDL monomer (8.9 wt%) was studied in DMSO-$d_6$ (89.3 wt%) under moisture (1.8 wt% water) at room temperature. DMDL decomposed to form compound **2** (Scheme 4.3) via hydrolysis (Figure 4.9 in Experimental Section). The extent of the DMDL hydrolysis was 5%, 11%, and 64% for 0.5 h, 12 h, and 4 days, respectively.

**Homopolymerizations of DMDL and PhDL.**

We conducted a homopolymerization of DMDL (100 equiv., 50 wt%) using 2,2′-azoisobutyronitrile (AIBN) (1 equiv.) as a radical initiator in toluene (50 wt%) at 70 °C for 12 h (Table 4.1, entry 1). The monomer conversion reached 82% (as determined with $^1$H NMR), yielding a PDMDL with $M_n$ = 10 300 and $Đ$ (= $M_w/M_n$) = 1.61, where $M_n$ and $M_w$ are the number- and weight-average molecular weights, respectively, and $Đ$ is the dispersity. The $M_n$ and $Đ$ values are not absolute values but PMMA-calibrated GPC values, where PMMA is poly(methyl methacrylate). The obtained PDMDL was soluble in organic solvents such as chloroform, tetrahydrofuran, and dimethylsulfoxide. Figure 4.1a and b show the $^1$H NMR spectra ($CDCl_3$) of DMDL (monomer) and PDMDL (polymer) (after purification via reprecipitation in hexane/diethyl ether (1/1 (v/v)) (non-solvent)), respectively. The vinyl protons (*a*) of DMDL appearing at 3.62 and 3.70 ppm were converted to the backbone methylene protons (*a*′) of PDMDL appearing at 2.17–3.25 ppm. For PDMDL (Figure 4.1b), the integration ratio of methylene protons (*a*′) and dimethyl protons (*b*′) was nearly 1 (*a*′) to 3 (*b*′), agreeing with the PDMDL structure.

**Table 4.1.** Homopolymerizations of DMDL and random copolymerizations of DMDL with co-monomers.

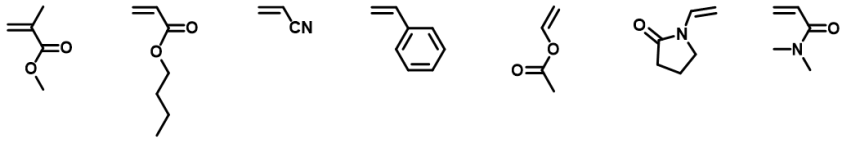


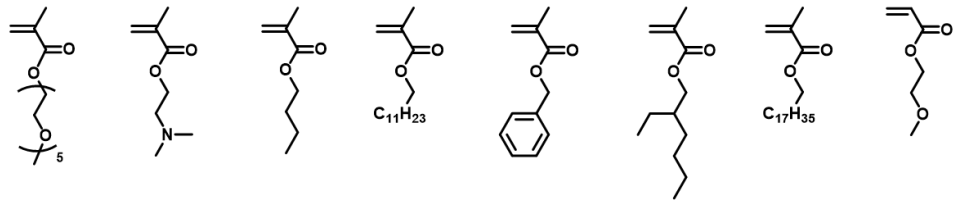


| Entry | Co-monomer (M) | Initiator | Solvent[a] | $[M]_0/[DMDL]_0/[initiator]_0$ (equiv) | $T$ (°C) | $t$ (h) | Conv. (M/DMDL) (%/%)[b] | $M_n$[c] | $Đ$[c] | $F_{DMDL}$ (%)[d] |
|---|---|---|---|---|---|---|---|---|---|---|
| 1 | None | AIBN | Toluene | 0/100/1 | 70 | 12 | NA/82 | 10300 | 1.61 | 100 (100) |
| 2 | None | AIBN | Bulk | 0/100/0.5 | 70 | 1.5 | NA/79 | 104000 | 2.04 | 100 (100) |
| 3 | MMA | AIBN | Toluene | 50/50/1 | 70 | 7 | 99/23 | 19000 | 1.78 | 18 (19) |
| 4 | BA | AIBN | Toluene | 50/50/1 | 70 | 1 | 98/56 | 130000 | 1.53 | 37 (36) |
| 5 | St | AIBN | Toluene | 50/50/2 | 80 | 12 | 79/NA[e] | 5100 | 1.46 | 8 (NA) |
| 6 | AN | AIBN | EC | 50/50/1 | 70 | 1 | 80/44 | 77000 | 1.54 | 34 (35) |
| 7 | VAc | AIBN | Toluene | 50/50/1 | 70 | 12 | 84/48 | 11000 | 1.60 | 35 (36) |
| 8 | NVP | AIBN | DMF | 50/50/1 | 70 | 2 | 96/28 | 29000 | 1.81 | 19 (23) |
| 9 | DMA | AIBN | Toluene | 50/50/1 | 70 | 1 | 100/39 | 91000 | 1.95 | 28 (29) |
| 10 | PEGMA | V65 | Toluene | 50/50/1 | 60 | 4 | 92/NA[e] | 39000 | 2.22 | 17 (NA) |
| 11 | DMAEMA | AIBN | Toluene | 50/50/1 | 70 | 4 | 98/20 | 27000 | 1.62 | 17 (17) |
| 12 | BMA | AIBN | Toluene | 50/50/1 | 70 | 5 | 93/11 | 46000 | 1.54 | 10 (11) |
| 13 | LMA | AIBN | Toluene | 50/50/1 | 70 | 3 | 85/15 | 42000 | 1.76 | 16 (15) |
| 14 | BzMA | AIBN | Toluene | 50/50/1 | 70 | 3 | 92/26 | 39000 | 1.76 | 19 (22) |
| 15 | EHMA | AIBN | Toluene | 50/50/1 | 70 | 2 | 97/18 | 38000 | 1.95 | 13 (16) |
| 16 | SMA | AIBN | Toluene | 50/50/1 | 70 | 2 | 77/29 | 86000 | 1.96 | 28 (27) |
| 17 | MEA | AIBN | Toluene | 50/50/1 | 70 | 1 | 100/54 | 82000 | 2.00 | 32 (35) |

[a]Dilution with 50wt% solvent for entries 1 and 3–17. EC is ethylene carbonate. DMF is *N*,*N*-dimethylformamide. [b]Monomer conversion obtained with $^1$H NMR. [c]PMMA-calibrated THF-GPC values for entries 1, 3–5, 7, and 12–17 and PMMA-calibrated DMF-GPC values for entries 2, 6, and 8–11. [d]$F_{DMDL}$ value determined by the $^1$H NMR analysis of the purified polymer. In the parenthesis, $F_{DMDL}$ value calculated from the monomer conversions of DMDL and co-monomer determined using $^1$H NMR is given. [e]Monomer conversion of DMDL was unable to determine because the DMDL monomer peak overlapped with the co-monomer peak in the $^1$H NMR spectrum.

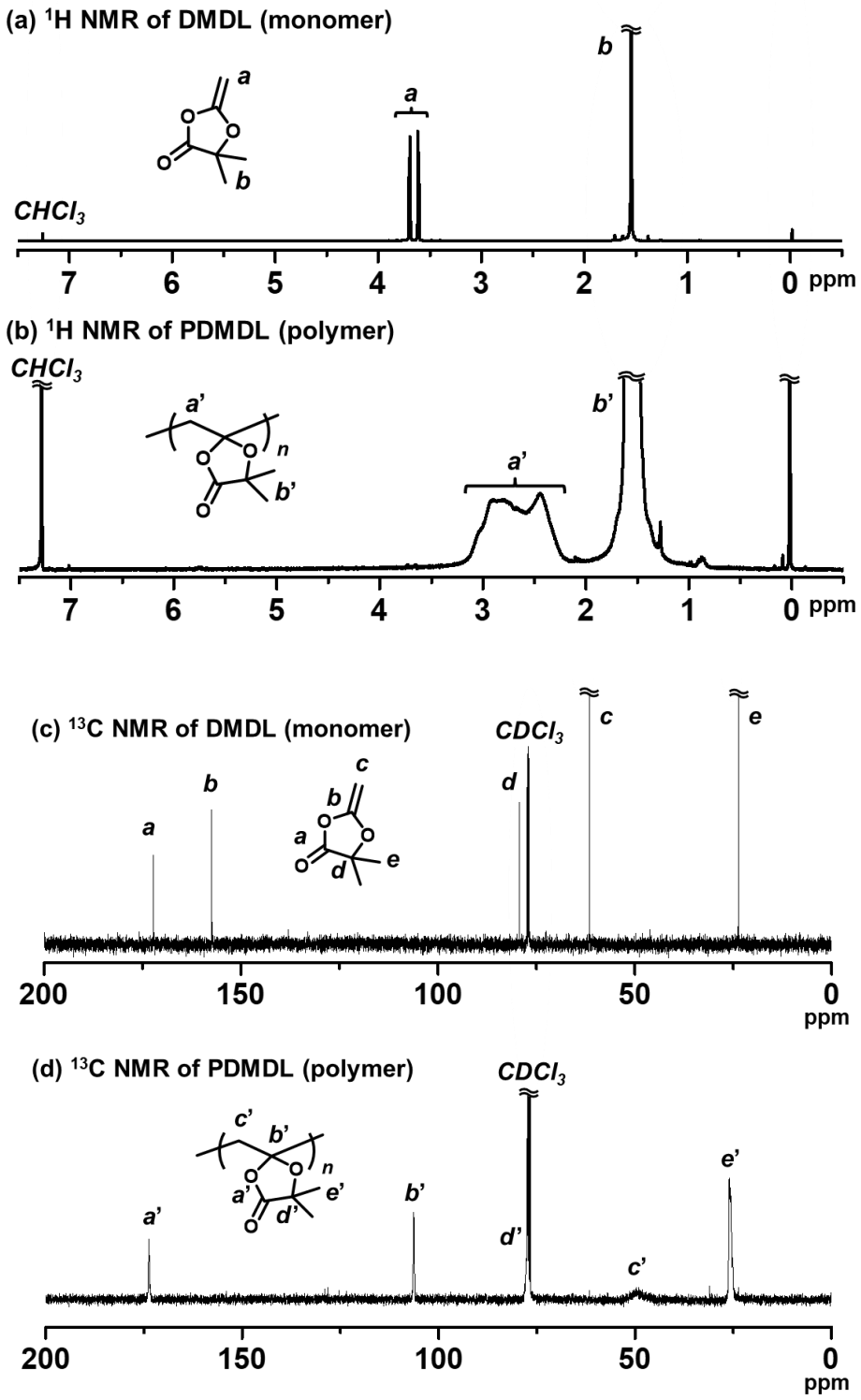


**Figure 4.1.** $^{1}H$ NMR spectra of (a) DMDL and (b) PDMDL. $^{13}C$ NMR spectra of (c) DMDL and (d) PDMDL. The synthesis of PDMDL is given in Table 4.1 (entry 1). 400 MHz for $^{1}H$ NMR (100 MHz for $^{13}C$ NMR) in $CDCl_3$.

As mentioned, there are two possible polymerization pathways, i.e., the ring-retaining and ring-opening pathways (Scheme 4.2). Figure 4.1c and d show the $^{13}C$ NMR spectra ($CDCl_3$) of DMDL and PDMDL, respectively. Through the polymerization, the vinyl carbon (*b*) of DMDL (Figure 4.1c) appearing at 157 ppm can be converted to the backbone quaternary carbon (*b*′) via the ring-retaining pathway (Figure 4.1d) or to a backbone anhydride carbonyl carbon via the ring-opening pathway (Scheme 4.2). The $^{13}C$ NMR spectrum of PDMDL (Figure 4.1d) shows a clear signal for the characteristic backbone quaternary carbon (*b*′) at 106 ppm, meaning the occurrence of the ring-retaining pathway. The signal of the ester carbonyl carbon (*a*) of DMDL appearing at 173 ppm (Figure 4.1c) was only slightly sifted to 174 ppm ((*a*′) in Figure 4.1d) in PDMDL, supporting the ring retention. If the ring-opened structure was also formed, an additional signal for the anhydride carbonyl carbon should have appeared, as anhydride carbonyl carbons generally appear at 160–170 ppm.[36] However, we observed only one signal (for the ester carbonyl carbon for the ring-retained structure) but did not observe other signals in the region at 160–180 ppm, where any carbonyl carbons are to appear. The result means that the obtained PDMDL predominantly contained the ring-retained monomer units and that the ring-opened monomer units were minor units if any present. A possible reason why the ring-opened radical was hardly generated (Scheme 4.2) is the presence of the trigonal carbonyl carbon in CKHE (DMDL). The trigonal carbonyl carbon can make the CKHE ring more planar than the CKA ring (without the trigonal carbonyl carbon), and the planar conformation may enhance the stabilization of the ring-retained radical.[37]

Instead of the solution polymerization in toluene (Table 4.1, entry 1) (described above), we carried out a bulk polymerization of DMDL (100 equiv.) using AIBN (0.5 equiv.) at 70 °C for 1.5 h (Table 4.1, entry 2). The absolute monomer concentration increased, and the viscosity of the polymerization solution increased, suppressing radical–radical termination by the so-

called gel effect and yielding a higher molecular weight PDMDL with $M_n$ = 104 000 and $Đ$ = 2.04 at a 79% monomer conversion.

Despite the higher molecular weight, the polymer was still soluble in organic solvents. We measured the glass transition temperature ($T_g$), crystallization temperature ($T_c$), melting temperature ($T_m$), and 50%-decomposition temperature ($T_d$) of this polymer (PDMDL) using differential scanning calorimetry (DSC) and thermogravimetric analysis (TGA). $T_d$ is the temperature at which a material begins to degrade thermally with a weight loss of 50% in this study.

The $T_g$, $T_c$, $T_m$, and $T_d$ values were 41 °C, 117 °C, 186 °C, and 269 °C, respectively (Figure 4.10).

The homopolymerization of PhDL (using AIBN) did not proceed at 70 °C. At an elevated temperature of 120 °C, the homopolymerization of PhDL (using *t*-butyl peroxybenzoate (TBPB)) slowly proceeded but yielded only an oligomer with $M_n$ <1000 (Table 4.2, entry 1) (Figure 4.11). In PhDL, one of the two methyl groups of DMDL is replaced by a phenyl group (Scheme 4.2). The steric hindrance of the bulky phenyl group might hinder the successive connection of the ring-retained monomer units. Another possibility is that the phenyl group of PhDL stabilizes the ring-opened radical and facilitates the formation of the ring-opened radical but that the radical might be too stable to polymerize. Also, the ring-opened radical might generate polymers with anhydride linkages but the anhydride linkages might be cleaved during the polymerization at a high temperature of 120 °C. These are not definitive but possible explanations. Due to the low molecular weight, the obtained oligomer was difficult to unequivocally analyze, and the exact explanation is not clear at this moment.

**Table 4.2.** Homopolymerization of PhDL and random copolymerizations of PhDL with co-monomers.

| Entry | Co-monomer (M) | Initiator[a,b] | $[M]_0/[PhDL]_0/[Initiator]_0$ (mM) | $T$ (°C) | $t$ (h) | Conv. (M/PhDL) (%/%)[c] | $M_n$[d] | $Đ$[d] | $F_{PhDL}$ (%)[e] |
|---|---|---|---|---|---|---|---|---|---|
| 1 | None | TBPB | 0/100/1 | 120 | 12 | NA/37 | <1000 | NA | 100 (100) |
| 2 | MMA | AIBN | 50/50/1 | 70 | 7 | 93/15 | 15000 | 1.83 | 11 (14) |
| 3 | MMA | TBPB | 50/50/1 | 120 | 5 | 94/33 | 21000 | 1.45 | 24 (26) |
| 4 | BA | AIBN | 50/50/1 | 70 | 3 | 96/39 | 47000 | 2.08 | 26 (29) |
| 5 | BA | TBPB | 50/50/1 | 120 | 3.5 | 96/48 | 13000 | 2.63 | 31 (33) |

[a]TBPB is *t*-butyl peroxybenzoate. [b]Dilution with 50 wt% solvent. [c]Monomer conversion obtained with $^1$H NMR. [d]PMMA-calibrated THF-GPC values. [e]$F_{PhDL}$ value determined by the $^1$H NMR analysis of the purified polymer. In the parenthesis, $F_{PhDL}$ value calculated from the monomer conversion (monomer consumption) determined using $^1$H NMR is given.

**Random Copolymerizations of DMDL and PhDL with Various Co-monomers.**

We carried out a random copolymerization of DMDL (50 mol%) with methyl methacrylate (MMA) (50 mol%) in toluene at 70 °C (Table 4.1, entry 3). Figure 4.2a shows the plots of the conversions of MMA (square) and DMDL (circle) *vs.* time. MMA was consumed faster than DMDL. After 7 h, the conversions of MMA and DMDL were 99% and 23%, respectively, yielding a random copolymer of MMA and DMDL with $M_n$ = 19 000 and $Đ$ = 1.78. The fraction ($F_{DMDL}$) of DMDL in the copolymer was 18%. The $^1$H and $^{13}$C NMR analysis showed that the polymer contained both MMA and DMDL units and the DMDL units were incorporated in the ring-retained form (Figures 4.12 and 4.13 in Experimental Section). The monomer reactivity ratio was determined by the Fineman-Ross method[38] (Figures 4.14–4.18 in Experimental Section) to be $r_{MMA}$ = 4.60 and $r_{DMDL} \approx 0$ (Table 4.3, entry 1). The result means that the MMA terminal radical reacts with both MMA and DMDL and 4.60 times more reacts with MMA than DMDL and that the DMDL terminal radical virtually exclusively reacts with MMA.

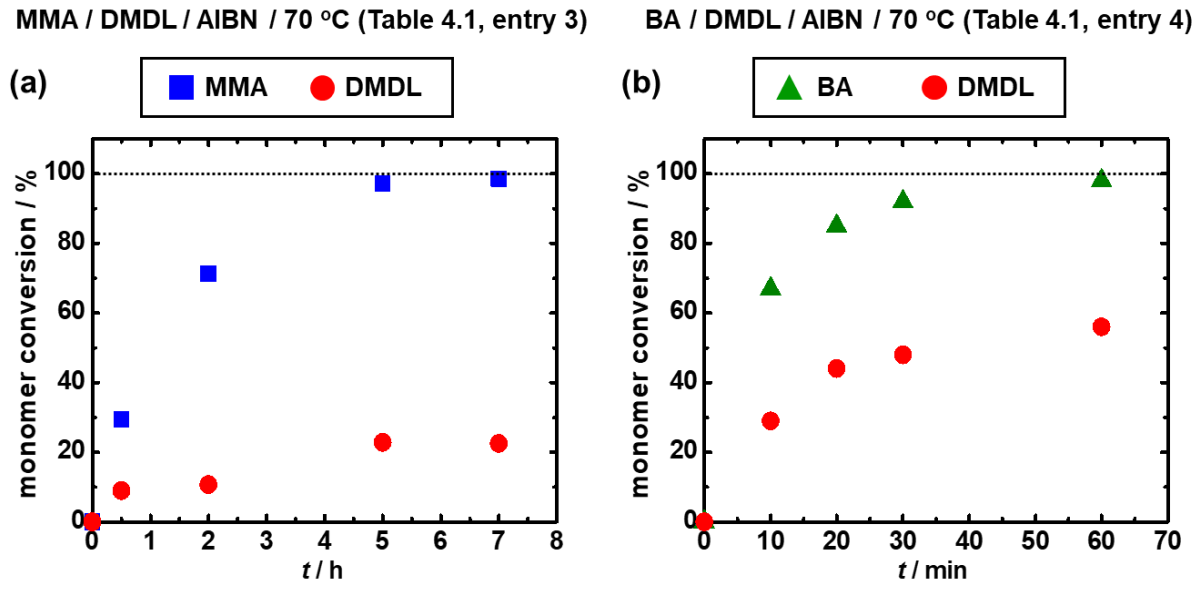


**Figure 4.2.** Plots of monomer conversion *vs.* time for (a) the MMA/DMDL/AIBN (50/50/1) system (70 °C) (Table 4.1, entry 3) and (b) the BA/DMDL/AIBN (50/50/1) system (70 °C) (Table 4.1, entry 4). The solvent was toluene (50 wt%) for both systems. The symbols are indicated in the figure.

**Table 4.3.** Monomer reactivity ratios[a] of co-monomers ($M_1$) and DMDL ($M_2$) determined by the Fineman-Ross method.

| Entry | $M_1$ | $T$ (°C) | $r_1$[a] | $r_2$[a] |
|---|---|---|---|---|
| 1 | MMA | 60 | 4.60 | Close to zero |
| 2 | BA | 60 | 0.83 | 0.03[b] |
| 3 | St | 80 | 1.08 | 0.01[b] |
| 4 | AN | 70 | 0.28 | 0.04[b] |
| 5 | VAc | 70 | 1.65 | 0.29 |

[a] $r_1 = r_{12}/r_{11}$ and $r_2 = r_{21}/r_{22}$. [b] $r_{DMDL}$ = 0–0.10 with an experimental error.

We studied *n*-butyl acrylate (BA) as another family of monomer. We carried out a random copolymerization of DMDL (50 mol%) with BA (50 mol%) in toluene at 70 °C (Table 4.1, entry 4). Figure 4.2b shows the plots of the conversions of BA (triangle) and DMDL (circle) *vs.* time. Similar to MMA, the co-monomer BA was consumed faster than DMDL. After 1 h, the conversions of BA and DMDL were 98% and 56%, respectively, yielding a random copolymer of BA and DMDL with $M_n$ = 130 000 and $Đ$ = 1.53 (Figure 4.19 in Experimental Section). The monomer reactivity ratios were $r_{BA}$ = 0.83 and $r_{DMDL} \approx 0.03$ (a range of 0–0.10 with an experimental error) (Table 4.3, entry 2). These values means that the

BA/DMDL system ($r_{BA}$ = 0.83 (Table 4.3, entry 2)) has a more alternating tendency than the MMA/DMDL system ($r_{MMA}$ = 4.60 (Table 4.3, entry 1)) but that the DMDL terminal radical still virtually exclusively reacts with BA over DMDL ($r_{DMDL} \approx 0.03$ (Table 4.3, entry 2)).

We also studied styrene (St), acrylonitrile (AN), and vinyl acetate (VAc) as other families of monomer (Table 4.1, entries 5–7). We carried out random copolymerizations of DMDL (50 mol%) with the co-monomer (50 mol%) in toluene (for St and VAc) or ethylene carbonate (for AN), yielding polymers with $M_n$ = 5100–77 000 and $Đ$ = 1.46–1.60 at $F_{DMDL}$ = 8–35% (Figure 4.20–4.22 in Experimental Section). For the St and AN systems, the monomer reactivity ratios were $r_{St}$ = 1.08 and $r_{DMDL} \approx 0.01$ (0–0.10 with an experimental error) (Table 4.3, entry 3) and $r_{AN}$ = 0.28 and $r_{DMDL} \approx 0.04$ (0–0.10 with an experimental error) (Table 4.3, entry 4). The $r_{St}$ and $r_{AN}$ values mean that the St terminal radical reacts nearly equally with DMDL and St, whereas the AN terminal radical reacts 3.6 (= 1/0.28) times more with DMDL than AN. The nearly zero $r_{DMDL}$ values mean that the DMDL terminal radical predominantly reacts with St and AN over DMDL. The VAc system had $r_{VAc}$ = 1.65 and $r_{DMDL}$ = 0.29 (Table 4.3, entry 5). The $r_{DMDL}$ value is not nearly zero in the VAc system (Table 4.3, entry 5), in contrast to the mentioned four systems (Table 4.3, entries 1–4). The result means that the DMDL terminal radical reacts with VAc slowly and hence can react with DMDL to some extent in the VAc system.

In the literatures, random copolymerizations of CKAs and vinyl co-monomers also showed similar tendency, i.e., slower consumption of CKAs than the co-monomers. The $r_{co\text{-}monomer}$ values are typically 2–8 and the $r_{CKA}$ values are 0.01–1 (Table 4.4 in Experimental Section).[29,39–43] For MBDO (previously reported CKHE monomer) (Scheme 4.2), its random copolymerization with VAc had $r_{VAc}$ = 0.587 and $r_{MBDO}$ = 1.51 (60 °C), showing that MBDO has higher reactivity than VAc.[31]

Thermal properties of the obtained DMDL copolymers (Table 4.1, entries 3 and 5–7) with MMA, St, AN, and VAc were studied (Figures 4.23–4.26 in Experimental Section). The $T_g$ values of the copolymers with MMA (104 (±5) °C), St (90 (±5) °C), and AN (76 (±5) °C) were slightly lower than those of homopolymers of MMA (*ca.* 105 °C),[44] St (*ca.* 90–100 °C),[44] and AN (*ca.* 95 °C),[44] while the $T_g$ value of the copolymer with VAc (38 (33–46) °C) was slightly higher than that of a homopolymer of VAc (*ca.* 30 °C),[44] because the $T_g$ value of a homopolymer of DMDL is 41 °C.

We further expanded the co-monomer scope to *N*-vinylpyrrolidone (NVP) and *N*,*N*-dimethylacrylamide (DMA) as other families of monomer (Table 4.1, entries 8 and 9) and functional methacrylates with poly(ethylene glycol) methyl ether (PEGMA), dimethylamino (DMAEMA), butyl (BMA), lauryl (LMA), benzyl (BzMA), ethylhexyl (EHMA), and stearyl (SMA) groups (Table 4.1, entries 10–16) as well as a functional acrylate with a methoxyethyl group (MEA) (Table 4.1, entry 17), yielding co-polymers with $M_n$ = 27 000–91 000 and $Đ$ = 1.54–2.22 at $F_{DMDL}$ = 10–32% (Figures 4.27–4.36 in Experimental Section). Such a wide range of amenable monomer families and functional monomers, including hydrophobic (BMA, LMA, BzMA, EHMA, SMA, and MEA), hydrophilic (NVP, DMA, PEGMA, and DMAEMA), and biocompatible (PEGMA and MEA) monomers, are attractive for polymer design by DMDL.

While the homopolymerization of PhDL generated only an oligomer (Table 4.2, entry1), PhDL was able to be copolymerized with a methacrylate and an acrylate (Table 4.2, entries 2–5). We carried out a random copolymerization of PhDL (50 mol%) with MMA (50 mol%) in toluene at 70 °C (Table 4.2, entry 2), which is the same condition as that in the DMDL/MMA system (Table 4.1, entry 3) except using PhDL instead of DMDL. After 7 h, the conversions of MMA and PhDL were 93% and 15%, respectively, yielding a random copolymer of MMA and PhDL with $M_n$ = 15 000 and $Đ$ = 1.83 (Figure 4.37 in Experimental Section). The conversion of PhDL (15%) was smaller than that of DMDL (23%) at similar conversions of

MMA (93–99%). In order to increase the conversion of PhDL, we elevated the polymerization temperature from 70 °C to 120 °C (Table 4.2, entry 3). After 5 h, the conversions of MMA and PhDL were 94% and 33%, respectively, yielding a random copolymer with $M_n$ = 21 000 and $Đ$ = 1.45. The conversion of PhDL increased by 18% (from 15% to 33%) by elevating the temperature from 70 °C to 120 °C at the similar (93–94%) conversions of MMA.

We also conducted a random copolymerization of PhDL (50 mol%) with BA (50 mol%) in toluene at 70 °C (Table 4.2, entry 4). After 3 h, the conversions of BA and PhDL were 96% and 39%, respectively, yielding a random copolymer with $M_n$ = 47 000 and $Đ$ = 2.08 (Figure 4.38 in Experimental Section). At a higher temperature of 120 °C, the conversions of BA and PhDL were 96% and 48%, respectively (Table 4.2, entry 5), showing an increase in the conversion of PhDL by 9% by elevating the temperature from 70 °C to 120 °C at the same (96%) conversion of BA.

Thus, DMDL and PhDL were able to be copolymerized with a range of vinyl monomers, offering a wide scope of accessible polymers. This feature is in sharp contrast to the limited co-monomer scope of the previously reported CKHE monomer, i.e., MBDO, which was copolymerized only with VAc.

**Hydroxide-assisted Degradation of PDMDL.**

We studied the degradation of PDMDL. We dissolved a PDMDL homopolymer ($M_n$ = 104 000 and $Đ$ = 2.04 (Table 4.1, entry 2)) (0.064 g, 2.4 wt%, 1 equiv. of the DMDL monomer unit) in DMSO-$d_6$ (2.08 g, 77.2 wt%), which was a colorless transparent solution. To this solution, a $D_2O$ solution of 1 M NaOH (0.55 g, 20.4 wt%, 1 equiv. of NaOH) was added at room temperature. The mixture became slightly turbid, because PDMDL chains became globular due to the presence of water ($D_2O$), but the mixture soon turned reddish brown and transparent upon stirring at room temperature. PDMDL seemed to degrade to small molecules.

The reaction mixture was subsequently analyzed using GPC and NMR within 5 h after the reaction started.

In the GPC chromatogram (DMF eluent) (Figure 4.3a), no peak was observed in the polymer region (molecular weight >2000), suggesting that PDMDL degraded. (The peak at the molecular weight <2000 observed in Figure 4.3a would be ascribed to generated oligomers and/or possible clusters of lithium bromide (LiBr) used in the DMF eluent.) The $^{1}H$ (Figure 4.3b) and $^{13}C$ (Figure 4.3c) NMR spectra also show no polymer (PDMDL) signals (no signal at 2.15–3.25 ppm for the backbone $CH_2$ protons in the $^{1}H$ NMR spectrum and no signal at 174 ppm for the ester carbon of the DMDL unit in the polymer in the $^{13}C$ NMR spectrum) (the $^{1}H$ and $^{13}C$ NMR spectra of (non-degraded) PDMDL (2.4 wt%) in the studied DMSO-$d_6$/$D_2O$ (77.2/20.4 wt%) mixed solvent are given in Experimental Section (Figures 4.39 and 4.40 in Experimental Section)). The only species clearly detected was HIBA (Scheme 4.3) whose $CH_3$ protons appeared at 1.13 ppm (Figure 4.3b) and whose $CH_3$ carbons, quaternary carbon, and carbonyl carbon appeared at 28, 73, and 181 ppm, respectively (Figure 4.3c).

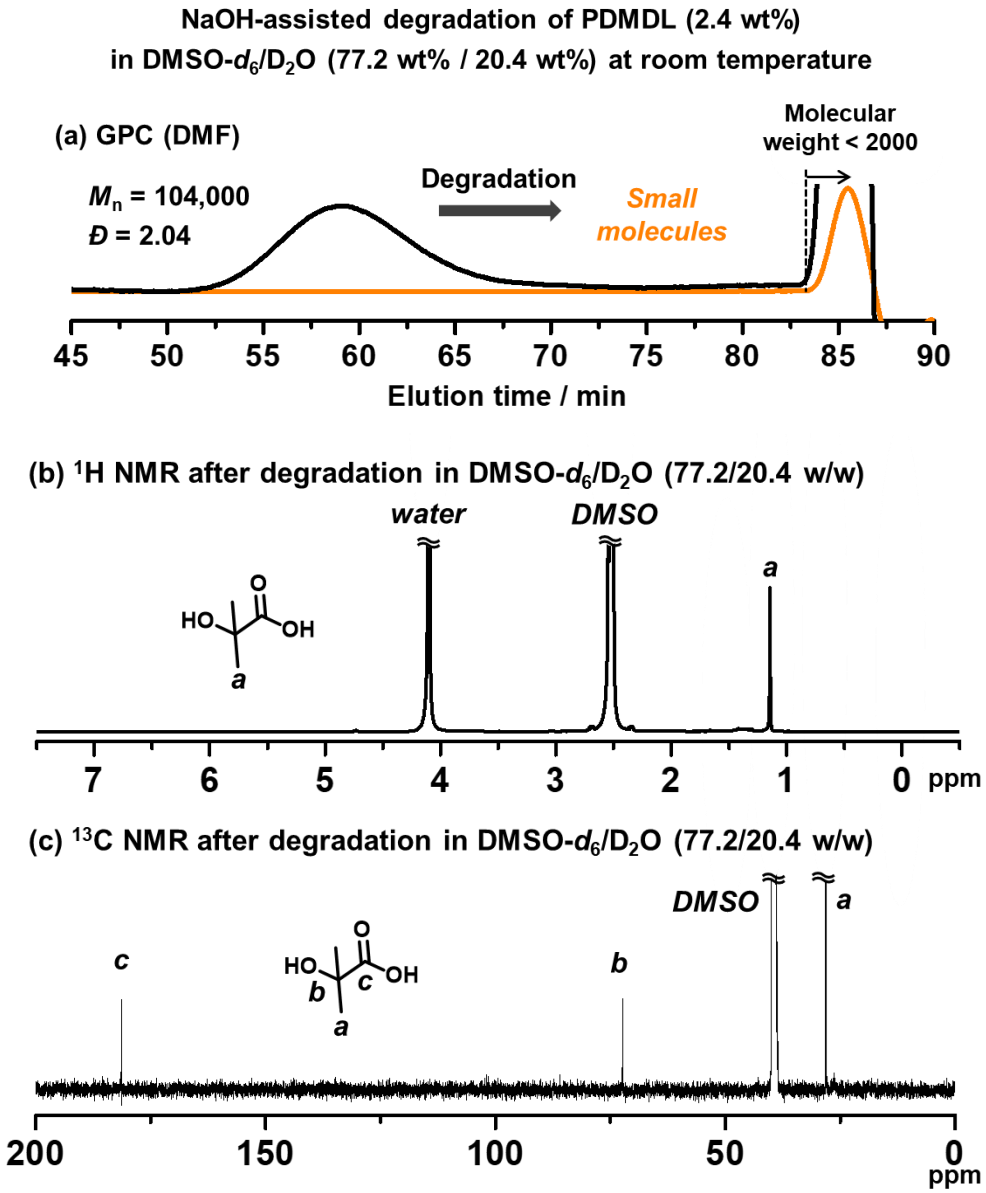


**Figure 4.3.** Degradation of PDMDL ($M_n$ = 104,000, $Đ$ = 2.04, 2.4 wt%, 1 equiv. of the DMDL monomer unit) using 1 equiv. of NaOH in a mixture of $D_2O$ (20.4 wt%) and DMSO-$d_6$ (77.2 wt%) at room temperature within 5 h. (a) GPC chromatogram before (black line) and after (orange line) degradation. (b) $^1$H NMR and (c) $^{13}$C NMR spectra of the reaction mixture after degradation (400 MHz for $^1$H NMR (100 MHz for $^{13}$C NMR) in DMSO-$d_6$/$D_2O$).

Scheme 4.4 shows a possible degradation mechanism of PDMDL in the presence of $OH^-$. It should be emphasized that this scheme is a possible mechanism but is not a definitive one at this moment. Firstly, $OH^-$ attacks the carbonyl carbon of the hemiacetal ester, generating an alkoxide anion (Scheme 4.4, compound **5**). A subsequent elimination can result in either (a)

the side-chain cleavage or (b) the main-chain cleavage. The side-chain cleavage can generate a ketone in the backbone chain (compound **6**) and HIBA. If the side-chain cleavage is significant, a polyketone can be generated. The main-chain cleavage can generate a carboxylic acid chain-end PDMDL (compound **8**) and a carboxylate chain-end PDMDL (compound **9**). These two compounds can further generate another form of carboxylic acid chain-end PDMDL (compound **10**) and a ketone chain-end PDMDL (compound **11**) as well as two molecules of HIBA. If the main-chain cleavage is significant, the polymers (compounds **8**–**11**) will further undergo the main-chain cleavage and degrade into small molecules. A main-chain cleavage mechanism was previously proposed for the degradation of the MBDO polymer, for which the mechanism was studied in an acidic condition.[31]

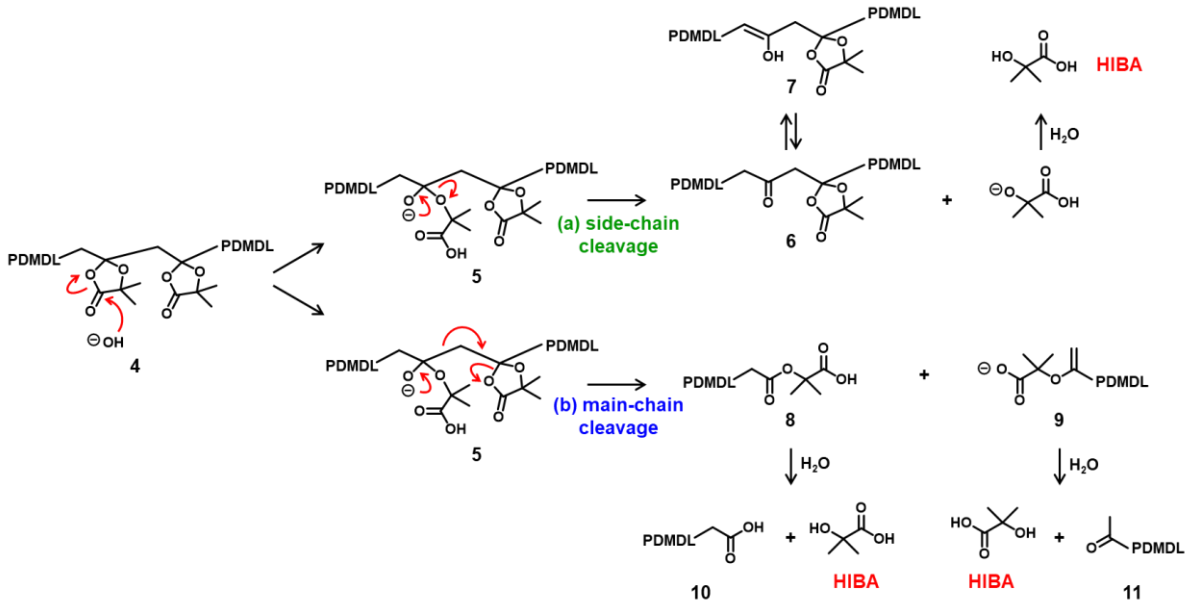


**Scheme 4.4.** Possible mechanisms of hydroxide-assisted degradation of PDMDL.

No polymer peak observed in the GPC chromatogram (Figure 4.3a) suggests that the main-chain cleavage operated significantly in the present system so that the polymer chains could degrade into small molecules or oligomers. The side-chain cleavage is not excluded at this moment and might also operate to some extent. HIBA is a product in both pathways. The observation of HIBA in the NMR analysis (Figures 4.3b and c) supports the proposed

degradation scheme (either or both of the two pathways). However, the $^{1}H$ and $^{13}C$ NMR analyses detected no other species, and the reason is unclear at the moment. When the main-chain cleavage operates, small molecules or oligomers with carboxylic acid (compounds **8** and **10**), carboxylate (compound **9**), and/or ketone (compound **11**) can be generated. However, the $^{13}C$ NMR analysis (Figure 4.3c) detected no other C=O carbons than that of HIBA. When the side-chain cleavage operates, a polyketone (compound **6**) or its isomer, i.e., a polyenol (compound **7**) can be generated, and the intramolecular cyclization of polyketone can also generate aromatic species.[45] However, the $^{13}C$ NMR analysis (Figure 4.3c) detected no ketone (>190 ppm), no enol (90–100 ppm), or no aromatic species (110–140 ppm). Small molecules that were possibly generated might be volatile and evaporate during the degradation. Thus, we also conducted the same experiment in a valved (sealed) NMR tube (Figure 4.41 in Experimental Section). However, again, only HIBA was detected. A possible reason for no detection of other species (compounds **6–11**) is the solubility of the product. To check this possibility, we studied the degradation of PDMDL in a more hydrophobic solvent (a mixture of THF-$d_8$ and $D_2O$ instead of a mixture of DMSO-$d_6$ and $D_2O$), as described in detail in Experimental Section. The $^{1}H$ NMR and $^{13}C$ NMR spectra of the reaction mixture (Figure 4.42 in Experimental Section) again showed only HIBA even in this more hydrophobic solvent. Thus, the reason for no detection of other species is not clear at this moment, and hence the proposed degradation scheme (Scheme 4.4) is viewed as a tentative mechanism.

Nevertheless, as an experimental fact, PDMDL clearly degraded in the presence of NaOH. The degradation occurred within 5 h at room temperature or markedly fast (within 30 min) at 50 °C, which would be an attractive feature of PDMDL.

**Acid-assisted Degradation of PDMDL.**

We also studied the degradation of PDMDL in an acidic condition, using the same condition as previously reported condition for the acid-assisted degradation of the MBDO polymer.[31] We dissolved a PDMDL ($M_n$ = 106 000 and $Đ$ = 1.88) (0.064 g, 2.4 wt%, 1 equiv. of the DMDL monomer unit) in DMSO (2.08 g, 78.7 wt%), which was a colorless transparent solution. To this solution, an aqueous 1 M HCl solution (0.5 g, 18.9 wt%, 1 equiv. of HCl) was added, and the mixture became turbid. The mixture was heated at 80 °C for 24 h, and the generated precipitate was analyzed with GPC (Figure 4.43 in Experimental Section). The precipitate was found to be unreacted PDMDL, and its $M_n$ (= 100 000) and $Đ$ (= 2.00) values were close to its original values ($M_n$ = 106 000 and $Đ$ = 1.88). The amount of the precipitate (unreacted PDMDL) was 0.057 g, which is 89% of the original amount (0.064 g). Thus, PDMDL did not degrade in the same condition as the MBDO polymer did, mainly because of the low solubility of PDMDL in the studied acidic condition.

Thus, we used a more hydrophobic solvent (a mixture of DMSO-$d_6$ (79.4 wt%) and $H_2O$ (1.4 wt%)) to dissolve PDMDL (10.2 wt%) and used an organic acid, i.e., trifluoroacetic acid (9 wt%), that is soluble in this solvent. We heated the mixture at 80 °C for 3 days and observed a decrease in the $M_n$ value by 25%, showing that PDMDL slowly degraded in this acidic condition (Figure 4.44 in Experimental Section). We observed HIBA in this acid-assisted degradation, as in the NaOH-assisted degradation. Furthermore, acetone was observed in the acid-assisted degradation (Figure 4.44 in Experimental Section), which may suggest a chain-end degradation of **11** in the acidic condition (Scheme 4.5 in Experimental Section), although this mechanism is a tentative mechanism. While the acid-assisted degradation of the MBDO polymer generated acetic acid,[31] we did not observe acetic acid in the degradation of PDMDL. The degradation mechanism might be different for the MBDO polymer and PDMDL.

**Amine-assisted Degradation of PDMDL.**

The NaOH-assisted degradation was too fast to monitor over time. Hence, we used a milder base, i.e., an amine to probe the degradation of PDMDL. The studied amine was a primary amine, i.e., pentylamine ($R–NH_2$). We dissolve a PDMDL ($M_n$ = 39 000 and $Đ$ = 1.42) (0.064 g, 4.0 wt%, 1 equiv. of the DMDL monomer unit) and pentylamine (0.065 g, 4.0 wt%, 1.5 equiv.) in $CD_3CN$ (1.48 g, 92.0 wt%), which was a colorless transparent solution. The solution was heated at 65 °C. Figure 4.4a and b show the GPC chromatograms and the plot of $M_n$ *vs.* the reaction time, respectively. The original $M_n$ (= 39 000) value of PDMDL started to decay ($M_n$ = 33 000) right after the addition of the amine and became approximately a half ($M_n$ = 20 000) after the heating for 4 h, approximately a quarter ($M_n$ = 10 000) for 8 h, and approximately 1/10 ($M_n$ = 3000) for 24 h. The polymer degraded to small molecules or oligomers ($M_n$ <2000) for 60 h.

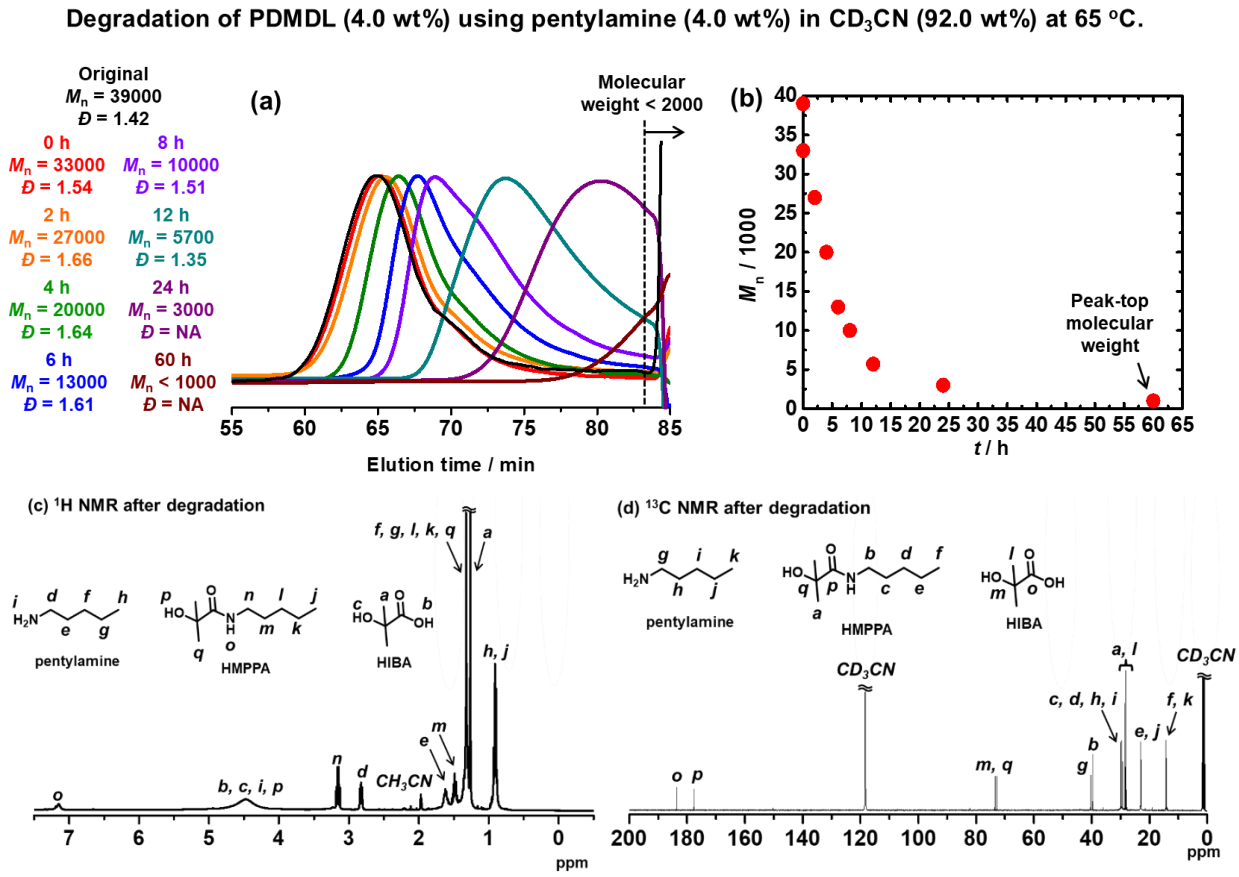


**Figure 4.4.** Degradation of PDMDL ($M_n$ = 39000, $Đ$ = 1.42, 4.0 wt%, 1 equiv. of the DMLD unit) using pentylamine (4.0 wt%, 1.5 equiv.) in $CD_3CN$ (92.0 wt%) at 65 °C. (a) GPC chromatograms and (b) plot of $M_n$ *vs.* degradation time. The 0 h sample in (a) is a sample right after the addition of pentylamine. (c) $^1H$ NMR and (d) $^{13}C$ NMR spectra of the reaction mixture after degradation for 60 h (400 MHz for $^1H$ NMR (100 MHz for $^{13}C$ NMR) in $CD_3CN$).

The $^1H$ (Figure 4.4c) and $^{13}C$ (Figure 4.4d) NMR spectra of the reaction mixture for 60 h show no polymer (PDMDL) signals (no signal at 2.38–3.13 ppm for the backbone $CH_2$ protons in the $^1H$ NMR spectrum or no signal at 174 ppm for the ester carbon of the DMDL unit in the polymer in the $^{13}C$ NMR spectrum) (the $^1H$ and $^{13}C$ NMR spectra of (non-degraded) PDMDL in the studied $CD_3CN$ are given in Figure 4.45 and 4.46 in Experimental Section). A possible mechanism is given in Scheme 4.6 in Experimental Section. We observed 2-hydroxy-2-methyl-*N*-pentylpropanamide (HMPPA) (product), HIBA (product), and pentylamine (remaining reactant) (Figure 4.4c and d), which were identified from the spectra of the isolated HMPPA, HIBA, and pentylamine (Figure 4.47 and 4.48 in Experimental

Section). The observation of HMPPA supports the proposed amine-assisted degradation scheme (Scheme 4.6 in in Experimental Section). The degradation was carried out without removing moisture. HIBA (Scheme 4.4) was generated probably because of the presence of moisture, which might provide hydroxide in the presence of the amine. However, similar to the NaOH-assisted degradation, no other products than HMPPA and HIBA were observed in the $^{1}$H and $^{13}$C NMR spectra (Figure 4.4c and d) for an unclear reason.

Although the degradation mechanism is yet to be definitive, this experiment demonstrated that PDMDL degraded even with a milder base (amine). The facile operation (no need to remove moisture) and mild temperature (65 °C) are attractive.

**Degradation of PPEGMA-*r*-PDMDL.**

Besides the PDMDL homopolymer, we studied the degradation of a PPEGMA-*r*-PDMDL random copolymer, where PPEGMA is poly(ethylene glycol) methyl ether methacrylate. This random copolymer is hydrophilic and soluble in water. We dissolved a PPEGMA-*r*-PDMDL ($M_n$ = 39 000, $Đ$ = 2.22, and $F_{DMDL}$ = 17%) (0.06 g, 1 wt%, 1 equiv. of the DMDL monomer unit) in a 0.9 M KOH aqueous solution (6.0 g, 99 wt%, 67 equiv. of KOH) and monitored the degradation at room temperature for 23 h. Figure 4.5a and b show the GPC chromatograms and the plot of $M_n$ *vs.* time. The original $M_n$ (= 39 000) value of the copolymer became approximately a half ($M_n$ = 21 000) for 1 h, approximately 1/3 ($M_n$ = 13 000) for 8 h, and approximately a quarter ($M_n$ = 9300) for 23 h. To confirm that the observed decrease in the $M_n$ value was not ascribed to the pendant chain cleavage of the PEGMA units, we studied the degradation of a PPEGMA homopolymer ($M_n$ = 72 000 and $Đ$ = 2.82) in the same condition. After 24 h, the $M_n$ value decreased from 72 000 to only 70 000 (Figure 4.49 in Experimental Section), confirming no significant pendant chain cleavage. Thus, the observed degradation (significant decrease in the $M_n$ value) of the PPEGMA-*r*-PDMDL is ascribed to the main-chain

cleavage of the DMDL units in the polymer. The $F_{DMDL}$ value of the PPEGMA-*r*-PDMDL was 17%, meaning that a DMDL unit was incorporated in every approximately 6 PEGMA units on average. Upon the full main-chain cleavage of the DMDL units, the $M_n$ value may decrease to 1800 (6 units of PEGMA). The observed $M_n$ value (=9400) after 23 h of the reaction was larger than 1800, possibly because of a compositional drift during the polymerization (smaller DMDL compositions in the polymers generated at an early stage of polymerization and larger DMDL compositions in those generated at a later stage of polymerization).[46] The degradation of PPEGMA-*r*-PDMDL by addition of 0.9 M KOH (Figure 4.5a) is slower than that of PDMDL by the addition of 1.0 M NaOH (Figure 4.3a) might be due to the poor solubility of PDMDL in water than in DMSO. In the degradation of PDMDL, we used DMSO to dissolve PDMDL then we added 1.0 M NaOH in $D_2O$. In the degradation of PPEGMA-*r*-PDMDL, we used aqueous KOH. The polymer is soluble, but the PDMDL is poorly soluble in water. Therefore, the degradation of PPEGMA-*r*-PDMDL is slower.

**Degradation of PLMA-*r*-PDMDL.**

We also studied the degradation of a PLMA-*r*-PDMDL random copolymer, where PLMA is poly(lauryl methacrylate). This random copolymer is hydrophobic. We used a mixture of methanol and THF to dissolve this hydrophobic copolymer. We dissolved a PLMA-*r*-PDMDL ($M_n$ = 42 000, $Đ$ = 1.76, and $F_{DMDL}$ = 16%) (0.04 g, 2.0 wt%, 1 equiv. of the DMDL monomer unit) in a mixture of a 0.9 M KOH methanol solution (0.16 g, 8.1 wt%, 3.5 equiv. of KOH) and THF (1.78 g, 89.9 wt%) and monitored the degradation at room temperature for 24 h (Figure 4.5c and d). The original $M_n$ (= 42 000) value of the copolymer became approximately its 60% ($M_n$ = 25 000) for 2 h, approximately its 45% ($M_n$ = 19 000) for 8 h, and approximately its 30% ($M_n$ = 13 000) for 24 h. Thus, the degradation of the PLMA-*r*-PDMDL successfully occurred.

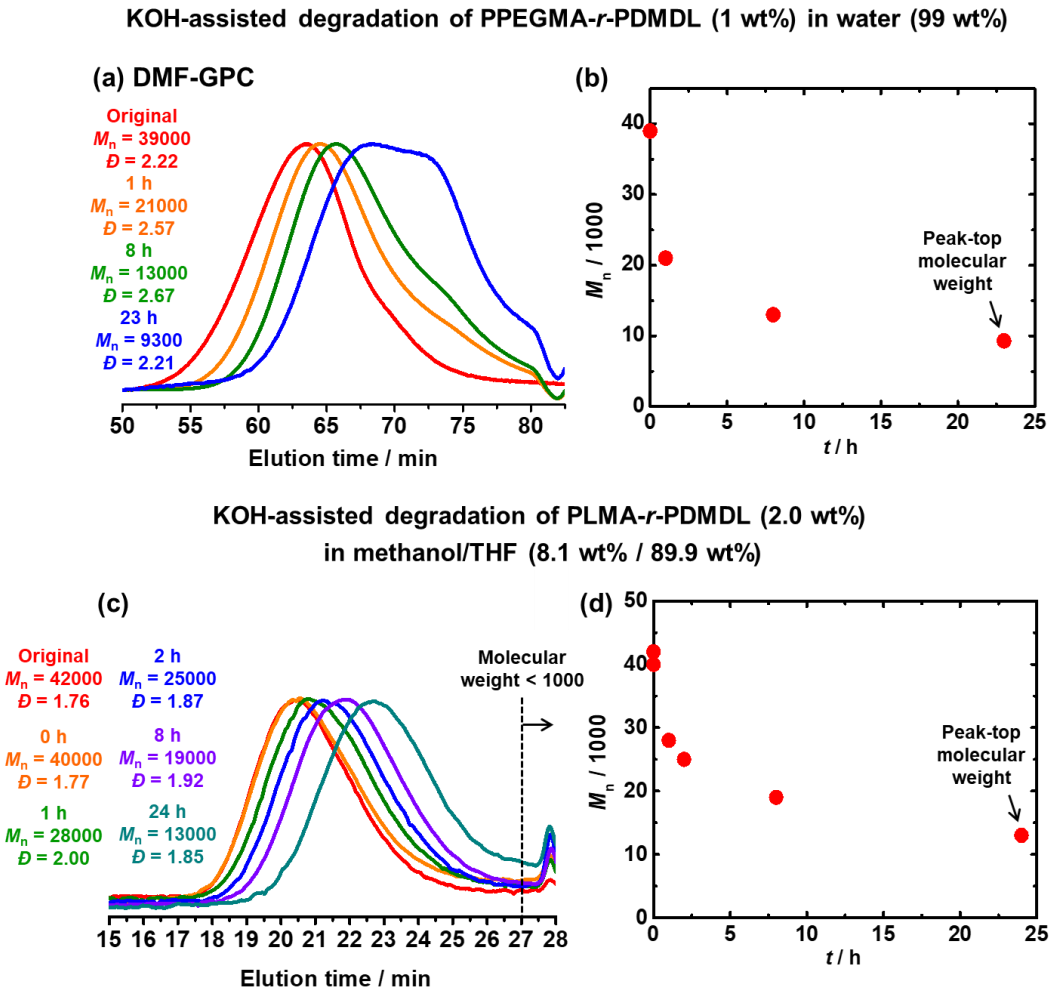


**Figure 4.5.** Degradation of PPEGMA-*r*-PDMDL ($M_n$ = 39000, $Đ$ = 2.22, and $F_{DMDL}$ = 17%) (1 wt%) using 67 equiv of KOH in water (99 wt%) at room temperature: (a) GPC chromatograms and (b) plot of $M_n$ *vs.* time. Degradation of PLMA-*r*-PDMDL ($M_n$ = 42000, $Đ$ = 1.76, and $F_{DMDL}$ = 16%) (1.8 wt%) with 3.5 equiv of KOH in a mixture of methanol (8.1 wt%) and THF (89.9 wt%) at room temperature; (c) GPC chromatograms and (d) plot of $M_n$ *vs.* time.

**Recovery of HIBA via NaOH-assisted Degradation of PDMDL.**

HIBA is the starting material (compound **1** ($R_1 = CH_3$) in Scheme 4.3) of the DMDL monomer. Hence, we attempted to recover HIBA after the NaOH-assisted degradation of PDMDL, use the recovered HIBA to synthesize DMDL monomer, and use this monomer to synthesize PDMDL for demonstrating the concept of the recycling of PDMDL (Scheme 4.3). As mentioned, four of the six carbons of the DMDL monomer are recycled via the recovery of HIBA.

A PDMDL ($M_n$ = 56 000 and $Đ$ = 2.47) (1.0 g, 1 equiv. of the DMDL monomer unit) was dissolved in a mixture of a 0.9 M KOH methanol solution (28 g, 4 equiv. of KOH) and THF (300 g) was stirred at room temperature for 1 h. The mixture of methanol and THF was used instead of a mixture of DMSO and water (Figure 4.3), because DMSO is difficult to evaporate (in the evaporation process below). KOH was used instead of NaOH (Figure 4.3), because KOH is soluble in the mixture of methanol and THF. After the reaction, acidic water and diethyl ether were added to the reaction mixture. HIBA was more soluble in the organic phase than in the aqueous phase in an acidic condition. After the extraction with diethyl ether three times, the collected organic layer was evaporated. The $^{1}$H and $^{13}$C NMR spectra (Figure 4.6) show that the compound extracted in the organic layer was nearly pure HIBA (we observed only HIBA). We collected 0.39 g of HIBA. The theoretically recoverable maximum amount of HIBA from 1 g of PDMDL is 0.81 g. Thus, the recovery yield was 48% (= (0.39 g)/(0.81 g)).

We used the recovered HIBA to synthesize DMDL (Figure 4.51-4.55 in Experimental Section). We carried out a polymerization of this DMDL (100 equiv.) with AIBN (0.5 equiv.) at 70 °C for 6 h (in the same condition as Table 4.1, entry 2) and obtained a PDMDL with $M_n$ = 52 000 and $Đ$ = 2.32 with an 80% monomer conversion. Thus, we successfully experimentally demonstrated the concept of the chemical recycling of PDMDL.

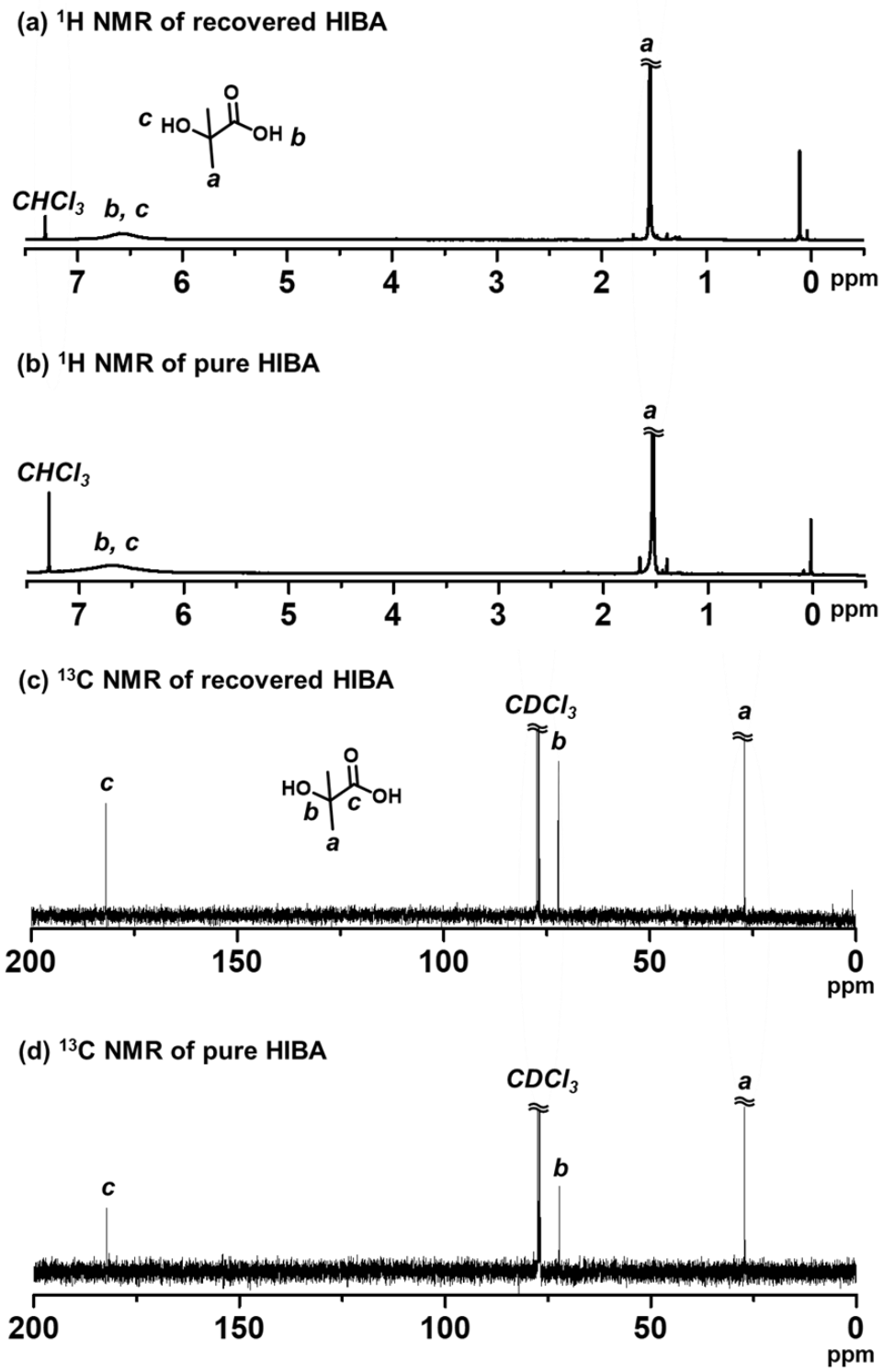


**Figure 4.6.** $^{1}H$ NMR spectra of (a) recovered HIBA and (b) pure HIBA. $^{13}C$ NMR spectra of (c) recovered HIBA and (d) pure HIBA. (400 MHz for $^{1}H$ NMR (100 MHz for $^{13}C$ NMR) in $CDCl_3$).

## 4.3. Conclusions

We successfully synthesized polymers using two new CKHE monomers (DMDL and PhDL). The two monomers were synthesized in high yields (80–90%), which is an attractive feature. DMDL generated homopolymers, and DMDL and PhDL were copolymerized with important families of vinyl monomers, i.e., methacrylates, acrylates, styrene, acrylonitrile, vinyl pyrrolidinone, and acrylamide, and various functional methacrylates and acrylate, exhibiting a wide scope of the accessible polymers. The obtained homopolymers and random copolymers of DMDL degraded in the presence of a hydroxide (NaOH or KOH) and an amine (pentylamine) at mild temperatures (room temperature to 65 °C). The degradation of the PDMDL homopolymer generated HIBA. We recovered HIBA, used the recovered HIBA to synthesize DMDL monomer, and used this monomer to synthesize PDMDL, demonstrating the concept of the chemical recycling of PDMDL. HIBA is not only an ingredient to regenerate DMDL but also a useful ingredient of other important chemicals such as methacrylic acid, tetramethylglycolide, and chloro- and amino-derivatives of HIBA[47,48] and can serve for a range of chemical recycling. The degradability and chemical recyclability of PDMDL may be useful for circular materials economy.

## 4.4. Experimental Section

### Materials.

2-Acetoxyisobutyryl chloride (>97%, Tokyo Chemical Industry (TCI)), 2-hydroxyisobutyric acid (>98%, TCI), acetyl chloride (≥99.0%, Sigma-Aldrich, USA), oxalyl chloride (≥99.0%, Sigma-Aldrich), triethylamine (>99.0%, TCI), anhydrous dichloromethane (DCM) (>99.0%, TCI), hexane (>99%, International Scientific, Singapore), diethyl ether (ACS reagent grade, VWR International, USA), ethanol (≥99.5%, absolute, Fisher Scientific, USA), chloroform (>99.2%, VWR Chemicals, USA), tetrahydrofuran (THF) (>99.5%, Kanto Chemical, Japan), N,N-dimethylformamide (DMF) (>99.5%, Kanto), 2,2′-azobis(2-methylpropionitrile) (AIBN) (95%, Wako Pure Chemical, Japan), 2,2'-azobis(2,4-dimethylvaleronitrile) (V65) (95%, Wako), ethylene carbonate (EC) (>99%, TCI), toluene (ACS reagent grade, VWR International), methanol (ACS reagent grade, VWR International), tert-butyl peroxybenzoate (TBPB) (≥98.0%, Sigma-Aldrich), methyl methacrylate (MMA) (>99.8%, TCI), poly(ethylene glycol) methyl ether methacrylate (PEGMA) (average molecular weight = 300) (98%, Sigma-Aldrich), butyl acrylate (BA) (>99%, TCI), acrylonitrile (AN) (>99%, TCI), butyl methacrylate (BMA) (>99.8%, TCI), styrene (St) (>99.8%, TCI), 2-(dimethylamino)ethyl methacrylate (DMAEMA) (≥98.5%, TCI), 2-methoxyethyl acrylate (MEA) (>98%, TCI), N,N-dimethylacrylamide (DMA) (>99.0%, TCI), vinyl acetate (VAc) (>99.0%, TCI), 1-vinyl-2-pyrrolidinone (NVP) (>99.0%, TCI), lauryl methacrylate (LMA) (>97.0%, TCI), benzyl methacrylate (BzMA) (>98.0%, TCI), 2-ethylhexyl methacrylate (EHMA) (>99.0%, TCI), stearyl methacrylate (SMA) (>97.0%, TCI), potassium hydroxide (KOH) (min. 85%, GCE, Sweden), sodium hydroxide (NaOH) (≥97.0%, VWR Chemicals), hydrochloric acid (1M, TCI), trifluoroacetic acid (TFA) (>99.0%, TCI), pentylamine (>98.0%, TCI), and anhydrous magnesium sulfate (>98.0%, TCI) were used as received.

**Measurements.**

The GPC analysis using THF as an eluent was performed on a Shimadzu i-Series Plus liquid chromatograph LC-2030c Plus (Kyoto, Japan) equipped with a Shodex (Japan) KF-804L mixed gel column (300 × 8.0 mm; bead size = 7 μm; pore size = 1500 Å) and a Shodex LF-804 mixed gel column (300 × 8.0 mm; bead size = 6 μm; pore size = 3000 Å). The flow rate was 0.7 mL/min (40 o C). The GPC analysis using DMF as an eluent was performed on a Shimadzu LC-2030c Plus equipped with two Shodex LF-804 mixed gel columns (300 × 8.0 mm; bead size = 6 μm; pore size = 3000 Å) and a Shodex KD-802 (300 × 8.0 mm; bead size = 6 μm; pore size = 150 Å). The flow rate was 0.34 mL/min (40 °C). The DMF eluent contained LiBr (10 mM). The sample detection was conducted using a refractive index detector (RID-20A) for THF-GPC and for DMF-GPC. The column system was calibrated with standard poly(methyl methacrylate)s (PMMAs) for both THF-GPC and DMF-GPC systems.

The NMR spectra were recorded on Bruker (Germany) BBFO400 spectrometer (400 MHz) at ambient temperature. $CDCl_3$, DMSO-$d_6$, THF-$d_8$ and $CD_3CN$ (Cambridge Isotope Laboratories, USA) were used as the solvents for the NMR analysis, and the chemical shift was calibrated using residual undeuterated solvents or tetramethylsilane (TMS) as the internal standard. The monomer conversions and the monomer compositions in the obtained polymers were determined with $^1H$ NMR.

The differential scanning calorimetry (DSC) curves were recorded with QSeries DSC Q50 model device (TA instrument, New Castle, US). The DSC analysis was conducted using an aluminium sample pan under flowing nitrogen at a flow rate of 50 mL/min. The samples were cooled down to –80 °C or –50 °C and heated up to 225–400 °C with a heating rate of 10 °C/min.

The thermal gravimetric analysis (TGA) curves were recorded with TGA Q500 model device (TA instrument). The TGA analysis was carried out in platinum pans under flowing air at a flow rate of 60 mL/min with a heating rate of 10 °C/min at a temperature range of 25–700 °C.

**Synthesis of DMDL.**

5,5-Dimethyl-2-methylene-1,3-dioxolan-4-one (DMDL) was synthesized according to reported literature.[32] A mixture of 2-acetoxyisobutyryl chloride (**3** (**$R_1$** = **$CH_3$**), 50.0 g, 0.30 mol), triethylamine (36.8 g, 0.36 mol), and anhydrous DCM (200 mL) was heated under reflux in nitrogen atmosphere. After 5 h, the mixture was cooled down and diluted with 200 mL of hexane/diethyl ether (1/1 (v/v)). The resulting suspension was filtered, and the solvent was evaporated with a rotary evaporator. The residual liquid was subjected to fractional distillation to give DMDL (30 g, 0.23 mol) at 15 Torr at 40 °C in 80% yield. **$^1$H NMR (400 MHz, $CDCl_3$)** δ 3.70 (d, *J* = 4.0 Hz, 1H), 3.62 (d, *J* = 4.0 Hz, 1H), 1.54 (s, 6H). **$^{13}$C NMR (100 MHz, $CDCl_3$)** δ 173.3, 157.4, 79.3, 61.5, 23.7.

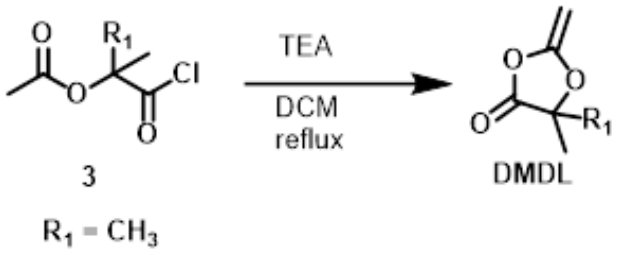


**Synthesis of PhDL.**

2-Acetoxy-2-phenylpropanoic acid (**2 ($R_1$ = Ph)**) was synthesized according to the reported literature.[33] 2-Hydroxy-2-phenylpropanoic acid hydrate (**1 ($R_1$ = Ph)**, 10.0 g, 60 mmol) was suspended in anhydrous DCM (60 mL) under Ar, followed by the addition of acetyl chloride (12 mL, 2.8 equiv., 168 mmol) dropwise. The mixture gradually became clear and was heated to reflux. After 2 h, the resulting solution was cooled down, and concentrated under

vacuum to remove all volatiles. The residue was crystallized to give **2 ($R_1$ = Ph)** (12.0 g, 57.6 mol) in 96% yield as a white solid. **$^1$H NMR (400 MHz, $CDCl_3$)** δ 7.59-7.55 (m, 2H), 7.45-7.34 (m, 3H), 2.23 (s, 3H), 1.99 (s, 3H). **$^{13}$C NMR (100 MHz, $CDCl_3$)** δ 177.6, 176.2, 139.1, 128.8, 128.6, 128.5, 124.9, 124.8, 81.3, 23.5, 21.1.

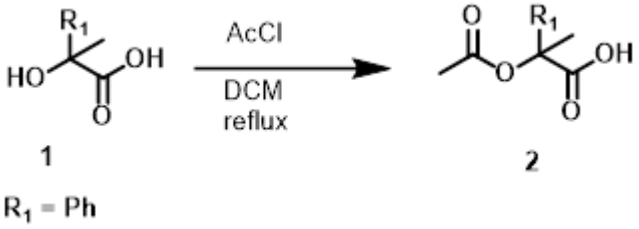


1

2

$R_1$ = Ph

1-Chloro-1-oxo-2-phenylpropan-2-yl acetate (**3 ($R_1$ = Ph)**) was synthesized using a modified procedure according to the reported literature.[34] 2-Acetoxy-2-phenylpropanoic acid (**2 ($R_1$ = Ph)**, 12.0 g, 57.6 mmol) was dissolved in anhydrous DCM (60 mL) under Ar, followed by the addition of *N*,*N*-dimethylformamide (0.45 mL, 10 mol%, 5.8 mmol) and oxalyl chloride (5.4 mL, 1.1 equiv., 63.4 mmol) with caution. The mixture was stirred at room temperature overnight. The resulting solution was concentrated under vacuum to remove all volatiles. The residue was directly used in the following step as **3 ($R_1$ = Ph)** (13.0 g, 57.4 mol, 99% yield) as a yellow sticky semi-solid. **$^1$H NMR (400 MHz, $CDCl_3$)** δ 7.52-7.49 (m, 2H), 7.42-7.37 (m, 3H), 2.28 (s, 3H), 1.98 (s, 3H). **$^{13}$C NMR (100 MHz, $CDCl_3$)** δ 173.2, 170.0, 136.5, 129.1, 128.9, 128.4, 125.1, 124.9, 86.6, 24.2, 21.1.

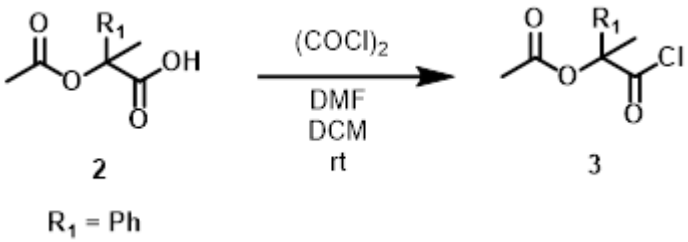


2

3

$R_1$ = Ph

5-Methyl-2-methylene-5-phenyl-1,3-dioxolan-4-one (PhDL) was synthesized using a modified procedure according to the reported literature. [32] The 1-chloro-1-oxo-2-phenylpropan-2-yl acetate (**3 ($R_1$ = Ph)**, 13.0 g, 57.4 mmol) obtained above was dissolved in

anhydrous DCM (100 mL), followed by the addition of triethylamine (37.6 g, 4.7 equiv., 270 mmol) under Ar. The mixture was heated to reflux. After 2 h, the mixture was cooled down, concentrated and precipitated with 100 mL of diethyl ether. The resulting suspension was filtered, and the solvent was evaporated with a rotary evaporator. The residual liquid was subject to fractional distillation to give PhDL (9.8 g, 51.5 mmol) at 0.1 Torr at 60 °C in 90% yield. **$^{1}$H NMR (400 MHz, $CDCl_3$)** δ 7.59-7.54 (m, 2H), 7.46-7.36 (m, 3H), 3.85 (d, *J* = 4.0 Hz, 1H), 3.83 (d, *J* = 4.0 Hz, 1H), 1.90 (s, 3H). **$^{13}$C NMR (100 MHz, $CDCl_3$)** δ 170.5, 157.5, 137.2, 129.1, 128.9, 124.6, 81.8, 62.1, 25.1.

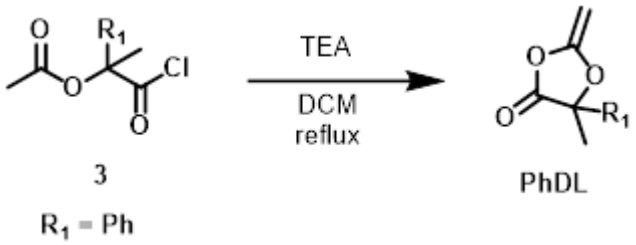


**Stability of DMDL under Moisture.**

DMDL (0.05 g, 8.9 wt%) and DMSO-d6 (0.50 g, 89.3 wt%) were mixed at room temperature in a vial. The mixture was transferred to an NMR tube. Water (0.01 g, 1.8 wt%) was added to the mixture. After a prescribed time *t*, the mixture was analyzed with NMR. In the presence of moisture, DMDL was hydrolyzed to form compound 2 (Scheme 3). We compared integrals of the vinyl protons (a) of DMDL at 3.62 and 3.70 ppm with and those of the methyl protons (c) of compound 2 and possibly further decomposed species of compound 2 from 1.86 to 2.09 ppm (Figure 4.9). The extents of the DMDL hydrolysis were determined to be 5%, 11%, and 64% at 0.5 h (Figure 4.9a), 12 h (Figure 4.9b), and 4 days (Figure 4.9c), respectively.

**General Procedure for Polymerization.**

In a typical run, a mixture (1.2–2.5 mL, typically) of a CKHE monomer, a co-monomer, AIBN or V65 or TBPB (radical initiator), and solvent was heated in a Schlenk flask at 60-120 °C under argon atmosphere with magnetic stirring. After a prescribed time *t*, an aliquot (0.1 mL) of the solution was taken out by a syringe, cooled to room temperature, and analyzed with GPC and $^1$H NMR. At the last date point of the reaction, the polymer solution was diluted with chloroform (acetonitrile for AN and DMA), and the polymer was reprecipitated in a mixture of hexane/diethyl ether (1/1 (v/v)) twice (methanol for BA, St, BMA, LMA, EHMA, and SMA) for purification. The collected polymer was dried in vacuo and analyzed with $^1$H NMR.

**Synthesis of PDMDL ($M_n$ = 104000 and $Đ$ = 2.04) (Table 4.1, entry 2) Used for Degradation.**

A mixture of DMDL (2.50 g, 19.5 mmol) and AIBN (16.0 mg, 0.0975 mmol) was heated in a Schlenk flask at 70 °C under argon atmosphere with magnetic stirring. After 1.5 h, the reaction was cooled to room temperature and analyzed with GPC and $^1$H NMR. The polymer solution was diluted with chloroform (5 mL), and the polymer was reprecipitated in a mixture of hexane/diethyl ether (1/1 (v/v)) (50 mL) twice. The collected polymer was dried in vacuo to give a PDMDL ($M_n$ = 104000 and $Đ$ = 2.04) as a white solid.

**Synthesis of PDMDL ($M_n$ = 39000 and $Đ$ = 1.42) Used for Degradation.**

A mixture of DMDL (2.50 g, 19.5 mmol), AIBN (16.0 mg, 0.0975 mmol), and toluene (10 wt%) was heated in a Schlenk flask at 70 °C under argon atmosphere with magnetic stirring. After 3 h, the reaction was cooled to room temperature and analyzed with GPC and $^1$H NMR. The polymer solution was diluted with chloroform (5 mL), and the polymer was reprecipitated in a mixture of hexane/diethyl ether (1/1 (v/v)) (50 mL) twice. The collected polymer was dried in vacuo to give a PDMDL ($M_n$ = 39000 and $Đ$ = 1.42) as a white solid.

**Synthesis of PPEGMA-*r*-PDMDL ($M_n$ = 39000 and $Đ$ = 2.22) (Table 4.1, entry 10) Used for Degradation.**

A mixture of PEGMA (1.17 g, 3.90 mmol), DMDL monomer (0.50 g, 3.90 mmol), V65 (19.4 mg, 0.0780 mmol), and toluene (50 wt%) was heated in a Schlenk flask at 60 °C under argon atmosphere with magnetic stirring. After 4 h, the reaction was cooled to room temperature and analyzed with GPC and $^1$H NMR. The polymer solution was diluted with chloroform (2 mL), and the polymer was reprecipitated in a mixture of hexane/diethyl ether (1/1 (v/v)) (20 mL) twice. The collected polymer was dried in vacuo to give a PPEGMA-*r*-PDMDL ($M_n$ = 39000 and $Đ$ = 2.22) as a transparent viscous solid.

**Synthesis of PPEGMA ($M_n$ = 72000 and $Đ$ = 2.82) Used for Degradation.**

A mixture of PEGMA (1.09 g, 3.63 mmol), V65 (9.02 mg, 0.0363 mmol), and toluene (50 wt%) was heated in a Schlenk flask at 60 °C under argon atmosphere with magnetic stirring. After 1.5 h, the reaction was cooled to room temperature and analyzed with GPC and $^1$H NMR. The polymer solution was diluted with chloroform (2 mL), and the polymer was reprecipitated in a mixture of hexane/diethyl ether (1/1 (v/v)) (20 mL) twice. The collected polymer was dried in vacuo to give a PPEGMA ($M_n$ = 72000 and $Đ$ = 2.82) as a transparent viscous solid.

**Synthesis of PLMA-*r*-PDMDL ($M_n$ = 42000 and $Đ$ = 1.76) (Table 4.1, entry 13) Used for Degradation.**

A mixture of LMA (1.00 g, 3.93 mmol), DMDL (0.50 g, 3.90 mmol), AIBN (12.8 mg, 0.0780 mmol), and toluene (50 wt%) was heated in a Schlenk flask at 70 °C under argon atmosphere with magnetic stirring. After 3 h, the reaction was cooled to room temperature and analyzed with GPC and $^1$H NMR. The polymer solution was diluted with chloroform (2 mL), and the polymer was reprecipitated in methanol (20 mL) twice. The collected polymer was dried in vacuo to give a PLMA-*r*-PDMDL ($M_n$ = 42000 and $Đ$ = 1.76) as a transparent viscous solid.

**Synthesis of PLMA ($M_n$ = 90000 and $Đ$ = 2.32) Used for Degradation.**

A mixture of LMA (1.00 g, 3.93 mmol), AIBN (12.8 mg, 0.0393 mmol), and toluene (50 wt%) was heated in a Schlenk flask at 70 °C under argon atmosphere with magnetic stirring. After 3 h, the reaction was cooled to room temperature and analyzed with GPC and $^1$H NMR. The polymer solution was diluted with chloroform (2 mL), and the polymer was reprecipitated in methanol (20 mL) twice. The collected polymer was dried in vacuo to give a PLMA ($M_n$ = 90000 and $Đ$ = 2.32) as a transparent viscous solid.

**Determination of Monomer Reactivity Ratios.**

The monomer reactivity ratio was determined at early stages of polymerization, where the monomer conversions were low, using the Fineman-Ross method. We varied the monomer feed compositions (*f*) of two monomers and determined the copolymer compositions (*F*) using $^1$H NMR. According to the Fineman-Ross equation, i.e., $G = r_1H - r_2$, where $G = x(y-1)/y$ and $H = x^2/y$ with $x = f_1/f_2$ and $y = F_1/F_2$, *G* was plotted against *H*. From the slope and intercept of the obtained straight line, $r_1$ and $r_2$ were determined (Figures 4.14–4.18).

For the comparison of the monomer reactivity ratios for DMDL and literature CKAs, examples of the monomer reactivity ratios for literature CKAs are summarized in Table 4.4.[29,39–43]

**Table 4.4.** Examples of monomer reactivity ratios for CKAs and vinyl Co-monomers.

| CKA[a] | Vinyl co-monomers | $r_{CKA}$ | $r_{co\text{-}monomer}$ | Polymerization condition[b] | Method[c] | Reference |
|---|---|---|---|---|---|---|
| MPDL | MMA | 0.01 | 4 | NMP, 90 ℃, 50 wt % toluene | NLLS | 4 |
| MDO | MMA | 0.04 | 3.5 | DTBP, 120 ℃, bulk | KT | 5 |
| MDO | VAc | 0.93 | 1.71 | AIBN, 60 ℃, bulk | FR | 6 |
| BMDO | MMA | 0.53 | 1.96 | ATRP, 120 ℃, bulk | KT | 7 |
| BMDO | BA | 0.08 | 3.7 | ATRP, 110 ℃, bulk | KT | 8 |
| BMDO | St | 1.08 | 8.53 | ATRP, 120 ℃, bulk | KT | 9 |

[a]The structures of MPDL, MDO, and BMDO are given in Scheme 1. [b]NMP is nitroxide mediated polymerization, DTBP denotes a conventional radical polymerization using di-*tert*-butyl peroxide, AIBN denotes a conventional radical polymerization using 2,2′-azobis(2-methylpropionitrile), and ATRP is atom transfer radical polymerization. [c]NLLS is the nonlinear least-square method, KT is the Kelen-Tüdős method, and FR is the Fineman-Ross method.

**Hydroxide-assisted Degradation of PDMDL ($M_n$ = 104000 and $Đ$ = 2.04 (DMF-GPC) and $M_n$ = 106000 and $Đ$ = 1.88 (THF-GPC)).**

A mixture of PDMDL ($M_n$ = 104000 and $Đ$ = 2.04) (0.064 g, 1 equiv. of the DMDL monomer unit, 2.4 wt%), 1M NaOH in $D_2O$ (0.55 g, 1 equiv. of NaOH, 20.4 wt%), and DMSO-$d_6$ (2.08 g, 77.2 wt%) was stirred at room temperature for 10 min. The mixture was analyzed with NMR and DMF-GPC within 5 h after the start of the reaction.

This experiment was also conducted using a valved NMR tube. PDMDL ($M_n$ = 104000 and $Đ$ = 2.04 (DMF-GPC)) (0.064 g, 1 equiv. of the DMDL monomer unit, 2.4 wt%) was dissolved in DMSO-$d_6$ (2.08g, 77.2 wt%) in a vial, and to this solution, 1M NaOH in $D_2O$ (0.55 g, 1 equiv. of NaOH, 20.4 wt%) was added. The mixture was transferred to a valved NMR tube,

and the tube was valved (sealed) within 15 seconds after the addition of NaOH. The mixture was analyzed with NMR after 10 min at room temperature and DMF-GPC within 5 h after the start of the reaction (Figure 4.41).

We also studied the degradation of PDMDL in a more hydrophobic solvent (a mixture of THF-$d_8$ and $D_2O$ instead of a mixture of DMSO-$d_6$ and $D_2O$). We dissolved PDMDL ($M_n$ = 106000 and $Đ$ = 1.88 (THF-GPC)) (0.064 g, 3.4 wt%, 1 equiv. of the DMDL monomer unit) in a mixture of THF-$d_8$ (1.4 g, 75.2 wt%) and $D_2O$ (0.20 g, 10.7 wt%), which was a colorless transparent solution. To this solution, NaOH (0.20 g, 10.7 wt%, 10 equiv.) was added, and the mixture was heated at 50 °C. We used an excess of NaOH (10 equiv.) and heated (50 °C) to accelerate the reaction. The reaction mixture turned to a reddish-brown suspension. After the heat treatment for 30 min, no polymer was observed in the GPC chromatogram (THF eluent) of the reaction mixture (Figure 4.42), meaning that PDMDL degraded. Because of the poor solubility of HIBA (carboxylic acid) in THF, the reaction mixture was cloudy. Therefore, the mixture was treated with HCl to adjust the pH to 3 before the analysis with NMR. At pH = 3, the mixture turned homogeneous. The $^1$H NMR and $^{13}$C NMR spectra of the reaction mixture (Figure 4.42a and b) again showed only HIBA even in this more hydrophobic solvent (THF-$d_8$/$D_2O$ mixture). Thus, the reason for no detection of other species is not clear at this moment, and hence the proposed degradation scheme (Scheme 4.4) is viewed as a tentative mechanism.

**HCl-assisted Degradation of PDMDL ($M_n$ = 104000 and $Đ$ = 2.04 (DMF-GPC) and $M_n$ = 106000 and $Đ$ = 1.88 (THF-GPC)).**

A mixture of PDMDL ($M_n$ = 106000 and $Đ$ = 1.88 (THF-GPC)) (0.064 g, 2.4 wt%, 1 equiv. of the DMDL monomer unit), 1M HCl aqueous solution (0.5 g, 18.9 wt%, 1 equiv. of HCl), and DMSO-$d_6$ (2.08 g, 78.7 wt%) was heated at 80 °C with magnetic stirring for 24 h. The mixture was cooled to room temperature. The cloudy mixture was centrifuged to separate

the white precipitate from the solution. The precipitate was dried in vacuum and analyzed with THF-GPC (Figure 4.43).

**Trifluoroacetic Acid-assisted Degradation of PDMDL ($M_n$ = 104000 and $Đ$ = 2.04 (DMF-GPC) and $M_n$ = 106000 and $Đ$ = 1.88 (THF-GPC)).**

We dissolved a PDMDL ($M_n$ = 104000 and $Đ$ = 2.04 (DMF-GPC)) (0.064 g, 10.2 wt%, 1 equiv. of the DMDL monomer unit) in DMSO (0.5 g, 79.4 wt%), which was a colorless transparent solution. We transferred this mixture to a valved NMR tube. To this solution, trifluoroacetic acid (0.057 g, 9 wt%, 1 equiv.) and water (9 mg, 1.4 wt%, 1 equiv.) were added, and the mixture was clear and colorless. The mixture was heated at 80 °C for 3 days and analyzed with NMR and DMF-GPC (Figure 4.44). The $M_n$ value decreased from 104000 (original PDMDL) to 73000 after heating at 80 °C for 3 days (Figure 4.44a). The $^1$H (Figure 4.44b) NMR spectrum showed the remained PDMDL signals (2.12-3.55 ppm for the backbone $CH_2$ protons and 1.00-1.85 ppm for the dimethyl protons), HIBA (1.26 ppm for the dimethyl protons) and acetone (2.06 ppm for the two methyl protons). The $^{13}$C (Figure 4.44c) NMR spectrum confirmed the presence of acetone in the reaction mixture (207 ppm for the carbonyl carbon and 31 ppm for the methyl carbons). Scheme 4.5 shows a possible mechanism for the acid-assisted degradation. This scheme is a possible mechanism but is not a definitive one.

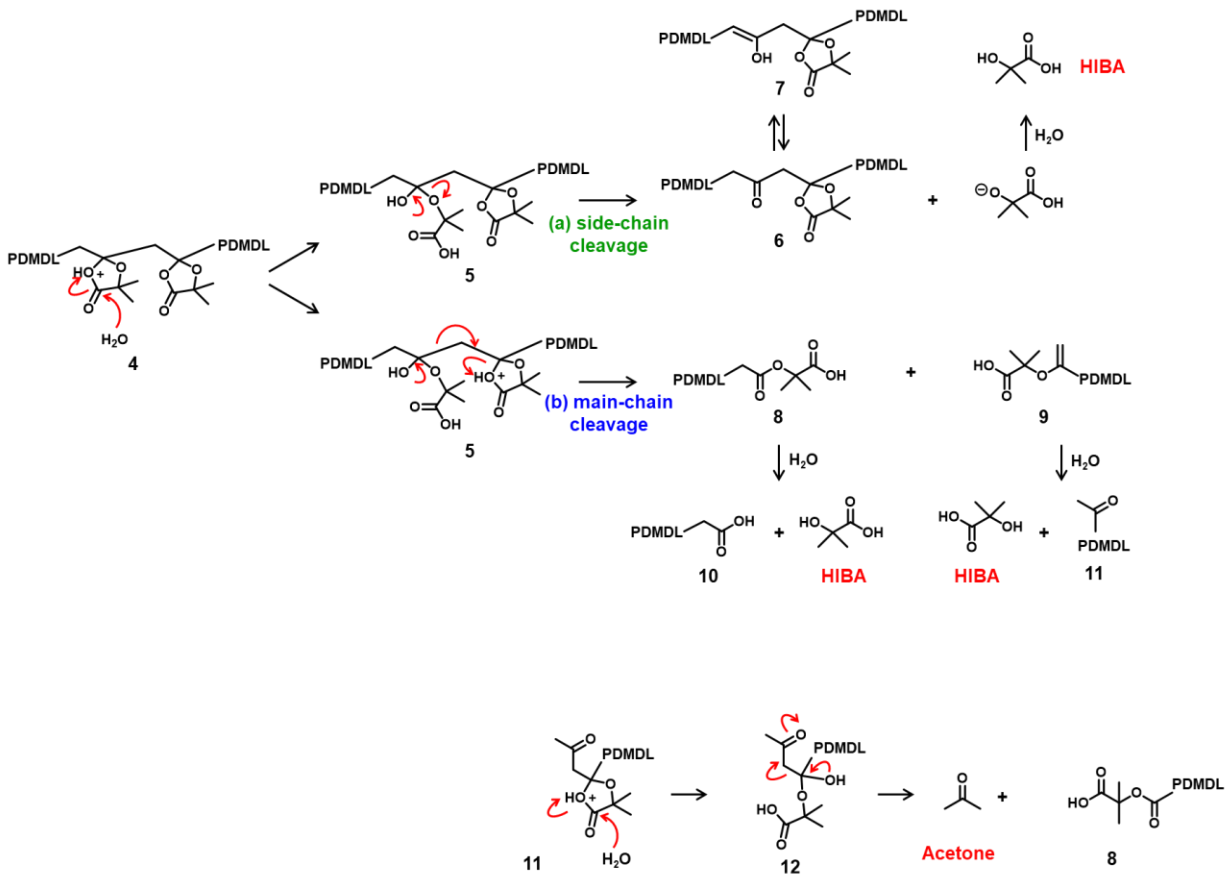


**Scheme 4.5.** Possible mechanisms of acid-assisted degradation of PDMDL.

**Amine-assisted Degradation of PDMDL ($M_n$ = 39000 and $Đ$ = 1.42).**

A mixture of PDMDL ($M_n$ = 39000 and $Đ$ = 1.42 (DMF-GPC)) (0.064 g, 4.0 wt%, 1 equiv. of the DMDL monomer unit), pentylamine (0.065g, 4.0 wt%, 1.5 equiv.), and $CD_3CN$ (1.48 g, 92.0 wt%) was heated at 65 °C with magnetic stirring. After a prescribed time *t*, an aliquot (0.1 mL) of the solution was taken out by a syringe, cooled to room temperature, and analyzed with DMF-GPC. At the last date point of the reaction, the mixture was analyzed with NMR.

Scheme 4.6 shows a possible mechanism for the amine-assisted degradation of PDMDL. Again, this scheme is a possible mechanism but is not a definitive one. R–$NH_2$ attacks the carbonyl carbon of the hemiacetal ester, generating an alkoxide anion (Scheme 4.6, compound 12). Then, either the side-chain or main-chain cleavage can occur. The side-chain cleavage can generate a ketone in the backbone (compound 6) and 2-hydroxy-2-methyl-*N*-

pentylpropanamide (HMPPA). The main-chain cleavage can generate amide (compounds 13 and 14), carboxylate (compound 9), and ketone (compound 11) chain-end PDMDLs as well as HMPPA.

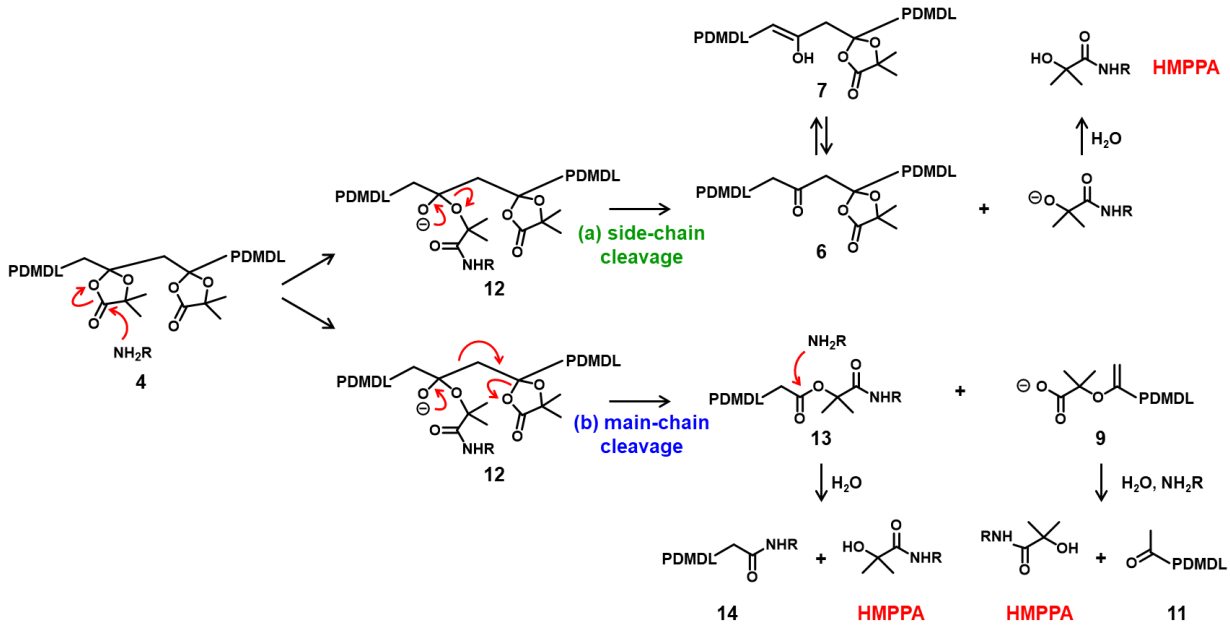


**Scheme 4.6.** Possible mechanisms of amine-assisted degradation of PDMDL.

**Degradation of PPEGMA-*r*-PDMDL ($M_n$ = 39000 and $Đ$ = 2.22).**

A mixture of PPEGMA-*r*-PDMDL ($M_n$ = 39000, $Đ$ = 2.22, and $F_{DMDL}$=17%) (0.06 g, 1 wt%, 1 equiv. of the DMDL monomer unit) and 0.9M KOH aqueous solution (6.0 g, 99 wt%, 67 equiv. of KOH) was stirred at room temperature. After a prescribed time *t*, an aliquot (0.1 mL) of the solution was taken out by a syringe and analyzed with DMF-GPC.

**Degradation of PPEGMA ($M_n$ = 72000 and $Đ$ = 2.82).**

A mixture of PPEGMA ($M_n$ = 72000 and $Đ$ = 2.82) (0.06 g, 1 wt%) and 0.9M KOH aqueous solution (6.0 g, 99 wt%) was stirred at room temperature. After 24 h, an aliquot (0.1 mL) of the solution was analyzed with DMF-GPC. The $M_n$ decreased (from 72000) to only 70000 and hence did not change significantly (Figure 4.49). Thus, the degradation (decrease in

the $M_n$ value) of the PPEGMA-*r*-PDMDL (Figure 4.5a) was ascribed to the main-chain cleavage of the DMDL units in the polymer.

**Degradation of PLMA-*r*-PDMDL ($M_n$ = 42000 and $Đ$ = 1.76).**

A mixture PLMA-r-PDMDL ($M_n$ = 42000, $Đ$ = 1.76, and $F_{DMDL}$ = 16%) (0.04 g, 2.0 wt%, 1 equiv. of the DMDL monomer unit), 0.9M KOH in methanol (0.16 g, 3.5 equiv. to the DMDL unit, 8.1 wt%), and THF (1.78 g, 89.9 wt%) was stirred at room temperature. After a prescribed time *t*, an aliquot (0.1 mL) of the solution was taken out by a syringe and analyzed with THF-GPC.

**Degradation of PLMA ($M_n$ = 90000 and $Đ$ = 2.32).**

A mixture PLMA ($M_n$ = 90000 and $Đ$ = 2.32) (0.04 g, 2.0 wt%), 0.9M KOH in methanol (0.16 g, 8.1 wt%), and THF (1.78 g, 89.9 wt%) was stirred at room temperature. After 24 h, an aliquot (0.1 mL) of the solution was analyzed with THF-GPC. The $M_n$ changed from 90000 to 91000 and hence did not change significantly (Figure 4.50). Thus, the observed degradation (decrease in the $M_n$ value) of the PLMA-*r*-PDMDL (Figure 4.5b) was ascribed to the main-chain cleavage of the DMDL units in the polymer.

**Recovery of HIBA via NaOH-assisted Degradation of PDMDL.**

A mixture of PDMDL ($M_n$ = 56000 and $Đ$ = 2.47) (1.0 g, 1 equiv. of the DMDL monomer unit), 0.9M KOH in methanol (28 g, 4 equiv. of KOH), and THF (300 g) was stirred at room temperature for 1 h. The mixture was acidified using an aqueous HCl (1M) solution to pH = 3. The mixture was extracted with diethyl ether (100ml) for three times. The collected organic layer was dried with anhydrous magnesium sulfate. The mixture was filtered and dried with rotary evaporator. HIBA (0.39g) (white solid) was obtained and analyzed with NMR.

**Synthesis of PDMDL Using Recovered HIBA.**

The HIBA (1 equiv.) recovered above was reacted with acetyl chloride (1.8 equiv.) under room temperature for 2 h, according to Scheme 4.3. The mixture was evaporated under vacuum, extracted with dichloromethane, dried with sodium sulfate, and then evaporated under vacuum, giving compound **2 ($R_1$ = $CH_3$)** (Figures 4.51 and 4.52) in an 80% yield. The purified compound **2 ($R_1$ = $CH_3$)** (1 equiv.) was subsequently reacted with oxalyl chloride (1.1 equiv.) in a mixture of dichloromethane (99%) and dimethyl formamide (1%) at room temperature overnight, giving compound **3 ($R_1$ = $CH_3$)** (Figures 4.53 and 4.54) in a 70% conversion (as determined with $^1$H NMR) after the evaporation under vacuum. The crude compound **3 ($R_1$ = $CH_3$)** (1 equiv.). was directly reacted in the presence of triethylamine (1.5 equiv.) in dichloromethane under reflux for 5 h, yielding DMDL. DMDL was purified by distillation and obtained in a 75% yield (based on the amount of compound **3 ($R_1$ = $CH_3$)**) after distillation (Figure 4.55).

**Spectral Data and Plots.**

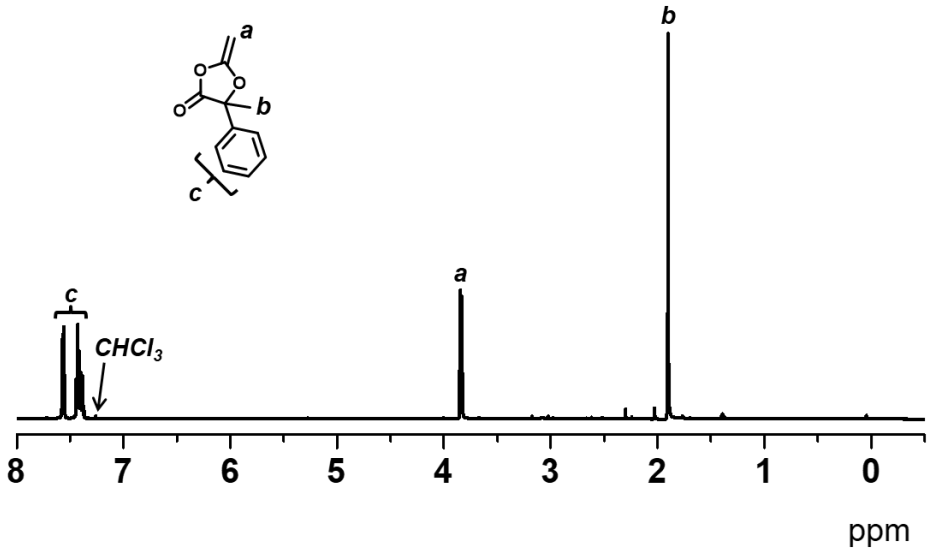


**Figure 4.7.** $^{1}H$ NMR spectrum of PhDL (400 MHz, 298 K, $CDCl_3$).

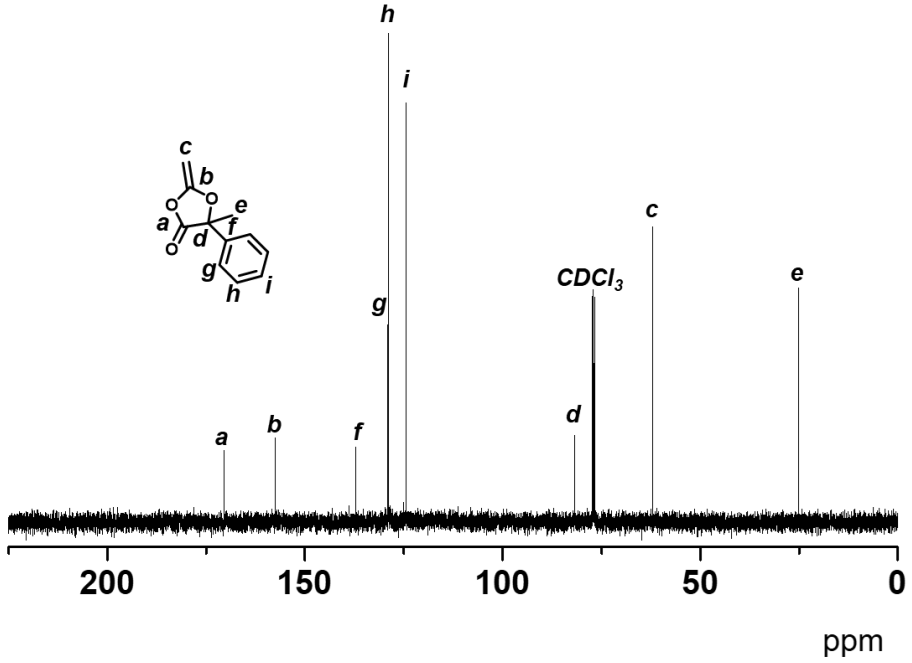


**Figure 4.8.** $^{13}C$ NMR spectrum of PhDL (100 MHz, 298 K, $CDCl_3$).

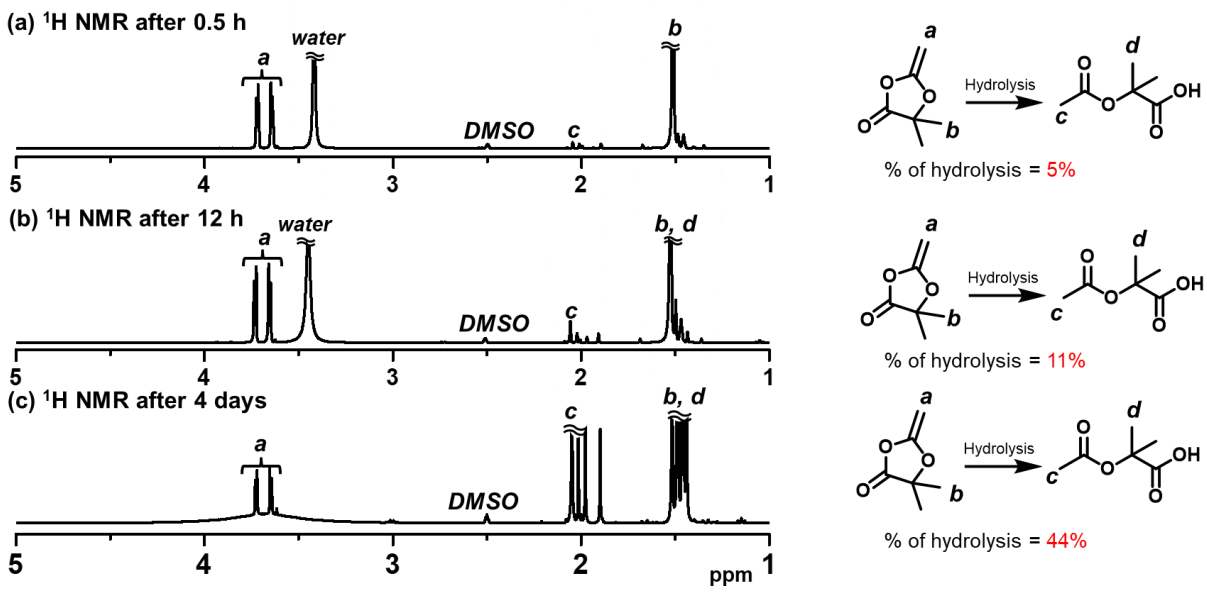


**Figure 4.9.** $^{1}$H NMR spectra of DMDL and water mixture at (a) 0.5 h (b) 12 h (c) 4 days (400 MHz, 298 K, DMSO-$d_6$).

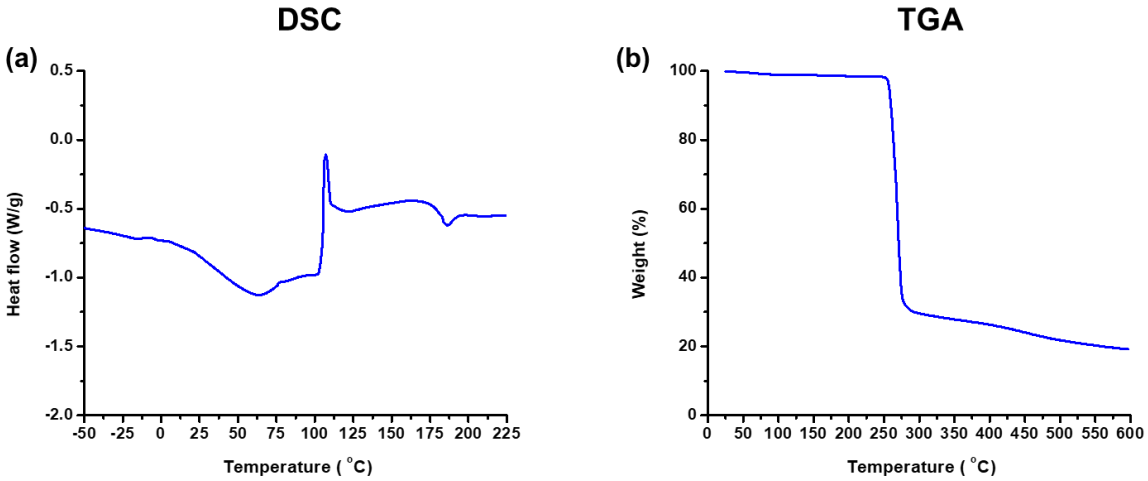


**Figure 4.10.** (a) DSC and (b) TGA curves of PDMDL (Table 4.1, entry 2) ($M_n$ = 104000 and $Đ$ = 2.04).

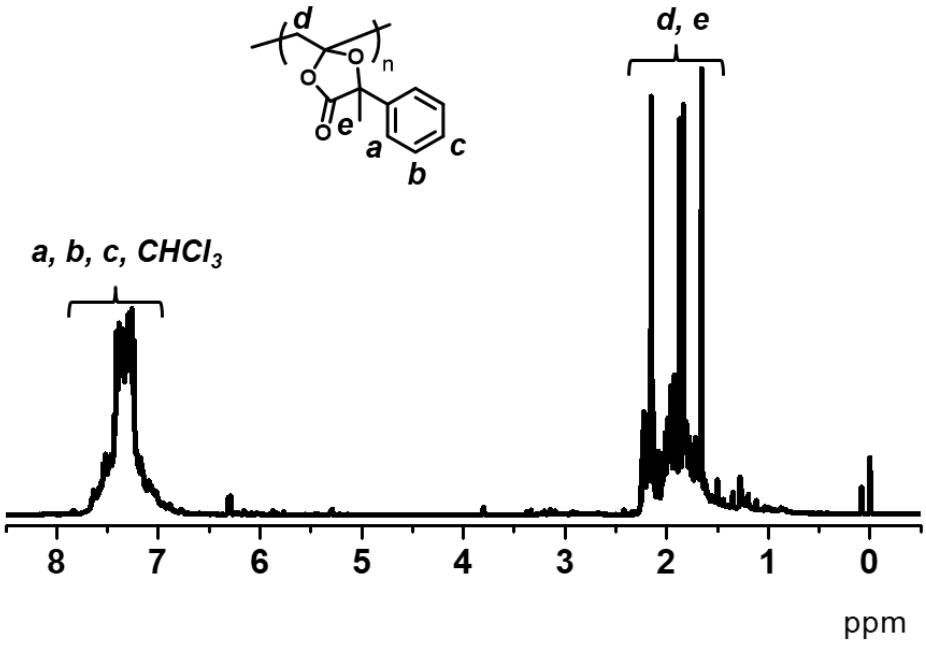


**Figure 4.11.** $^{1}$H NMR spectrum of PPhDL (Table 4.2, entry 1) (400 MHz, 298 K, $CDCl_3$).

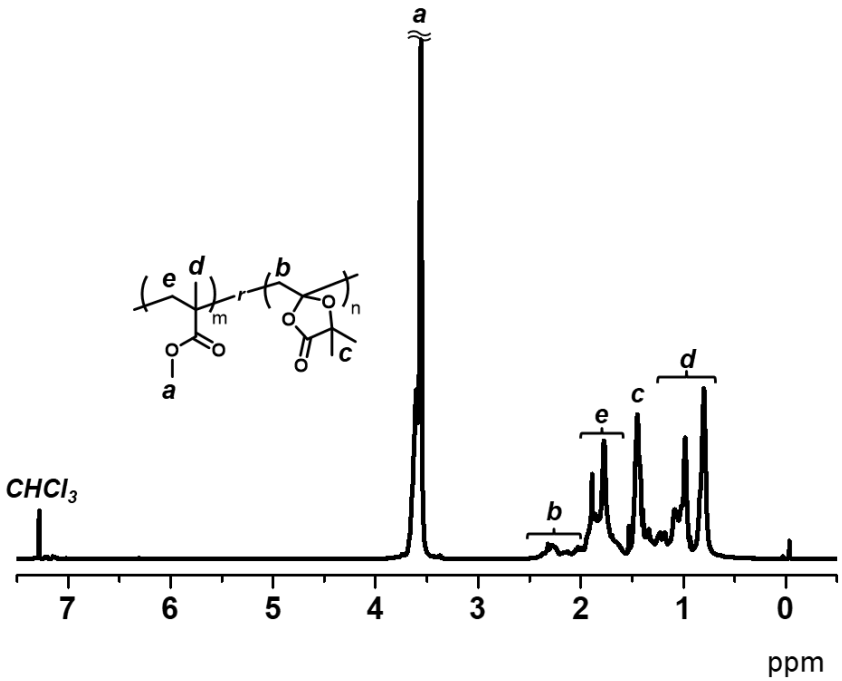


**Figure 4.12.** $^{1}$H NMR spectrum of PMMA-*r*-PDMDL (Table 4.1, entry 3) (400 MHz, 298 K, $CDCl_3$).

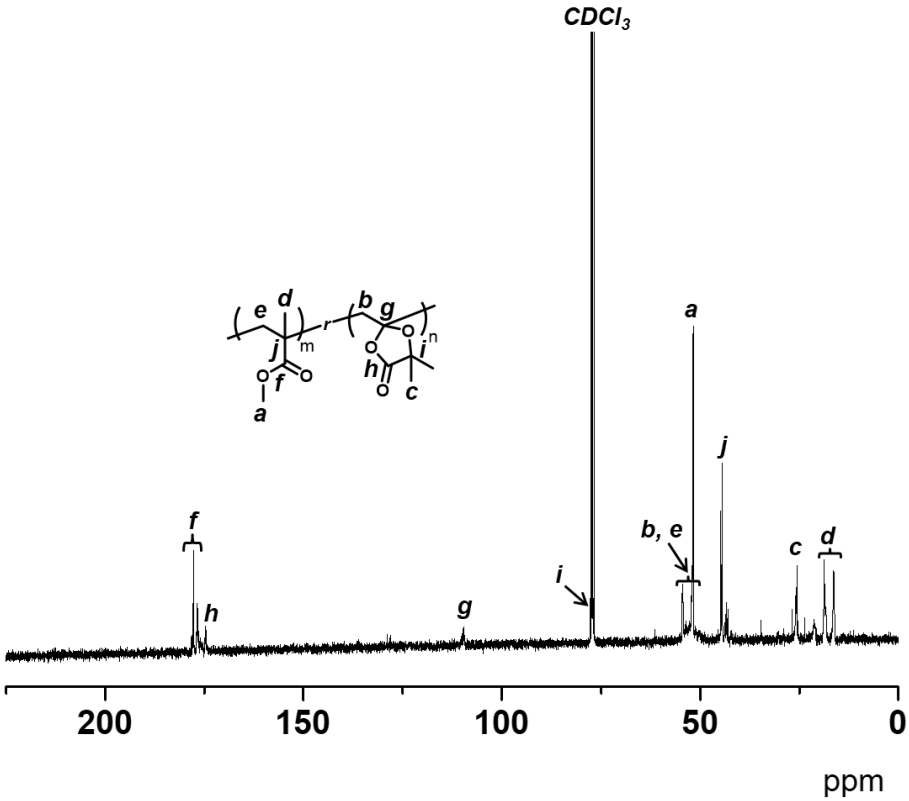


**Figure 4.13.** $^{13}C$ NMR spectrum of PMMA-*r*-PDMDL (Table 4.1, entry 3) (100 MHz, 298 K, $CDCl_3$).

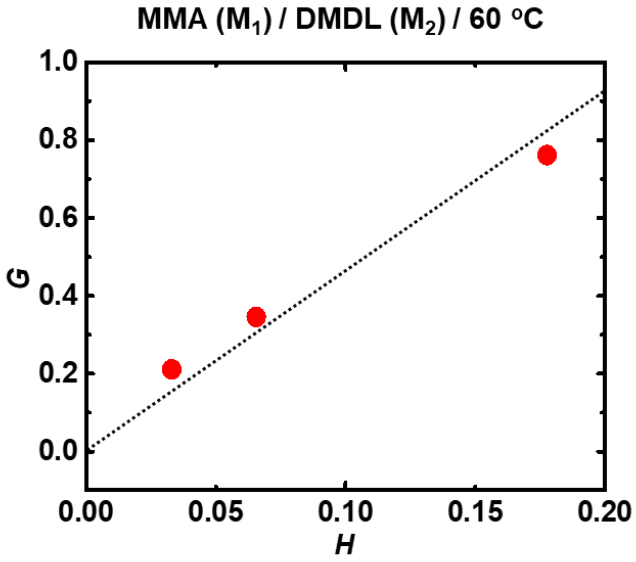


**Figure 4.14.** Fineman-Ross plot of MMA ($M_1$) and DMDL ($M_2$) (Table 4.3, entry 1).

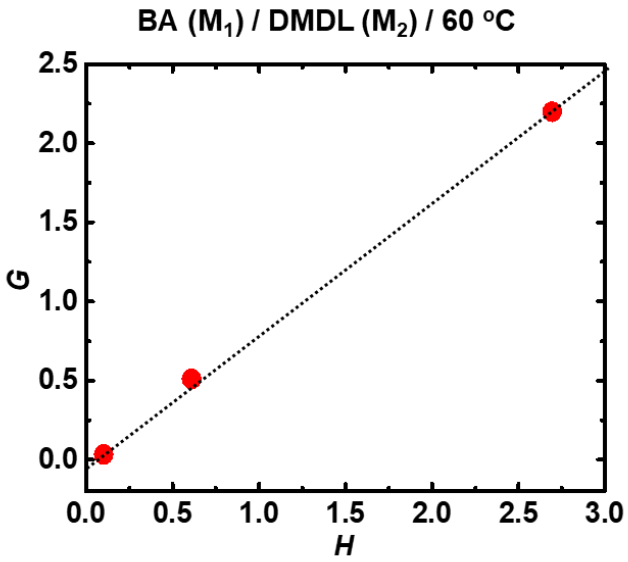


**Figure 4.15.** Fineman-Ross plot of BA ($M_1$) and DMDL ($M_2$) (Table 4.3, entry 2).

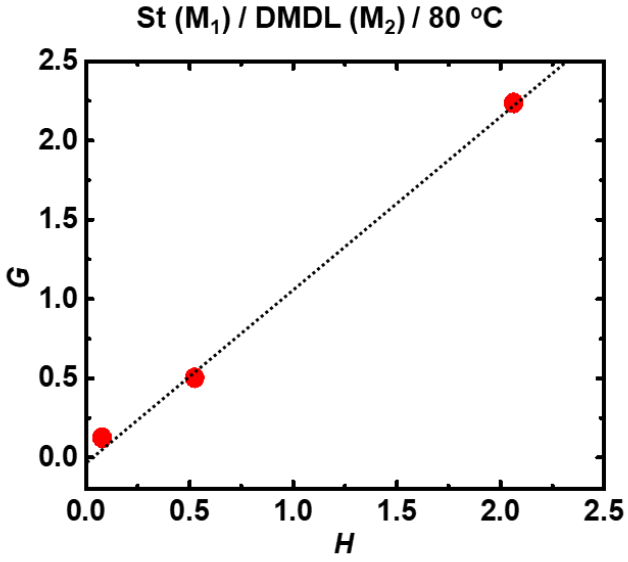


**Figure 4.16.** Fineman-Ross plot of St ($M_1$) and DMDL ($M_2$) (Table 4.3, entry 3).

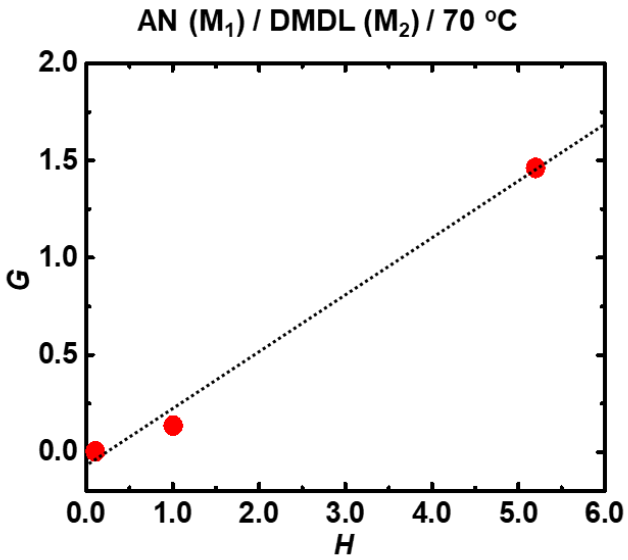


**Figure 4.17.** Fineman-Ross plot of AN ($M_1$) and DMDL ($M_2$) (Table 4.3, entry 4).

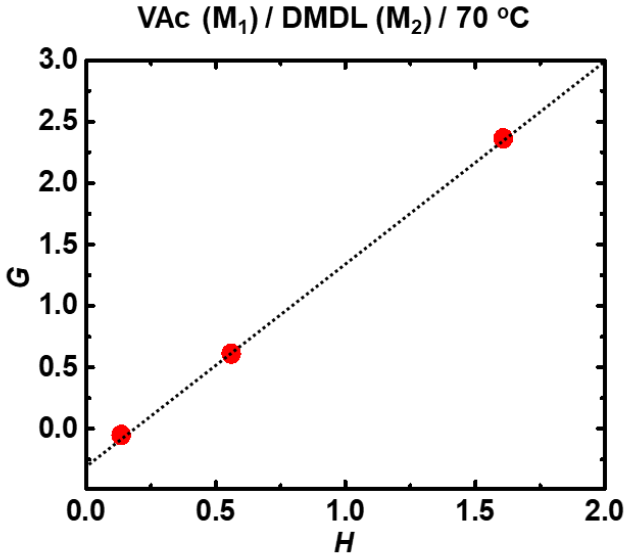


**Figure 4.18.** Fineman-Ross plot of VAc ($M_1$) and DMDL ($M_2$) (Table 4.3, entry 5).

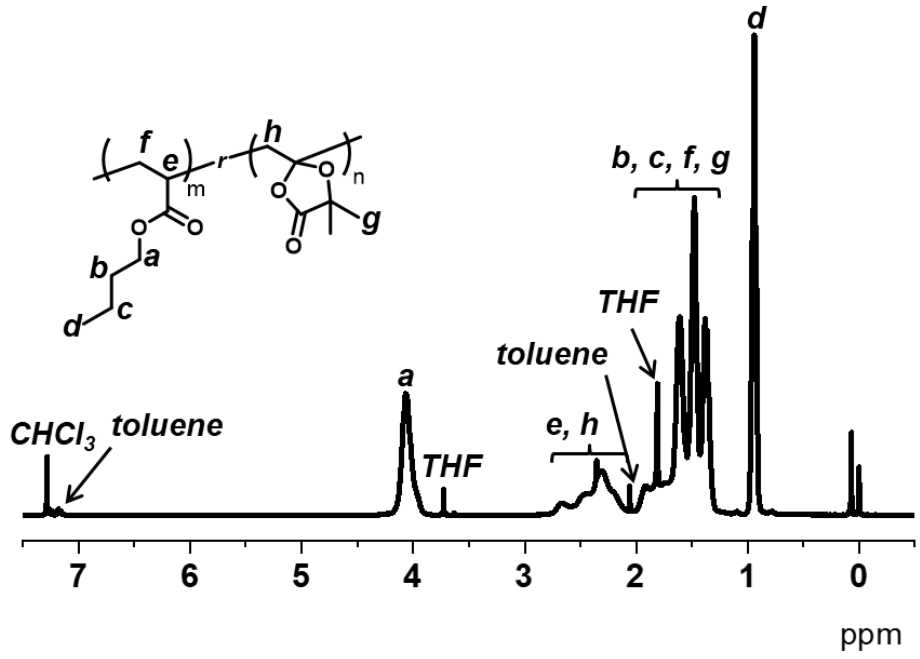


**Figure 4.19.** $^{1}$H NMR spectrum of PBA-*r*-PDMDL (Table 4.1, entry 4) (400 MHz, 298 K, $CDCl_3$).

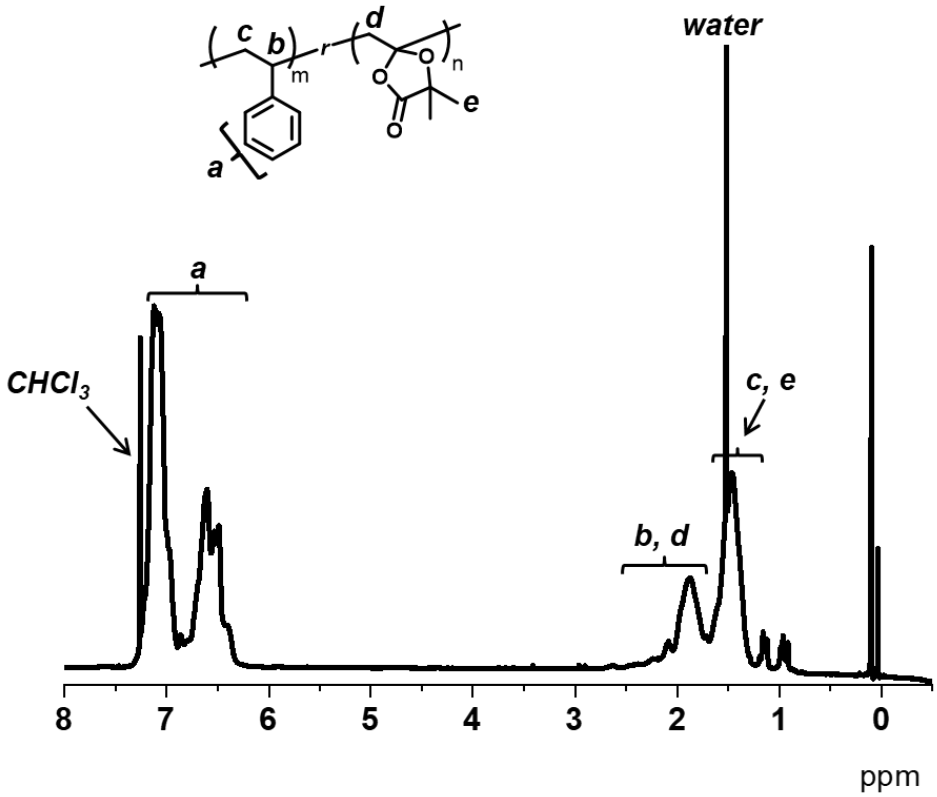


**Figure 4.20.** $^{1}$H NMR spectrum of PSt-*r*-PDMDL (Table 4.1, entry 5) (400 MHz, 298 K, $CDCl_3$).

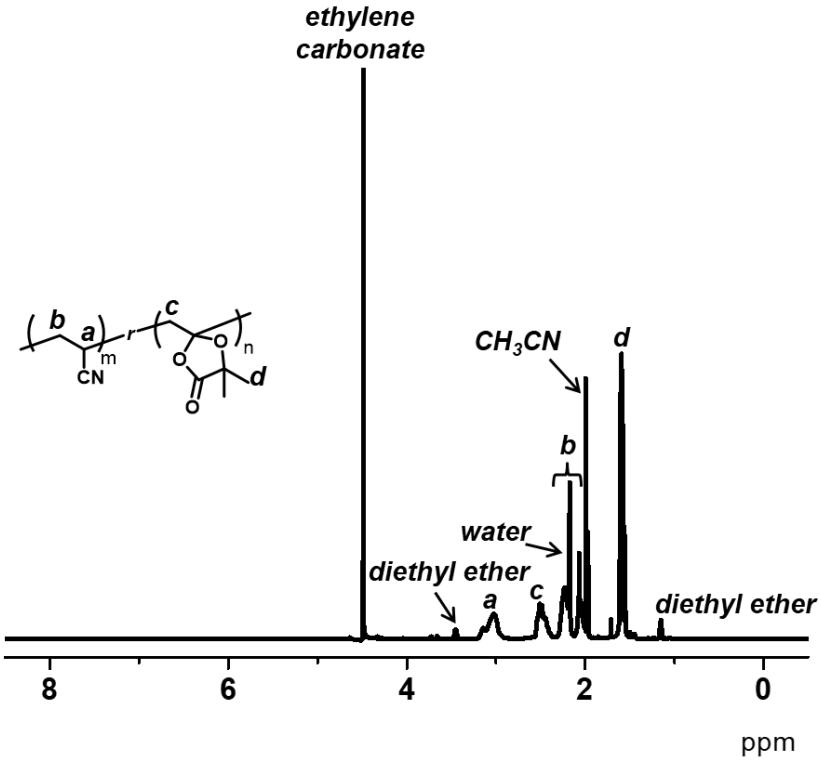


**Figure 4.21.** $^{1}$H NMR spectrum of PAN-*r*-PDMDL (Table 4.1, entry 6) (400 MHz, 298 K, $CD_3CN$).

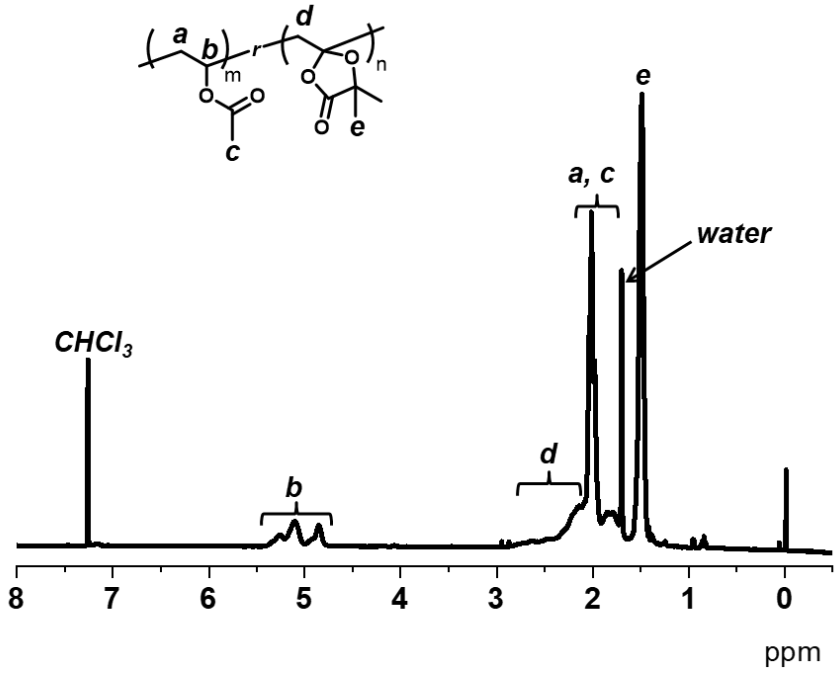


**Figure 4.22.** $^{1}$H NMR spectrum of PVAc-*r*-PDMDL (Table 4.1, entry 7) (400 MHz, 298 K, $CDCl_3$).

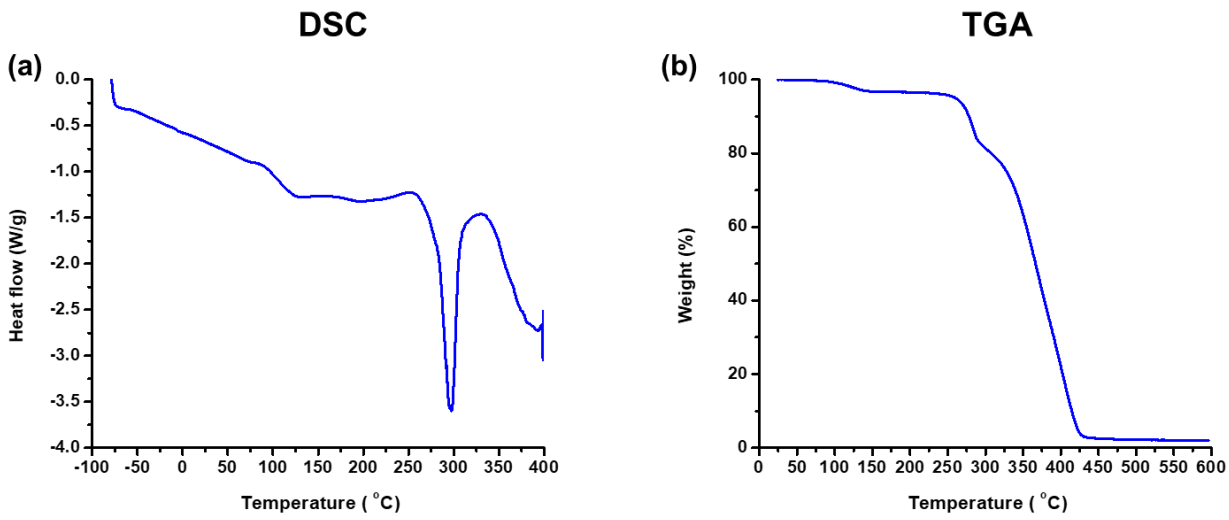


**Figure 4.23.** (a) DSC and (b) TGA of PMMA-*r*-PDMDL (Table 4.1, entry 3) ($M_n$ = 19000 and $Đ$ = 1.78). The $T_g$ and $T_d$ values were 104 (± 5 °C) °C and 366 °C, respectively.

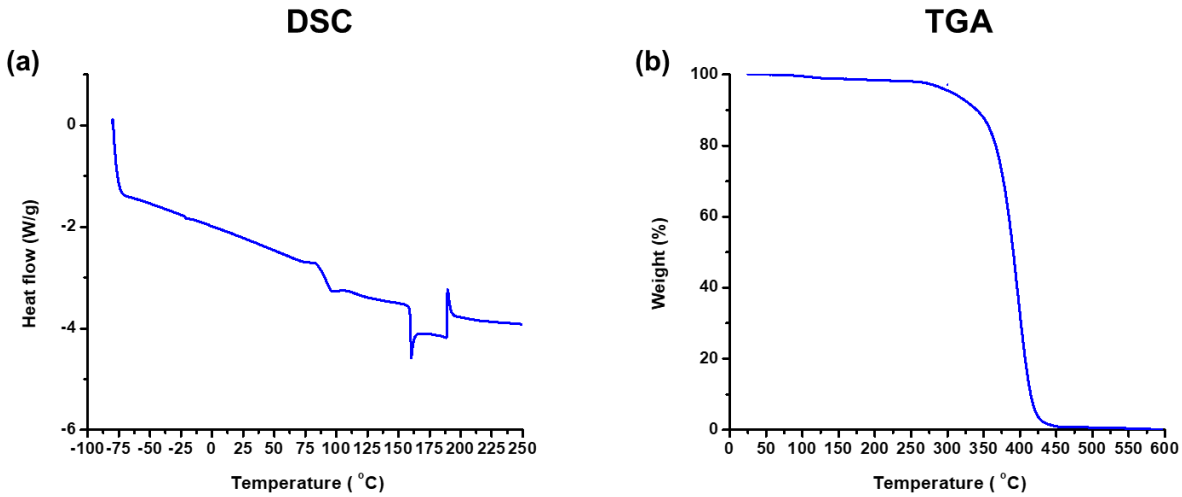


**Figure 4.24.** (a) DSC and (b) TGA of PSt-*r*-PDMDL (Table 4.1, entry 5) ($M_n$ = 5100 and $Đ$ = 1.46). The $T_g$ and $T_d$ values were 90 (± 5 °C) °C and 391 °C, respectively.

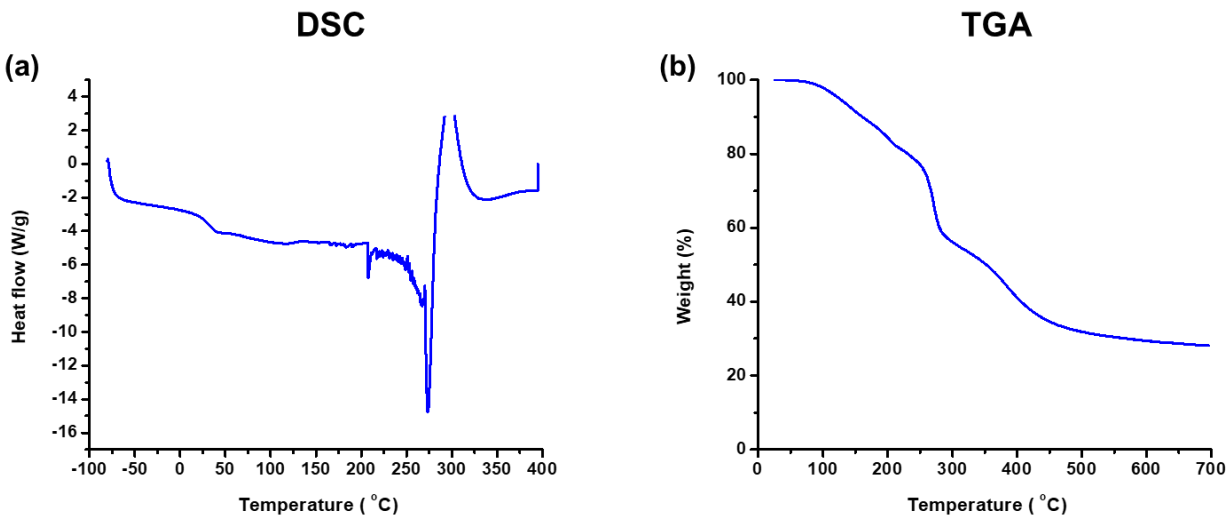


**Figure 4.25.** (a) DSC and (b) TGA of PAN-*r*-PDMDL (Table 4.1, entry 6) ($M_n$ = 77000 and $Đ$ = 1.54). The $T_g$ and $T_d$ values were 76 (± 5 °C) °C and 350 °C, respectively. (The decay in the 20–40 °C region in the DSC curve would be ascribed to the ethylene carbonate (EC) remaining in the polymer (melting point of EC = 36 °C)

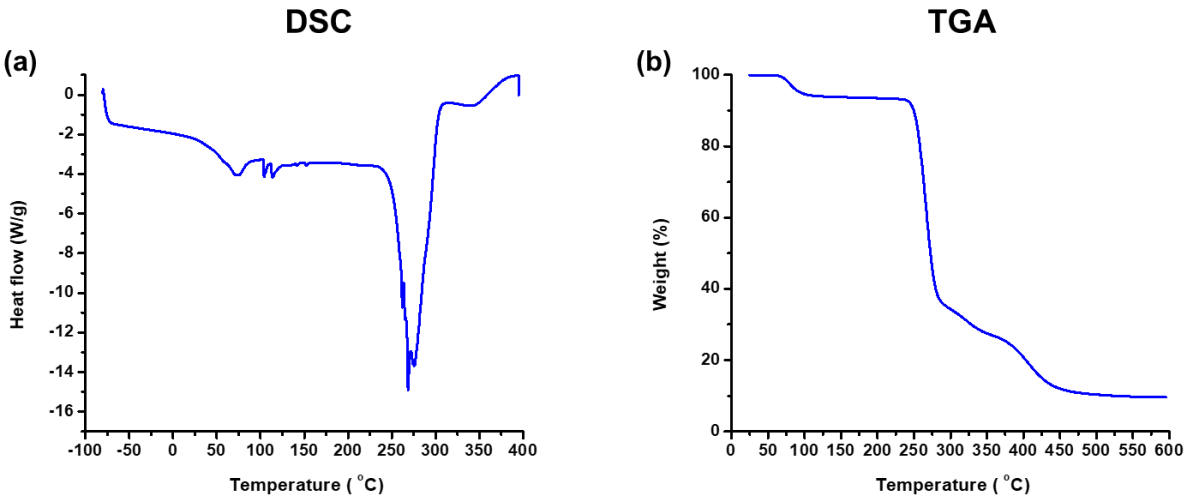


**Figure 4.26.** (a) DSC and (b) TGA of PVAc-*r*-PDMDL (Table 4.1, entry 7) ($M_n$ = 11000 and $Đ$ = 1.60). The $T_g$ and $T_d$ values were 38 (33–46) °C and 272 °C, respectively.

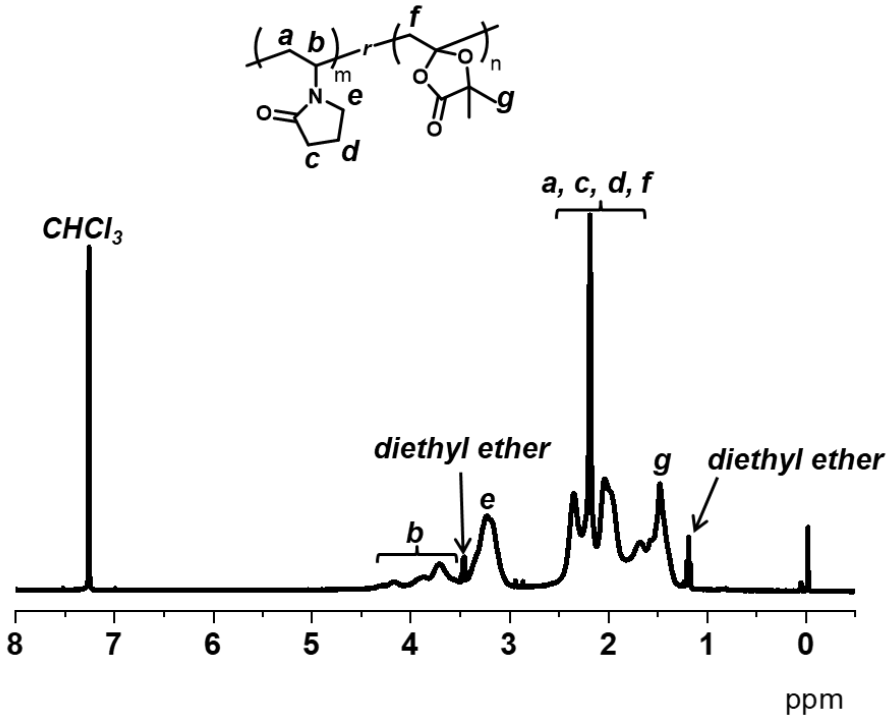


**Figure 4.27.** $^{1}$H NMR spectrum of PNVP-*r*-PDMDL (Table 4.1, entry 8) (400 MHz, 298 K, $CDCl_3$).

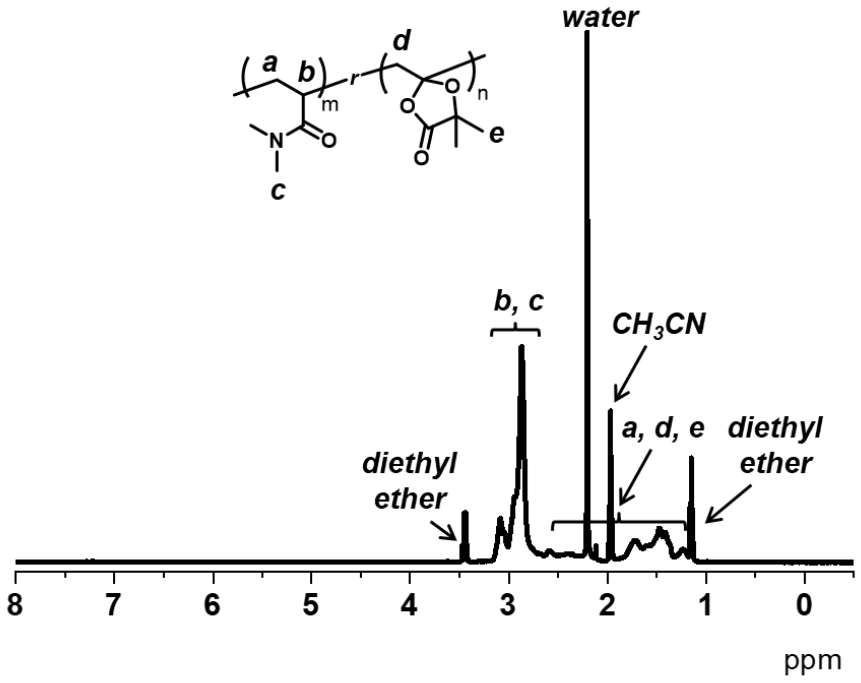


**Figure 4.28.** $^{1}$H NMR spectrum of PDMA-*r*-PDMDL (Table 4.1, entry 9) (400 MHz, 298 K, $CD_3CN$).

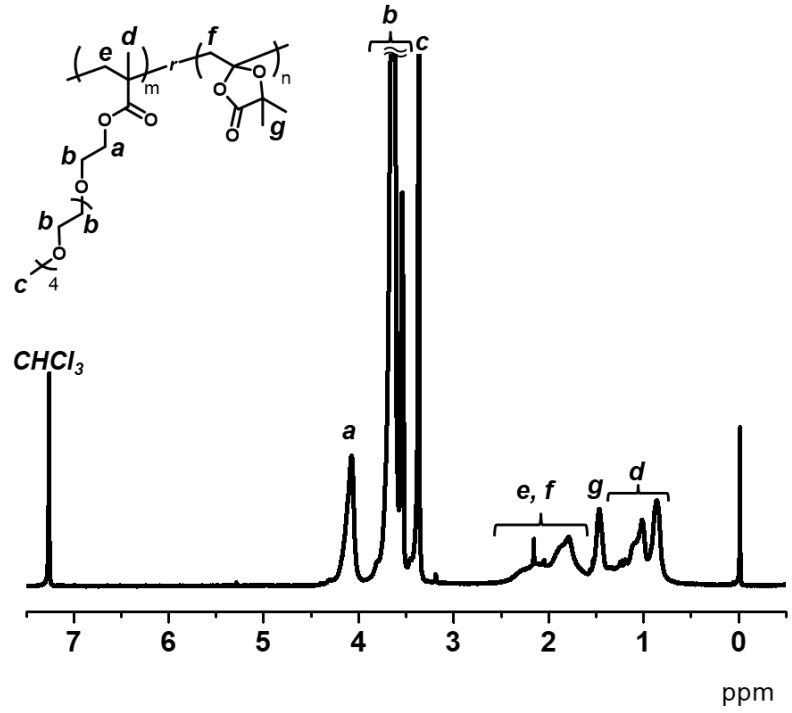


**Figure 4.29.** $^{1}$H NMR spectrum of PPEGMA-*r*-PDMDL (Table 4.1, entry 10) (400 MHz, 298 K, $CDCl_3$).

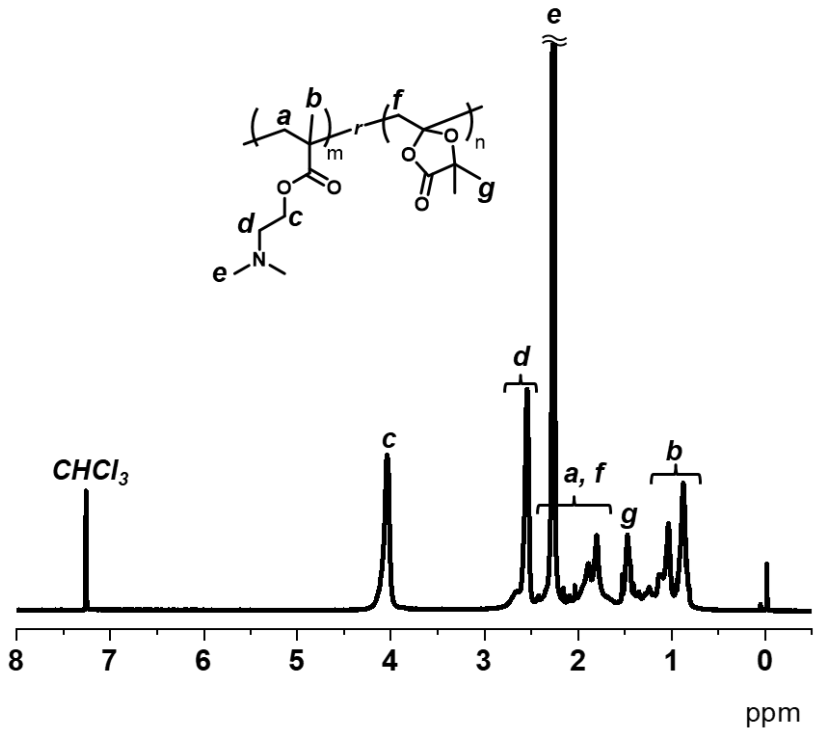


**Figure 4.30.** $^{1}$H NMR spectrum of PDMAEMA-*r*-PDMDL (Table 4.1, entry 11) (400 MHz, 298 K, $CDCl_3$).

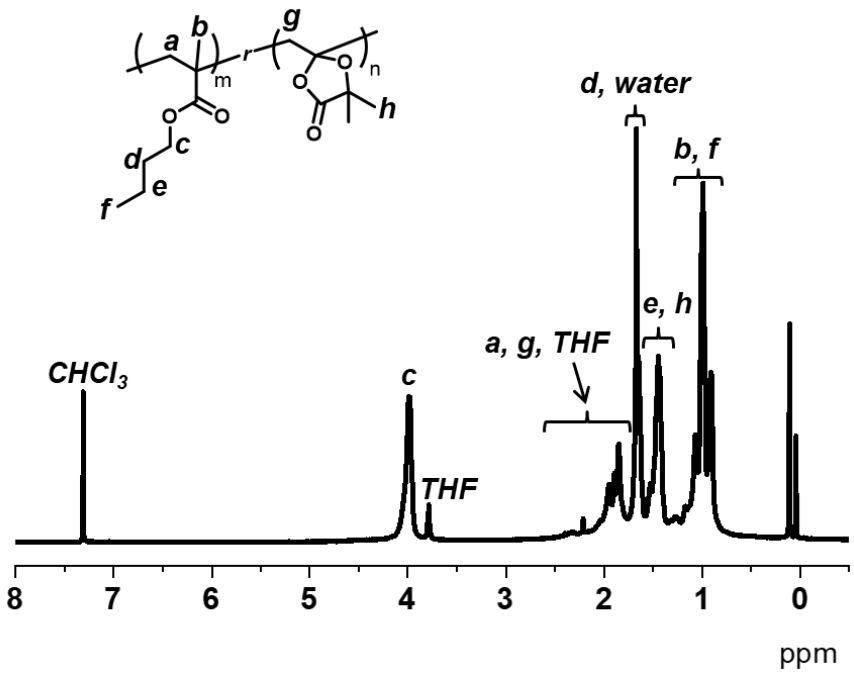


**Figure 4.31.** $^{1}$H NMR spectrum of PBMA-*r*-PDMDL (Table 4.1, entry 12) (400 MHz, 298 K, $CDCl_3$).

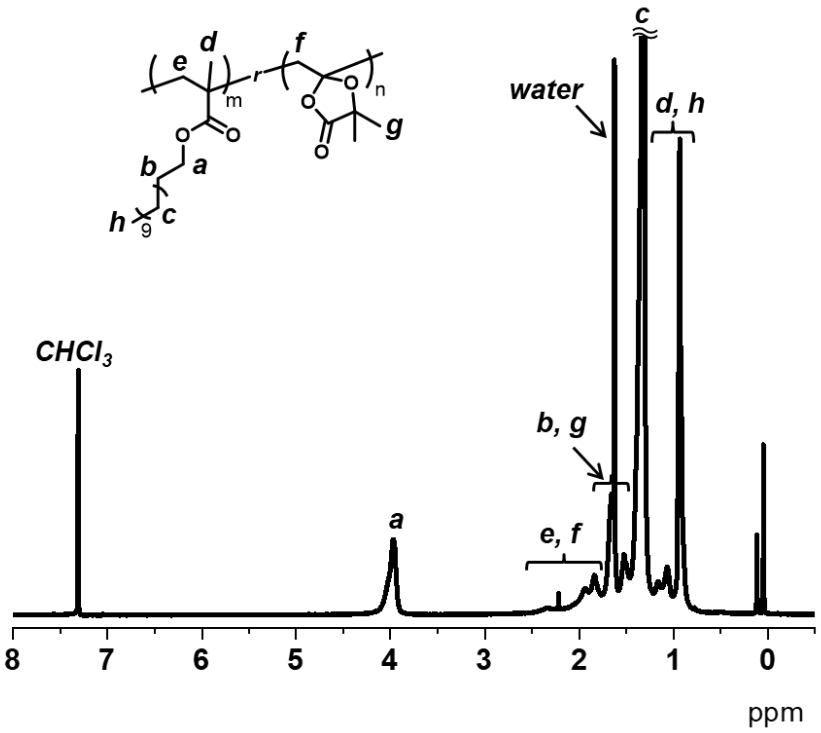


**Figure 4.32.** $^{1}$H NMR spectrum of PLMA-*r*-PDMDL (Table 1, entry 13) (400 MHz, 298 K, $CDCl_3$).

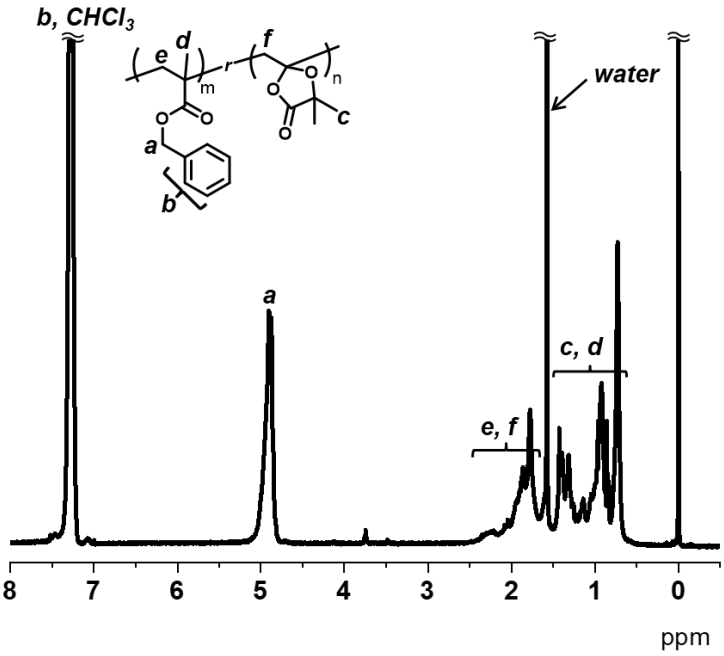


**Figure 4.33.** $^{1}$H NMR spectrum of PBzMA-*r*-PDMDL (Table 4.1, entry 14) (400 MHz, 298 K, $CDCl_3$).

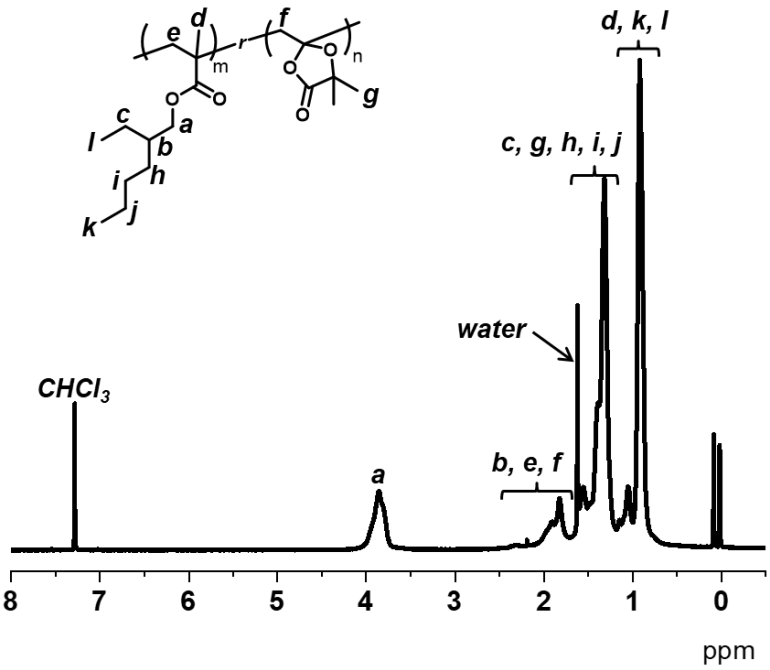


**Figure 4.34.** $^{1}$H NMR spectrum of PEHMA-*r*-PDMDL (Table 4.1, entry 15) (400 MHz, 298 K, $CDCl_3$).

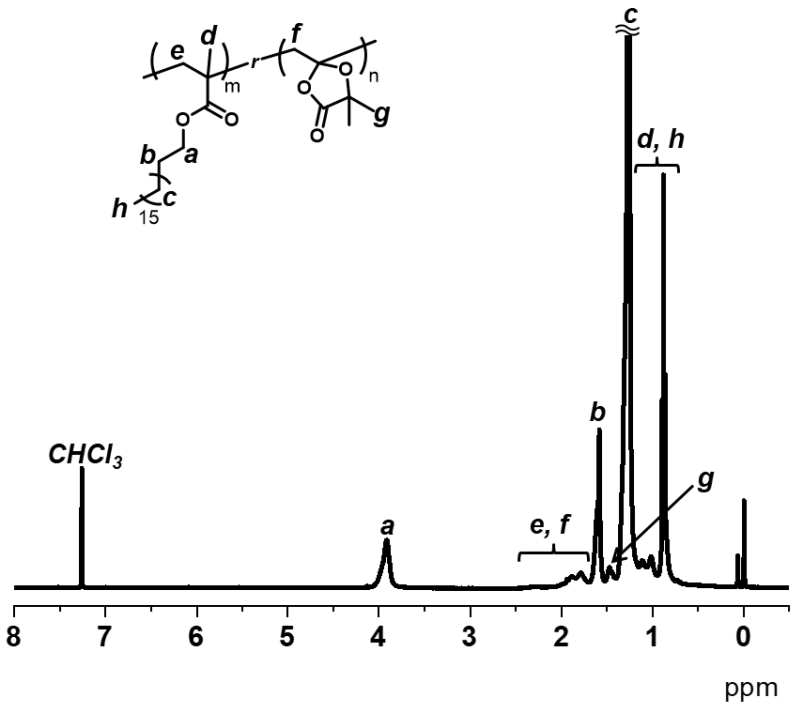


**Figure 4.35.** $^{1}$H NMR spectrum of PSMA-*r*-PDMDL (Table 4.1, entry 16) (400 MHz, 298 K, $CDCl_3$)

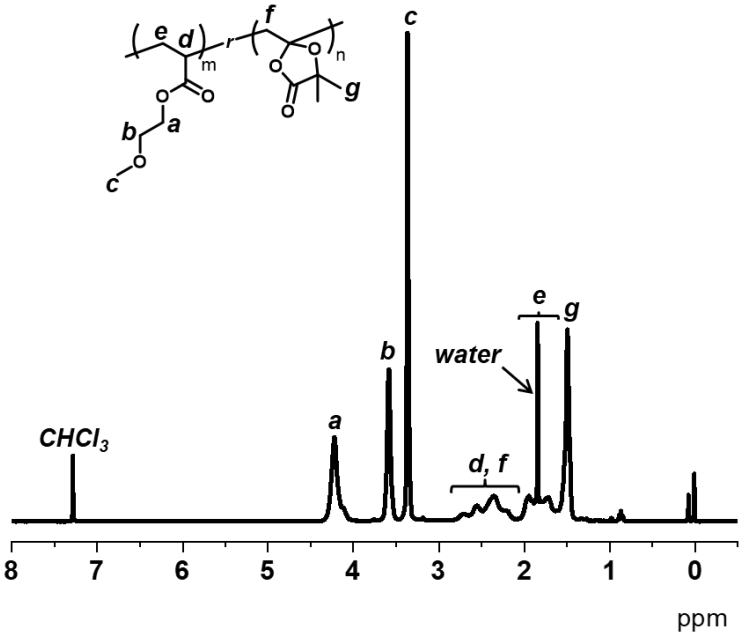


**Figure 4.36.** $^{1}$H NMR spectrum of PMEA-*r*-PDMDL (Table 4.1, entry 17) (400 MHz, 298 K, $CDCl_3$).

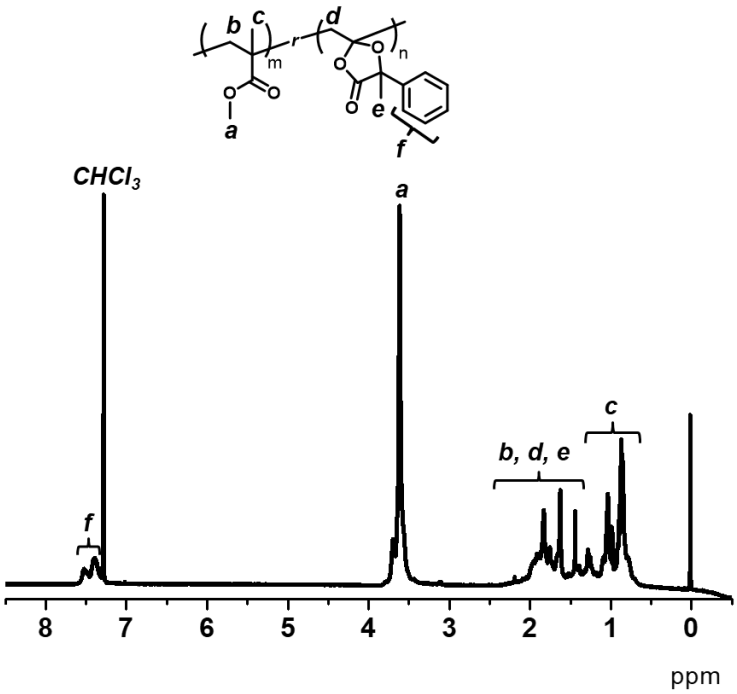


**Figure 4.37.** $^{1}$H NMR spectrum of PMMA-*r*-PPhDL (Table 4.2, entry 2) (400 MHz, 298 K, $CDCl_3$).

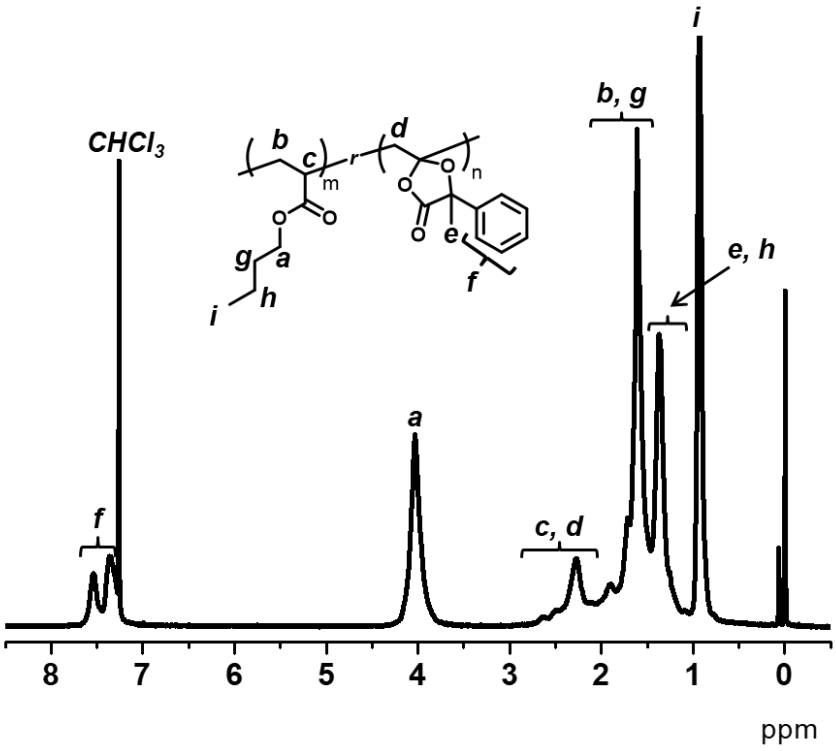


**Figure 4.38.** $^{1}$H NMR spectrum of PBA-*r*-PPhDL (Table 4.2, entry 4) (400 MHz, 298 K, $CDCl_3$).

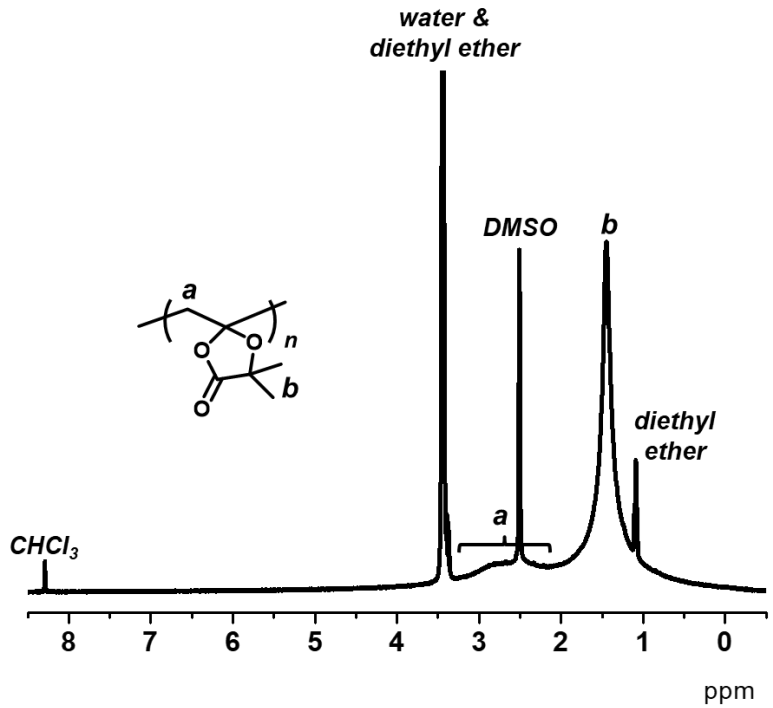


**Figure 4.39.** $^{1}$H NMR spectrum of non-degraded PDMDL in DMSO-$d_6$/$D_2O$ (77.2/20.4 wt%) mixture (400 MHz, 298 K, $CDCl_3$).

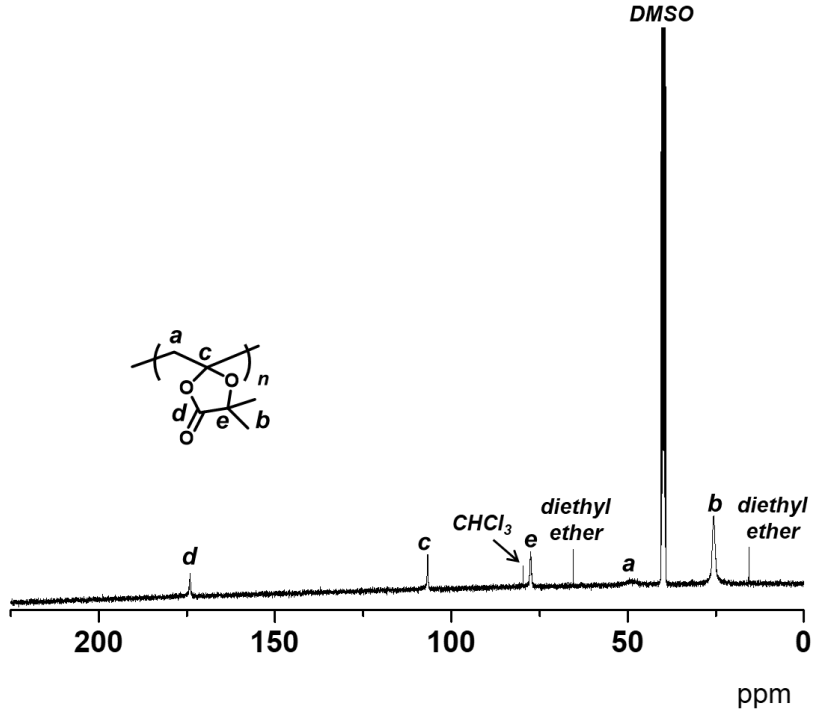


**Figure 4.40.** $^{13}$C NMR spectrum of non-degraded PDMDL (2.4 wt%) in DMSO-$d_6$/$D_2O$ (77.2/20.4 wt%) mixture (100 MHz, 298 K, $CDCl_3$).

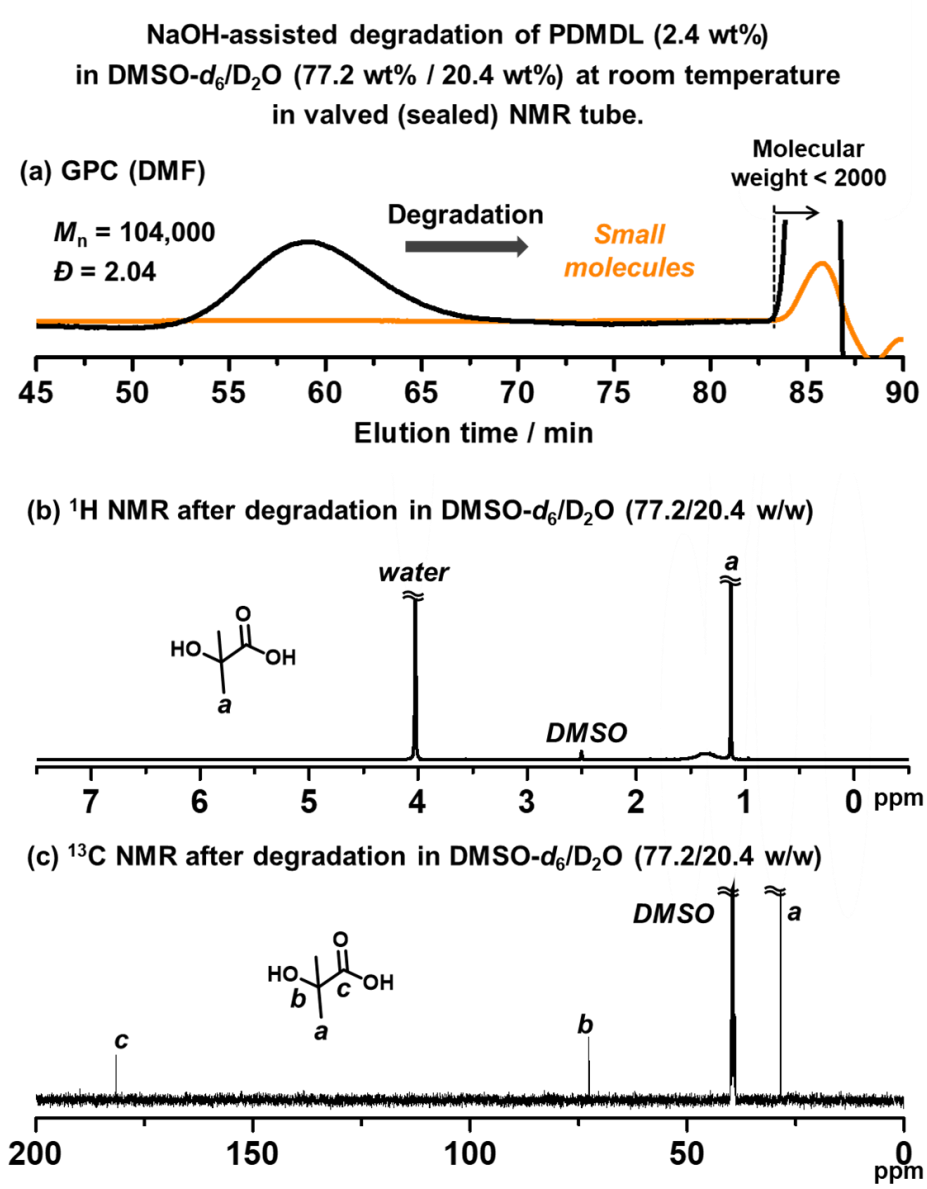


**Figure 4.41.** Degradation of PDMDL ($M_n$ = 104,000, $Đ$ = 2.04, 2.4 wt%, 1 equiv. of the DMDL monomer unit) using 1 equiv. of NaOH in a mixture of $D_2O$ (20.4 wt%) and DMSO-$d_6$ (77.2 wt%) at room temperature within 5 h. The reaction was conducted in a valved (sealed) NMR tube. The PDMDL used in Figure 4.41 is the same as that given in Table 4.1 (entry 2), Figure 4.3a, 4.42, 4.43, and 4.44. The $M_n$ and $Đ$ values of PDMDL determined with DMF-GPC (Table 4.1 (entry 2), Figure 4.3a, 4.41, and 4.44) were 104,000 and 2.04, respectively, and those determined with THF-GPC (Figure 4.42 and 4.43) were 106,000 and 1.88, respectively. (a) GPC chromatogram before (black line) and after (orange line) degradation. (b) $^1$H NMR and (c) $^{13}$C NMR spectra of the reaction mixture after degradation (400 MHz for $^1$H NMR and 100 MHz for $^{13}$C NMR) (in DMSO-$d_6$/$D_2O$).

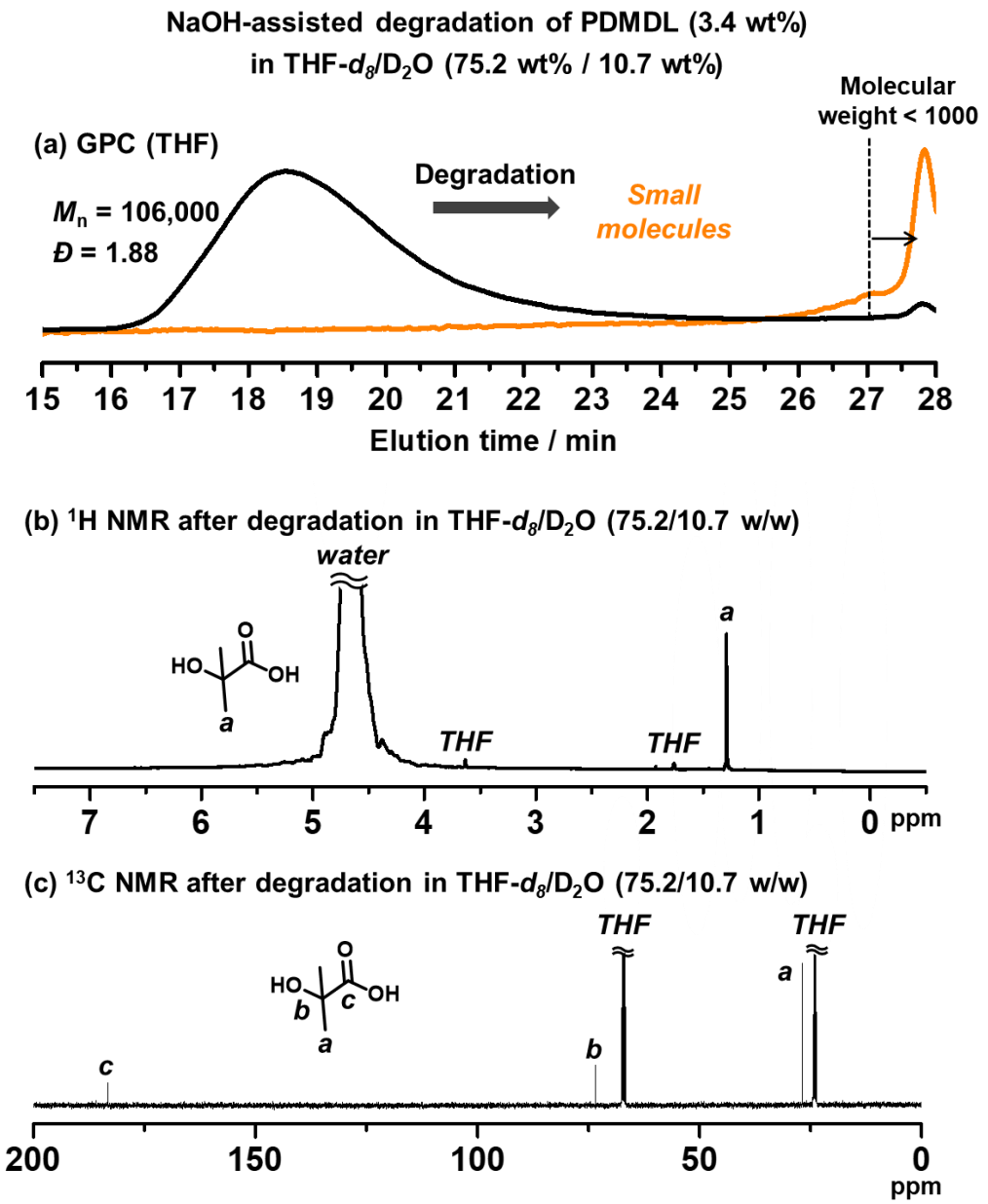


**Figure 4.42.** Degradation of PDMDL ($M_n$ = 106,000, $Đ$ = 1.88, 3.4 wt%) using 10 equiv. of NaOH (10.7 wt%) in $D_2O$ (10.7 wt%) and THF-$d_8$ (75.2 wt%) at 50 °C for 30 min. The PDMDL used in Figure 4.42 is the same as that given in Table 4.1 (entry 2), Figure 4.3a, 4.41, 4.43, and 4.44. The $M_n$ and $Đ$ values of PDMDL determined with DMF-GPC (Table 4.1 (entry 2), Figure 4.3a, 4.41, and 4.44) were 104,000 and 2.04, respectively, and those determined with THF-GPC (Figure 4.42 and 4.43) were 106,000 and 1.88, respectively. (a) GPC chromatogram before (black line) and after (orange line) degradation. (b) $^1$H NMR and (c) $^{13}$C NMR spectra of the reaction mixture after degradation (400 MHz for $^1$H NMR and 100 MHz for $^{13}$C NMR) (in THF-$d_8$/$D_2O$).

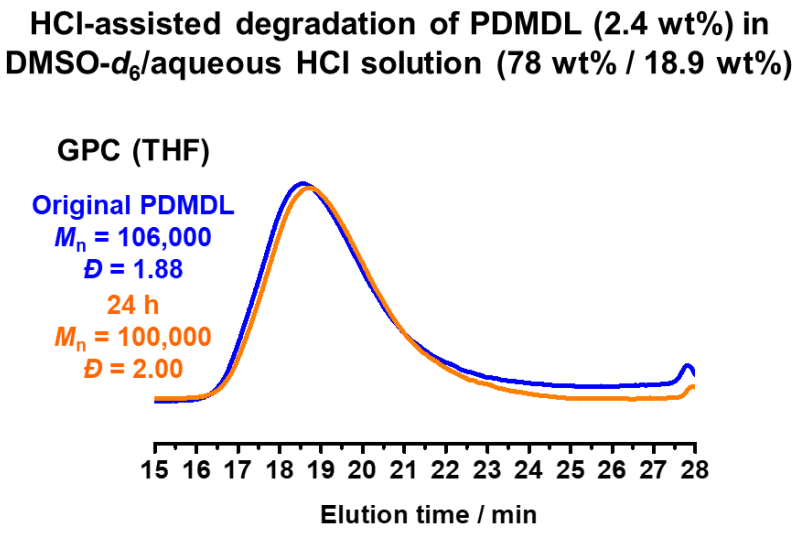


**Figure 4.43.** HCl-assisted degradation of PDMDL ($M_n$ = 106,000, $Đ$ = 1.88) (2.4 wt%) in a mixture of 1M HCl aqueous solution (18.9 wt%) and DMSO-$d_6$ (78.7 wt%) at 80 °C. The PDMDL used in Figure 4.43 is the same as that given in Table 4.1 (entry 2), Figure 4.3a, 4.41, 4.42, and 4.44. The $M_n$ and $Đ$ values of PDMDL determined with DMF-GPC (Table 4.1 (entry 2), Figure 4.3a, 4.41, and 4.44) were 104,000 and 2.04, respectively, and those determined with THF-GPC (Figure 4.42 and 4.43) were 106,000 and 1.88, respectively.

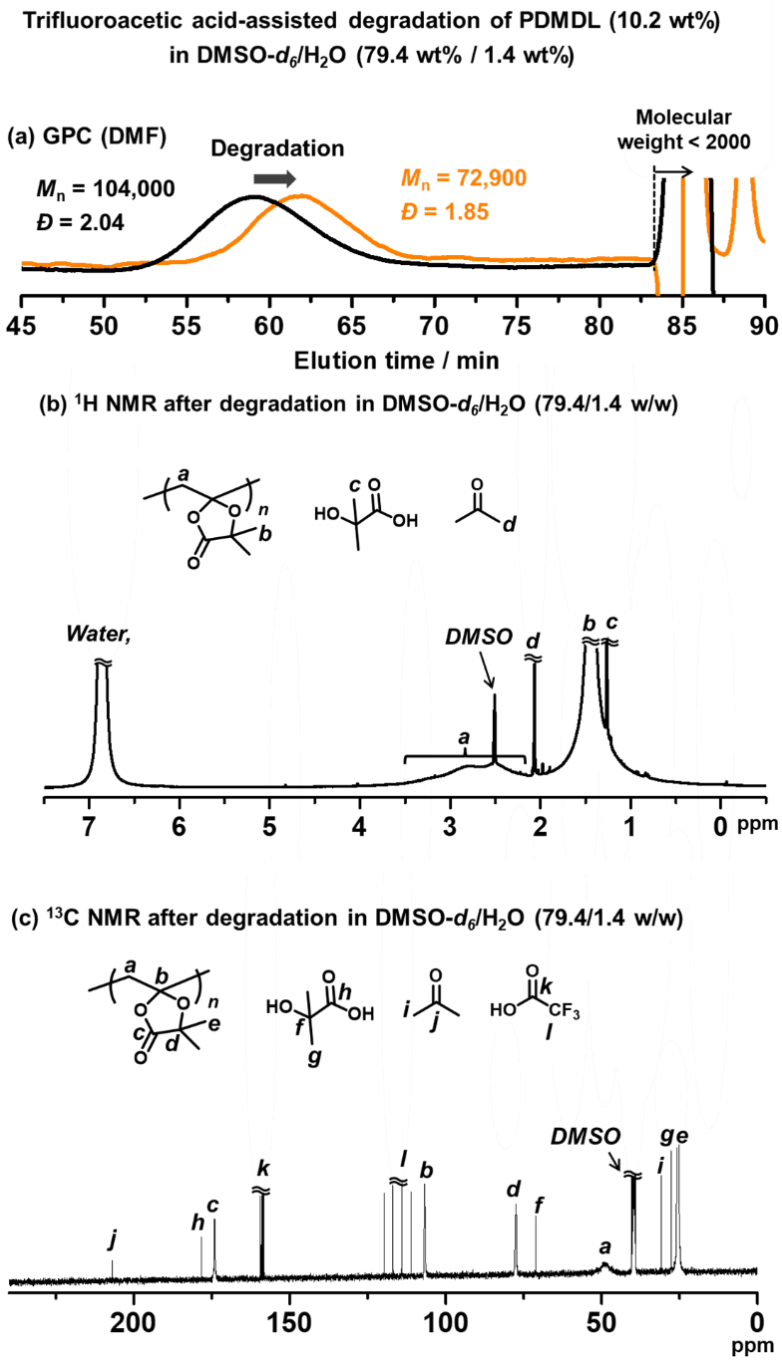


**Figure 4.44.** Degradation of PDMDL ($M_n$ = 104,000, $Đ$ = 2.04, 10.2 wt%, 1 equiv. of the DMDL monomer unit) using 1 equiv. of trifluoroacetic acid (9.0 wt%) and $H_2O$ (1.4 wt%) in DMSO-$d_6$ (79.4 wt%) at 80 °C for 3 days. The reaction was conducted in a valved (sealed) NMR tube. The PDMDL used in Figure 4.44 is the same as that given in Table 4.1 (entry 2), Figure 4.3a, 4.41, 4.42, and 4.43. The $M_n$ and $Đ$ values of PDMDL determined with DMF-GPC (Table 4.1 (entry 2), Figure 4.3a, 4.41, and 4.44) were 104,000 and 2.04, respectively, and those determined with THF-GPC (Figure 4.42 and 4.43) were 106,000 and 1.88, respectively. (a) GPC chromatogram before (black line) and after (orange line) degradation. (b) $^1$H NMR and (c) $^{13}$C NMR spectra of the reaction mixture after degradation (400 MHz for $^1$H NMR and 100 MHz for $^{13}$C NMR) (in DMSO-$d_6$/$H_2O$).

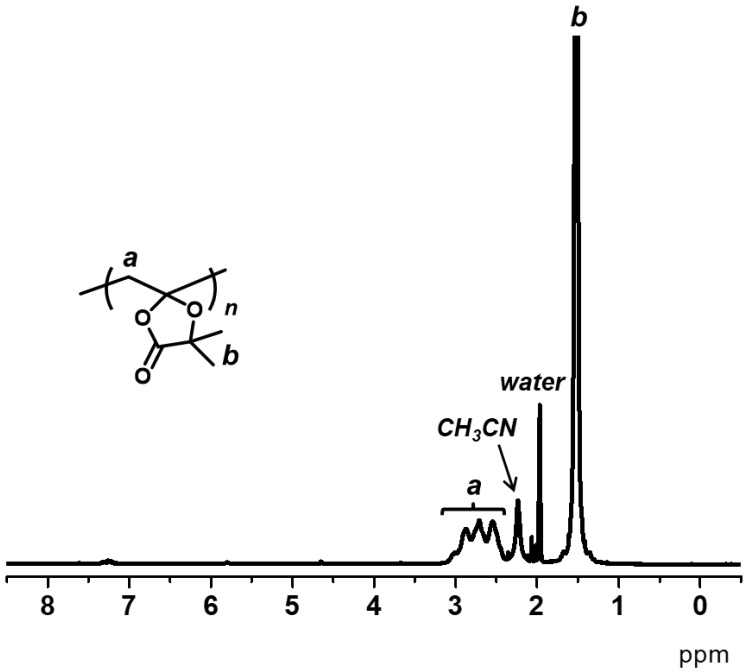


**Figure 4.45.** $^{1}H$ NMR spectrum of non-degraded PDMDL (4.2 wt%) in $CD_3CN$ (95.8 wt%) mixture (400 MHz, 298 K, $CDCl_3$).

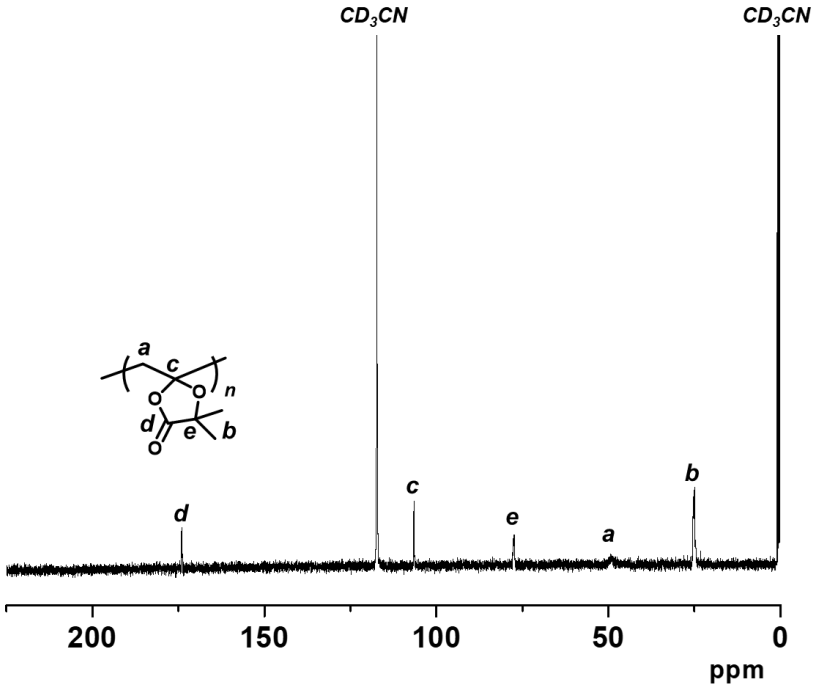


**Figure 4.46.** $^{13}C$ NMR spectrum of non-degraded PDMDL (4.2 wt%) in $CD_3CN$ (95.8 wt%) mixture (100 MHz, 298 K, $CDCl_3$).

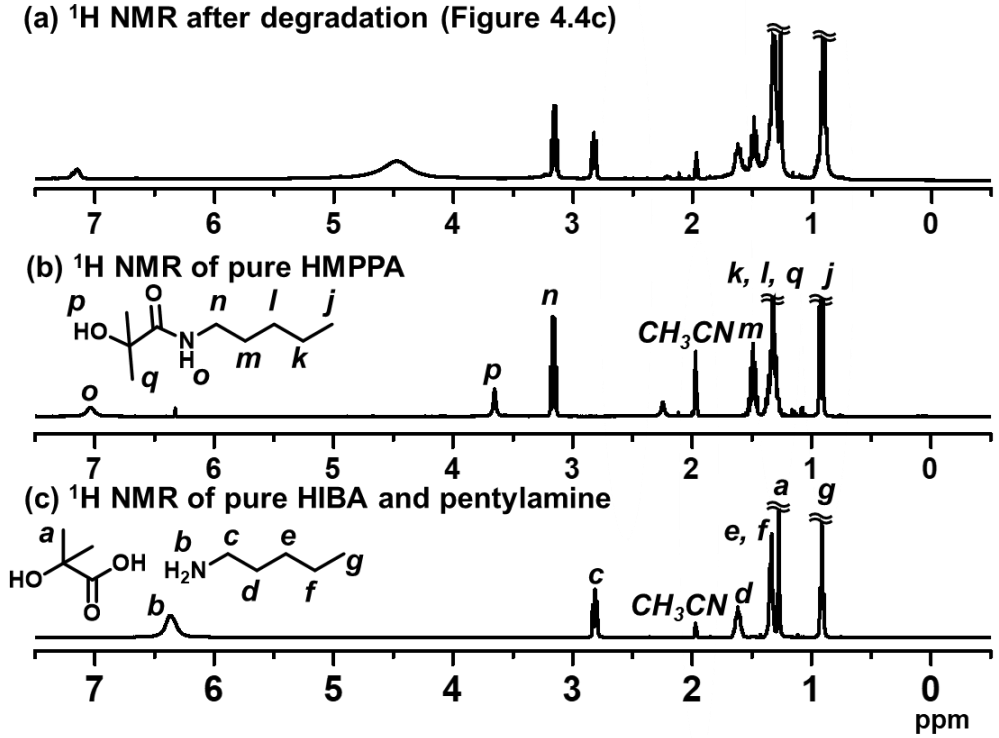


**Figure 4.47.** $^{1}H$ NMR of (a) the reaction mixture after degradation (b) pure HMPPA (c) pure HIBA and pentylamine (400 MHz, 298K, $CD_3CN$).

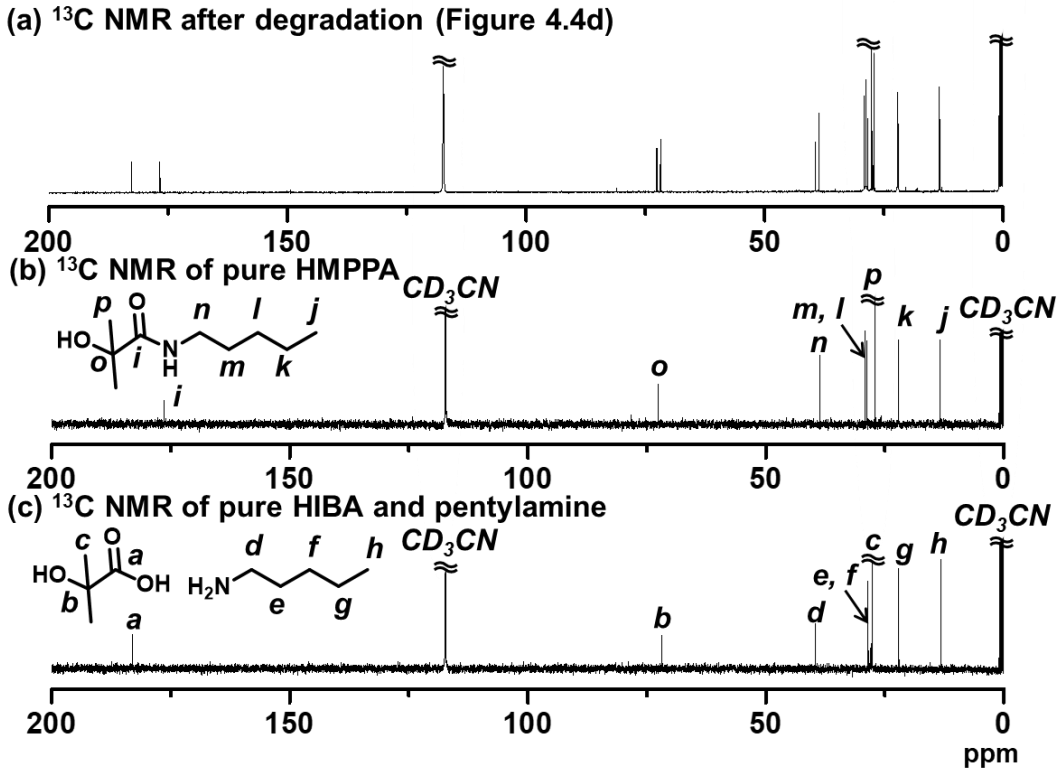


**Figure 4.48.** $^{13}C$ NMR of (a) the reaction mixture after degradation, (b) pure HMPPA, (c) pure HIBA and pentylamine (100 MHz, 298K, $CD_3CN$).

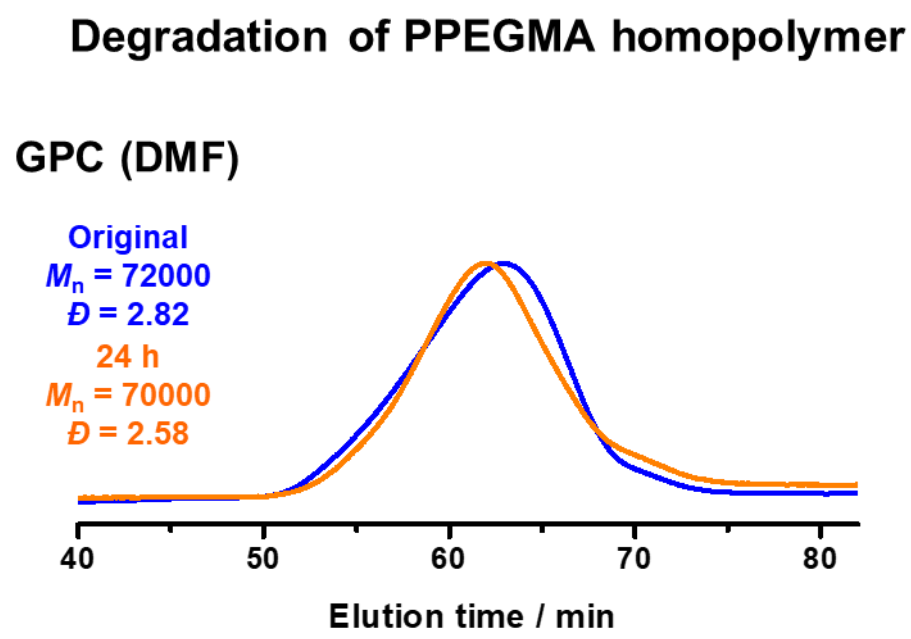


**Figure 4.49.** Degradation of PPEGMA ($M_n$ = 72000, $Đ$ = 2.82) (1 wt%) using 0.9M KOH aqueous solution (99 wt%) at room temperature for 24 h.

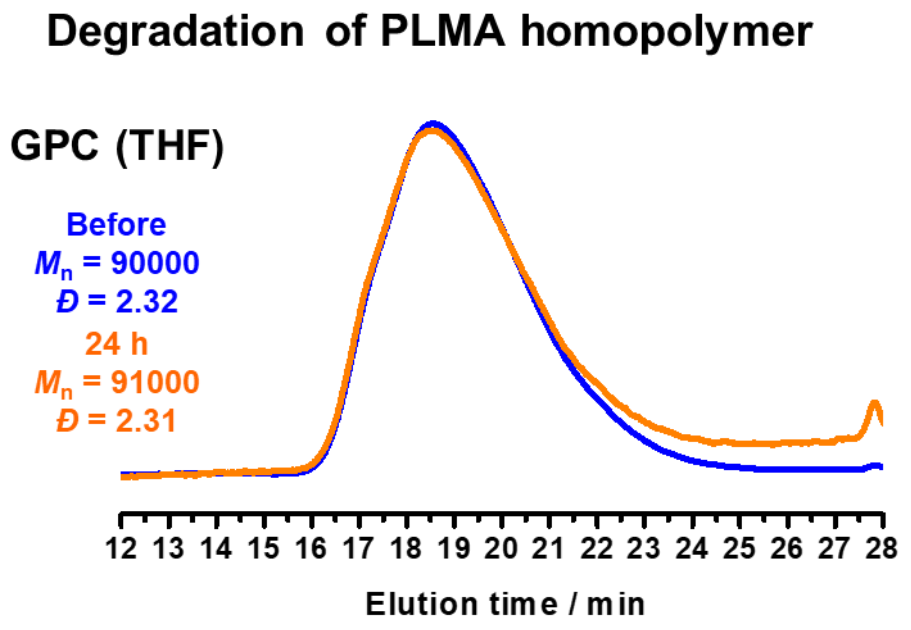


**Figure 4.50.** Degradation of PLMA ($M_n$ = 90000, $Đ$ = 2.32) (2.0 wt%) using 0.9M KOH in a mixture of methanol (8.1 wt%) and THF (89.9 wt%) at room temperature for 24 h.

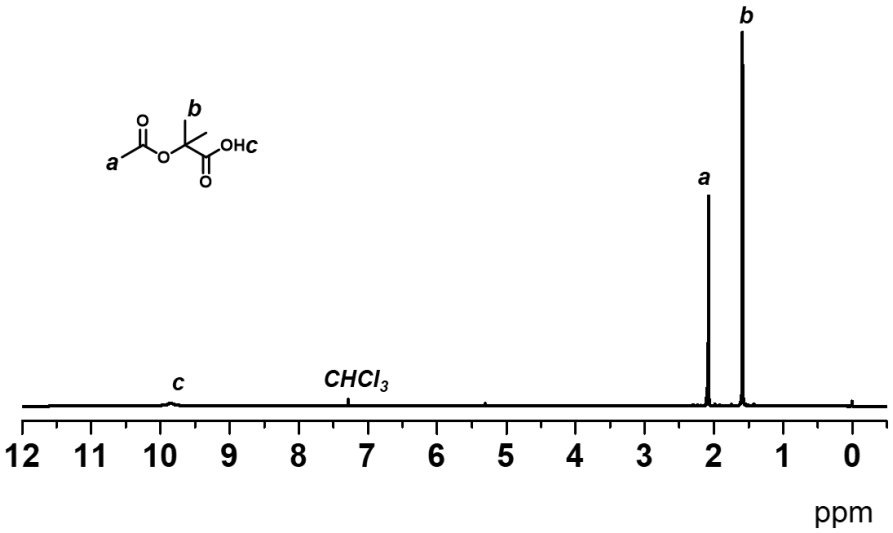


**Figure 4.51.** $^{1}$H NMR spectrum of compound **2 ($R_1$ = $CH_3$)** synthesized from recovered HIBA (400 MHz, 298 K, $CDCl_3$).

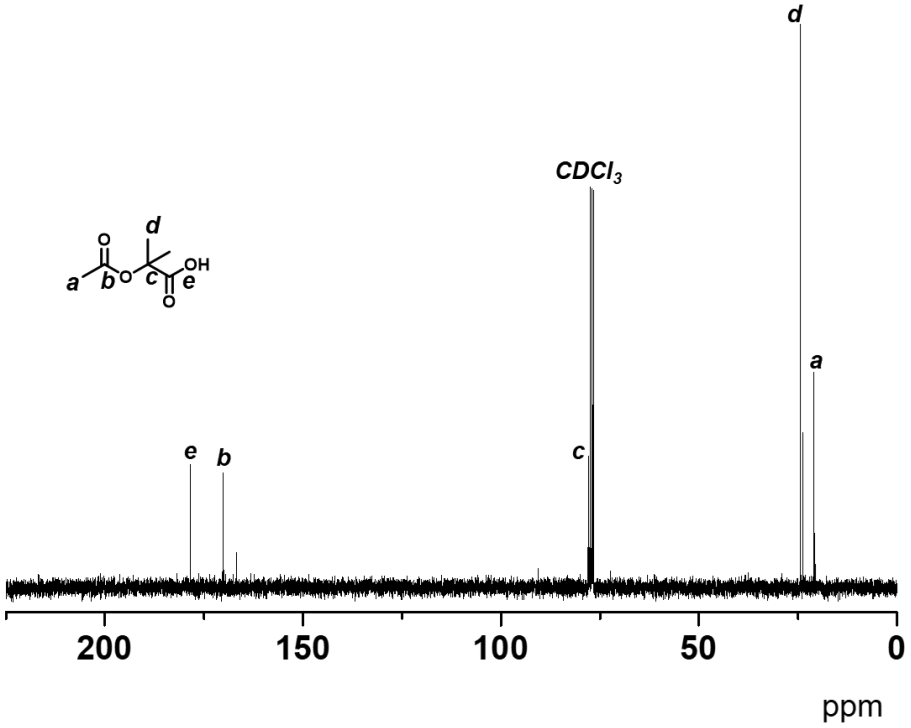


**Figure 4.52.** $^{13}$C NMR spectrum of compound **2 ($R_1$ = $CH_3$)** synthesized from recovered HIBA (100 MHz, 298 K, $CDCl_3$).

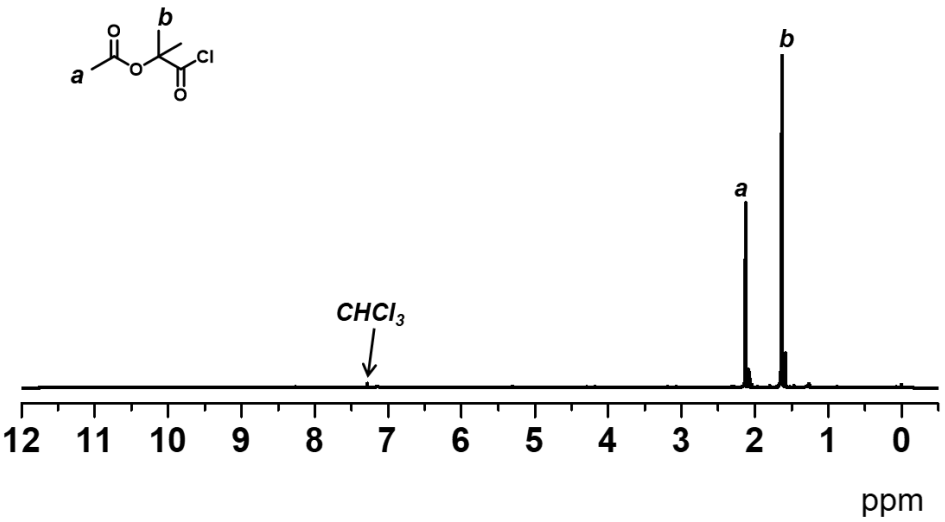


**Figure 4.53.** $^{1}$H NMR spectrum of compound **3 ($R_1$ = $CH_3$)** synthesized from recovered HIBA (400 MHz, 298 K, $CDCl_3$).

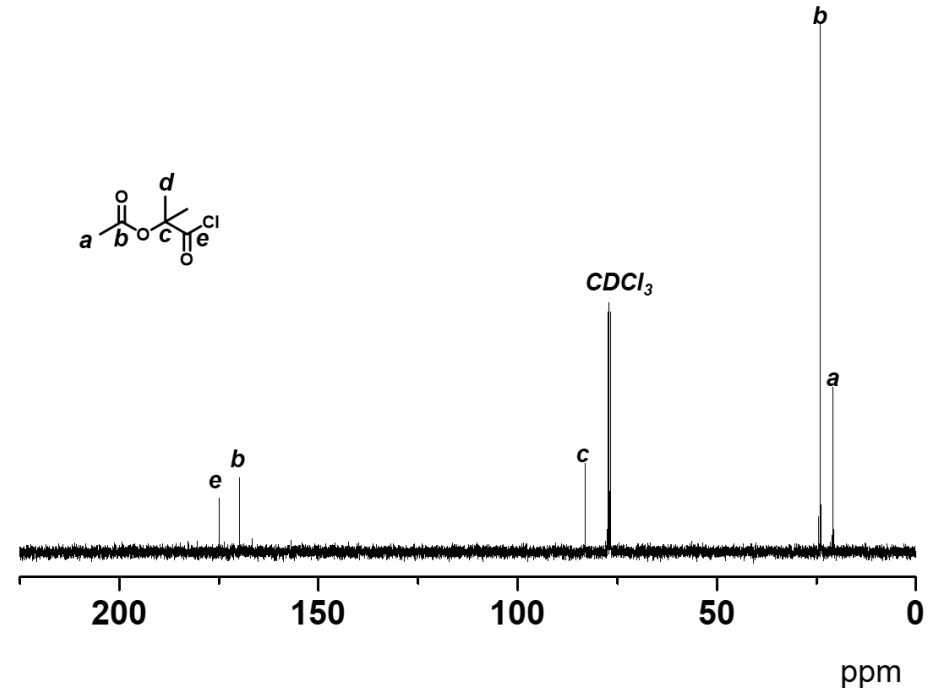


**Figure 4.54.** $^{13}$C NMR spectrum of compound **3 ($R_1$ = $CH_3$)** synthesized from recovered HIBA (100 MHz, 298 K, $CDCl_3$).

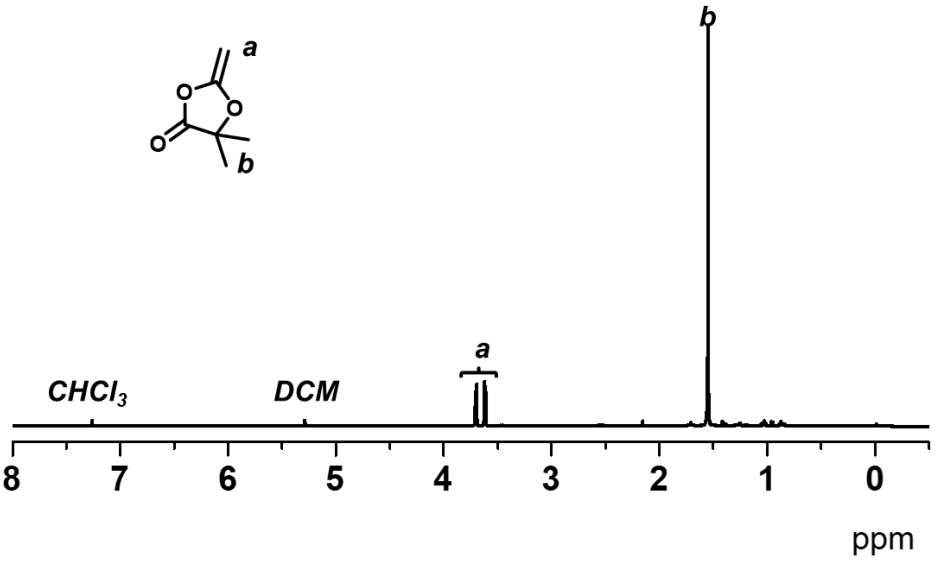


**Figure 4.55.** $^{1}H$ NMR spectrum of DMDL synthesized from recovered HIBA (400 MHz, 298 K, $CDCl_3$).

## References


1. Kamaly, N.; Yameen, B.; Wu, J.; Farokhzad, O. C. *Chem. Rev.* **2016**, *116*, 2602-2663.
2. Hong, M.; Chen, E. Y. X. *Green Chem.* **2017**, *19*, 3692-3706.
3. Guegain, E.; Tran, J.; Deguettes, Q.; Nicolas, J. *Chem. Sci.* **2018**, *9*, 8291-8306.
4. Haider, T. P.; Volker, C.; Kramm, J.; Lanfester, K.; Wurm, F. R. *Angew. Chem. Int. Ed.* **2019**, *58*, 50-62.
5. Paek, K. H.; Im, S. G. *Green Chem.* **2020**, *22*, 4570-4580.
6. Meereboer, K. W.; Misra, M.; Mohanty, A. K. *Green Chem.* **2020**, *22*, 5519-5558.
7. Barron, A.; Sparks, T. D. *iScience* **2020**, *23*, 101353.
8. Xu, Y.; Sen, S.; Wu, Q.; Zhong, X.; Ewoldt, R. H.; Zimmerman, S. C. *Chem. Sci.* **2020**, *11*, 3326.
9. Yang, J.; Xia, Y. *Chem. Sci.* **2021**, *12*, 4389.
10. Tardy, A.; Nicolas, J.; Gigmes, D.; Lefay, C.; Guillaneuf, Y. *Chem. Rev.* **2017**, *117*, 1319-1406.
11. Jackson, A. W. *Polym. Chem.* **2020**, *11*, 3525-3545.
12. Folini, J.; Murad, W.; Mehner, F.; Meier, W.; Gaitzsch, J. *Eur. Polym. J.* **2020**, *134*, 109851.
13. Pesenti, T.; Nicolas, J. *ACS Macro Lett.* **2020**, *9*, 1812-1835.
14. Folini, J.; Huang, C.-H.; Anderson, J. C.; Meier, W. P.; Gaitzsch, J. *Polym. Chem.* **2019**, *10*, 5285.
15. Bailey, W.; Ni, Z.; Wu, S-R. *J. Polym. Sci. Polym. Chem. Ed.* **1982**, *20*, 3021-3030.
16. Tardy, A.; Honoré, J.-C.; Siri, D.; Nicolas, J.; Gigmes, D.; Lefay, C.; Guillaneuf, Y. *Polym. Chem.* **2017**, *8*, 5139-5147.
17. Hedir, G. G.; Arno, M. C.; Langlais, M.; Husband, J. T.; O'Reilly, R. K.; Dove, A. P. *Angew. Chem. Int. Ed.* **2017**, *56*, 9178-9182.
18. Tran, J.; Pesenti, T.; Cressonnier, J.; Lefay, C.; Gigmes, D.; Guillaneuf, Y.; Nicolas, J. *Biomacromolecules* **2019**, *20*, 305-317.
19. Lena, J.-B.; Jackson, A. W.; Chennamaneni, L. R.; Wong, C. T.; Andriani, Y.; Thaniyot, P.; Herk, A. M. V. *Macromolecules* **2020**, *53*, 3994-4011.
20. Jackson, A. W.; Chennamaneni, L. R.; Thaniyot, P. *Eur. Polym. J.* **2020**, *122*, 109391.
21. Carter, M. C. D.; Hejl, A.; Woodfin, S.; Einsla, B.; Janco, M.; DeFelippis, J.; Cooper, R. J.; Even, R. C. *ACS Macro Lett.* **2021**, *10*, 591-597.
22. Zeng, T-Y.; Xia, L.; Zhang, Z.; Hong, C.-Y.; You, Y.-Z. *Polym. Chem.* **2021**, *12*, 165.
23. Komatsu, S.; Sato, T.; Kikuchi, A. *Polym. J.* **2021**, *53*, 731-739.
24. Bailey, W.; Ni, Z.; Wu, S-R. *Macromolecules* **1982**, *15*, 711-714.
25. Xie, F.; Deng, X.; Kratzer, D.; Cheng, K. C. K.; Friedmann, C.; Qi, S.; Solorio, L.; Lahann, J. *Angew. Chem. Int. Ed.* **2017**, *56*, 203-207.
26. Zhu, C.; Nicolas, J. *Polym. Chem.* **2021**, *12*, 594-607.
27. Bailey, W.; Wu, S-R.; Ni, Z. *Makromol. Chem.* **1982**, *183*, 1913-1920.
28. Hill, M. R.; Guégain, E.; Tran, J.; Figg, C. A.; Turner, A. C.; Nicolas, J.; Sumerlin, B. S. *ACS Macro Lett.* **2017**, *6*, 1071-1077.
29. Tran, J.; Guégain, E.; Ibrahim, N.; Harrisson, S.; Nicolas, J. *Polym. Chem.* **2016**, *7*, 4427-4435.

30. Guegain, E.; Zhu, C.; Giovanardi, E.; Nicolas, J. *Macromolecules* **2019**, *52*, 3612-3624.
31. Kazama, A.; Kohsaka, Y. *Polym. Chem.* **2019**, *10*, 2764-2768.
32. Friary, R. *J. of Heterocycl. Chem.* **1978**, *15*, 63-64.
33. Igglessi- Markopoulou, O.; Athanasellis, G.; Detsi, A.; Prousis, K.; Markopoulos, J. *Synthesis* **2003**, 2015-2022.
34. Zheng, L.; Zheng, D.; Wang. Y.; Yu, C.; Zhang, K.; Jiang, H. *Org. Biomol. Chem.* **2019**, *17*, 9573-9577.
35. Ma, P. J.; Tang, F.; Yao, Y.; Lu, C. D. *Org Lett* **2019**, *21*, 4671-4675.
36. Haim-Zada, M.; Basu, A.; Hagigit, T.; Schlinger, R.; Grishko, M.; Kraminsky, A.; Hanuka, E.; Domb, A. J. *Biomacromolecules* **2016**, *17*, 2253-2259.
37. Beckwith, A. L. J.; Brumby, S.; Chai, C. L. L. *J. Chem. Soc. Perkin Trans.* **1992**, *2*, 2117-2121.
38. Rudin, A.; Choi, P. *The Elements of Polymer Science & Engineering*, 3rd edn.; Academic Press, 2013, ch. 9, pp. 402-406.
39. Agarwal, S. *Polym. J.* **2007**, *39*, 163-174.
40. Undin, J.; Illanes, T.; Finne-Wistrand, A.; Albertsson, A.-C. *Polym. Chem.* **2012**, *3*, 1260-1266.
41. Wickel, H.; Agarwal, S.; Greiner, A. *Macromolecules* **2003**, *36*, 2397-2403.
42. Huang, J.; Gil, R.; Matyjaszewski, K. *Polymer* **2005**, *46*, 11698-11706.
43. Wickel. H.; Agarwal, S. *Macromolecules* **2003**, *36*, 6152-6159.
44. Inokuma, Y.; Yoneda, T.; Ide, Y.; Yoshioka, S. *Chem. Commun.* **2020**, *56*, 9079-9093.
45. Gigmes, D.; Steenberge, P. H. M. Van; Siri, D.; D'hooge, D. R.; Guillaneuf, Y.; Lefay , C. *Macromol. Rapid Commun.* **2018**, 1800193.
46. Rohwerder, T.; Müller, R. H. *Microb. Cell Factories* **2010**, *9*, 13.
47. Pirmoradi, M.; Kastner, J. R. *ACS Sustain. Chem. & Eng.* **2016**, *5*, 1517-1527.

# Chapter 5. Controlled Radical Polymerization of 4,4-Disubstituted Five-Membered Cyclic Ketene Hemiacetal Ester (CKHE) Monomer


## Abstract

Controlled radical polymerization of a 4,4-disubstituted five-membered cyclic ketene hemiacetal ester (CKHE) monomer, i.e., 4,4-dimethyl-2-methylene-1,3-dioxolan-5-one (DMDL) was performed using reversible addition-fragmentation chain-transfer (RAFT) polymerization and reversible complexation mediated polymerization (RCMP), yielding low-dispersity homopolymers, random (gradient) copolymers, and a block copolymer of DMDL. Various vinyl monomers such as (functional) methacrylates, (functional) acrylates, vinyl acetate, *N*,*N*-dimethylacrylamide and acrylonitrile were used as co-monomers for the copolymerizations. The obtained PDMA-*r*-PDMDL random copolymer degraded in a basic condition at room temperature.

## 5.1. Introduction

In chapter 4, we synthesized cyclic ketene hemiacetal esters (CKHE) monomers and used them in conventional radical polymerization. Because of the nature of conventional radical polymerization, the dispersity (*Đ*) was high, and the number of average molecular weight ($M_n$) was not controlled. In the present chapter (chapter 5), we used a CKHE monomer in controlled radical polymerization for obtaining polymers with low dispersity and controlled molecular weights. Homopolymers, random (gradient) copolymers, and a block copolymer were synthesized via reversible addition-fragmentation chain-transfer (RAFT) polymerization and reversible complexation mediated polymerization (RCMP).

The *Đ* value is a fundamental parameter in determining polymer properties such as rheological properties, thermal properties, and self-assembly behaviors.[1] Low-dispersity polymers may be useful in obtaining specific properties. An advantage of controlled radical polymerization is its capability for yielding block copolymers and also gradient copolymers when the reactivities of two monomers are largely different. Degradable block copolymers and degradable gradient copolymers are not obtainable via conventional radical polymerization. Self-assemblies (micelles and vesicles) of degradable block copolymers can decompose upon degrading stimuli and are used for drug delivery applications.[2-4] Gradient copolymers are copolymers in which the comonomer sequence gradually changes from one monomer species to the other species. Gradient copolymers can still self-assemble because of different properties along the chain. Gradient copolymers may degrade more heterogeneously, generating short oligomers upon degradation, while block copolymers degrade specifically, generating small molecules from the degradable segment and polymer chains from the non-degradable segment. Degradable gradient copolymers have been utilized in biomedical applications such as drug delivery,[5,6] gene/DNA transfection,[7] and tissue engineering.[8] Lu et al. used degradable gradient copolymers to form doxorubicin (DOX)-loaded micelles, releasing DOX (drug molecule) upon

pH changes.[5] Non-spherical egg-shaped micelles were also prepared by degradable gradient block copolymers which then degraded by lipase (enzyme) completely.[6]

Vinyl monomers are classified into "more activated" monomers (MAMs) and "less activated" monomers (LAMs) based on the stability of the generated propagating radical.[9] MAMs generally bear conjugated substituents such as phenyl, carbonyl, and nitrile groups on the polymerizable vinyl group and generate stabilized propagating radicals. LAMs generally do not bear conjugated substituents and generate less stabilized propagating radicals. In RAFT polymerization, choice of RAFT agents (chain transfer agents (CTAs)) is important for different monomers (MAMs and LAMs). Figure 5.1 shows examples of CTAs, which bear a leaving alkyl group (R group) and a stabilizing group (Z group). They are dithiocarbamates (Z = *N*-alkyl), xanthates (Z = *O*-alkyl), trithiocarbonates (Z = *S*-alkyl), and dithiobenzoates (Z = Ph). Scheme 5.1 shows the RAFT process, where $P_n$–SCSZ is a polymer dormant species. The propagating radical ($P_m^{\bullet}$) undergoes addition to the thiocarbonylthio compounds (S=C(Z)S–$P_n$), generating an intermediate radical ($P_m$-SC$^{\bullet}$S–Z). The intermediate radical subsequently undergoes fragmentation, forming a polymer dormant species ($P_m$–SCSZ) and a propagating radical ($P_n^{\bullet}$) (Scheme 5.1). Through the addition and fragmentation processes, the transfer between the propagating radical ($P_m^{\bullet}$) and the dormant species ($P_n$–SCSZ) completes. To ensure a frequent chain transfer, the C=S bond of the CTA must be sufficiently reactive for the addition of the propagating radical. The reactivity of the C=S bond largely depends on the Z group, because the Z group controls the stability of the intermediate radical formed in the RAFT process (Scheme 5.1). When the Z group better stabilizes the intermediate radical, the addition rate constant ($k_{add}$ (Scheme 5.1)) increases, thereby resulting in a more frequent chain transfer. The $k_{add}$ value increases in the order of Z = *N*-alkyl < *O*-alkyl < *S*-alkyl < Ph. Hence, dithiobenzoates (Z = Ph) and trithiocarbonates (Z = *S*-alkyl) are generally efficient CTAs and are used for MAMs such as methacrylate. However, for LAMs, the propagating radicals are

less stable. The intermediate radicals can be more stable than the propagating radicals of LAMs, resulting in the accumulation of the intermediate radicals. Thus, termination between the intermediate radical and propagating radical and termination among the intermediate radicals can be significant, causing a retardation in the polymerization rate and a significant generation of dead polymer chains. Thus, less stabilized Z groups need to be used to make the intermediate radical less stable (make the fragmentation faster). Hence, dithiocarbamates (Z = *N*-alkyl) and xanthates (Z = *O*-alkyl) are suitable for LAMs such as vinyl acetate (VAc).

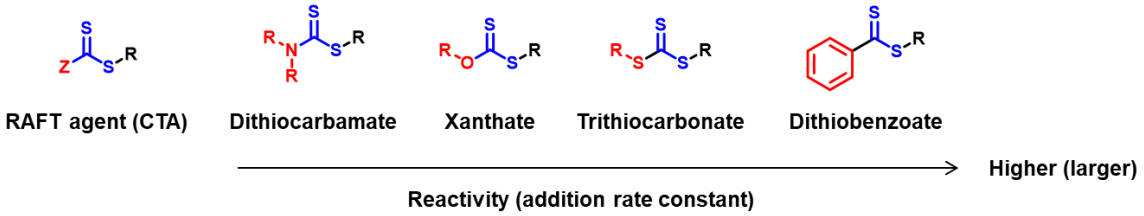


**Figure 5.1.** Examples of RAFT agents (CTAs).

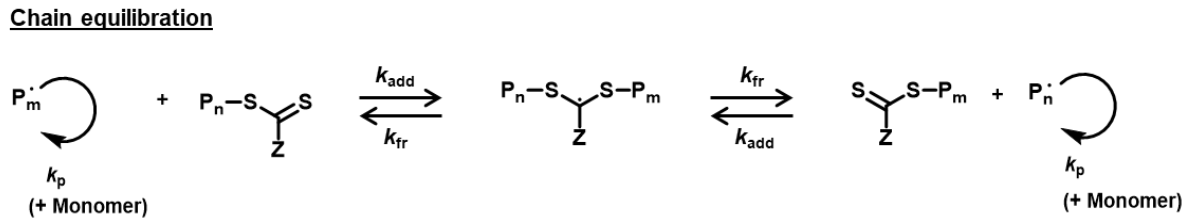


**Scheme 5.1.** RAFT process.

RCMP employs polymer–iodide (Polymer–I) as the dormant species and an iodide anion ($I^-$) as the catalyst, for example (Scheme 5.2).[10] $I^-$ is used in the forms of salts such as tetrabutylammonium iodide ($Bu_4N^+I^-$) (BNI). Polymer–I and $I^-$ form a halogen-bonding complex (Polymer–I---$I^-$), which can reversibly generate the propagating radical (Polymer•) and $I_2^{\bullet-}$ (Scheme 5.2).

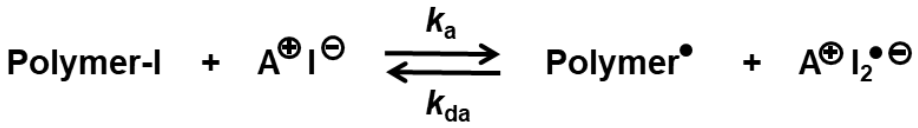

**Scheme 5.2.** Reversible activation in RCMP.

In the present chapter, we used 4,4-dimethyl-2-methylene-1,3-dioxolan-5-one (DMDL) (Figure 5.2) as a CKHE monomer and synthesized its homopolymers, random (gradient) copolymers and a block copolymer via the RAFT polymerization and its homopolymer and random copolymers via RCMP. The studied co-monomers are shown in Figure 5.2.

## 5.2. Results and Discussion

### Homopolymerizations of DMDL Using RAFT Polymerization.

We carried out RAFT homopolymerizations of DMDL using three different CTAs (Figure 5.2), i.e., ethyl 2-[(ethoxycarbonothioyl)thio]propionate (ECP) (Z = *O*-alkyl), 2-cyanopropan-2-yl *N*-methyl-*N*-(pyridin-4-yl)carbamodithioate (CMPC) (Z = *N*-aryl), and 4-cyano-4[[(dodecylthio)carbonothioyl]thio]pentanoic acid (CDPA) (Z = *S*-alkyl). We heated mixtures of DMDL (100 equiv.), CTA (1 equiv.), and 2,2'-azoisobutyronitrile (AIBN) (0.2 equiv.) at 70 °C for 4–5.5 h. When ECP was used as a CTA, the monomer conversion reached 56 % (as determined with $^1$H NMR) for 5.5 h, yielding a poly(4,4-dimethyl-2-methylene-1,3-dioxolan-5-one) (PDMDL) with $M_n$ = 6400 and $Đ$ (=$M_w/M_n$) = 1.37 (Table 5.1, entry 1), where $M_w$ is the weight-average molecular weight. The $M_n$ and $Đ$ values are not absolute values but PMMA-calibrated gel permeation chromatography (GPC) values, where PMMA is poly(methyl methacrylate). The monomer (DMDL) conversion increased with an increase in time (Figure 5.3a). The $M_n$ value increased with an increase in the monomer conversion (Figure 5.3b). The deviation of the $M_n$ value from the theoretical values is ascribed to the PMMA-calibrated GPC values. The $Đ$ value was approximately 1.4 throughout the polymerization. Thus, a relatively low-dispersity PDMDL was obtained. Figure 5.4 shows the $^1$H NMR

spectrum ($CDCl_3$) of PDMDL after purification (reprecipitation in a hexane/diethyl ether mixture (1/1 (v/v)) (non-solvent)). The backbone methylene protons (*a*) of PDMDL and methylene proton (*c*) of ECP appear at 2.13–3.16 ppm. The dimethyl protons (*b*) of PDMDL and methyl protons (*d, f, h*) appear at 1.12–1.77 ppm. The methylene protons (*e*, *g*) of ECP appearing at 4.02–4.19 ppm (*e*) and 4.62–4.72 ppm (*g*). For PDMDL, the integration ratio of methylene protons (*a*) and dimethyl protons (*b*) was nearly 1 (*a*) to 3 (*b*), agreeing with the PDMDL structure.

The use of CMPC as a CTA (Table 5.1, entry 2) resulted in a slower polymerization than the use of ECP (Table 5.1, entry 1). The monomer conversion was 20 % for 4 h, yielding a PDMDL with $M_n$ = 3600 and $Đ$ = 1.39 (Table 5.1, entry 2). Although the polymerization was slow, a relatively low-dispersity PDMDL was obtained. When CDPA was used as a CTA, the polymerization was even slower. The monomer conversion reached 19 % for 5.5 h, yielding a PDMDL with a peak-top molecular weight of 1100 (Table 5.1, entry 3). (The polymer chains were too short, and the $M_n$ and $Đ$ values were not accurately determined by GPC.)

DMDL bears no conjugated substituents but two non-conjugated (ether) substituents and would be considered as a LAM. The propagating radical of DMDL is a tertiary carbon-centered radical with two non-conjugated carbon-oxygen linkages and would be a "less stabilized" radical. The observed retardation in the polymerization rate using CDPA (*Z* = *S*-alkyl) would be ascribed to the slow fragmentation of the intermediate radical and thereby caused terminations of the intermediate radical, as mentioned above. CMPC bears an *N*-aryl (not *N*-alkyl). Because of the presence of the aryl group (pyridyl group), the intermediate radical of CMPC might be stabilized, which would result in the observed slow polymerization. Therefore, for the homopolymerization of DMDL, ECP was the best suitable CTA of the three studied CTAs with respect to the polymerization rate.

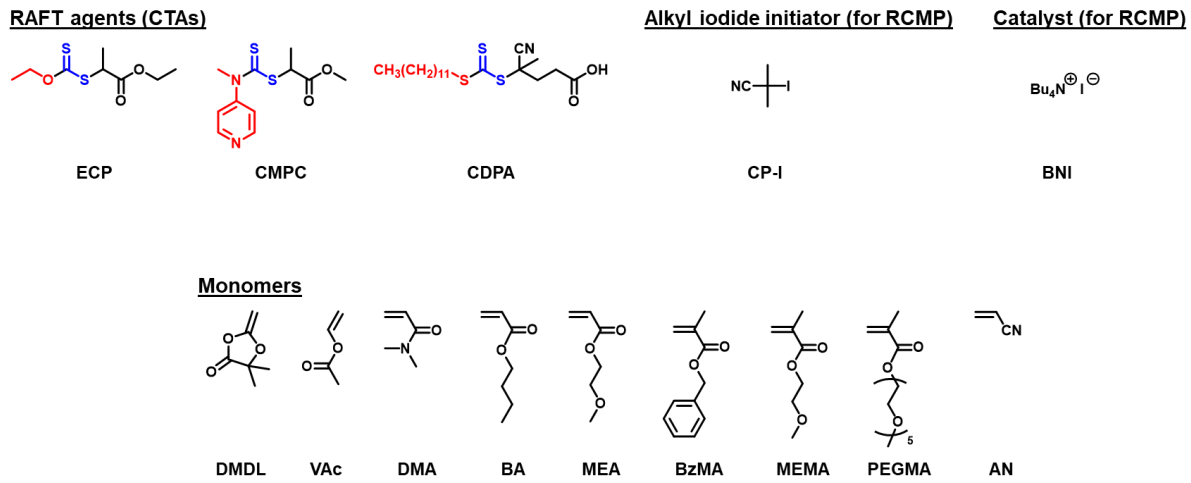


**Figure 5.2.** RAFT agents (CTAs), alkyl iodide initiator (for RCMP), catalyst (for RCMP), and monomers used in this work.

**Table 5.1.** RAFT polymerizations of DMDL monomer with CTAs.

| Entry | CTA | $[DMDL]_0/[CTA]_0/[AIBN]_0$ (equiv.) | $T$ (°C) | $t$ (h) | Conv. (%)[a] | $M_n$[b] ($M_{n,theo}$[c]) | $Đ$[b] |
|---|---|---|---|---|---|---|---|
| 1 | ECP | 100/1/0.2 | 70 | 5.5 | 56 | 6400 (7200) | 1.37 |
| 2 | CMPC | 100/1/0.2 | 70 | 4 | 20 | 3600 (2600) | 1.39 |
| 3 | CDPA | 100/1/0.2 | 70 | 5.5 | 19 | 1100[d] (2400) | NA |

[a]Monomer conversions determined with $^1$H NMR. [b]PMMA-calibrated GPC values (THF eluent). [c]Theoretical $M_n$ calculated according to ($[DMDL]_0/[CTA]_0$)×(monomer conversion)×(molecular weight of monomer). [d]GPC peak-top molecular weight.

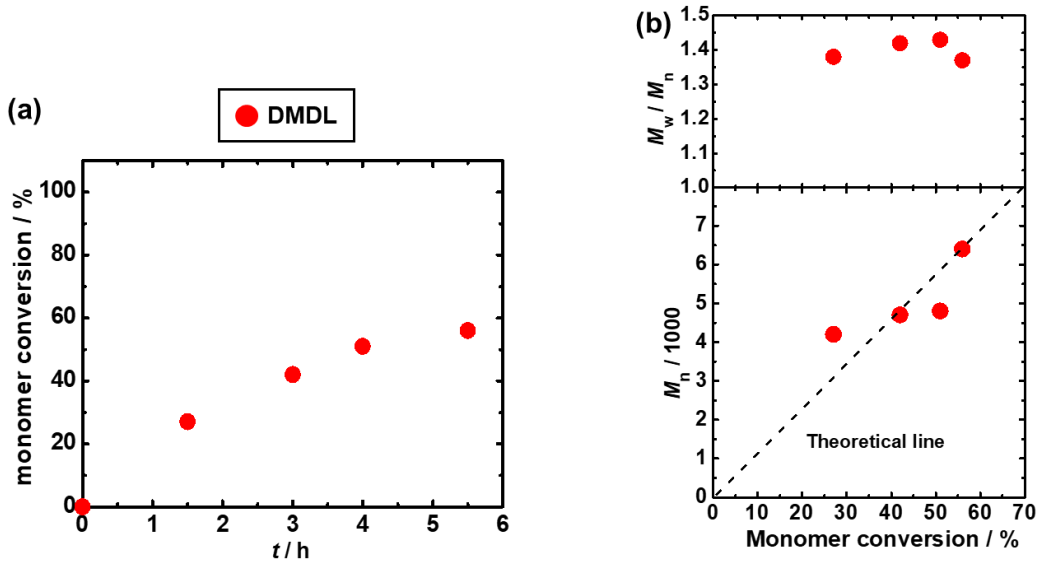


**Figure 5.3.** Plots of (a) monomer conversion *vs*. polymerization time ($t$) and (b) $M_n$ and $M_w/M_n$ *vs*. monomer conversion for the DMDL/ECP/AIBN system (70 °C). The reaction condition is given in Table 5.1, entry 1.

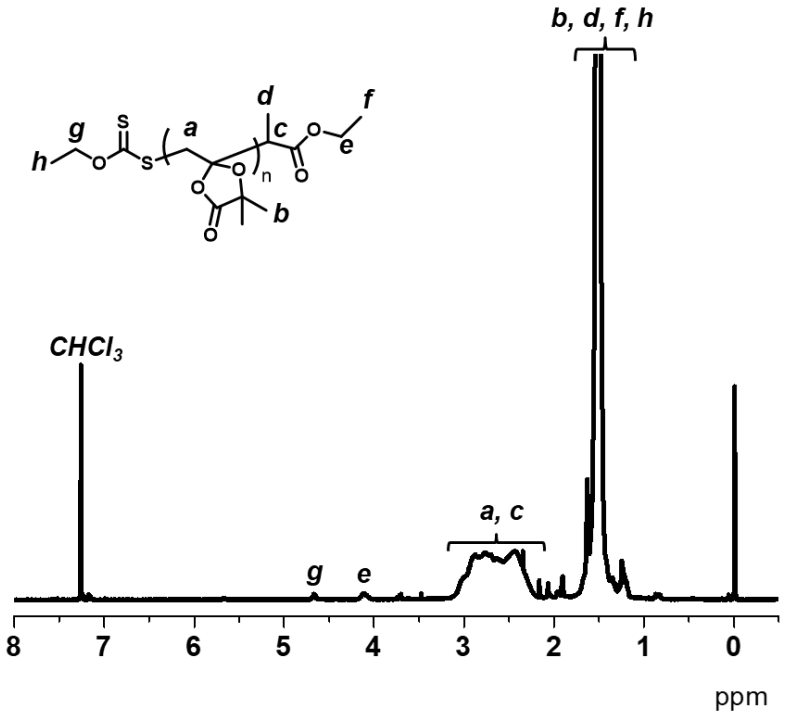


**Figure 5.4.** $^{1}$H NMR spectrum of PDMDL (Table 5.1, entry 1) (400 MHz, 298 K, $CDCl_3$).

**Random Copolymerizations of DMDL Using RAFT Polymerization.**

We studied random copolymerizations of DMDL with vinyl co-monomers, i.e., VAc, *N*,*N*-dimethylacrylamide (DMA), butyl acrylate (BA), and 2-methoxyethyl acrylate (MEA) (Figure 5.2) using ECP and CDPA as CTAs (Table 5.2). VAc is a LAM. DMA, BA, and MEA are MAMs. We heated mixtures of DMDL (50 equiv.), co-monomer (50 equiv.), CTA (1 equiv.), and AIBN (0.2 equiv.) at 70 ℃ for 2–5 h. The (initial) monomer composition was 50% for DMDL and 50% for the co-monomer. We chose ECP as a CTA for the copolymerization with the LAM (VAc) and CDPA for those with the MAMs (DMA, BA, and MEA).

**Table 5.2.** RAFT random copolymerizations of DMDL with several vinyl co-monomers.

| Entry | Co-monomer (M) | CTA | $[M]_0/[DMDL]_0/[CTA]_0/[AIBN]_0$ (equiv.) | $T$ (°C) | $t$ (h) | Conv. (M/DMDL) (%/%)[a] | $M_n$[b] ($M_{n,theo}$[c]) | $Đ$[b] | $F_{DMDL}$ (%)[d] |
|---|---|---|---|---|---|---|---|---|---|
| 1 | VAc | ECP | 50/50/1/0.2 | 70 | 4 | 85/68 | 7700 (8000) | 1.16 | 47 (44) |
| 2 | DMA | CDPA | 50/50/1/0.2 | 70 | 2 | 100/43 | 9900 (7700) | 1.16 | 24 (30) |
| 3 | BA | CDPA | 50/50/1/0.2 | 70 | 5 | 97/59 | 13000 (10000) | 1.23 | 37 (38) |
| 4 | MEA | CDPA | 50/50/1/0.2 | 70 | 2.5 | 93/40 | 11000 (8600) | 1.17 | 28 (30) |

[a]Monomer conversions determined with $^1$H NMR. [b]PMMA-calibrated GPC values (THF eluent) for entries 1, 3, and 4. PMMA-calibrated GPC values (DMF eluent) for entry 2. [c]Theoretical $M_n$ calculated according to $([M]_0/[CTA]_0)\times$(co-monomer conversion)×(molecular weight of co-monomer) + $([DMDL]_0/[CTA]_0)\times$(DMDL monomer conversion)×(molecular weight of DMDL monomer). [d]$F_{DMDL}$ value determined by the $^1$H NMR analysis of the purified polymer. In the parenthesis, $F_{DMDL}$ value calculated from the monomer conversions of DMDL and co-monomer determined using $^1$H NMR is given.

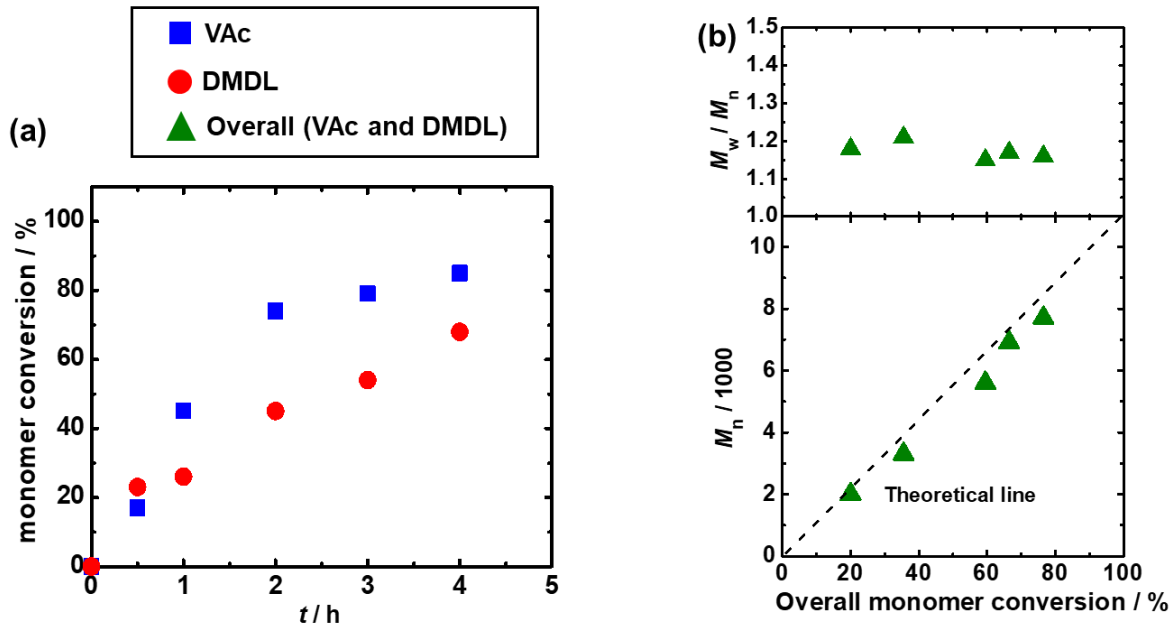


**Figure 5.5.** Plots of (a) monomer conversion *vs*. time ($t$) and (b) $M_n$ and $M_w/M_n$ *vs*. overall monomer conversion for the VAc/DMDL/ECP/AIBN system (70 °C). The reaction condition is given in Table 5.2, entry 1. The symbols are indicated in the figure. In Figure 5.5b, the overall monomer conversion is (conversion of DMDL)×0.5 + (conversion of co-monomer)×0.5.

The copolymerization with VAc yielded a PVAc-*r*-PDMDL ($M_n$ = 7700, $Đ$ = 1.16, and $F_{DMDL}$ = 47 %) (Table 5.2, entry 1) for 4 h, where PVAc is poly(vinyl acetate) and $F_{DMDL}$ is the fraction of DMDL in the copolymer. Figure 5.5a shows the plots of monomer conversion

*vs.* time for each of DMDL (red circle) and VAc (blue square). In chapter 4, the monomer reactivity ratios of DMDL and VAc were determined to be $r_{VAc}$ = 1.65 and $r_{DMDL}$ = 0.29 which means that VAc is more reactive than DMDL in the monomer consumption. Thus, VAc was consumed faster than DMDL (Figure 5.5a). Conventional radical polymerization (in chapter 4) can yield a mixture of VAc-rich polymer chains (that can be generated at an early stage of polymerization) and DMDL-rich polymer chains (that can be generated at later stage of polymerization). In contrast, controlled radical polymerization (chapter 5) can yield gradient copolymer chains, because living polymer chains grow over a history of the monomer consumption and record the history in the copolymer sequence. Thus, in the present system (chapter 5), the polymer chain would contain more VAc units at an early stage of polymerization and more DMDL units at a later stage of polymerization, forming a gradient copolymer. Figure 5.5b shows the plots of $M_n$ and $Đ$ *vs.* the overall monomer conversion, where the overall monomer conversion of the two monomers is (conversion of DMDL)×(initial fraction of DMDL (0.5)) + (conversion of co-monomer)×(initial fraction of co-monomer (0.5)). The $M_n$ value increased with an increase in the overall monomer conversion. The $Đ$ value was low (1.15-1.21) throughout the polymerization up to 77 % overall monomer conversion. Thus, we obtained low-dispersity PVAc-*r*-PDMDL copolymers.

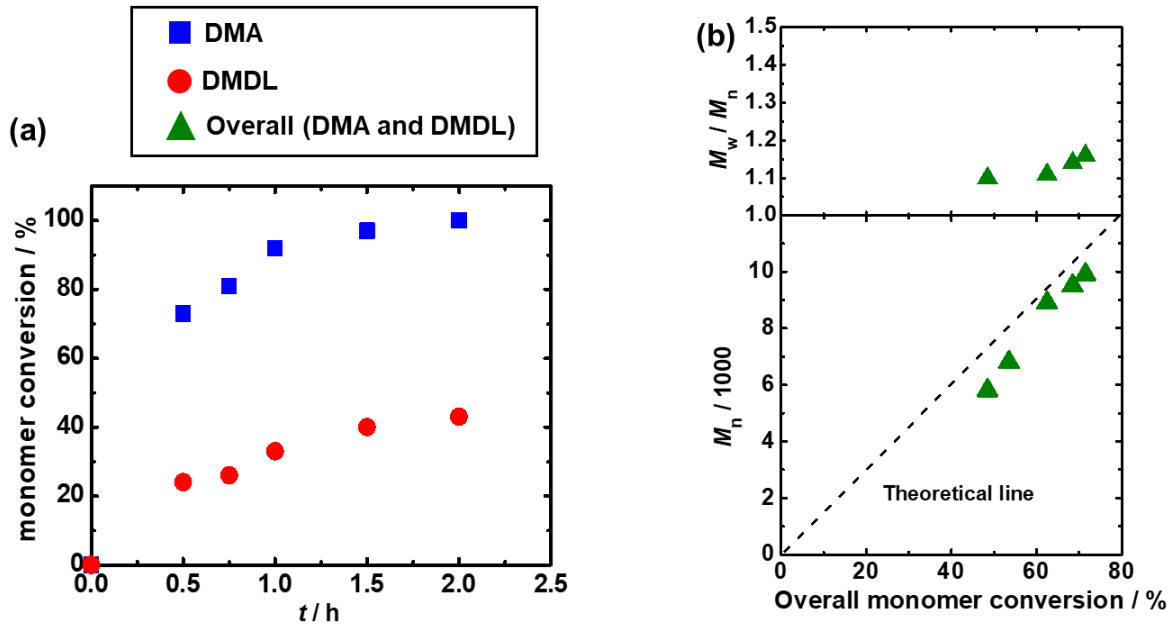


**Figure 5.6.** Plots of (a) monomer conversion *vs*. time (*t*) and (b) $M_n$ and $M_w/M_n$ *vs*. overall monomer conversion for the DMA/DMDL/CDPA/AIBN system (70 °C). The reaction condition is given in Table 5.2, entry 2. The symbols are indicated in the figure, the overall monomer conversion is (conversion of DMDL)×0.5 + (conversion of co-monomer)×0.5.

The use of DMA as a co-monomer yielded a PDMA-*r*-PDMDL ($M_n$ = 9900, $Đ$ = 1.16, and $F_{DMDL}$ = 24 %) (Table 5.2, entry 2) for 2 h, where PDMA is poly(*N*,*N*-dimethylacrylamide). The gradient was more pronounced in the DMA/DMDL system (Figure 5.6a) than in the VAc/DMDL system (Figure 5.5a). The DMA conversion was 81% at the DMDL monomer conversion of 26% (for 0.75 h in Figure 5.6a), while the conversion of VAc was 45% at the similar DMDL conversion of 26% (for 1 h in Figure 5.5a), meaning that DMA is more reactive than VAc in the copolymerizations of DMDL. Thus, the gradient in the DMA and DMDL units in the copolymer would be larger than that in the VAc and DMDL units in the copolymer. The $M_n$ value increased with an increase in the overall monomer conversion, and the $Đ$ value was low (1.10–1.16) throughout the polymerization up to 72 % overall monomer conversion (Figure 5.6b).

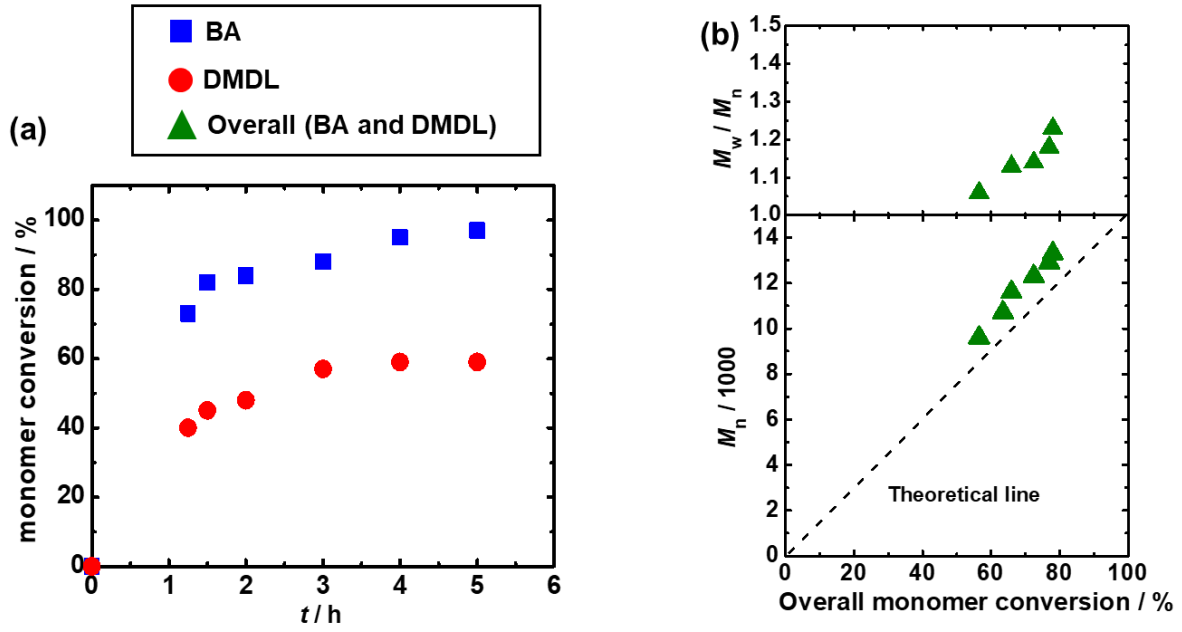


**Figure 5.7.** Plots of (a) monomer conversion *vs*. time (*t*) and (b) $M_n$ and $M_w/M_n$ *vs*. overall monomer conversion for the BA/DMDL/CDPA/AIBN system (70 °C). The reaction condition is given in Table 5.2, entry 3. The symbols are indicated in the figure, the overall monomer conversion is (conversion of DMDL)×0.5 + (conversion of co-monomer)×0.5.

The use of acrylate co-monomers (BA and MEA) yielded a PBA-*r*-PDMDL ($M_n$ = 13000, $Đ$ = 1.23, and $F_{DMDL}$ = 37 %) (Table 5.2, entry 3) for 5 h and a PMEA-*r*-PDMDL ($M_n$ = 11000, $Đ$ = 1.17, and $F_{DMDL}$ = 28 %) (Table 5.2, entry 4) for 2.5 h, where PBA is poly(butyl acrylate) and PMEA is poly(2-methoxyethyl acrylate). In chapter 4, the monomer reactivity ratios of DMDL and BA were determined to be $r_{BA}$ = 0.83 and $r_{DMDL}$ = 0.03, meaning that BA is much more reactive than DMDL. Therefore, like the DMA/DMDL system (Figure 5.6a), the BA/DMDL system (Figure 5.7a) gave a large gradient in the BA and DMDL units in the copolymer. The $M_n$ value increased with an increase in the overall monomer conversion, and the $Đ$ value was low (1.06–1.23) throughout the polymerization up to 78 % overall monomer conversion (Figure 5.7b). Thus, we obtained low-dispersity radon (gradient) copolymers of DMDL using the four different co-monomers.

**Block Copolymerization of DMDL Using RAFT Polymerization.**

We prepared a PDMDL macroinitiator using ECP as a CTA. We heated a mixture of DMDL (100 equiv.), ECP (1 equiv.), and AIBN (0.2 equiv.) at 70 ℃ for 2 h (Table 5.3). The reaction condition was the same as shown in Table 5.1 (entry 1) and Figure 5.3. We stopped the polymerization at the relatively short time (2 h) (monomer conversion = 37 %) to retain a high fraction of the xanthate moiety at the chain end. After the purification by reprecipitation in hexane/diethyl ether mixture (1/1 (v/v)) (non-solvent)), we obtained a PDMDL with $M_n$ = 5100 and $Đ$ = 1.27 (Table 5.3). The $Đ$ value (1.27) of the purified polymer was smaller than those of the unpurified polymers (approximately 1.4 (Table 5.1, entry 1, and Figure 5.3)), suggesting that a part of oligomers (as well as monomers and other small molecules) was removed during the purification (reprecipitation).

**Table 5.3.** Synthesis of PDMDL Macroinitiator Using RAFT Polymerization.

| $[DMDL]_0/[ECP]_0/[AIBN]_0$ (equiv.) | $T$ (°C) | $t$ (h) | Conv. (%)[a] | $M_n$[b] ($M_{n,theo}$[c]) | $Đ$[b] |
|---|---|---|---|---|---|
| 100/1/0.2 | 70 | 2 | 37 | 5100 (4700) | 1.27 |

[a]Monomer conversion determined with $^1$H NMR. [b]PMMA-calibrated GPC values (THF eluent) of PDMDL after purification (reprecipitation). [c]Theoretical $M_n$ calculated according to $([DMDL]_0/[ECP]_0)\times$(monomer conversion)×(molecular weight of monomer).

The purified PDMDL was used as a macroinitiator in the polymerization of VAc. We heated a mixture of VAc (150 equiv.), PDMDL macroinitiator (1 equiv.), and AIBN (0.2 equiv.) in toluene (25 wt%) at 70 ℃ for 22 h. The $M_n$ value increased from 5100 to 7100 with a VAc conversion of 49 % (Table 5.4). The GPC chromatograms before (dashed line) and after (solid line) the block polymerization (Figure 5.8) showed that a large fraction of the macroinitiator (PDMDL) extended to the block copolymer (PDMDL-*b*-PVAc).

**Table 5.4.** Block polymerization of VAc using PDMDL macroinitiator ($M_n$ = 5100, $Đ$ = 1.27).

| $[VAc]_0/[PDMDL\ macroinitiator]_0/[AIBN]_0$ (equiv.)[a] | $T$ (°C) | $t$ (h) | Conv. (%)[b] | $M_n$[c] ($M_{n,theo}$[d]) | $Đ$[c] |
|---|---|---|---|---|---|
| 150/1/0.2 | 70 | 22 | 49 | 7100 (11000) | 1.35 |

[a]Dilution with 25 wt% toluene. [b]Monomer conversion determined with $^1$H NMR. [c]PMMA-calibrated GPC values (THF eluent). [d]Theoretical $M_n$ calculated according to ((($[VAc]_0/[PDMDL]_0$)×(monomer conversion)×(molecular weight of monomer)) + (molecular weight of PDMDL).

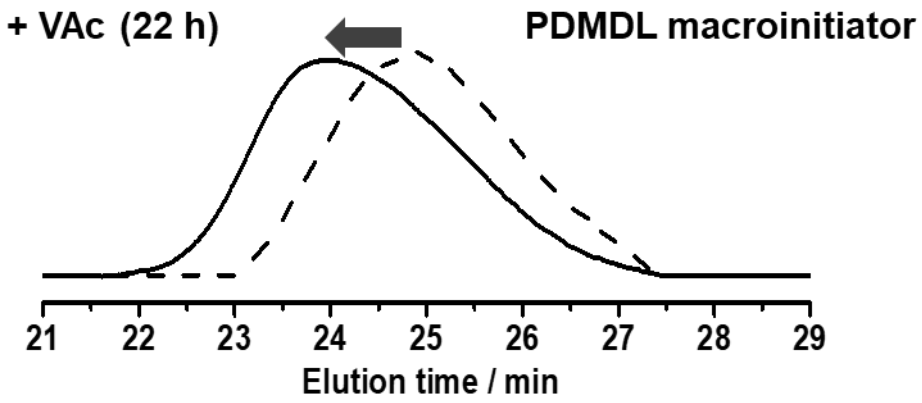


**Figure 5.8.** GPC chromatograms before (dashed line) and after (solid line) block polymerization of VAc using PDMDL macroinitiator. The reaction condition is given in Table 5.4.

**Homopolymerization of DMDL Using RCMP.**

We carried out RCMP of DMDL (homo-polymerization). We heated a mixture of DMDL (100 equiv.), 2-iodo-2-methylpropionitrile (CP-I) (alkyl iodide initiating dormant species (Figure 5.2), 1 equiv.), BNI (catalyst, 1 equiv.), and AIBN (1 equiv.) at 70 °C(Table 5.5 and Figure 5.9). AIBN was added to increase the polymerization rate. Without AIBN, the polymerization was very slow (conversion < 5% for 5h), generating only oligomers ($M_n$ < 1000). Azo initiators are used to decrease the deactivator concentration and hence effectively increase the polymerization rate in RCMP[11] and other living radical polymerization systems.[12] After 5 h, the monomer (DMDL) conversion reached 88 %, yielding a PDMDL homopolymer with $M_n$ = 15000 and $Đ$ = 1.86 (Table 5.5) The $Đ$ values (= 1.75–1.86) were relatively large during the course of polymerization (Figure 5.9b), suggesting a relatively slow activation of the carbon–iodide bond of the PDMDL–iodide using the BNI catalyst. However, as described

below, the addition of co-monomers (random copolymerizations of DMDL with co-monomers) generated low-dispersity copolymers, probably because the terminal monomer unit was replaced by the co-monomers to some extents so that the polymer-iodide can be activated more frequently overall.

**Table 5.5.** RCMP of DMDL homopolymerization.

| $[DMDL]_0/[CP\text{-}I]_0/[BNI]_0/[AIBN]_0$ (equiv.) | $T$ (°C) | $t$ (h) | Conv. (%)[a] | $M_n$[b] ($M_{n,theo}$[c]) | $Đ$[b] |
|---|---|---|---|---|---|
| 100/1/1/1 | 70 | 5 | 88 | 15000 (11000) | 1.86 |

[a]Monomer conversion determined with $^1$H NMR. [b]PMMA-calibrated GPC values (THF eluent) [c]Theoretical $M_n$ calculated according to $([DMDL]_0/[CP\text{-}I]_0)\times$(monomer conversion)×(molecular weight of monomer).

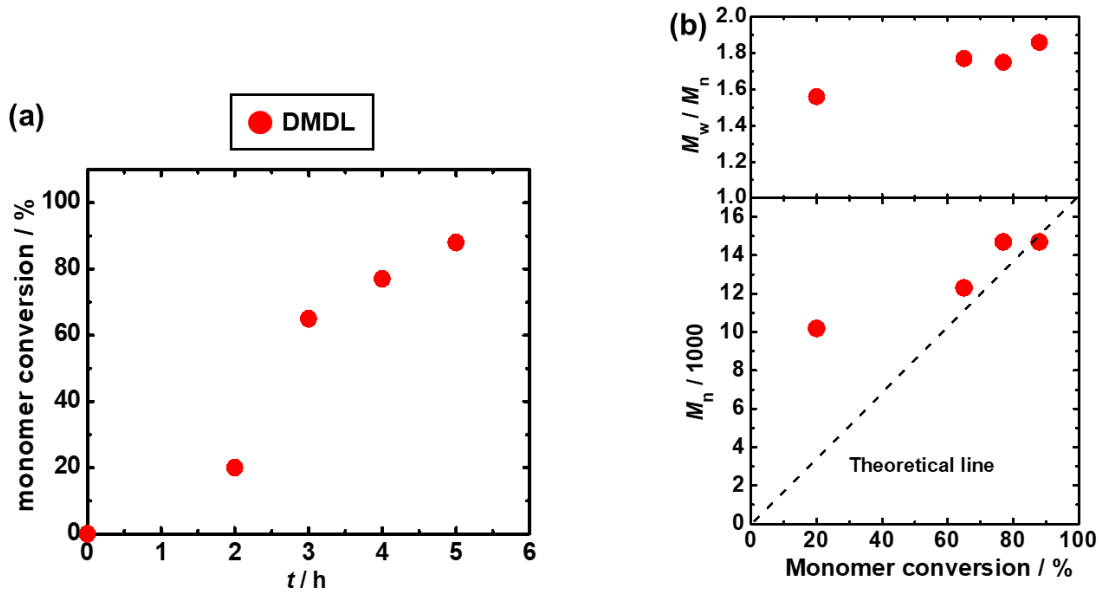


**Figure 5.9.** Plots of (a) monomer conversion *vs.* polymerization time ($t$) and (b) $M_n$ and $M_w/M_n$ *vs.* monomer conversion for the DMDL/CP-I/BNI/AIBN system (70 °C). The reaction condition is given in Table 5.5.

**Random Copolymerizations of DMDL Using RCMP.**

We studied RCMPs (random copolymerizations) of DMDL with several co-monomers (Figure 5.2), i.e., four different methacrylates (methyl methacrylate (MMA), benzyl methacrylate (BzMA), 2-methoxyethyl methacrylate (MEMA), poly(ethylene glycol) methyl ether (PEGMA), acrylonitrile (AN), and an acrylate (MEA). We heated mixtures of DMDL (25 equiv.), co-monomer (75 equiv.), CP-I (1 equiv.), and BNI (1-4 equiv.) at 60–110 $^{o}$C for 2-24 h (Table 5.6). Using 50/50 molar ratio of DMDL and co-monomer, we obtained only oligomers with relatively low monomer conversions. Therefore, we increased the fraction of the co-monomer. We chose a 25/75 molar ratio of DMDL and co-monomer (DMDL/co-monomer ratio), thereby yielding polymers.

The random copolymerizations with the four methacrylates yielded random copolymers with $M_n$ = 5600–16000, $Đ$ = 1.27–1.32, and $F_{DMDL}$ = 4–7% (Table 5.6, entries 1–4). Thus, we obtained low-dispersity degradable hydrophobic and amphiphilic random copolymers with methyl (MMA), benzyl (BzMA), poly(ethylene glycol) (PEGMA), and 2-methoxyethyl (MEA) groups. In chapter 4, we determined the monomer reactivity ratios of DMDL and MMA to be $r_{MMA}$ = 4.60 and $r_{DMDL} \approx 0$, suggesting that methacrylates are almost exclusively consumed over DMDL in methacylate/DMDL random copolymerizations. Therefore, the $F_{DMDL}$ was low (4–7%) in the studied random copolymerizations (Table 5.6, entries 1–4). The random copolymerizations with AN and MEA (acrylate) yielded random copolymers with $M_n$ = 6700–8400, $Đ$ = 1.14–1.25, $F_{DMDL}$ = 11% (Table 5.6, entries 5 and 6). The $F_{DMDL}$ values (11%) for AN and the acrylate were slightly larger than those (4-7%) for methacrylates, which is because of the slightly more alternating tendency in the AN ($r_{AN}$ = 0.28 and $r_{DMDL} \approx 0.04$) and acrylate ($r_{BA}$ = 0.83 and $r_{DMDL} \approx 0.03$) systems. Thus, we obtained low-dispersity degradable random copolymers using methacrylates, AN, and an acrylate.

**Table 5.6.** Random copolymerizations of DMDL with several co-monomers using RCMP.

| Entry | Co-monomer (M) | $[M]_0/[DMDL]_0/[CP\text{-}I]_0/[BNI]_0$ (equiv.)[a] | $T$ ($^oC$) | $t$ (h) | Conv. (M/DMDL) (%/%)[b] | $M_n$[c] ($M_{n,theo}$[d]) | $Đ$[c] | $F_{DMDL}$ (%)[e] |
|---|---|---|---|---|---|---|---|---|
| 1 | MMA | 75/25/1/1 | 70 | 2 | 61/8 | 5600 (5300) | 1.27 | 4 |
| 2 | BzMA | 75/25/1/1 | 70 | 6 | 54/12 | 8300 (7500) | 1.30 | 7 |
| 3 | MEMA | 75/25/1/1 | 70 | 8 | 57/7 | 8800 (6400) | 1.31 | 4 |
| 4 | PEGMA | 75/25/1/1 | 60 | 22 | 60/9 | 16000 (14000) | 1.32 | 5 |
| 5 | AN | 75/25/1/1 | 75 | 15 | 33/12 | 6700 (1700) | 1.14 | 11 |
| 6 | MEA | 75/25/1/4 | 110 | 24 | 71/26 | 8400 (7800) | 1.25 | 11 |

[a]Bulk polymerizations for entries 1-4 and 6 and solution polymerization (in 50 wt% ethylene carbonate) for entry 5. [b]The co-monomer conversions were determined from the decay in the co-monomer peaks using $^1$H NMR. The DMDL monomer conversions were too low to be accurately determined in the same way. Therefore, the DMDL monomer conversions were calculated from the co-monomer conversion and the $F_{DMDL}$ value (DMDL unit fraction determined in the purified copolymer), because the co-monomer conversion and the $F_{DMDL}$ value were relatively large and relatively accurately determined. [c]PMMA-calibrated GPC values (THF eluent) for entries 1-3 and 6. PMMA-calibrated GPC values (DMF eluent) for entries 4 and 5. [d]Theoretical $M_n$ calculated according to $([M]_0/[CP\text{-}I]_0)\times$(co-monomer conversion)$\times$(molecular weight of co-monomer) + $([DMDL_0/[CP\text{-}I]_0)\times$(DMDL monomer conversion)$\times$(molecular weight of DMDL monomer). [e]$F_{DMDL}$ value determined by the $^1$H NMR analysis of the purified polymer.

**Degradation of PDMA-*r*-PDMDL.**

We tested the degradation of the PDMA-*r*-PDMDL random copolymer ($M_n$ = 8800, $Đ$ = 1.16, and $F_{DMDL}$ = 20 %) synthesized in the RAFT polymerization (Table 5.2, entry 2). This random copolymer is hydrophilic and soluble in water. We dissolved the polymer (0.06 g, 6 wt%, 1 equiv. of the DMDL monomer unit) in a 1M NaOH aqueous solution (1 g, 94 wt%, 11 equiv. of NaOH) and monitored the degradation at room temperature. Figure 5.10a and b show the GPC chromatograms and the plot of $M_n$ *vs.* degradation time. The peak-top molecular weight ($M_p$) decreased from 12000 (original polymer) to 7900 and 3600 for 2 h and further decreased to 6000 and 3000 for 15 h. Apparent two peaks were observed for 2, 6, 9, and 15 h. The two peaks would be apparent and would not be ascribed to two distinct species. According to the proposed mechanism of degradation in Chapter 4 (Scheme 4.4), shorter polymer chains ($M_n$ smaller than 8800) and small molecule HIBA were generated after the degradation of the

PDMA-*r*-PDMDL random copolymer. The peaks were broad and appeared probably because the PDMA-*r*-PDMDL is a gradient copolymer and degraded to a mixture of longer and shorter polymer chains. The relative intensity (peak height) of the two apparent peaks also changed over time. The higher molecular-weight peak became smaller over time, while the lower-molecular weight peak became larger. Thus, the PDMA-*r*-PDMDL random copolymer degraded in the basic condition.

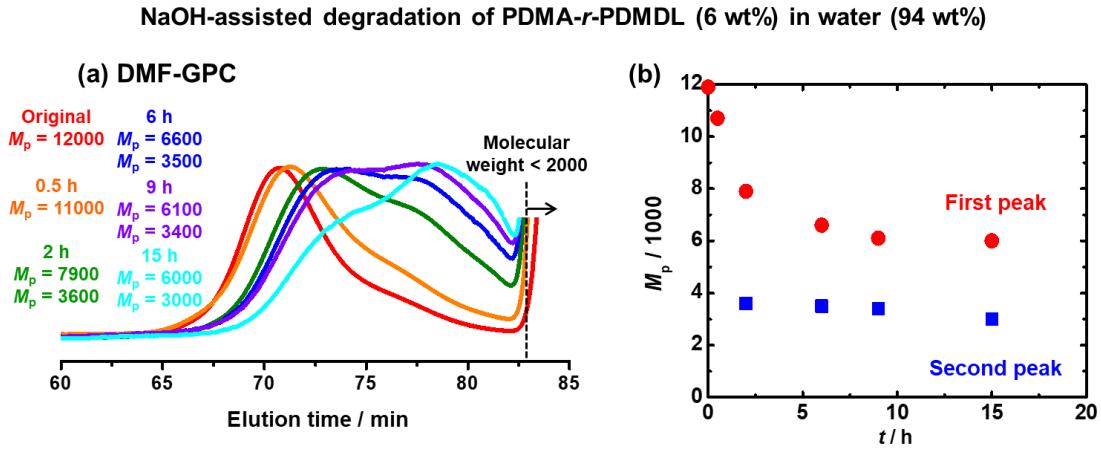


**Figure 5.10.** Degradation of PDMA-*r*-PDMDL ($M_n$ = 8800, $Đ$ = 1.16, and $F_{DMDL}$ = 20 %) (6 wt%) using 11 equiv. of NaOH in water (94 wt%) at room temperature: (a) GPC chromatograms and (b) plot of $M_n$ *vs.* degradation time (red circles represent $M_p$ of the first peak eluted and blue squares represent $M_p$ of the second peak eluted).

.

## 5.3. Conclusions

We successfully prepared homopolymers, random copolymers, and a block copolymer of DMDL with controlled molecular weights and low dispersities using RAFT polymerization and RCMP. For the RAFT polymerizations, ECP (xanthate) was the most effective CTA of the three studied CTA and was useful for a homopolymerization, random copolymerizations and a block copolymerization with VAc. CDPA (trithiocarbonate) was more suitable for random copolymerizations with an acrylamide and acrylates. RCMP was effective for random (gradient) copolymerizations with several (functional) methacrylates, acrylonitrile, and an acrylate. The PDMA-r-PDMDL prepared via RAFT polymerization successfully degraded in basic condition (1M NaOH). Low-dispersity and controlled molecular weight of DMDL homopolymer and random (gradient) copolymers may be useful in applications for specific physical properties. Also, gradient copolymers and a block copolymer of DMDL generate either shorter oligomers or longer polymer chains may be practical for biomedical applications.

## 5.4. Experimental Section

### Materials.

Anhydrous dichloromethane (DCM) (>99.0%, TCI), 2-hydroxyisobutyric acid (>98%, TCI), 2,2′-azobis(2-methylpropionitrile) (AIBN) (95%, Wako Pure Chemical, Japan), acetyl chloride (≥99.0%, Sigma-Aldrich, USA), oxalyl chloride (≥99.0%, Sigma-Aldrich), triethylamine (>99.0%, TCI), hexane (>99%, International Scientific, Singapore), diethyl ether (ACS reagent grade, VWR International, USA), chloroform (>99.2%, VWR Chemicals, USA), tetrahydrofuran (THF) (>99.5%, Kanto Chemical, Japan), *N*,*N*-dimethylformamide (DMF) (>99.5%, Kanto), ethylene carbonate (EC) (>99%, TCI), toluene (ACS reagent grade, VWR International), methanol (ACS reagent grade, VWR International), methyl methacrylate (MMA) (>99.8%, TCI), poly(ethylene glycol) methyl ether methacrylate (PEGMA) (average molecular weight = 300) (98%, Sigma-Aldrich), butyl acrylate (BA) (>99%, TCI), acrylonitrile (AN) (>99%, TCI), 2-methoxyethyl acrylate (MEA) (>98%, TCI), *N*,*N*-dimethylacrylamide (DMA) (>99.0%, TCI), vinyl acetate (VAc) (>99.0%, TCI), 1-vinyl-2-pyrrolidinone (NVP) (>99.0%, TCI), benzyl methacrylate (BzMA) (>98.0%, TCI), ethyl 2-[(ethoxycarbonothioyl)thio]propionate (ECP) (>95.0%, TCI), 4-cyano-4-[[(dodecylthio)carbonothioyl]thio]pentanoic acid (CDPA) (>97.0%, TCI), (2-iodo-2-methylpropionitrile (CP–I) (>95%, TCI), 2-acetoxyisobutyryl chloride (>97%, Tokyo Chemical Industry (TCI)), tetrabutylammonium iodide (BNI) (>98%, TCI), sodium hydroxide (1 mol/L in water) (NaOH) (0.95 to 1.05 mol/L, TCI) were used as received.

### Measurement.

A Shimadzu i-Series Plus liquid chromatograph LC-2030c Plus (Kyoto, Japan) equipped with a Shodex (Japan) KF-804L mixed gel column (300 × 8.0 mm; bead size = 7 μm; pore size = 1500 Å) and a Shodex LF-804 mixed gel column (300 × 8.0 mm; bead size = 6 μm;

pore size = 3000 Å) was used with THF eluent for the GPC analysis. The flow rate was 0.7 mL/min (40 $^{o}$C). A Shimadzu LC-2030c Plus equipped with two Shodex LF-804 mixed gel columns (300 × 8.0 mm; bead size = 6 μm; pore size = 3000 Å) and a Shodex KD-802 (300 × 8.0 mm; bead size = 6 μm; pore size = 150 Å) was used with DMF eluent for the GPC analysis. The flow rate was 0.34 mL/min (40 °C). The DMF eluent contained LiBr (10 mM). A refractive index detector (RID-20A) was used for sample detection for THF-GPC and for DMF-GPC. For both THF-GPC and DMF-GPC systems, standard poly(methyl methacrylate)s (PMMAs) was used to calibrate the column system.

The NMR spectra were recorded on Bruker (Germany) BBFO400 spectrometer (400 MHz) at ambient temperature. $CDCl_3$ and $CD_3CN$ (Cambridge Isotope Laboratories, USA) were used as the solvents for the NMR analysis, and the chemical shift was calibrated using residual undeuterated solvents or tetramethylsilane (TMS) as the internal standard. The monomer conversions and the monomer compositions in the obtained polymers were determined with $^{1}$H NMR.

**General Procedure for Polymerization.**

In a typical run, a mixture (1.2–2.5 mL, typically) of a DMDL monomer, a co-monomer, RAFT CTAs or alkyl iodide initiator (CP-I), AIBN (radical initiator), and solvent was heated in a Schlenk flask at 60-110 °C under argon atmosphere with magnetic stirring. After a prescribed time *t*, an aliquot (0.1 mL) of the solution was taken out by a syringe, cooled to room temperature, and analyzed with GPC and $^{1}$H NMR. At the last date point of the reaction, the polymer solution was diluted with chloroform (DMSO for AN), and the polymer was reprecipitated in a mixture of hexane/diethyl ether (1/1 (v/v)) twice (methanol for BA) for purification. The collected polymer was dried in vacuo and analyzed with $^{1}$H NMR.

**Synthesis of PDMDL Macroinitiator.**

DMDL (5 g, 39 mmol), ECP (87 mg, 0.39 mmol), and AIBN (13 mg, 0.078 mmol) was added to a Schlenk flask and heated at 70 ℃ under argon atmosphere with magnetic stirring. After 2 h, the polymerization mixture was dissolved in chloroform (10 mL) and subsequently reprecipitated into hexane in a mixture of hexane/diethyl ether (1/1 (v/v)) twice for purification. The polymer was stored under vacuum to dry and give PDMDL macroinitiator (monomer conversion = 37 %, $M_n$ = 5100 and $Đ$ = 1.31 after purification) as a pale-yellow powder.

**Block Copolymerization.**

In a typical run, a mixture of VAc (0.5 g), a PDMDL macroinitiator, and AIBN was heated in a Schlenk flask at 70 °C under argon atmosphere with magnetic stirring. After cooling to room temperature, an aliquot (0.1 mL) of the solution was analyzed with $^1$H NMR for monomer conversion and GPC for $M_n$ and $Đ$.

**Degradation of PDMA-*r*-PDMDL.**

A mixture of PDMA-*r*-PDMDL ($M_n$ = 8800, $Đ$ = 1.16, and $F_{DMDL}$ = 20 %) (0.06 g, 6 wt%, 1 equiv. of the DMDL monomer unit) and 1M NaOH aqueous solution (1 g, 94 wt%, 11equiv. of NaOH) was stirred at room temperature. After a prescribed time *t*, an aliquot (0.1 mL) of the solution was taken out by a syringe and analyzed with DMF-GPC.

## References


1. Whitfield, R.; Truong, N. P.; Messmer, D.; Parkatzidis, K.; Rolland, M.; Anastasaki, A. *Chem. Sci.* **2019**, *10*, 8724-8734.
2. Barouti, G.; Jarnouen, K.; Cammas-Marion, S.; Loyer, P.; Guillaume, S. M. *Polym. Chem.* **2015**, *6*, 5414-5429.
3. Cajot, S.; Lecomte, P.; Jérôme, C.; Rivaa, R. *Polym. Chem.* **2013**, *4*, 1025-1037.
4. Jundi, A. E.; Buwalda, S. J.; Bakkour, Y.; Garric, X.; Nottelet, B. *Adv. Colloid Interface Sci.* **2020**, *283*, 102213.
5. Grabe, N.; Zhang, Y.; Agarwal, S. *Macromol. Chem. Phys.* **2011**, *212*, 1327–1334.
6. Xiao, N.; Liang, H.; Lu, J. *Soft Matter* **2011**, *7*, 10834-10840.
7. Ganda, S.; Jiang, Y.; Thomas, D. S.; Eliezar, J.; Stenzel, M. H. *Macromolecules* **2016**, *49*, 4136– 4146.
8. Gao, Y.; Böhmer, V. I.; Zhou, D.; Zhao, T.; Wang, W.; Paulusse, J. M. J. *J. Control. Release* **2016**, *244*, 375-383.
9. Perrier, S. *Macromolecules* **2017**, *50*, 7433–7447.
10. Goto, A.; Ohtsuki, A.; Ohfuji, H.; Tanishima, M.; Kaji, H. *J. Am. Chem. Soc.* **2013,** *135*, 11131-11139.
11. Wang, C-G; Chang, J. J.; Yong, E. J. F.; Niino, H.; Chatani, S.; Hsu, S. Y.; Goto, A. *Macromolecules* **2020**, *53*, 51-58.
12. Goto, A.; Fukuda, T. *Prog. Polym. Sci.* **2004**, *29*, 329−385.

## Chapter 6. Conclusions

The objective of this doctoral thesis was to prepare functional polymers in a sustainable way. Self-catalyzed RCMP, recycled use of RCMP heterogeneous catalyst, dual catalysts nano-capsule, and degradable vinyl polymers with chemical recyclability were reported in this thesis.

In chapter 2, QAI containing monomers were used for self-catalyzed RCMP. Synthesis of $C_6$MAI (a QAI containing monomer) is simple and attainable in a large scale (i.e., 100-gram scale). This self-catalyzed RCMP does not need an extra catalyst to catalyze the polymerization of functional monomers (i.e., methacrylates and acrylates). It is amenable to various monomers and highly versatile. The purification process is simple therefore fewer chemical wastes are generated.

Further exploration of self-catalyzed RCMP was conducted in chapter 3, where heterogeneous RCMP catalyst and dual catalysts nano-capsule were synthesized. Recycle of the heterogeneous RCMP catalyst is simple (i.e., precipitation from a toluene mixture). The recovered heterogeneous RCMP catalyst is applicable for an MMA polymerization up to ten cycles to achieve consistently high monomer conversion and relatively low-dispersity polymers. Furthermore, dual catalysts nano-capsule was explored with MMA polymerization taking place on both outer surface and inner core. This novel nano-capsule (i.e., polymerization occur in the inner core) may be useful as a functional nano reactor for different interesting applications (i.e., block copolymerization in micro-phase separation nanoparticles or selective hydrophilic and hydrophobic monomers polymerization).

In chapter 4, degradable and chemically recyclable polymers were synthesized with CKHE monomers (i.e., DMDL and PhDL). The degradable polymers are attractive for use in preparing degradable materials. Also, chemical recycling of monomer precursor after degradation of DMDL homopolymer confidently shows the sustainability to the environment.

The precursor can be recovered in a simple way (i.e., extraction) and reused for DMDL monomer synthesis.

Chapter 5 further studied the CRP (i.e., RAFT polymerization and RCMP) of CKHE monomer (i.e., DMDL) where CKHE monomers were studied in conventional radical polymerization in chapter 4. CRP is useful in synthesizing low-dispersity polymers with controlled molecular weights. The DMDL homopolymers, random (gradient) copolymers, and a block copolymer obtained via CRP are controllable in molecular weights with low dispersity. Physical properties are displayed differently with different dispersities. Therefore, DMDL polymers with controllable molecular weight and low dispersity are attractive for design of polymeric materials with different physical properties (i.e., durability and thermal property).

Synthesis of functional polymers in a sustainable way was demonstrated in this thesis. In Chapter 2 and 3, we used the catalytic monomers to catalyze polymerizations without additional catalyst. In Chapter 3, we prepared a heterogeneous catalyst with the catalytic monomer for recycle use in polymerizations. A sustainable self-catalyzed process is useful for industrial applications that can avoid the use of an external catalyst. A heterogeneous catalyst with recycle use preparing by self-catalyzed RCMP may capture more interest because this combination substantially reduces the waste and cost. Following work of this project will involve the use of the catalytic nano-capsule as nano-reactor to synthesize solvophilic polymer nano-particles in their soluble media. In Chapter 4 and 5, we synthesized degradable polymers and recovered the degradation product for monomer synthesis. Degradable polymers are useful for many applications such as drug delivery and tissue scaffold. In addition, recycle of product generated after polymer degradation leads to lesser waste imposed to the environment. Future work of this project will involve the use of suitable RAFT agent to prepare random copolymers of DMDL and methacrylates. We demonstrated the sustainability concept with the self-

catalyzed process without additional catalyst, the recycle use of a heterogeneous catalyst, and the synthesis of degradable polymers with its recycled use of degradation product.